Aus dem Institut für Physiologie und Pathophysiologie

Geschäftsführender Direktor: Prof. Dr. Dominik Oliver
des Fachbereichs
Medizin der Philipps-Universität Marburg

Titel der Dissertation:

Dissecting the role of tyrosine phosphorylation of WAVE in macrophage migration

Inaugural-Dissertation zur Erlangung des
Doktorgrades der Naturwissenschaften
dem Fachbereich Medizin der Philipps-Universität Marburg

Vorgelegt von
Marike Rüder aus Bad Segeberg
Marburg 2021

Angenommen vom Fachbereich Medizin der Philipps-Universität Marburg
am: 19.05.2021
Gedruckt mit Genehmigung des Fachbereichs Medizin

Dekanin: Prof. Dr. Denise Hilfiker-Kleiner

Referent: Prof. Dr. Sven Bogdan

1. Korreferent: Prof. Dr. Ralf Jacob

Contents

I List of abbreviations

Abi	Abelson interactor
Abl	Abelson
AdoR	Adenosine receptor
ADP	Adenosine diphosphate
APS	Ammonium persulfate
Arg	Abl-related genes
Arp	Actin related protein
ATP	Adenosintriphosphate
attB	bacterial attachment site
BCM	border cell migration
BCR	Breakpoint cluster region
BSA	Bovine serum albumin
CDK	Cyclin-dependent kinase
Co-IP	Co-Immunoprecipitations
D	Aspartic acid
DAMPs	damage-associated molecular patterns
ddH2O	Double-distilled water
Dia	Diaphanous
DNA	desoxyribonucleic acid
DTT	Dithiothreitol
DUOX	dual oxidase
E	Glutamic acid
ECM	extracellular matrix
EDTA	Ethylenediaminetetraacetic acid
eGFP	Enhanced green fluorescent protein
EGTA	Ethylene glycol-bis(β-aminoethyl ether)-N,N,N',N'-tetraacetic acid
EMS	Ethylmethansulfonat
Ena	Enabled
ERK	Extracellular signal-regulated kinase
EVH1	Ena/VASP homology 1
F	Phenylalanine
F-actin	Filamentous actin
FH2	Formin homology 2
FLP	Flippase
FRT	Flippase recombination target
g	Gram
G-actin	Monomeric actin
GBD	GTPase binding domain
GEF	Guanine nucleotide exchange factor
GTP	Guanosine triphosphate
HMMS	Histogram-based macrophage migration score

HSPC300	Hematopoietic stem progenitor cell 300
ITAM	Immunoreceptor tyrosine-based activation motif
kDa	Kilo Dalton
LMOD	Leiomodin
M	Molar
mg	Milligram
ml	Milliliter
NADPH	Nicotinamide adenine dinucleotide phosphate
Nap-1	Nck-associated protein 1
NPFs	Nucleation promoting factors
N-WASP	Neural WASP
PBS	Phosphate buffered saline
PBT	PBS + TritonX
PCR	Polymerase chain reaction
PDGF	Platelet-derived growth factor
PFA	Paraformaldehyd
PI(3)K	Phosphoinositide 3-kinase
PIP2	Phosphatidylinositol 4,5-bisphosphate
PIP3	Phosphatidylinositol 4,5,6-trisphosphate
PRD	Proline rich domain
PTP61F	Protein tyrosine phosphatase 61F
Pvr	Platelet-derived growth factor/vascular endothelial growth factor related receptor
Rac	Ras-related C3 botulinum toxin substrate
RNA	Ribonucleic acid
RNAi	RNA interference
rpm	Rounds per minutes
RT	Room temperature
S	Serine
Scar	Suppressor of cAMP receptor
SDS	Sodium dodecyl sulfate
SDS-PAGE	SDS polyacrylamide gel electrophoresis
sec	Seconds
SH2	Src homology 2 domain
SH3	Src homology 3 domain
Sra-1	Specifically Rac associated protein 1
T	Threonine
UAS	Upstream activating sequence
VASP	Vasodilator-stimulated phosphoprotein
VCA	Verprolin, cofilin, acidic
VDGF	Vascular endothelial growth factor
WASH	Wiskott-Aldrich syndrome and Scar homolog
WASP	Wiskott-Aldrich syndrome protein
WAVE	WASP family verprolin homologous protein

WH2	WASP homology 2
WHD	WAVE homology domain
WIRS	WRC interacting receptor sequence
WRC	WAVE Regulatory Complex
Y	Tyrosine

II List of figures

List of Supplementary Figures

III List of tables

List of Supplementary Tables

1 Introduction

1.1 Cell movement builds the fundament of multicellular life

In multicellular organisms many developmental processes like gastrulation, dorsal closure, or organ differentiation as well as immune cell migration are based on movement of either single cells or entire epithelial sheets (Barrett et al., 1997; Genova et al., 2000; Tilney et al., 1995). Establishing cell polarity is the initial and fundamental part of all cellular migratory processes. Cells receive external position information from surrounding cells or tissues by direct contact or via external secreted signaling factors and can translate this information to initiate an asymmetric rearrangement of their cytoskeleton. Thus, the cytoskeleton itself builds the scaffold of the cell but also coordinates morphological processes by dynamic changes of the cell shape. The cytoskeleton is composed of three different components – microtubules, intermediate filaments and actin filaments. The majority of cell shaping processes rely on fast assembly and disassembly of actin filaments. At the cell membrane, the assembly of filaments generates forces pushing the membrane outwards to form protrusive structures, which are called lamellipodia and filopodia. These dynamic protrusive structures form the so-called leading-edge which is responsible for directional movement of the cell (Ananthakrishnan and Ehrlicher, 2007; Pollard and Borisy, 2003). The main functions of these two structures differ. Filopodia are finger-like structures, whose function mainly lies in exploring the environment. Therefore, they also play a critical role in collective and invasive cell migration. In contrast, lamellipodia are flat, leaf-like structures, which are especially important for cell migration.
Cell migration can be differentiated in single cell migration and collective cell migration. Since one of the first publications on single cells migration focusses on lamellipodial driven movements, this outstanding findings shaped many of the following research in this area (Abercrombie et al., 1970a, 1970c, 1970b). Since then, the knowledge about actin regulated morphological flexibility has extended enormously. In the classical model of single cell migration, experiments were performed on cells migrating on a 2D surface like a coated Petri dish or *in vivo* on an epithelial layer. In all experimental models, extracellular signals initiate cell shape changes resulting in directed cell migration. The force generation, induced by F-actin assembly at the leading edge of the cell, leads to an increase in cell membrane tension. The cell membrane is then pushed forward by the forced, opposing the expanding actin

filament and pushes them backwards. This can be observed in the characteristic retrograde actin flow at the membrane. Cells adhere to the surface/substrate through integrin-mediated adhesions. These adhesions are constantly rebuilt at the cell front – the leading-edge – and are released at the cell rear to allow constant cell movement. Actin-myosin contractions in the rear facilitate the retraction of the cell body (Vicente-Manzanares et al., 2009).

When it comes to 3D migration, protrusive structures need to be more complex. Cells combine not only filopodial and lamellipodial structures or cylindrical-shaped lobopodia composing features of lamellipodia, but membrane blebs can appear in addition or exclusively (Sander et al., 2013; Sixt, 2012).

During collective cell migration, the movement of entire groups of cells is coordinated. The main principles for collective cell migration are the same as for single cell migration. As in single cell migration, the directional information can be received by external signals. However, in collective cell migration it is sufficient that only a few tip cells receive the signal. This signal is passed on to the other cells in the structure and translated into collective cell movement. To ensure the integrity of the group, the cell junction contacts in the group are constantly maintained between the moving cells (Aman and Piotrowski, 2010).

1.1.1 *Drosophila* as a model for cell migration in a physiological context

In the last decades, advanced genetic tools and high-resolution imaging techniques have improved the toolboxes available to scientists enormously. *In vitro* approaches have provided the necessary insights into cellular processes, but they lack the ability to investigate cell dynamics in a multicellular context. Furthermore, cell culture experiments cannot entirely substitute the environmental impact on the migratory behavior of cells *in vivo*. As most actin regulated migratory processes are highly conserved across species, knowledge obtained from a model organism can be transferred to other organisms. For at least 100 years, *Drosophila melanogaster* is commonly used as a model organism in the life sciences. Observations made in *Drosophila* have a huge impact on our knowledge about both collective and single cell migration (Table 1).

Table 1: Examples for actin-based processes in Drosophila and their relevance as model function in mammalian system

Drosophila model	**Actin dependent process/ structure**	**Mammalian Equivalent**	**Reference**
border cell migration (BCM)	collective cell migration	neural crest cell migration (Shellard and Mayor, 2016)	(Montell, 2003)
egg rotation	collective cell migration	epithelial morphogenesis	(Squarr et al., 2016)
myoblast fusion	cell–cell fusion, podosome or invadopodia-like structure; invadopodia-like fingers/protrusions	myoblast fusion	(Önel and Renkawitz-Pohl, 2009; Schäfer et al., 2007)
cellular wound response	single cell migration	single cell migration, cancer metastasis	(Sander et al., 2013; Wood et al., 2006)
bristles development	bundled F-actin	brush-border of epithelial intestine cells (Tilney & Mooseker, 1971)	(Bogdan et al., 2004)
cells extravasation from vessels	invadopodium	cancer metastasis	(Thuma et al., 2018)

Drosophila egg chamber development in particular provides an excellent model to study collective cell migration in a multicellular context. During oogenesis, egg chamber maturation undergoes 14 different stages until the matured egg. In these 2.5 to 3 days, the egg chamber grows massively in size and changes its shape to end in an elongated conformation (Lin and Spradling, 1993). This process is driven by so-called follicle cells surrounding the egg chamber. The collective migration of follicle cells induces egg rotation, which is necessary for the maturation of the egg. The simultaneous reorganization of the actin cytoskeleton in these cells leads to cell polarization and enables the generation of unidirectional forces (Squarr et

al., 2016). Observation of this mechanism provides general insights into epithelial sheet movement.

Another fascinating and well-established model for collective cell migration, is the border cell migration (BCM). The border cell cluster is composed of six to ten cells deriving from the follicle cell epithelium. These cells migrate collectively through the egg chamber towards the oocyte and finally upwards to form the micropyle. The cluster moves between the nurse cells, a process guided by at least three different secreted growth factors. Successful BCM is highly dependent on cell cluster integrity based on cadherin-mediated adhesion. Furthermore, cell cluster motility is highly dependent on cell polarity and the extension of actin regulated protrusion (Llense and Martín-Blanco, 2008; McDonald et al., 2006; Prasad and Montell, 2007; Silver et al., 2005) . In mammals, a comparable mechanism is found in neural crest cell migration (Shellard and Mayor, 2016).

A convenient system to study single cell migration events, which do not depend on the cellular integrity of a cell cluster, are *Drosophila* macrophages. In their migratory behavior, these cells are comparable to mammalian immune or cancer cells. They travel long distances, whereby their motion is tightly controlled by their actin machinery. Upon external stimulation, for example by a pathogen or a wounding incidence, *Drosophila* macrophages switch from random to directed migration, comparable with mammalian cellular immune response (Sander et al., 2013).

1.1.2 Single cell migration of *Drosophila* macrophages

Once a pathogen passes the physical barrier and infiltrates the organism it needs to be recognized and eliminated by the host organism to prevent damage. In all multicellular organisms, the first and immediate immune response relies on multiple defense strategies of the innate immune system. Many reactions are highly conserved across species. Vertebrates further possess an adaptive immune system, whose response is slower but more specific on pathogens. The crosslinks between innate and adaptive immune response in vertebrates makes it difficult to investigate single components independently. Therefore, the high similarity of the *Drosophila* innate immune response is used to study the general underlying mechanisms.

Immune cells make up a large part of the innate immune defense. Together with the humoral immune response, including antimicrobial peptides, the cellular immune response of insects is an effective system to fight bacterial infections and induce wound healing (Lemaitre and Hoffmann, 2007). While vertebrates possess a full set of specialized cell types, *Drosophila* immune cells, so-called hemocytes, are divided into three classes: hemocytes, crystal cells and lamellocytes. However, novel findings based on bulk RNA sequencing suggest a more

heterogeneous immune cell population (Cattenoz et al., 2020). Plasmatocytes are the most frequent cell type that account for up to 95 % of *Drosophila* immune cell population. These cells share similar functions to vertebrate macrophages and are therefore also called *Drosophila* macrophages (from here on out referred to as macrophages). Macrophages have important roles in both development and tissue homeostasis and are able to secrete antimicrobial peptides and extracellular matrix components. Their major task is the defense against pathogens and the recognition and clearance of cellular debris after wound healing (Wynn et al., 2013).

The second type of *Drosophila* immune cells are called crystal cells, named after their crystalline structures harboring prophenoloxidase. They are essential in wound healing processes. After cell rupture, a proteolytic cascade eventually leads to the melanisation at the wound site and the additional release of reactive oxygen species induces a systematic immune response (Eleftherianos and Revenis, 2011; Theopold et al., 2014). Crystal cells make up less than five percent of the immune cell population. The third class of immune cells known as lamellocytes appear even more rarely. They only emerge upon immune challenging conditions. These giant immune cells encapsulate large immune targets. It has been shown that parasitic wasp infections trigger the differentiation of lamellocytes from macrophages (Sorrentino et al., 2002).

Hemocytes development occurs during the embryonic, larval and pupal development of *Drosophila* in three waves depicted in Figure 1 (Gold and Brückner, 2014). The progenitors emerge in the head mesoderm in the embryonic stage 7 and differentiate into 600 – 700 macrophages and a few crystal cells. While crystal cells stay clustered at their origin, macrophages migrate through the embryo until they population is dispersed throughout the hole embryo in stage 15. Macrophages are motile until the larval stage where they cluster in so-called hematopoietic pockets. Here, the rapid proliferation of the existing embryonic macrophages occurs in a second wave (Makhijani et al., 2011).

The second origin for hemocytes is the lymph gland (Figure 1, Holz, 2003). In the embryonic stage, lymph gland hemocytes undergo a low rate of proliferation until the second larval stage. In the third instar, larval hemocytes differentiate into macrophages and expand during the third wave extensively in number. Crystal cells and lamellocytes are only present in small numbers. In the pupal stage, both populations of macrophages are released from the hematopoietic pockets and the lymph gland and start to circulate in the hemolymph of the pupae and later the adult fly to fulfil their immune function. In these developmental stages, only a weak hematopoietic activity is observable (Gold and Brückner, 2014; Parsons and Foley, 2015).

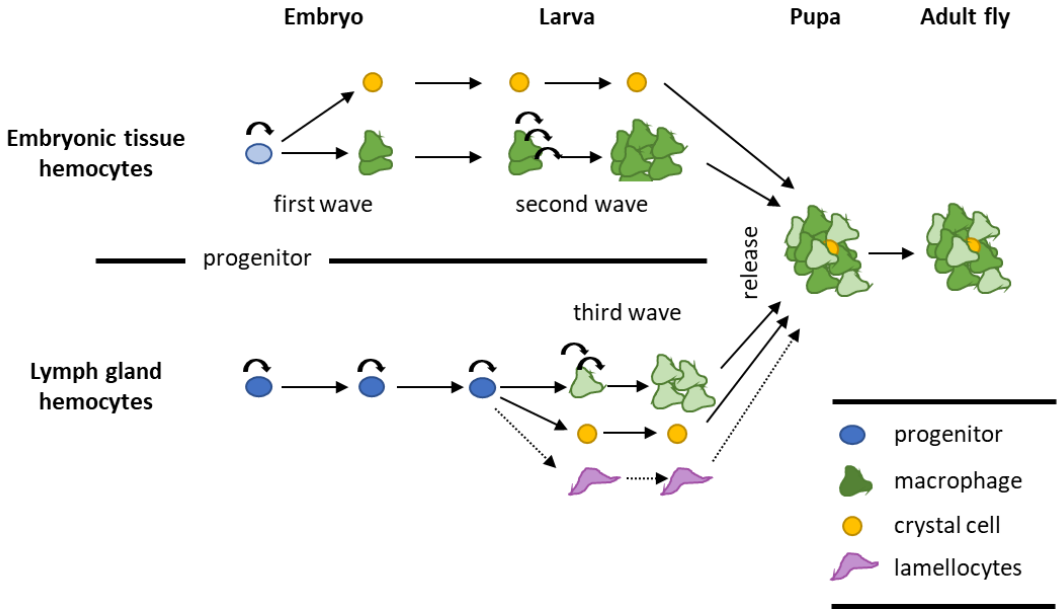

Figure 1: Scheme of *Drosophila* hematopoiesis. Macrophage differentiation occurs in three waves. Embryonic tissue hemocytes differentiate and proliferate in the embryonal stage and further proliferate in the larva. lymph gland macrophages differentiate and proliferate in the late larval stage. Both populations are related to the hemolymph of the pupa. Under normal conditions, crystal cells and especially lamellocytes make up under five percent of the hemocyte population (modified from Gold & Brückner, 2014)

1.1.3 Chemotactic guidance of macrophage migration during development and wound response

The majority of macrophages originating in the pupal stage are polarized and increased in size compared to embryonic and larval macrophages (Sampson and Williams, 2012; Sander et al., 2013). These macrophages are dispersed throughout the entire animal. Macrophages, which are attached to the epithelium, show large protruding lamellipodia embedding few stress fibers formed by actin bundles. For effective cell migration of *Drosophila* macrophages and mesenchymal cells, a high level of relevance is attached to these flat lamellipodial structures at the leading edge of cells (Sander et al., 2013). However, it is still under debate, whether lamellipodia are dispensable for migration (Suraneni et al., 2012; Wu et al., 2012).

Figure 2: Schematic view of a migration macrophage. Macrophages show a broad flat lamellipodium at the leading edge. This is composed of few actin bundles and a dense branched actin network.

Hemocyte migration depends on adhesion to the extracellular matrix (ECM) (Ananthakrishnan and Ehrlicher, 2007). In classical models, it is proposed that ECM is exogenously present to the migrating cell (Olofsson and Page, 2005; Urbano et al., 2009). However, it also has been shown that embryonic macrophages are able to secrete autocrine produced laminin and other ECM components. Previous studies underline the importance of the presence of ECM for the regulation of protrusion stability, dynamics and effective cell migration (Urbano et al., 2017). *Drosophila* macrophages migrate as single cells, reacting to extracellular signals and are able to pass cell barriers. By the expression of chemotactic molecules, the guidance and the survival of the hemocytes is coordinated in time and space (Kockel et al., 2004; Ratheesh et al., 2015). Early studies have already shown that at the end of embryonic stage 10, macrophages start actively migrating through the embryo following three major routes (Cho et al., 2002; Tepass et al., 1994). One subpopulation in stage 12 passes the cellular barrier of the germband epithelium and moves into the yolk sac (Ratheesh et al., 2015; Siekhaus et al., 2010). The specific dispersal pattern of macrophages at the ventral midline is coordinated by Platelet-derived growth factor/ vascular endothelial growth factor (PDGF/VEGF) signaling (Wood et al., 2006). The developmental dispersal of the macrophages is a relatively slow process to ensure that all cells reach their destination in a certain time frame. In contrast, wound response requires a rapid but also precise orchestrated reaction upon wound signals.

In studies investigating directed immune cell migration in *Drosophila*, laser-induced wounding was inflicted on the organism to identify potential signaling pathways. Wood and colleagues claim at least two independent mechanisms for an exact developmental dispersal of macrophages and the fast, directed response on wound signals. They demonstrate the Phosphoinositide 3-kinase (PI(3)K) is a crucial component in chemotaxis towards wounds in *Drosophila*, but dispensable in coordination of ventral midline dispersal (Heit et al., 2002;

Wood et al., 2006). Hydrogen peroxide (H_2O_2) and ATP are small and fast diffusing molecules that get released after wounding and might act as potential chemoattractant. $H_2O_2$is postulated to signal through the Src42A-Draper-Shark cascade, which is conserved in vertebrates and known as Src family kinase immunoreceptor tyrosine-based activation motif (ITAM)-Syk immune pathway (Evans et al., 2015; Yoo et al., 2012, 2011). This signaling mechanism is further supported by the production of the NADPH dual oxidase enzyme (DUOX) at the wound rim of damaged cells (Razzell et al., 2013). However, other data challenges these findings. In Weaver et al. (2016) the spatiotemporal properties of a wound attracted gradient were defined and a potential diffusion rate of 200 μm^2/min for a hypothetical chemoattractant upon laser induced wounding was calculated. These findings speak against fast diffusing molecules like H_2O_2 and ATP as direct immune cues (Weavers et al., 2016). Further support for this hypothesis comes from the mutation of the *Drosophila* purinoreceptor Adenosine receptor (AdoR), which does not alter the immune response upon wounding (Moreira et al., 2010).

Conclusively, inflammatory response signaling is not yet fully understood. However, current data suggests redundant functions of different signal cascades on multiple damage-associated molecular patterns (DAMPs). This hypothesis is also consistent with reports from leucocyte system in vertebrates (Mcdonald et al., 2010). Furthermore, it is still unclear how the extracellular signal gets further transduced to the cytoskeleton machinery. This critical step in the local rearrangement of the actin network after wounding and its regulation needs to be investigated in more detail.

1.2 The actin cytoskeleton as the fundament for structure and dynamics

A network of actin filamentous structures builds the scaffold of cells and allows cell movement by fast and precise reorganization. The reorganization is driven by continuous assembly at the barbed end and disassembly at the pointed end of the filaments. Cells use a diverse set of proteins to control the polymerization of actin filaments. Actin monomers (G-actin) can self-assemble into filaments *in vitro*. Nevertheless, under physiological conditions, the majority of free actin monomers are bound to monomer binding proteins like profilin and thymosine-ß4, decreasing spontaneous polymerization events compared to *in vitro* data (Ozaki and Hatano,

1984; Safer and Nachmias, 1994; Skruber et al., 2018). This pool of G-actin is only available for the actin polymerization machinery under certain conditions. However, the formation of a filament nucleus consisting of an actin trimeric is kinetically unfavored (Cooper et al., 1983). Thus, the spontaneous polymerization turns out to be inefficient and slow. To overcome this, cells have evolved several control steps to tightly regulate actin polymerization as well as depolymerization. To do so, cells use the so-called actin nucleators, which share the ability to mimic the trimeric state and build the origin of a new actin filament but promote nucleation by distinct mechanisms.

The Arp2/3 complex is highly conserved across species and is a very well characterized actin nucleator. It consists of seven subunits in which the actin-related subunits Arp2 and Arp3 show structural similarities to monomeric actin itself (Goley and Welch, 2006). The formation of a nucleus, catalyzed by the Arp2/3 complex, is most efficient at a pre-existing mother filament. The daughter filament emerges in a 70° angle, giving rise to a branched actin network structure. To slow down the dissociation, cortactin can bind the filament. As a class II activator, its N-terminal end contains equivalent amino acids to bind Arp2/3, but it lacks the G-actin binding site (Ammer and Weed, 2008). Several mechanisms are based on this network, such as the clathrin-mediated endocytosis, where Arp2/3 dependent actin patches are crucial. The most prominent structures based on actin branched networks are leaf-like protrusions named lamellipodia (Small et al., 2002). With ongoing growth of the filament, the Arp2/3 complex is shifted backwards to the cell rear and finally dissociates. Depletion of Arp2/3 activity results in the complete loss of lamellipodia (Suraneni et al., 2012; Wu et al., 2012).

Another class of actin nucleators, so-called tandem-monomer-binding nucleators, contain a tandem cluster of three or more actin binding WASP homology 2 (WH2) domains. In contrast to the Arp2/3 complex, these nucleators are involved in unbranched F-actin formation. Until now, three members are identified: Cordon-bleu (COBL), whose function seems to be restricted to vertebrates, the muscle-specific nucleator Leiomodin (LMOD) and Spire, which was first identified in *Drosophila* and is required during egg development (Campellone and Welch, 2010). Current data on Spire promotes its function as actin nucleator facilitating polymerization of filaments by bringing actin monomers in close proximity to the WH2 domain. However, other data suggests that Spire, if bound to actin, can also result in a stable sequestration complex and abolishes polymerization (Rasson et al., 2015). To promote the formation of microtubule-actin meshwork, Spire cooperates with the Formin Cappuccino (Bor et al., 2015; Rodal et al., 2015).

Formins are the third prominent class of nucleators. In animal cells, Formins are key factors in the formation of linear actin filaments and can additionally initiate actin bundles. They

provide the basis of many cellular structures like filopodia (Schirenbeck et al., 2005), but are also involved in stress fiber formation (Lammel et al., 2014; Satoh and Tominaga, 2001), long range cytoplasmic transport actin networks and other processes (Breitsprecher and Goode, 2013). Once a filament is initiated, the elongation also needs to be regulated. A majority of the Formin members remain associated with the growing barbed end and therefore favor further polymerization. The Formin homology 2 (FH2) domain is crucial for the interaction with the actin filament . They build homodimers and each carries two F-actin binding sites. The dimeric FH2 domain walks progressively with the growing end of the newly build filament. It constantly switches between an open state, favoring the addition of an actin monomer, and an inactive closed state (Paul and Pollard, 2009; Zigmond et al., 2003). The different Formin family members vary in the time they spend in the closed position or open position, which characterizes their cellular function. Formins can therefore slow down polymerization but also support elongation. Murine Diaphanous 1 (mDia1) is an example for a Formin predominantly present in an open position (Kovar et al., 2006). To perform properly, Dia-like Formins are dependent on profilin-bound actin as an actin source that is rapidly added to the existing filament by their Formin homology 1 (FH1) domain.

In contrast, elongation mechanisms based on Ena/Vasodilator-stimulated phosphoproteins (VASP) proteins are dependent on pre-existing actin filaments and show a rather weak ability to nucleate filaments *de novo*. At the barbed end, Ena acts antagonistically to capping proteins and supports further filament elongation (Bear et al., 2002). The protein family shows a highly conserved structure with N-terminal Ena/VASP homology 1 (EVH1) domain, a proline-rich domain and the C-terminal EVH2 domain (Krause et al., 2003). They act as a trimer, while one of its arms holds contact to the filament, the other offer three binding sites for G-actin (Brühmann et al., 2017).

The intact actin turnover is just as important as the growth control of filaments. One option to terminate elongation, as described above, is the blocking of the filament by Formins in major inactive gated states (Shemesh et al., 2005). Additionally, there are specialized proteins, referred to as capping proteins. They mask the barbed end and make it inaccessible for elongation factors (Schafer et al., 1996).

Maturing actin monomers within the filament undergo conformational changes by the hydrolysis of ATP, which prepares this part of the polymer for disassembly (Blanchoin and Pollard, 2002). The actin-depolymerization factor cofilin also contains an actin-binding site but prefers binding to ADP-bound actin filaments (Tanaka et al., 2018). In comparison, Twinfilin promotes disassembly on both sites of the filament, whereas Cofilin just acts at the pointed end (Johnston et al., 2015). Crucial for the turnover of branched network is Coronin,

so far, the only known Arp2/3 inhibitor. High levels of Coronin influence Arp2/3-dependent polymerization negatively, whereas depletion of Coronin increases cofilin phosphorylation, resulting in elevated protein activity (Cai et al., 2007).
Within an equilibrium of assembly and disassembly continuous treadmilling of the filament can be observed and provides the basis of the dynamic of the actin cytoskeleton (Pantaloni et al., 2001). This rapid and very efficient machinery needs to be precisely coordinated at the site of action. To avoid spontaneous and unregulated polymerization, the Arp2/3 complex is cytoplasmatically present in its inactive form. It can be activated by so-called nucleation promoting factors (NPFs), which are crucial for the site-specific activation in many actin driven processes.

1.2.1 Regulation of branched nucleation by WASP family members

The fast but controlled nucleation of actin filaments is fundamental for many cellular processes. Proteins of the Wiskott-Aldrich syndrome protein (WASP) family have been identified as acting as NPFs in the activation of the Arp2/3 complex. In mammals, WASP family members are divided in five subfamilies including WASP and neuronal-WASP (N-WASP), three isoforms of the WASP family verproline homologs (WAVE1-3), WHAMM, WASH and JYM. *Drosophila* expresses only four WASP family proteins (Campellone and Welch, 2010): of each, WASP, WAVE (also known as suppressor of cyclic AMP receptor (SCAR), Figure 3) and WASH, one orthologue is expressed. The last identified NPF is WHAMY, which originated from a *wasp* gene duplication (Brinkmann et al., 2015). All members share a characteristic C-terminal VCA (or WCA: WH2 connecting and acidic) domain consisting of the verprolin-homology domain binding monomeric actin, the cofilin-homology/ center domain and the acidic domain (Figure 3) interacting with the Arp2/3 complex (Campellone and Welch, 2010; Pantaloni et al., 2001; Stradal and Scita, 2005).
The N-terminus each family member consists of individual unique domains, which regulate their interaction with other proteins and specify their localization within the cell. WASP is intrinsically present in its folded autoinhibitory state, so the VCA domain is inaccessible for Arp2/3 binding (Figure 3). At the N-terminus, WASP exhibits a WASP homology 1 (WH1) domain that binds to members of the WASP-interacting protein (WIP) family (Ramesh et al., 1997) and is required for WASP stabilization in vertebrates. The WH1 domain further negatively influences WASP activity (Dai et al., 2001). In contrast, binding of the small GTP-bound form of Cdc42 to the GTPase binding domain (GBD) unfold WASP and releases the VCA domain (Kim et al., 2000), leading to it being accessible for Arp2/3 binding.

In contrast, WAVE proteins are incorporated into a regulatory hetero-pentameric complex controlling WAVE activity. It is composed of Kette (Nap1), specifically Rac1-associated protein 1 (Sra1), Abelson interactor (Abi), Hematopoietic stem progenitor cell protein 300 (HSPC300) and WAVE itself (Bogdan et al., 2004; Takenawa and Suetsugu, 2007) with Sra and Kette forming an elongated dimer. WAVE binds Abi and HSPC300 with its WHD to form a trimer, which aligns on the platform offered by the Sra:Kette dimer (Chen et al., 2010). The interference with a single subunit, potentially by degradation, disrupts complex integrity and WAVE regulatory complex (WRC) function (Steffen et al., 2004; Stradal and Scita, 2005). A diminished amount of the other members underlines the complex as a functional unit. However, in *Dictyostelium*, individual mutants of WRC subunits display different phenotypes indicating additional roles of each member. At least for Abi, initial evidence shows that interaction with VASP may nucleate actin in a non-classical way (Litschko et al., 2017).

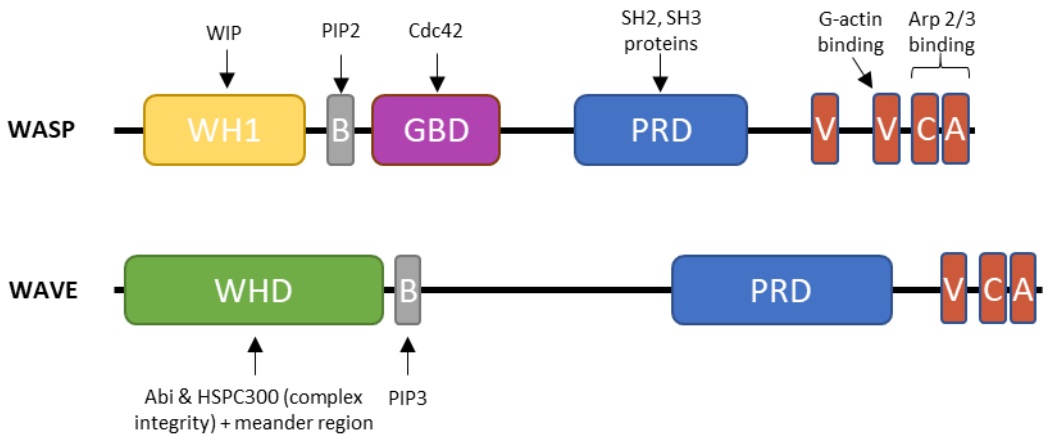

Figure 3: Comparison of protein domain structure of Drosophila WASP and WAVE. At the C-terminus they share the characteristic VCA domain (or WCA: WH2 connecting and acidic) domain consisting of the verprolin-homology domain binding monomeric actin, the cofilin-homology/ center domain and the acidic domain, a basic region (B) and a proline-rich domain (PRD). At the N-terminus WASP exhibits a WASP homology domain 1 (WH1) and a GTPase binding domain (GBD). WAVE N-terminally contains the WAVE homology domain (WHD) including the meander region at the end (not shown). Further indicated are potential interacting proteins.

1.2.2 Spatial regulation of the WRC at the leading edge

The local induction of the branched actin network relies on the regulated recruitment of a molecular scaffold to the leading edge (Buracco et al., 2019). WAVE as the main activator of the Arp2/3 complex is a key factor for efficient lamellipodia based migration (Campellone and Welch, 2010). The local regulation has been the focus of investigations for many years. WAVE is normally present in its inactive, folded form, incorporated in the WRC. The VCA domain

is sequestered by various interactions of its verprolin domain (V) and the center/cofilin (C) binding to both Sra1 and the meander region of WAVE abolishing G-actin as well as Arp2/3 complex binding (Chen et al., 2010). Thus, upstream signals need to activate and recruit the WRC to the membrane to induce site-specific actin assembly. Many proteins interact with WAVE or other WRC family members, leading to the conclusion that cooperative functions are essential for the ideal activation of the complex (Figure 4).

A large body of evidence supports the small Rho GTPases Rac1 to be central to activating the WRC and trigger actin polymerization (Abou-kheir et al., 2008; Mehidi et al., 2019; Ridley et al., 1992; Steffen et al., 2004). For a long time, only one conserved binding surface at the C-terminus of Sra1 close to the VCA-binding site was postulated (now named A-site). The allosteric binding of Rac-GTP to the A-Site of the WRC subunit Sra-1 destabilizes its binding to the meander region and inducing the release of the WAVE VCA domain (Chen et al., 2010; Mehidi et al., 2019) (Steffen et al., 2004). Recent studies identified an additional binding site, the so-called D-site near the C-terminus of Sra-1 which turned out expendable for WRC activation but still functionally relevant for optimal lamellipodial formation and protrusive velocity (Mehidi et al., 2019, 2018)(Carver et al., 2017). Both binding sites contribute to actin assembly. Whereas the A-site remains the major WRC activation site, the D-site facilitates efficiency of actin assembly (Schaks et al., 2018). Constitutive active WRC with mutations in both Rac binding sites is partially able to rescue lamellipodia formation and migration defects. This implies that Rac is an important factor for WRC activation, but not essential for the recruitment of the WRC to the membrane (Schaks et al., 2018). Single molecule tracking of the Rac and WRC components showed that Rac immobilization at the lamellipodium tip strongly correlates with its activity in turn depends on its effector binding e.g., to the immobilized fraction of the WRC. Thus, WRC-RAC binding is not essential for recruitment, maintenance and turnover of the WRC at the lamellipodium. Single molecule tracking of different WRC subunits shows immobilization of free diffusing WRC increases at the lamellipodial tip (Mehidi et al., 2018). This implies that a local diffusion-trapping mechanism is responsible for the local recruitment to and accumulation of the WRC at the lamellipodial tip.

Membrane curvature as well as phosphoinositide lipid composition highly affects WRC binding affinity to the membrane. The membrane lipid phosphatidylinositol (3,4,5) trisphosphate (PIP3), a product of PI(3)K phosphorylating PI(4,5)P2. PIP3 binds WAVEs´ positively charged basic region and facilitates the recruitment of the WRC to the membrane (Lebensohn and Kirschner, 2009) (Oikawa et al., 2004).. Generally, the electrostatic charge distribution on the surface of the WRC further supports the binding of the predominate

positively charged complex face of the Sra-1:Kette platform adjected to the basic region to phospholipid rafts. The other part of the complex, harboring the WAVE:Abi:HSPC300, is negatively charged and facing the cytoplasm (Chen et al., 2010). This renders the VCA and the meander region of WAVE accessible for other regulators like kinases or especially the Arp2/3 complex as the main effector. The asymmetric distribution of PIP3 and PIP2 therefore might be involved in the specificity of WAVE localization at the leading edge. Rac is also activated by PIP3 via the activation and locally restricted recruitment of guanine-nucleotide exchange factors (GEFs). Furthermore, Rac activity and mediated actin assembly also stimulates PI(3)K activity (Welch et al., 2003). This feedback mechanism supports proper local enrichment of Rac and PI(3)K recruitment and therefore further WAVE activation (Figure 4).

For a local activation of the actin machinery upon extracellular signals, these signals need to be transduced into the cell and further translated into cell motion. Interestingly, numerus membrane receptors and membrane associated proteins have been identified to be carrying a WRC interacting receptor sequence (WIRS). This short peptide sequence (Φ-x-T/S-F-X-X) is present in an abundance of membrane receptors and membrane-associated proteins including cell adhesion receptors, guidance receptors, and tyrosine kinase receptors (Figure 4). It directly links potential WIRS ligands to a conserved surface on the WRC formed by the Sra-1 and Abi subunits (B. Chen et al., 2014). Fat2 contains a WIRS motive, which interaction with the WCR has been demonstrated to drive collective cell migration in follicle cells during *Drosophila* oogenesis (Squarr et al., 2016). So far, this mechanism is only predicted to be involved in macrophage guidance.

Although the phosphorylation of WAVE is frequently reported to influence actin polymerization, the precise mechanism remains unknown. There is evidence that WAVE might be activated and recruited to the membrane by a combination of membrane receptors containing a WIRS motive, PIP3, GTP-bound Rac, phosphorylation and other factors. Some of these can be substituted, but others are critical, e.g. the Rac-dependent activation of WAVE. In conclusion, they all need to be tightly coordinated for lamellipodial driven cell motion.

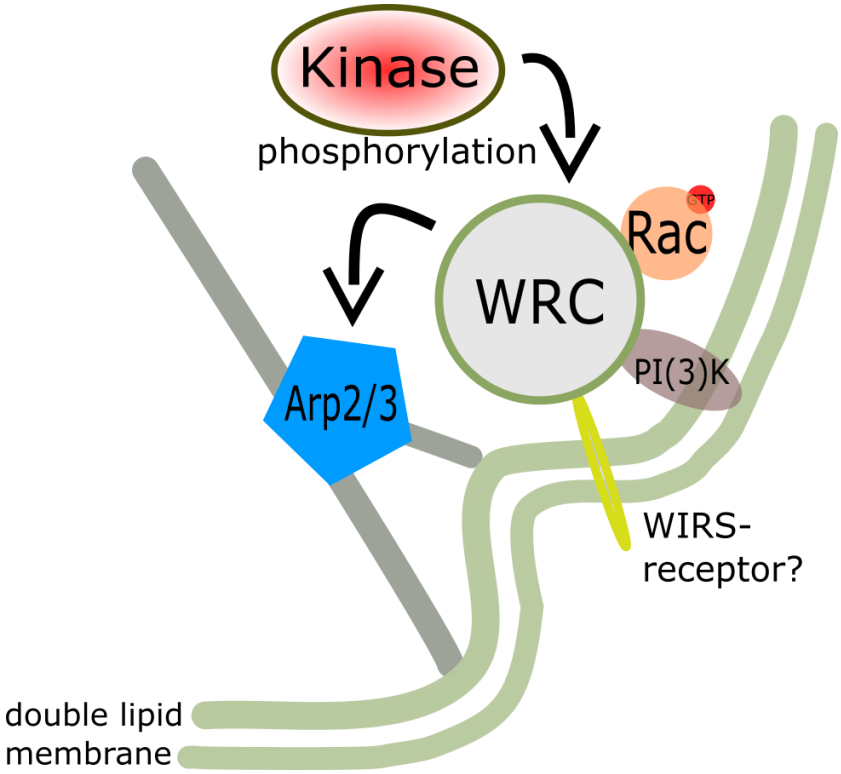

Figure 4: Scheme of predicted WAVE dependent lamellipodia formation. Different depicted factors influence WRC recruitment and activity at the membrane. GTP bound Rac facilitate the release of the VCA domain and further activates the Arp2/3 complex. Negatively charged PI(3)K bind the basic region of WAVE and facilitate membrane localization. WIRS-receptors are assumed to transmit external signal to the actin machinery. WAVE is targeted by many kinases that influence its activity.

1.2.3 The influence of phosphorylation on WAVE activity

Phosphorylation is a well described reversible post-transcriptional modification and has been known to play a critical role in the regulation of diverse cellular processes including, but not restricted to, growth, apoptosis, receptor-dependent and intracellular signal transduction. Phosphorylation is carried out by kinases, catalyzing the energy consuming transfer of a γ-phosphoryl group to a serine, threonine or tyrosine (Cohen, 2002; Fischer et al., 1959). Phosphorylation can lead to conformational changes and either activation or inactivation of the protein. Furthermore, it can change the binding affinity and thus enables the recruitment of the protein to distinct targets. The modification can be reversed by specific phosphatases.

1.2.3.1 Kinase specific targeting of WAVE regulatory domains

Phosphorylation is known to influence WAVE function and localization. Within its regulatory domains, WAVE contains many serine, threonine and tyrosine residues being a potential target

for diverse protein kinases. Many of the identified residues are species-specific but also isoform-specific within species (Krause and Gautreau, 2014; Mendoza, 2013). Nevertheless, the specific kinase regulation seems to be restricted to a certain functional WAVE domain (Figure 5).

The VCA domain is crucial for WAVE polymerization function and its release activates WRC to further induce Arp2/3-dependent actin nucleation. Casein kinases phosphorylate WAVE2 at five Serine residues within the VCA domain (Figure 5), whereby three sites (WAVE2 – Ser482, Ser484, Ser488) are conserved in all isoforms and across species (Mendoza, 2013a). However, the exact effect of VCA phosphorylation on WAVE activity is still a matter of controversial discussion (Nakanishi et al., 2007; Pocha and Cory, 2009; Ura et al., 2012).

In mammals, the Proline rich domain (PRD) of WAVE is mainly controlled by serin-phosphorylation via Cyclin-dependent kinase (CDK) and extracellular signal-regulated kinase (ERK) (Figure 5). CDKs only regulate WAVE1 and act negatively on WAVE function, whereas ERK is described to phosphorylate WAVE2, which results in its activation (Mendoza et al., 2011). Nevertheless, none of these residues are conserved in invertebrates (Mendoza, 2013). The question of whether PRD phosphorylation is negligible in invertebrates or whether its function has been taken over by other kinases needs further investigation.

Tyrosine-dependent WAVE regulation is restricted to the WHD domain, where the two prominent tyrosine kinases Src and Abelson (Abl) are reported to phosphorylate WAVE in the meandering region and therefore act on WAVE's active state. In mammals, CDK5 is reported to additionally support WAVE function via the phosphorylation of WAVE2 at S137 in mouse oligodendrocyte precursor cell or T137 in human WAVE1 (Chen et al., 2010; Miyamoto et al., 2008).

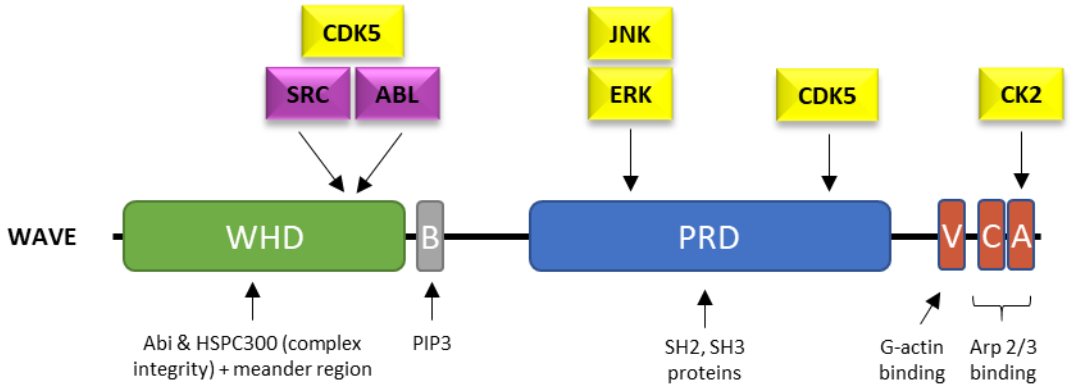

Figure 5: Kinase specific phosphorylation of WAVE domains. Domain structure of *Drosophila* WAVE. Local regulation by: Serin/threonine kinases in yellow and tyrosine kinases in purple.

1.2.3.2 Regulation of WAVE tyrosine phosphorylation

The Abl tyrosine kinase has repeatedly been described to direct phosphorylate WAVE2 at the conserved Y150 (Table 2). This tyrosine residue is located in the WHD meander region and maps downstream of the Abi binding site (**Figure 6**). WAVE activity is increased in the presence of Abi and Abl but abrogated in WAVE mutated in the Y150F phosphorylation site (phospho-mutant). Hereby, Abi WAVE interaction facilitates WAVE phosphorylation (Stuart et al., 2006). The indispensability of Abi in WAVE phosphorylation is still under debate.

Crystal structure of WAVE1 identified Y151 to localize within the hydrophobic pocket of the WRC formed by Sra1 and WAVE. Chen et al. (2010) hypothesized that phosphorylation of this residue destabilizes the binding of the C-Helix of the VCA domain, caused by a disruption of Sra1 binding to the meander region. Phosphorylation site-mutation, with an amino acid substitution of WAVE Y150D (Table 2) mimicking a phosphorylated state, displays high actin assembly activity and increase lamellipodia formation. Other studies found that the phospho-mimicking of conserved WAVE1 Y125– predicted as a Src phosphorylation site within the meander region – shows similar actin polymerization activity to that described for Y150 (Ardern et al., 2006; Chen et al., 2010). This data suggests another alteration mechanism beside the Rac1 induced release of the VCA domain leading to WCR activation (Chen et al., 2010).

Remarkably, phospho-mutation in WAVE2 Y150 but not in WAVE3 Y151 (Table 2) completely blocks Abl-mediated phosphorylation (Sossey-Alaoui et al., 2007; Stuart et al., 2006). In WAVE3, Y248, Y337 and Y486 (Table 2) need to be additionally modified to completely inhibit phosphorylation (Sossey-Alaoui et al., 2007). This might indicate an Abl phosphorylation-dependent mechanism that is not restricted to the WHD domain.

Table 2 Conserved tyrosine residues of WAVE orthologous and corresponding reported effector kinase.

WAVE1	**WAVE2**	**WAVE3**	***Drosophila* WAVE**	**Kinase/ Phosphatase**	**Source**
Y125	**Y124**	Y125	Y127	**Src**	(Ardern et al., 2006; Chen et al., 2010; Mendoza, 2013)

Y151	**Y150**	**Y151**	Y153	**Abl**	(Joseph et al., 2017; Krause and Gautreau, 2014; Leng et al., 2005; Mendoza, 2013; Stuart et al., 2006)
Y151	Y150	**Y151**	Y153	**Abl**	(Sossey-Alaoui et al., 2007)
not conserved	not conserved	**Y248**	not conserved	**Abl**	
not conserved	not conserved	**Y337**	not conserved	**Abl**	
Y543 (alignment)	Y480 (alignment)	**Y486**	not conserved	**Abl**	
not conserved	not conserved	not conserved	**Y234**	**PTP61F** (Abl consensus)	(Chang et al., 2008; Huang et al., 2007)
not conserved	not conserved	not conserved	**Y247**	**PTP61F**	
not conserved	Y230 (alignment)	not conserved	**Y253**	**PTP61F** (Src consensus)	

In total, *Drosophila* WAVE exhibits 15 potential tyrosine residues (Figure 6) of which one is located at the N-terminal part of WAVE, four residues are located in the WHD domain and the remaining ten residues map between the basic region and the PRD domain. The WHD domain as well as the four tyrosine residues, located in the meandering region of the domain, are highly conserved across species. This region is critical for the autoinhibitory binding of the VCA domain and the intermolecular binding of the heteromeric WRC complex (Chen et al., 2010).

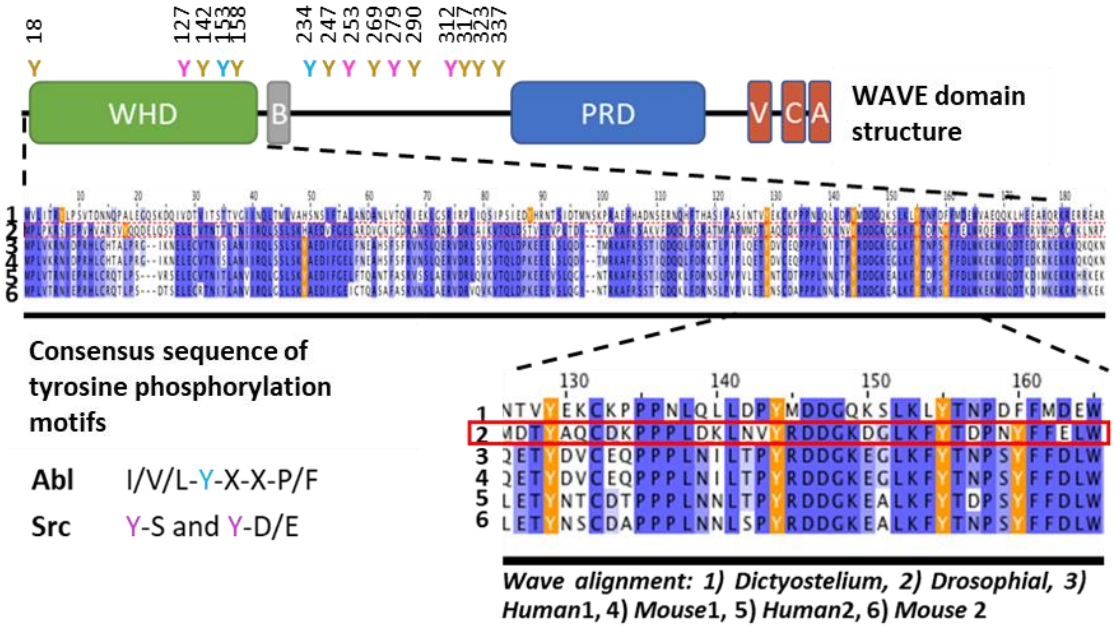

Figure 6: WAVE tyrosine phosphorylation. *Drosophila* WAVE domain structure with highlighted tyrosine residues. Consensus-sequence of WAVE homology domain in 1) Dictyostelium *wave*, 2) Drosophila *wave*, 3) human *wave1*, 4) mouse *wave1*, 5) human *wave2*, 6) mouse *wave2* with tyrosine sides highlighted in orange. Predicted Abl (cyan) and Src (magenta) kinase tyrosine targets based on reported consensus sequence.

Most studies claim WAVE WHD phosphorylation facilitates WAVE activation and mainly acts positively on actin polymerization. However, in T-cells WAVE2 phosphorylation is described to induce WAVE protein degradation from the membrane. It has been shown that degradation is initiated when the autoinhibitory state is dissolved and lysine 45 is accessible for ubiquitination. This process is reduced in phospho-deficient transgenes of Abl phosphorylation site Y150 (Joseph et al., 2017). The similar mechanism was reported for N-WASP (Frame, 2002).

To reverse kinase protein modification, phosphatases are essential to remove added phospho-residues. In phospho-tyrosine trapping experiments, potential substrates for phosphatase PTP61F (Huang et al., 2007) – the counterpart phosphatases of Abl – were identified. WAVE fragments 220-267, carrying three tyrosine (Y234, Y247, Y253 (Table 2)), are found in *Drosophila* S2 cells. But it must be mentioned, that aside from Y150 and Y125, no physical relevance has been associated with other WAVE tyrosine residues so far.

Conclusively, phosphorylation is a complex interaction of different kinases and is reversibly controlled by phosphatases. Further evidence shows that phosphorylation may not only influence protein activity but can also lead to WAVE degradation. All these interactors

additionally influence their activity reciprocally. It has to be further determined how the phosphorylation state of different residues as well as kinase composition act on actin dynamics *in vivo*.

1.2.4 Structure and regulation of tyrosine kinase Abelson

The non-receptor tyrosine kinase Abelson (Abl = Abelson murine leukemia) is involved in development and cell shape changes by regulating the activity and localization of target proteins. It has been identified in patients with chronic myeloid leukemia. The reciprocal translocation of Abl to the breakpoint cluster region (BCR) of the BCR gene results in a new chimeric gene with enhanced tyrosine kinase activity (Fogerty et al., 1999; Owen-Lynch and Whettno, 1993; Price et al., 1988). Increased levels of constitutive active Abl during eye development results in a rough eye phenotype (Fogerty et al., 1999).

Abl, as well as Src, belongs to the non-receptor tyrosine kinase superfamily. Both are proto-oncogenes and share a high domain structural similarity (Nagar et al., 2003). In both proteins, a tandem Src-homology domain 3 (SH3) localizes to the N-terminus mediating the complex assembly by binding the proline rich domain of target proteins. The SH3 domain is followed by a Src-homology domain 2 (SH2) that procures binding to tyrosine phosphorylated residues of interaction partners (Waksman et al., 2004). The kinase domain of Abl is located central (Figure 7). Abl predominantly phosphorylates tyrosine residues in the consensus sequence I/V/L-Y-X-X-P/F (Figure 6, Mendoza, 2013). C-terminal Abl carries a unique F-actin binding domain, which is connected via a long and less conserved linker carrying a PXXP motive (Figure 7). However, this direct interaction has only been shown for mammalian Abl-related gene (Arg, or Abl2) and is only predicted based on sequence homology for *Drosophila* (Figure 7, Galkin et al., 2005; MacGrath and Koleske, 2012; Rogers et al., 2016). Furthermore, modification of this actin-binding site in *Drosophila* has no effect on fly development or morphology (Rogers et al., 2016). Additionally, Abl, as well as Src, contain a WIRS motive, known to facilitate the interaction of membrane-associated proteins and the WRC.

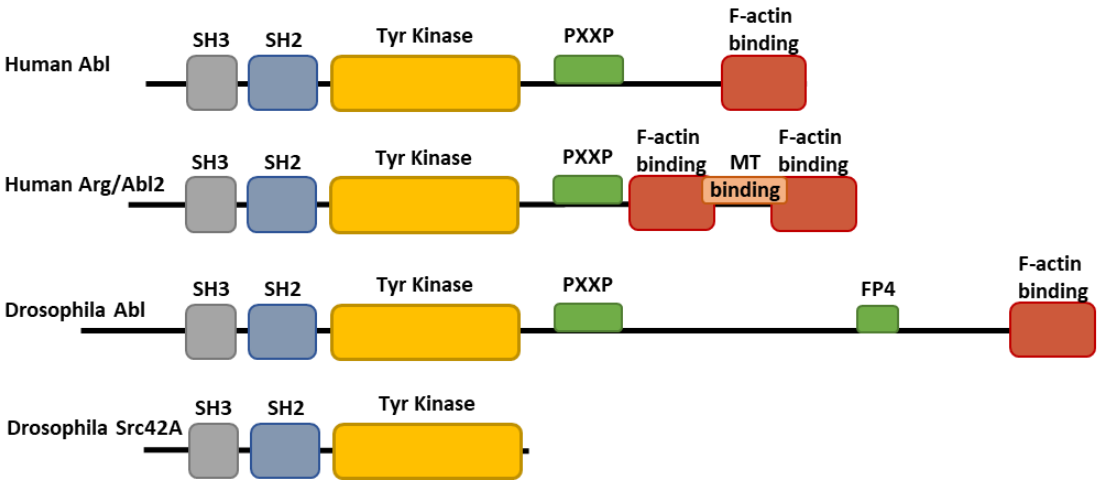

Figure 7: Comparison of protein domain structure of Abl orthologs and *Drosophila* Src42A. At the C-terminus Abl orthologs possess a SH3 domain interacting with Proline rich regions, followed by the SH2 domain binding to phosphorylated tyrosine residues. The tyrosine kinase domain is central in Abl orthologs but terminate Src kinases. In Abl kinases a C-terminal F-actin binding site is connected by a linker carrying a PXXP motive. Human Arg/Abl2 also possess a microtubule binding motive. *Drosophila* Abl further carries a FP4 motive involved in ENA recruitment and inhibition.

Abl, as well as Src, are present in an inactive state, in which the SH2 and SH3 domains fold back to mask the kinase domain. In case of Abl, a hydrophobic pocket in the kinase domain interacts with a myristoyl group (Nagar et al., 2003). The binding of an interaction partner leads to a release of lash and a switch to the unfolded confirmation. Additional phosphorylation events on tyrosine Abl Y245 (Arg Y272), close to the SH2 domain and Abl Y412 (Arg Y439) in the kinase activation loop, lead to a proper orientation of the catalytic site and additionally prevent a re-closure of the active confirmation to gain full kinase activity. This step can either occur by autophosphorylation in trans by a neighboring Abl or Arg molecule, or by another Src kinase family member (Brasher and Van Etten, 2000; Schindler et al., 2000). After stimulation with growth factors (EGF and PDGF) Abl is phosphorylated and activated. However, this is an indirect mechanism described to depend on Src-family kinases (Plattner et al., 1999). Activation further is transmitted via integrin adhesion or various adaptor molecules binding to the SH3/2 domain or the N-terminal PXXP motive. This links adaptors like Crk, Nck and the WRC member Abi to Abl (Bradley and Koleske, 2009; Reichman et al., 2005; Waksman et al., 2004).

1.2.5 Abelson associated modification of actin regulation

Abl's domain structure suggests that it bridges various proteins, alters their activity and influences cytoskeletal regulation. Initial studies already indicated that Abl supports actin

dynamics. PDGF induced activation of Abl in fibroblast leads to membrane ruffling (Plattner et al., 1999). Abl is a well-known antagonist of actin regulator Ena (Gertler et al., 1990). Via Abl phosphorylation, Ena activity is suppressed by an altered binding affinity to interaction targets. In the absence of Abl, Ena is accumulated and ectopically located, leading to an increase of bundled actin structures (Gates et al., 2007).

Moreover, the interaction of the WRC subunit Abi (Abelson interacting protein) with Abl, is dissected early and clearly connects Abl to branched actin regulation (Juang and Hoffmann, 1999). Abl phosphorylates Abi at four distinct positions and has been shown to promote protein stability and the incorporation into the WRC. Additionally, Abl mediated phosphorylation of Abi supports a re-localization of Abi and Abl to the cell cortex. The mutation of four predicted Abl target tyrosine residues decreases the membrane localization and reduces the half–life of the protein (Huang et al., 2007). These findings suggest that Abl is crucial for the recruitment of the WRC to the membrane and further acts on WRC activation via Abi phosphorylation. However, the expression of Abl in cancer cells leads to ubiquitin dependent degradation of Abi (Dai et al., 2001).

Further, Abi fulfils different functions by modulating Abl activity and is claimed to facilitate the interaction with WAVE. It has been shown that the WAVE2 proline rich region (PXXP) is necessary for Abl binding, most likely via its SH3 domain. However, this binding is weakened in the absence of the WAVE WHD domain, known to be crucial for WAVE Abi binding (Leng et al., 2005; Stuart et al., 2006). Other data shows that WAVE3 is also able to physically interact with Abl without the facilitative function of Abi (Sossey-Alaoui et al., 2007). This indicates that, at least in cell culture experiments, there might be at least two different interaction modes of Abl with WAVE. As described previously, Abl also directly phosphorylates WAVE2 at the conserved tyrosine residue 150 (Table 2). *In vitro* and in cell culture the phospho-mimicking mutant of WAVE exhibits an increased activity in actin polymerization (Chen et al., 2010; Leng et al., 2005; Sossey-Alaoui et al., 2007). However, its impact on actin dynamics *in vivo* has not yet been elucidated.

Abl can also act indirectly on WAVE activation by stimulating the Rho guanine nucleotide exchange factor (GEF) Trio that activates WAVE-Arp2/3 dependent actin branching via Rac1. The absence of Abl activates Ena and the equilibrium shifts towards filamentous actin. Here, Abl is claimed as a regulator that manipulates the proportion of branched and linear actin filaments (Kannan et al., 2017). Further, new data underlines the regulatory importance of the first C-terminal quarter carrying the PXXP element for Ena regulation during axon guidance. Still, they indicate that the same motive may be relevant for Abl interacting with Abi and Trio causing WRC activity as well (Sian et al., 2020).

Taken together, Abl kinase is a very versatile protein. On one hand, it acts as a scaffold protein for various interaction partners and on the other hand it directly phosphorylates target proteins via its kinase domain to modulate their activity. This makes the Abl kinase a key regulator of many cellular processes.

1.3 Aim of the project

Drosophila macrophage-like immune cells are highly motile cells patrolling in the hemolymph. When migrating on epithelia surface, they extend large protruding lamellipodia. They switch from random to directed migration in reaction to external immune cues. To achieve this, cells rely on the recognition of extracellular signals and their further translation into a cell specific response. Therefore, they provide an excellent genetically tractable model to investigate actin dynamics in single cell migration.

The WAVE regulatory complex (WRC) is crucial for cell morphology and cell migration by activating the evolutionary conserved Arp2/3 complex, which induces branched actin nucleation during lamellipodia formation. The underlying mechanisms need to be tightly regulated to induce the fast and exact reorganization of the actin cytoskeleton. Several upstream factors control the side specific activation of WAVE.

There is still little knowledge about the direct recruitment of WAVE to the leading edge in response to external signals. Previous studies identified a conserved WRC interacting receptor sequence (WIRS) that is part of several membrane and membrane associated proteins. It provides a direct interaction platform between those WIRS-ligand and actin machinery via the binding of WRC. This thesis addresses the impact of this interaction in immune cell migration. Further, the aim of this study is to identify and characterize novel interactors and regulatory processes of WAVE at the leading edge. An intriguing mechanism in the activation of the WRC is phosphorylation of the subunits. *Drosophila* WAVE possess 15 tyrosine residues, of which two – Y127 and Y153 – within the WHD have been previously linked to effect F-actin formation. Y127 is assumed as Src kinase target, whereas Y153 is phosphorylated by Abl kinase. The non-receptor tyrosine kinase Abl has been known to be an interaction partner of WAVE for a long time and assumed to act as a key regulator influencing WAVE activity. However, the effect on cell dynamics has only been insufficiently investigated so far. *Drosophila* macrophages as an *in vivo* model combined with high resolution live imaging allows us to analyze Abl function and the impact of side specific WAVE phosphorylation on cell migration.

2 Material and Methods

2.1 Solutions and buffers

All required chemicals for solutions, buffers and media are obtained in a pro-analysis grade of quality level from the following companies unless otherwise indicated. The buffers and solutions are according to standard published protocols or mentioned specifically in the respective, following chapters.

GIBCO (Eggenstein)	Roche (Mannheim)
Baker (Groß-Gerau)	Roth (Karlsruhe)
Biomol (Hamburg)	Merck (Darmstadt)
Biozym (Hamburg)	New Englang Biolabs (Frankfurt)
Sigma-Aldrich (Taufkirchen)	Clontech (Heidelberg)
Qiagen (Hilden)	ChromoTek GmbH (Planegg)
Kobe (Marburg)	Thermo Fisher Scientific (Dreieich)

2.2 Molecular biology

2.2.1 Transformation of chemically competent cells

Chemically competent cells (Top10, Mach1 T1®) are thawed on ice and 1-5 µL of the plasmid DNA is gently mixed in. After an incubation time of 30 minutes on ice, a heat shock at 42 °C for 30 seconds is performed in a water bath. Cells are kept for two additional minutes on ice, before adding 250 µL pre-warmed S.O.C. medium. The mix is incubated at 37 °C for 1 hour (180-220 rpm) in a shaking incubator. 20-200 µL from each sample are spread on LB-agar, supplemented with the appropriate antibiotics.

2.2.2 PCR and site directed mutagenesis

For polymerase chain reaction (PCR) Q5 DNA Polymerase (NEB) with a proofreading function is used. PCR reaction is performed according to manufacturer´s instructions.

Single mutations are generated via quick change mutagenesis. Site directed mutagenesis is achieved by long primer pairs harboring the designated mutation site. The following PCR mix is set up:

- DNA (10ng/µl)
- Primer sense (10µM)
- Primer antisense (10µM)
- dNTP-Mix (10mM)
- (Quick solution just by vector > 5kb)
- Buffer 5x
- Q5
- ddH_2O to final volume of 25µl

1. 95°C → 1`
2. 95°C → 50``
3. 62°C → 50``
4. 72°C → 30`` per 1000 bp

} 18x

5. 72°C → 7`

Incubate the reaction after the PCR on ice for 2 min. Then add DpnI to the mix, incubate for 1 hour at 37 °C and run a test gel afterwards. Transform 5 µL of reaction into chemical competent E. coli cells and spread on LB-agar plates supplemented with the appropriate antibiotics. Primer for Quick-change mutagenesis are attached in supplementary material.

tyrosine → glutamic acid/ glutamate	TAT/ TAC → GAA	phospho-mimic
tyrosine → phenylalanine	TAT/ TAC → TTC	phospho-mutant

2.2.3 Plasmid DNA preparation

For amplification and preparation of plasmid DNA, chemical competent E. coli (Top10, Mach1 T1®) are transformed. For mini (2-5 mL) or midi (50-100 mL) plasmid purification, bacteria are incubated over night with an appropriate antibiotic at 37 °C and 180 rpm.

Mini preparation using E.Z.N.A® Plasmid DNA Mini Kit I (Omega BIO-TEK) and Midi preparation using Plasmid *Plus* Midi Kit (QIAGEN) is performed according to manufacturer´s instructions.

2.2.4 Gateway cloning

Gateway cloning is a restriction independent cloning technique. An insert is generated via the PCR technic, whereby the product must carry a CACC-Sequence at the 3´ end. For cloning, the pENTR/D-TOPO cloning kit produced by Invitrogen/Thermo Fisher is used according to the manufacturer´s instructions. The correct pENTR vector is identified by colony PCR or restriction after a mini plasmid purification.
The final cloning into the destination UASp/t-attB-site vector is performed via recombination exchange of the attL and the attR site entry and the destination vector (Clonase® II Enzyme mix, Thermo Fisher scientific). The LR reaction is transformed into E. coli cells using the appropriate transformation protocol.

2.2.5 Plasmid DNA restriction

DNA restriction is performed prior to ligation or for test digestion after Mini and Midi preparation. Digestion is performed according to fitting conditions for appropriate enzymes (NEB).

2.2.6 DNA Sequencing

For sequencing 700 to 1200 ng DNA, with the optional addition of specific primers, is sent in a total volume of 15 µL to Microsynth SeqLab. Sequencing is performed using single tube option.

2.2.7 Vectors and plasmids

Plasmid	Comment	Source/References
pENTR-D/TOPO®	Cloning vector, gateway cloning technology	Invitrogen/ Thermo Fisher Scientific
pENTR/TOPO-TA®	Cloning vector, gateway cloning technology	Invitrogen/ Thermo Fisher Scientific
pUASt-attB-rfa	ΦC31 mediated germline transformation vector for untagged proteins; gateway in vitro cloning;	Stephan, 2008 (PhD)

	contains HSP70 promotor for expression from embryonic stage 17 onwards	
pUASp-attB-rfa	ΦC31 mediated germline transformation vector for untagged proteins; gateway *in vitro* cloning; contains a P-transposase promotor allowing germline expression	Stephan, 2008 (PhD)
pUASp-attB-rfa-eGFP	ΦC31 mediated germline transformation vector for C-terminal eGPF tagged proteins; gateway *in vitro* cloning; contains a P-transposase promotor allowing germline expression	Stephan, 2008 (PhD)
pUASp-attB-rfa-myc	ΦC31 mediated germline transformation vector for C-terminal myc tagged proteins ; gateway *in vitro* cloning; contains a P-transposase promotor allowing germline expression	Stephan, 2008 (PhD)
pUASp-attB-myc-rfa	ΦC31 mediated germline transformation vector for N-terminal myc tagged proteins ; gateway *in vitro* cloning; contains a P-transposase promotor allowing germline expression	Stephan, 2008 (PhD)
pENTR-WAVE	gateway expression vector, insert WAVE	Christina Gohl (PhD)
pENTR-WAVE	gateway expression vector, insert WAVE with STOP	this work (based on Christina Gohl (PhD))
pENTR-WAVE Y127,153F	gateway expression vector, insert WAVE with single mutation: Y→F 127, 153 with and without STOP	this work
pENTR-WAVE Y127F	gateway expression vector, insert WAVE with single mutation: Y→F 127 with and without STOP	this work
pENTR-WAVE Y127E	gateway expression vector, insert WAVE with single mutation: Y→E 127	this work

	with and without STOP	
pENTR-WAVE Y153F	gateway expression vector, insert WAVE with single mutation: Y→F 153 with and without STOP	this work
pENTR-WAVE Y153E	gateway expression vector, insert WAVE with single mutation: Y→E 153 with and without STOP	this work
pUASp-attB-WAVE	gateway expression vector; insert WAVE full-length	Marianne von Cann, master thesis
pUASp-attB-WAVE Y15E	gateway expression vector, insert WAVE with single mutation: Y→E 18, 127, 142, 153, 158, 234, 247, 253, 269, 279, 290, 312, 317, 323, 337	Rita Kottmeier, bachelor thesis
pUASp-attB-WAVE Y15F	gateway expression vector, insert WAVE with single mutation: Y→F 18, 127, 142, 153, 158, 234, 247, 253, 269, 279, 290, 312, 317, 323, 337	Rita Kottmeier, bachelor thesis
pUASp-attB-WAVE Y127,153F	gateway expression vector, insert WAVE with single mutation: Y127,153F	this work
pUASp-attB-WAVE Y127,153E	gateway expression vector, insert WAVE with single mutation: Y127,153E	this work
pUASp-attB-WAVE Y127F	gateway expression vector, insert WAVE with single mutation: Y127F	this work
pUASp-attB-WAVE Y127E	gateway expression vector, insert WAVE with single mutation: Y127F	this work
pUASp-attB-WAVE Y153F	gateway expression vector, insert WAVE with single mutation: Y153F	this work
pUASp-attB-WAVE Y153E	gateway expression vector, insert WAVE with single mutation: Y127,153E	this work
pUASp-attB-myc-WAVE	gateway expression vector with C-terminal myc-Tag	this work
pUASp-attB-myc-WAVE 15E	gateway expression vector with C-terminal myc-Tag, insert WAVE with single mutation: Y→E	Rita Kottmeier, bachelor thesis

	18, 127, 142, 153, 158, 234, 247, 253, 269, 279, 290, 312, 317, 323, 337	
pUASp-attB-myc-WAVE 15F	gateway expression vector with C-terminal myc-Tag, insert WAVE with single mutation: Y→F 18, 127, 142, 153, 158, 234, 247, 253, 269, 279, 290, 312, 317, 323, 337	Rita Kottmeier, bachelor thesis
pUASp-attB-myc-WAVE Y127,153F	gateway expression vector with C-terminal myc-Tag, insert WAVE with single mutation: Y127, 153F	this work
pUASp-attB-myc-WAVE Y127F	gateway expression vector with C-terminal myc-Tag, insert WAVE with single mutation: Y127F	this work
pUASp-attB-myc-WAVE Y153F	gateway expression vector with C-terminal myc-Tag, insert WAVE with single mutation: Y153F	this work
pEB2-mScarlet	mScarlet red fluorescent protein inserted in pEB2 vector	(Balleza et al., 2018), addgene #104006
pm-mScarlet-H_C1	mScarlet-H stable red fluorescent protein inserted in pm vector	(Bindels et al., 2017), addgene #85043
pEB2-mScarlet-I	mScarlet-H high insensitivity red fluorescent protein inserted in pEB2 vector	(Balleza et al., 2018) addgene #104007
pENTR-TOPO-TA-mScarlet	gateway entry vector with mScarlet	this work
pENTR-TOPO-TA-mScarlet-I	gateway entry vector with mScarlet-I	this work
pENTR-TOPO-TA-mScarlet-H	gateway entry vector with mScarlet-H	this work
pUASt-attB-rfA-mScarlet	ΦC31 mediated germline transformation vector for C-terminal mScarlet tagged proteins; gateway in vitro cloning; contains HSP70 promotor for expression from embryonic stage 17 onwards	this work
pUASt-attB-rfA-mScarlet-I	ΦC31 mediated germline transformation vector for C-terminal mScarlet-I tagged proteins; gateway in vitro cloning; contains HSP70	this work

	promotor for expression from embryonic stage 17 onwards	
pUASt-attB-rfA-mScarlet-I	ΦC31 mediated germline transformation vector for C-terminal mScarlet-H tagged proteins; gateway in vitro cloning; contains HSP70 promotor for expression from embryonic stage 17 onwards	this work
pENTR-alphaTub84B	gateway entry vector, insert alpha tubulin84B without stop	this work
pUASt-attB-alphaTub84B-mScarlet	gateway expression vector with C-terminal mScarlet-Tag, insert tubulin	this work
pUASt-attB-alphaTub84B-mScarlet-I	gateway expression vector with C-terminal mScarlet-I-Tag, insert tubulin	this work
pUASt-attB-alphaTub84B-mScarlet-H	gateway expression vector with C-terminal mScarlet-H-Tag, insert tubulin	this work
pUASt-attB-alphaTub84B-mCherry	gateway expression vector with C-terminal mCherry-Tag, insert tubulin	this work
pENTR-src42A^{CA}_stop	gateway entry vector, insert constitutive active form of Src42A without Amino acid replacement: Y511F.	this work
pUASp-attB-src42A^{CA}	gateway expression vector, insert constitutive active form of Src42A without Amino acid replacement: Y511F	this work
pDEST-HemmarG-eGFP	modified pDEST-Hemmar-G- vector for cloning any enhancer to drive expression of eGFP	(Han et al., 2011) addgene # 31221, modified by Rita Kottmeier, master thesis
pDEST-HemmarG-Stinger-eGFP	modified pDEST-Hemmar-G-vector for cloning any enhancer to drive expression of nuclear eGFP	(Han et al., 2011) addgene # 31221, modified by Rita Kottmeier, master thesis
pENTR-*hmlΔ*	gateway entry vector, with truncated *hml* promotor region (Z. Chen et al., 2010; Steffen et al., 2004)	this work

pDEST-HemmarG *hml*Δ-StingerEGFP	gateway expression vector with promotor fused *hml* promotor region to nuclear eGFP	this work
pDEST-HemmarG *hml*Δ-eGFP	gateway expression vector with promotor fused *hml* promotor region to eGFP	this work
pENTR-WIRS-GGSx4-eGFP	gateway expression vector, with four inserted WIRS-peptide motifs flanked by 10 amino acids which are linked with an GGS-linker.	Malte Kreft, bachelor thesis
pUASp-attB-WIRS-GGSx4-eGFP	with four inserted WIRS-peptide motifs flanked by 10 amino acids which are linked with an GGS-linker.	Malte Kreft, bachelor thesis

Maps of generated plasmids in this work are provided digitally.

2.3 Fly genetics

2.3.1 Maintenance and crossing

All flies are kept on *Drosophila* standard food in plastic tubes at either 18 °C, 25 °C or room temperature. For interbreeding, female virgins are collected and crossed in a 3:1 ratio with male flies at 25 °C (29 °C for RNAi expression).

***Drosophila* standard food for 54 L**

1. boil up 430 g agar and 3950 g corn flour in 41 L water
2. mix 930 g dry yeast and 540 g soy flour in 4 L water and add to the first mixture
3. add 2500 g malt extract
4. mix 1900 g treacle in 4 L water and add to the mix
5. boil up for 10 min stirring constantly
6. add 5 kg ice and chill to 60°C stirring constantly
7. add 275 mL propionic acid and 830 mL methyl-4-hydroxybenzoate 10% (w/v) in 70% (v/v) ethanol

2.3.2 List of flies

Table 3: Wild type and balancer stocks

FLYSTOCK	COMMENT	CHROMOSOME	SOURCE/REFERENCES
w1118	w-, wild type	X	(Lindsley and Zimm, 1992)
w;; TM3, e, Sb/TM6B, e Hu Tb	balancer for chromosome 3	3	Christian Klämbt, unpublished
w; CyO-$^{Wee\text{-}P\text{-}GFP}$/Sp; TM2, e Ubx/TM6B, e Hu Tb	balancer for chromosome 2 and 3	2,3	Thomas Hummel, unpublished
y, w, hs-flp ; Sp / CyO ; MKRS / TM6 ;	heat shock FLP on the X chromosome, balancer for chromosome 2 and 3	x, 2, 3	Bloomington stock center

Table 4: Mutations, transposon, insertions

FLYSTOCK	COMMENT	CHROMOSOME ARM	SOURCE/REFERENCES
***abi*^{A20}**	Transposon excision using P{Epgy2}*abiEY20423*; genomic locus deletion	3R: 88A9	(Stephan et al., 2011)
***abl*^{1}**	EMS induced allele of the *abl l*ocus	3L: 73B1 – B4	(Gertler et al., 1989) BL 8566
***abl*^{2}**	EMS induced allele of the *abl l*ocus	3L: 73B1 – B4	(Gertler et al., 1989) BL 8565
***abl*^{4}**	EMS induced allele of the *abl l*ocus	3L: 73B1 – B4	(Gertler et al., 1989) BL 3553
FRT40A, *scar*$^{\Delta 37}$	Transposon excision using *scark13811*, genomic deletion in	2L: 32C1	(Zallen et al., 2002)

	the *scar* and *piwi* locus		
***Src42A*$^{26-1}$**	P-element excision of *Src42A*^{k10108} (enhancer trap line), Loss of function allele	2R: 42A6-42A7	(Takahashi, 2005)
neoFRT80B, *arp3*^{83F}	Point mutation, lethal	3L: 66B6-66B6	BL 39727, used in this thesis

Table 5:Gal4 activator lines and promotor fusion constructs

FLYSTOCK	COMMENT	CHROMOSOME	SOURCE/REFERENCES
***act5C*Gal4**	*actin5C* promotor fusion; drives ubiquitous expression	2	Bloomington stock center
***da*-Gal4**	*daughterless* promotor/intron fusion; drives ubiquitous expression	3	(Wodarz et al., 1995)
GR1-Gal4	Enhancer trap, drives expression in all somatic cells during oogenesis	3	BL 36287
en-Gal4	*engrailed* promoter fusion, construct under control of engrailed regulatory sequences	2	Bloomington stock center
hmlΔ-Gal4	truncated *hemolectin* promotor fusion, expresses GAL4 in lymph glands and	2 3	BL 30139 BL30141 (Sinenko and Mathey-Prevot, 2004)

	circulating hemocytes		
slbo-Gal4	Gal4 expression in border cells a partial follicle cells	2	Montel Lab
c306-Gal4	GAL4 expression pattern in oocyte: stalk cells, border cells	x	BL 3743
***tub*-Gal4**	Drives ubiquitous expression	3	Bloomington stock center
***hmlΔ*-DsRed**	Promotor fusion construct to mark hemocytes, cytoplasmic expression	2	(Makhijani et al., 2011) Bückner lab.
***hmlΔ*-stinger-eGFP**	Promotor fusion construct to mark hemocytes, nuclear expression	2	this work

Table 6: UAS- effector lines inclusive RNAi

FLYSTOCK	COMMENT	CHROMOSOME	SOURCE/REFERENCES
pUASp-Abi^{WT}	express a full-length Abi	3	Julia Squarr, (B. Chen et al., 2014)
pUASp-Abi$^{\Delta WIRS}$	express a full-length Abi protein, point mutations at position 118 (R→A) & 122 (G→W)	3	Klaus Brinkmann, (B. Chen et al., 2014)
UAS-Abl^{FL}	express a full-length Abl	2	BL28993

UAS-Abl.K417N/ UAS-Abl^{DN}	expression on kinase dead Abl protein	2	BL 8566
UAS-p185Bcr-Abl	expression of C-terminal truncated Abl protein, truncation leads to an active form of Abl	2	(Fogerty et al., 1999)
UAS-mCD8-GFP	express mouse CD8a fused at the C-terminus to the coding region of GFP	2	Klämbt lab
UAS-LifeAct-eGFP	LifeAct c-terminal tagged to eGFP, visualize actin filaments	2	Bloomington stock center
UAS-eGFP	eGFP expression under UAS control	2 3	BL 6874 BL 6658
UAS- Src42A^{CA}	expression of a constitutively active form of the Src42A Protein, Amino acid replacement: Y511F	3	(Tateno et al., 2000)
UAS-Src42A^{DN}	express the kinase dead form of the Src42A Protein, Amino acid replacement: K295M	3	(Shindo et al., 2008)
UAS- abl RNAi	to express double-stranded RNAi against the *abl* gene product	2	BL 61170

UAS-*src42A* RNAi	to express double-stranded RNAi against the *src42A* gene product	2	VDRC 100708
UAS-*src42A* RNAi	to express double-stranded RNAi against the *src42A* gene product	3	BL 55868
UAS-scar RNAi	to express double-stranded RNAi against the *scar* gene product	2	NIG 4636R-2
pUASt-WAVE	expression of WAVE full-length protein, in landing site M{3xP3-RFP.attP'}ZH-68E	3	Bogdan stock collecktion
pUASt-WAVE-15E	expression of phosphor-mimic WAVE protein, all 15 Y→E, in landing site M{3xP3-RFP.attP'}ZH-68E	3	Rita Kottmeier, bachelor thesis
pUASt-WAVE 15F	expression of phosphor-mutant WAVE protein, all 15 Y→F, in landing site M{3xP3-RFP.attP'}ZH-68E	3	Rita Kottmeier, bachelor thesis
pUASp-WAVE	expression of WAVE full-length protein, in landing site M{3xP3-RFP.attP'}ZH-68E	3	Marianne von Cann, master thesis

pUASp-WAVE Y127F+Y153F	expression of WAVE full-length protein, in landing site M{3xP3-RFP.attP'}ZH-68E with single mutation: Y127F+Y153F	3	this work
pUASp-WAVE Y127E+Y153E	expression of WAVE full-length protein, in landing site M{3xP3-RFP.attP'}ZH-68E with single mutation: Y127E+Y153E	3	this work
pUASp-WAVE Y127F	expression of WAVE full-length protein, in landing site M{3xP3-RFP.attP'}ZH-68E with single mutation: Y127F	3	this work
pUASp-WAVE Y127E	expression of WAVE full-length protein, in landing site M{3xP3-RFP.attP'}ZH-68E with single mutation: Y127E	3	this work
pUASp-WAVE Y153F	expression of WAVE full-length protein, in landing site M{3xP3-RFP.attP'}ZH-68E with single mutation: Y153F	3	this work
pUASp-WAVE Y153E	expression of WAVE full-length protein, in landing site M{3xP3-RFP.attP'}ZH-68E	3	this work

	with single mutation: Y153E		

Table 7: Stocks for gene dosage experiments

FLYSTOCK	COMMENT	CHROMOSOME	SOURCE/REFERENCES
***hmlΔ*-Gal4, UAS-eGFP ; *abl*^{4}/TM6,Tb**	eGFP marked hemocytes in *abl* mutant background, crossing with *abl*^{2}	2, 3	this work
***hmlΔ*-Gal4, UAS-lifeAct-eGFP ; *abl*^{4}/TM6,Tb**	eGFP filamentous marked hemocytes in *abl* mutant background, crossing with *abl*^{2}	2, 3	this work
FRT40A *scar*$^{\Delta 37}$/ CyO$^{\text{Wee-P-GFP}}$; *abl*^{2}/TM6,Tb	gene dosage experiment to reduce WAVE protein amount in *abl* mutant background	2, 3	this work
***Src42A*$^{26\text{-}1}$/ CyO$^{\text{Wee-P-GFP}}$; *abl*^{2}/TM6,Tb**	gene dosage experiment to reduce Src42A protein amount in *abl* mutant background	2, 3	this work

Table 8: Stocks for genetic mosaics

FLYSTOCK	COMMENT	CHROMOSOME	SOURCE/REFERENCES
hsFLP; FRT40A,Gal80/ CyO; **tub-Gal4, UAS-CD8-GFP/TM6b**	to induce cell mutant clones; used for MARCM analysis	x, 2, 3	Stephan, 2008 (PhD)

hsFLP; FRT40A,Gal80/ CyO; *hmlΔ*-Gal4, UAS-eGFP/(TM6b)	to induce hemocyte specific cell mutant clones; used for MARCM analysis	x, 2, 3	this work
hsFLP;;FRT80B ubi-GFP/TM6b	to induce ubiquitously mutant cell clones; negative marking	x, 3	Christina Gohl, 2010 (PhD)

Table 9: Constructs for rescue experiments

FLYSTOCK	COMMENT	CHROMOSOME	SOURCE/REFERENCES
***hmlΔ*-dsRed, FRT40A *scar*$^{\Delta 37}$/ CyO$^{Wee\text{-}P\text{-}GFP}$; *da*-Gal4 / TM6B ;**	for ubiquitous expression of recue constructs in *wave (scar)* mutant background, cytoplasmic expression of dsRed in hemocytes	2, 3	this work
FRT40A *scar*$^{\Delta 37}$/ CyO$^{Wee\text{-}P\text{-}GFP}$; pUASt-WAVE/ (TM6B, ubiGFP)	expression of WAVE full-length construct in *wave* mutant background	2, 3	this work
FRT40A *scar*$^{\Delta 37}$/ CyO$^{Wee\text{-}P\text{-}GFP}$; pUASt-WAVE15E/ (TM6B, ubiGFP)	expression of WAVE phosphor-mimic construct in *wave* mutant background	2, 3	this work
FRT40A *scar*$^{\Delta 37}$/ CyO$^{Wee\text{-}P\text{-}GFP}$; pUASp-WAVE15F/ (TM6B, ubiGFP)	expression of WAVE phosphor-mutant construct in *wave*	2, 3	this work

	mutant background		
FRT40A *scar*$^{\Delta 37}$/ CyO$^{Wee\text{-}P\text{-}GFP}$; pUASp-WAVE/ (TM6B, DfdGFP)	expression of WAVE full-length construct in *wave* mutant background	2, 3	this work
FRT40A *scar*$^{\Delta 37}$/ CyO$^{Wee\text{-}P\text{-}GFP}$; pUASp-WAVEY127,153E/ (TM6B, ubiGFP)	expression of WAVE phosphor-mimic (Y127,153E) construct in *wave* mutant background	2, 3	this work
FRT40A *scar*$^{\Delta 37}$/ CyO$^{Wee\text{-}P\text{-}GFP}$; pUASp-WAVEY127,153F/ (TM6B, ubiGFP)	expression of WAVE phosphor-mutant (Y127,153F) construct in *wave* mutant background	2, 3	this work
FRT40A *scar*$^{\Delta 37}$/ CyO$^{Wee\text{-}P\text{-}GFP}$; pUASp-WAVEY127E/ (TM6B, ubiGFP)	expression of WAVE phosphor-mimic (Y127E) construct in *wave* mutant background	2, 3	this work
FRT40A *scar*$^{\Delta 37}$/ CyO$^{Wee\text{-}P\text{-}GFP}$; pUASp-WAVEY127F/ (TM6B, ubiGFP)	expression of WAVE phosphor-mutant (Y127F) construct in *wave* mutant background	2, 3	this work
FRT40A *scar*$^{\Delta 37}$/ CyO$^{Wee\text{-}P\text{-}GFP}$; pUASp-WAVEY153E/ (TM6B, ubiGFP)	expression of WAVE phosphor-mimic (Y153E) construct in *wave* mutant background	2, 3	this work

FRT40A *scar*$^{\Delta 37}$/ CyO$^{Wee\text{-}P\text{-}GFP}$; pUASp-WAVEY153F/ (TM6B, ubiGFP)	expression of WAVE phosphor-mutant (Y153F) construct in *wave* mutant background	2, 3	this work
***hmlΔ*-dsRed/ CyO$^{Wee\text{-}P\text{-}GFP}$; *abi*$^{\Delta 20}$, *da*-Gal4/ TM6B**	for ubiquitous expression of recue constructs in *abi* mutant background, cytoplasmic expression of dsRed in hemocytes	2, 3	this work, based on (B. Chen et al., 2014) and (Makhijani et al., 2011)
***hmlΔ*-dsRed / CyO$^{Wee\text{-}P\text{-}GFP}$; Abi^{FL}/ TM6B**	expression of Abi full-length construct in *wave* mutant background	2, 3	this work, based on (B. Chen et al., 2014) and (Makhijani et al., 2011)
***hmlΔ*-dsRed / CyO$^{Wee\text{-}P\text{-}GFP}$; Abi$^{\Delta WIRS}$/ TM6B**	expression of Abi$^{\Delta WIRS}$ (R106A/G110W) construct in *wave* mutant background	2, 3	this work, based on (B. Chen et al., 2014) and (Makhijani et al., 2011)

2.3.3 Mosaic analysis using the FLP/FRT system

To generate genetic mosaics in macrophages, the flippase recombination target/flippase (FRT/FLP) system was applied. It is a site-directed recombination system original derived from *Saccharomyces cerevisiae* and involves the recombination between FRT sites (flipase recognition target sites) mediated by the flipase recombinase (FLP). To induce homozygous mutant cells, a fly line with a temperature sensitive FLP is used, which expresses the FLP recombinase under 37 °C conditions. The generated mutant cell clones can be identified either by the absence of the marker gene expression (e.g. negatively labelled by GFP expression) or, as in this case, by the presence of the marker gene expression (GFP) only in the mutant cells (Lee and Luo, 2001; Perrimon, 1992).

The induction of heat shock clones in macrophages has been described previously in Moreira et al. (2013). The heat shocks are set for one hour at 37 °C in a water bath. Afterwards flies

are kept on 18 °C for one hour and finally returned on 25 °C. This procedure is repeated the next two days as depicted in Figure 8 (Moreira et al., 2013).

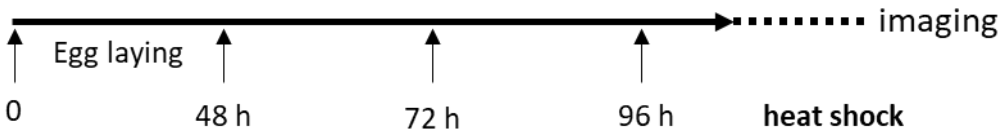

Figure 8: Timeline for heat shock after crossing.

2.3.4 Germline transformation and establishing of a transgenic fly line

2.3.4.1 Injection

Germline transformation is performed using the germline specific FC31 integration system (Z. Chen et al., 2010; Steffen et al., 2004). The chorion of 30 min old embryos (25 °C) is removed by a 2-minute incubation in a 50 % sodium hypochlorite solution. Afterwards, the embryos are washed with tap water. For injection they are lined up in the same orientation. For injection they are stamped on a parcel tape heptane glue covered cover slip. After drying for 5 minutes, they are overlaid with 10 S oil (Voltalef®).
The injection mix contains 3-5 µg DNA in add to a final volume of 15 µL with injection buffer.

Injection buffer (10x):

1 mM	phosphate buffer
50 mM	KCl
pH 7,4	

Injection is performed using a FemtoJet microinjector (Eppendorf). Injected embryos are placed in an apple agar dish with a water pond. They are kept at 18 °C for one day and are placed in the evening at 25 °C until they hatch the next day. Larvae are collected and transferred in a food vial close to a spot with fresh baker´s yeast.

2.3.4.2 Establishment of a transgenic fly strain and recombinant flies

Transgenic flies

After injection, hatching males are crossed with white minus balancer female virgins in a batch. In the F1 generation flies with integrated injected DNA express the *white* gen and can be selected *via* their orange/red eyes. *white* positive males are crossed in single crosses with balancer female virgins to remove the *integrase* gene on the first chromosome. If in any crossing step a female is the origin of the cross an additional crossing step need to be performed. Finally, the stable line is established by crossing identical genotypes with each other.

Recombinants

In the F1 generation, trans-heterozygous female virgins for our genes of interest are collected and are then crossed against balancer males. The F2 generation is screened for markers of the genes or tested *via* PCR for a positive recombination. A stable line of positive tested strain is established.

2.4 Biochemical approaches and immunohistochemistry

2.4.1 Antibodies

Table 10: Primary antibodies

ANTIBODY	CONJUGATION	DILUTION	REFERENCE/SOURCE
α Abelson	rabbit	1:500 (PA in IH)	Gininger Lab, NINDS USA
α myc	rabbit	1:500 (WB)	Santa Cruz
α Phospho-Tyrosine (pTyr)	mouse	1:1000 (WB)	Cellsignaling Technology® #9411

α Src42A	guinea pig	1:500 (WB)	Müller Lab, Kassel
α Tubulin	mouse	1:1000 (WB)	DSHB
α WAVE	guinea pig	1:1000 (IH, WB)	(Bogdan et al., 2005)
α WAVE	rabbit	1:500 (IH)	unpublished

Table 11: Secondary antibody

ANTIBODY	CONJUGATION	DILUTION	REFERENCE/SOURCE
α guinea pig	Alexa Fluor™ 488, -568, -647	1:1000 (IH)	Thermo Fisher Scientific, 488: A11073 568: A11075 647: A21450
α mouse	Alexa Fluor™ 488, -568, -647	1:1000 (IH)	Thermo Fisher Scientific, 488: A11029 568: A11031 647: A21236
α rabbit	Alexa Fluor™ 488, -568, -647	1:1000 (IH)	Thermo Fisher Scientific, 488: A11034 568: A11036 647: A21045
α guinea pig	800CW, 680RD/LT	1:10000 (WB)	LI-COR Biosciences
α mouse	800CW, 680RD	1:10000 (WB)	LI-COR Biosciences
α rabbit	800CW, 680RD	1:10000 (WB)	LI-COR Biosciences
Phalloidin	Alexa Fluor™ 488, -568, -647	1:100 (IH) (647 1:50)	Thermo Fisher Scientific, 488: A12379 568: A12380 647: A22297

2.4.2 Transfection of S2R+ cells

Drosophila S2R+-cells are cultured on 1 x Schneider's medium ($M3^{+/+}$, Gibco) in T-flasks (75 cm2, Corning) at 25 °C. The minimal medium $M3^{-/-}$ is supplemented with 10 % fetal bovine serum, penicillin (50 U/mL) and streptomycin (50 µg/mL) to generate the $M3^{+/+}$ medium. One day prior to transfection, cells are seeded in 24 well plate (3 x 105 cells/ mL; 1 mL/well).
The cells are co-transfected with 1 µg DNA of pUASt- or pUASp expression constructs and act5c-Gal4 0.6 µg DNA using FuGENE® HD Transfection Reagent (Promega). Prior to adding 100 µL transfection mix, 600 mL of the total of 1000 mL culture medium are removed.

Transfection mix (100 µl)

1 µg	pUASp/pUASt exp. construct
0.6 µg	Act5c-Gal4 DNA
4 µl	Fugene HD
ad 100 µl	$M3^{-/-}$

2.4.3 Protein extraction from *Drosophila* hemocytes

For protein extraction 30 wandering third instar larvae are washed in PBS and carefully rolled on tissue paper to remove the cell from the body wall. Larvae are prepared in $M3^{-/-}$ medium by opening the body wall lateral with forceps and shaking them slightly. The medium containing the isolated cells is transferred into a reaction tube and paced on ice until further processing. Cell are centrifuged for 10 min at 500 g at 4 °C. The medium is removed and cells are resolved in 10 µL 2x Laemmli buffer (Laemmli, 1970). The sample is boiled for 5 min and further analyzed on an SDS page.

2.4.4 Protein extraction from S2R+ cells

For protein extraction from transfected S2R+ cells, cells are resuspended in ice cold lysis buffer and transferred in a reaction tube. Cells are placed on ice for 15 min and vortexted three times in the meantime to lyse the cells. To analyze phosphorylated proteins, phosphatase inhibitors are added to the lysis buffer. Cells are spinned down for 15 min at maximum speed, 4 °C. The supernatant is boiled with Laemmli buffer for 5 min.

Lysis buffer (5 mL)

20mM	Tris pH 7.7	100 µL, 1M stock
150 mM	NaCl	750 µL, 1M stock
1 mM	EDTA	10 µL, 0.5 stock
1 mM	EGTA	10 µL, 0.5 stock
1 %	Triton-X	100 %
½ Tablet	Protease inhibitor	cOmplete Mini, EDTA-free, Roche
2.5 mM	Pyrophosphate	50 µL, 250 mM stock
1 mM	Glycerolphosphate	50 µL, 100 mM stock
1 mM	Vanadate	50 µL, 200 mM stock

2.4.5 Immunoprecipitation and Co-Immunoprecipitation

The ChromoTek Trap® system is used for immunoprecipitation of proteins. Therefore, eight transfected wells per sample are resolved in lysis buffer optional with phosphatase inhibitors. The further procedure is performed according to the manufacturer´s instructions. The samples can be stored at -20°C or directly be loaded on an SDS gel.

2.4.6 SDS polyacrylamide gel electrophoresis (SDS-PAGE)

To separate and analyze protein samples, a SDS polyacrylamide gel electrophoresis (PAGE) under denaturating conditions is performed. For phosphorylated samples the ratio of Acrylamide und Bis-acrylamide in the running buffer is altered (see below, after (Singh et al., 2020)).

3-4 x stacking gels 5 %

4.1	ddH_2O
1	30 % Polyacrylamide
0.75	0.5 Tris pH 6.8
0.06	10 % SDS
0.06	10 % APS
0.006	TEMED

2 x running gels 10 %

6.3	ddH_2O
5.33	30 % Polyacrylamide
4	1.5 Tris pH 8.8
0.16	10 % SDS
0.16	10 % APS
0.016	TEMED

2 x Phospho-running gels 10 %

5.82	ddH_2O
5.3	30 % Acrylamide
0.48	2 % Bisacrylamide
4	1.5 Tris pH 8.8
0.16	10 % SDS
0.16	10 % APS
0.016	TEMED

The gel is transferred into a vertical electrophoresis chamber (BioRad, Mini-PROTEAN Tetra Vertical Electrophoresis Cell) filled with SDS running buffer and samples are loaded onto the gel. In the initial phase a current voltage of 80 V is used. As soon the samples have reached the running gel, voltage is increased to 140-180 V. As protein standard Precision All Blue Protein Standards is used.

10 x SDS Running buffer

25 mM	Tris
192 mM	Glycine
0.1 % SDS (w/v)	SDS

Dilute 1:10 in ddH_2O to obtain 1x solution.

10 x SDS Transfer buffer

25 mM	Tris
192 mM	Glycine

Dilute 1:10 in ddH_2O and add 10 % MeOH to obtain 1x solution.

2.4.7 Western Blot analysis

The Western Blot technique is used to visualize separated proteins. Therefore, the PVDF membrane (Immobilon®-FL Transfer Membrane, pore size: 0.45 µm, Merck Milipore) is activated 30 sec in Methanol and incubated 10 min in a transfer buffer as well as two thin and two thick layers of Whatman® blotting papers. The gel is placed onto the membrane in a sandwich of thin a thick Whatman papers. The transfer is performed using Trans-Blot Turbo Transfer System (BioRad) using preset standard program (1.3 A for a single mini format gel, 2.5 A for a single midi or two mini format gels).

Afterwards, the membrane is blocked for 30 min using Intercept® (TBS) Blocking Buffer (LI-COR Biosciences) 1:1 with TBS. The primary antibody is diluted in the blocking buffer with additional 0.2 % Tween20 and incubated at 4 °C rotation overnight. The membrane is washed three times for 15 min, rotating with TBS-Tween before incubating with the corresponding antibody for 1 hour at room temperature. Finally washing the membrane three times with TBS-Tween and once with TBS. For protein detection after staining, Odyssey® Sa imager system (LI-COR Biosciences) is used.

2.4.8 Fixation and immunostaining staining of Drosophila macrophages and S2R+ cells

Per coverslip, 10-15 wandering third instar larvae or 3-5 prepupae ~3 hours after pupae formation (APF) are washed in PBS and carefully rolled on tissue paper to remove cells from the body wall. The larvae are place in $M3^{-/-}$ medium and the body wall is opened lateral with forceps and then shaken slightly. The medium including the isolated cells is transferred into a reaction tube and paced on ice until further processing. In the meantime, coverslips are coded with Concanavalin A (ConA, Sigmar) for 30 min. After removing ConA, coverslips are washed once with PBS. Then, cells are incubated 1 h at 25 °C on the coated coverslips.

Afterwards, cells are fixed with PFA for 12 min and then permeabilized with 0.1 PBS-T and immediately removed and washed three times with PBS for 5 min. After blocking for 30 min with 3 % BSA in PBS, cells are stained for 2 h with a primary antibody diluted in 3 % BSA in PBS in a humid chamber. The coverslip is dipped two times in PBS for washing and then stained for 1 hour with the secondary antibody including optional added phalloidin. The coverslip is dipped two times in ddH_2O and finally mounted in Mowiol.

Mowiol

12 g	Mowiol
30 g	glycerol (analytical grade)
30 ml	ddH2O
60 ml	Tris-HCl buffer, pH 8.5

- magnetic stirrer at 56°C for 10 min
- centrifuge at 5000g for 15 min

2.4.9 Fixation and immunostaining staining of wing imaginal discs

Wandering third instar larvae are transferred into a dissection dish with PBS. For preparation the anterior part is separated and turned inside out. The surrounding tissue of the wing disks is removed, and the dissected tissue is selected in a 0.2 mL collection tube filled with PBS. The PBS is removed, and the tissue is covered in 4 % PFA for fixation for 45 min rotating in a 50 mL tube. Then, the PFA discarded and the tissue rinse ones with PBS-T 0.3 % before washing it twice in PBS-T 0.3 %, once PBS-T 0.5 % rotating and twice again in PBS-T 0.3 % rotating. For blocking, the sample is covered with 3 % BSA for one hour. The primary antibody is dissolved in 3 % BSA-T 0.3 % and incubated at 4 °C overnight for one hour. The next day it is washed out for 15 minutes three times with PBS-T 0.3 %. The secondary antibody and optional Phalloidin (1:100) are dissolved in 3 % BSA-T 0.3 % and incubated for one hour at room temperature rotating. The tissue is washed three times for 15 minutes with PBS. Finally, the complete liquid is removed, and the tissue is embedded in Fluoromount at 4 °C (at least 2 hours).

The dissection of the imaginal disks takes place on an imaging-slide in Fluoromount and can be stored at 4°C.

2.4.10 Fixation and immunostaining staining of female egg chamber

Young adult females and a few males are collected and transferred into a fly-vial with additional fresh baker´s yeast. To analyze border cell migration, flies are kept for 36-48 h at 25 °C (29°C for RNAi experiments). Time is dependent on temperature and on the desired egg chamber stages.

Female flies are anaesthetized using CO_2 and dissection takes place in a dissection dish filled with cold M3+/+. For preparation the fly is fixated with forceps and the abdomen is ripped up. Carefully the ovaries are pushed out in the medium. Single egg chambers are isolated out of the muscle tube by carful pulling at the anterior part of the ovary. They are transferred with

per saturated and cut of piped tip into a 0.2 mL tube. The tissue is fixed for 20 minutes in 4 % PFA at RT. Afterward, it is rinsed once with PBS and is then washed and permeabilized once with PBS-T 0.5 % and three times with PBS-T 0.1 %, each for 20 minutes rotating upside down. The primary antibody is dissolved in 3 %, BSA is incubated at 4 °C overnight for one hour while rotating. Then, the tissue is washed for 20 minutes while rotating three times with PBS-T 0.1 %. Then, the secondary antibody and optional Phalloidin (1:100) in 3 % BSA is incubated for 1 h at room temperature while rotating. Finally, the tissue is washed for 15 minutes while rotating upside down with PBS.
After removing the entire liquid, the tissue is embedded in Fluoromount at 4 °C for at least two hours. Then, the egg chambers are mounted on an imaging-slide in Fluoromount and stored at 4°C.

2.5 Quantification and statistical analysis

2.5.1 Imaging acquisition and processing

Images of total flies or detailed body structures are acquired with Fluorescent Stereo Microscope Leica M165 FC equipped with a Leica DFC7000 T camera. Standard confocal fluorescent images are recorded using a Leica TCS SP8 Confocal Laser Scanning Microscope with Light sheet unit. Structure illumination microscopy images are taken with an ELYRA S.1 Microscope (CellObserver SD, 63x/1.4 oil-immersion objective; Carl Zeiss AG). Live imaging analysis is performed using a Carl Zeiss AG spinning disc confocal unit (Cell Observer SD with Yokogawa CSU-X1 scanning unit). Ablation experiments are done using a 355 nm pulsed UV Laser (Rapp, Optoelectronics). Images and movies are processed using Fiji (ImageJ) software and the Imaris 9.3.0 software update.

2.5.2 Morphology analyzes of isolated macrophages

To analyze cell morphology larval or prepupae macrophages are isolated and stained with phalloidin as described in chapter 2.4.8 overview images are taken and analyzed using FIJI shape descriptor parameter. Beside Area and Perimeter following parameters are calculated:

Circularity:	$4\pi \times \frac{[\mathbf{Area}]}{[\mathbf{Perimeter}]\text{^}\mathbf{2}}$
Aspect ratio (AR):	$\frac{[\text{Major Axis}]}{[\text{Minor Axis}]}$
Roundness:	$4 \times \frac{[\text{Area}]}{\pi \times [\text{Major axis}]\text{^}2}$
Solidity:	$\frac{[\text{Area}]}{[\text{Convex area}]}$

Furthermore, lamellipodia width is measured. Lamellipodia is defined as dens actin structure stained with phalloidin. The mean of five measurements per one cell is calculated form three independent measurements.

2.5.3 Fluorescence intensity measurement

To determine the level of cellular fluorescence, correlated total cell fluorescence (CTCF) is calculated. “Area integrated” intensity and “mean grey value” are set in FIJI measurement setup. Cells of interest are circled with the free hand tool. For backup measurement an area close to the cell is selected.

CTCF is calculated as followed:

> *Integrated Density – (Area of selected cell X Mean fluorescence of background readings)*

To analyze membrane fluorescence intensity of macrophages, overview images acquired in the counting modus (confocal Leica SP8) are used.

Use FIJI and proceed as followed:
Set line width to two and surround the cell exactly at the outer border with the free hand tool. Start at the cell rim (check Phalloidin staining) an choose part with the lowest fluorescence. Convert “area to line”, “plot profile” and extract list of data. Draw a line inside the cell for expression level control. Normalize measurements by subtracting cytoplasmic florescence. And normalizes cell perimeter to 100 %.

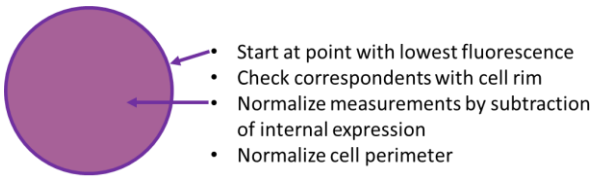

2.5.4 Analyzes of border cell migration

For analyzing Border cell migration at stage 10 A egg chambers are analyzed, when follicle cells are in line with the oocyte (Figure 9). The real migrated distance of the BCC is taken in relation to total migrated distance is calculated using FIJI (chapter 7.1.3).

$$Normalized\ distance = \frac{migrated\ distance}{total\ distance}$$

This method gives continues data, that makes it more sensitive in statistical analyzes. For visualization, the migration route is separated in quartiles beginning at the anterior tip of the egg chamber.

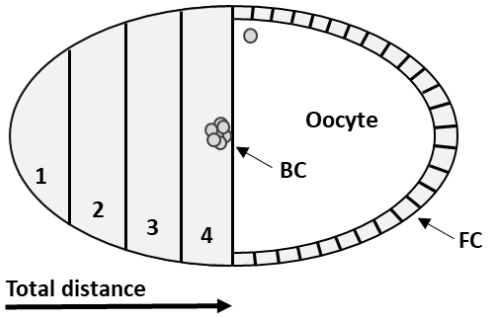

Figure 9: Schematic illustration of BCM and corresponding analyzes method. Border cell (BC) cluster already migrated from the anterior tip towards the oocyte. Stage 10 A can be identified when follicle cells (FC) reached the same high as the oocyte.

2.5.5 Quantification of F-actin staining in imaginal wing discs

To analyze the influence of a certain protein on F-actin, it is expressed in the posterior part of the wing disc using *engrailed* Gal4 driver line. Wing discs are isolated and stained as described in chapter 2.4.9.

For further investigation, close-up images are taken with the Leica SP8 confocal microscope in the counting modus. The procedure is illustrated in Figure 10 and the quantification method is described in more detail.

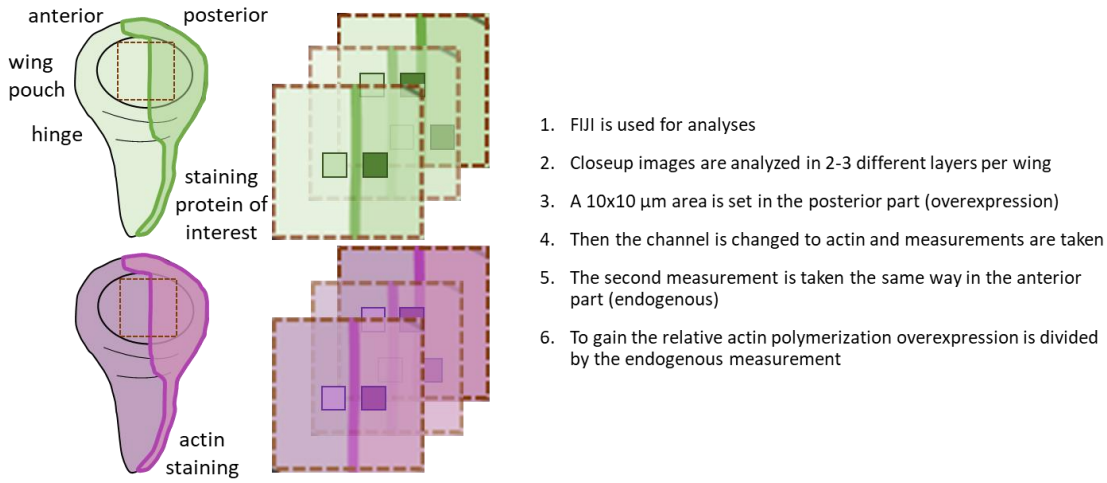

Figure 10: Schematic illustration of F-actin level quantification. Posterior expression by *en*-Gal4 driver in *Drosophila* imaginal wing disc is compared to anterior expression.

2.5.7 Live-cell imaging of S2R+ cells and isolated *Drosophila* macrophages

For live cell imaging of either transfected S2R+ cells or isolated *Drosophila* macrophages are placed in an 8-well imaging chamber, pre-incubated with ConA (Sigmar) for 30 minutes. Per well, 50-100 µL of either transfected cells (*in vitro*) or isolated macrophages (*ex vivo*) from 5 larvae/ 1-2 prepupae are diluted with $M3^{+/+}$ and incubated for 30 minutes in an 8-well chamber.

2.5.8 *In vivo* imaging of *Drosophila* macrophages

For *in vivo* live imaging of random migration of macrophages, prepupae are fixed with heptane glue on a cover slip ~3 h APF. The cover slip is placed in a wet imaging chamber and placed under the microscope. Imaging is performed in the anterior part dorsal of the prepupae.
Live imaging of directed migration is performed in drosophila pupal wing. Therefore, third instar larvae are transferred onto a water wettened tissue and incubated for 20 h at 25°C/ 16 hours 29°C. For imaging, the puparium is removed, and the pupa is placed on the wing or thorax in a wet imaging chamber and placed under the microscope. For precise laser induced wounding, a 355 nm pulsed UV Laser (Rapp, Optoelectronics) is used. Both procedures have been published and illustrated and described in detail (Rüder et al., 2018).

2.5.9 Tracking of macrophages by Imaris and analysis of migratory behavior

Time lapse movies are analyzed using the Imaris 9.3.0 software update. For random migration, a reference frame is set in offset position. For directed migration the reference frame is set at the ablation site. The spots mode option is used to track cells over time with parameters listed

in. Quality is adjusted manually for best detection result. After automatic tracking all time lapse movies are checked for correct results and are manually corrected.

2.5.10 Analysis of migration

To analyze the migratory behavior of cells, different parameters can be taken into account. "Track speed mean" can be directly extracted from Imaris. Graphs and statistical analysis (also see statistical analysis) are performed using Prism 7/8 or by R studio with ggplot package. Further analysis of migratory behavior is based on the three-dimensional position data of an object/cell over time. With this information motion vectors can be calculated, which describes the displacement of an object.

Motion vector: $$\overrightarrow{AB} = \begin{pmatrix} x_b - x_a \\ y_b - y_a \\ z_b - z_a \end{pmatrix}$$

Length of a vector:

$$\left|\overrightarrow{AB}\right| = \sqrt{x^2 + y^2 + z^2}$$

Track speed mean: average speed calculated by the track length divided by the time between first and last object.

The persistence angle of two vectors gives information about the persistence of a cell, whereas the bias angle reflects the directionality toward a wound/source. The R script is giving the option to set an outer and an inner radius within that the positions/cells are relevant for data calculation.

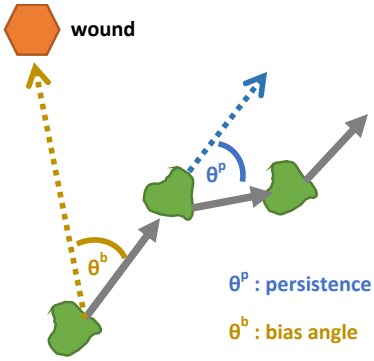

Scalar: $\vec{a} \circ \vec{b} = \begin{pmatrix} a_x \\ a_y \\ a_z \end{pmatrix} \circ \begin{pmatrix} b_x \\ b_y \\ b_z \end{pmatrix}$

$$= a_x * b_x + a_y * b_y + a_z * b_z$$

Angle: $\cos\theta = \frac{\vec{a} \circ \vec{b}}{|\vec{a}| * |\vec{b}|}$

Cell straightness and displacement form origin are both rough values for cell movement. Both are highly sensitive to variance in track duration. Therefore, displacement form origin is normalized by time.

$$Speed = \frac{|\overrightarrow{X_{t1}X_{t0}}|}{t_1 - t_0}$$

For directed cell migration track speed mean is just taken for cells in r radius between 15-70 µm from wounding site. This can be either extracted via direct filter using Imaris or the attached r-script.

$$Straightness = \frac{|\overrightarrow{X_{t0}X_{tEnd}}|}{\sum X_{t0} + X_{tn}}$$

$$Displacement\ from\ origin\ over\ time:\ DOT = \frac{|\overrightarrow{X_{t0}X_{tEnd}}|}{Frames} * Frames\ per\ minut$$

2.5.11 Statistical analyzes

For statistical analyzes GraphPad Prism 7 and 8 are used. Before analysis, groups are checked for data distribution using Shapiro-Wilk-test (column statistics). For normally distributed data, parametric tests are performed. Otherwise, nonparametric tests are used for analyses.

To compare to two unpaired experiments either the t-test (parametric data) or the Mann-Whitney test (non-parametric data) are used. For experiments with multiple groups, either parametric or non-paramedic multiple comparison tests are performed. There, all groups are compared with the corresponding control group.

3 Results

3.1 *wave* depleted macrophages show a disturbed lamellipodial migration but still respond to wound signals

Migration of cells is highly dependent on the temporal and spatial reorganization of the actin network. In the last decades, research has identified hundreds of factors that are important in the processes of modulating and regulating actin assembly as well as disassembly. The Arp2/3 complex has been identified as actin nucleator on preexisting mother filaments. For proper function, it must be activated by NPFs of the WASP family, which are conserved across species (Campellone and Welch, 2010). At the leading edge, migrating cells extend large protruding lamellipodia, consisting of branched actin (Abercrombie et al., 1970c). *Drosophila* macrophages provide a powerful system to address the role of lamellipodia in random but even more outstanding in directed migration *in vivo* (Sander et al., 2013; Weavers et al., 2016; Wood et al., 2006).

Additionally, macrophages can be easily isolated from white prepupae to analyze their cell shape and visualize actin structures. WAVE induced activation of the Arp2/3 complex is required for the formation of branched actin filament at the leading edge of macrophages. Isolated macrophages show a broad lamellipodium at the cell front and denser actin structure at the rear (Figure 12A+A´). WAVE is predominantly localized at the rim of the lamellipodium, but also detectable in the cytoplasm (Figure 12A´´).

Mutations of *wave* as well as single Arp2/3 subunits lead to embryonal lethality (Zallen et al., 2002). Therefore, macrophage specific RNAi-mediated gene knockdown experiments were performed to confirm the requirement of WAVE in lamellipodia formation. Suppression of Arp2/3-mediated actin polymerization in cells depleted for *wave* (Figure 12B, green cells) causes the almost complete disruption of lamellipodial structures. Cells exhibit finger-like filopodial protrusion and show a stellate shape as it has been previously described in S2R+ cells and *Drosophila* macrophages (Rogers et al., 2003; Rüder et al., 2018; Sander et al., 2013; Zobel and Bogdan, 2013).

Moreia et al. established a protocol based on the MARCM (Mosaic Analysis with a Repressible Cell Marker) system to induce homozygous lethal mutations in *Drosophila* macrophages in viable mosaic flies (Lee and Luo, 2001; Moreira et al., 2013). This method was used to investigate the first *wave* mutant macrophages *in vivo*. FRT recombination is

induced by a temperature sensitive flippase (hs-FLP) to generate homozygote mutant cell in an otherwise wild typic background (Figure 11). There, *wave* mutant macrophages are labeled with a fluorescent eGFP marker (Figure 12C) and show an even stronger stellar phenotype in comparison to the cells generated by RNAi mediated knock down experiment. Mutant cells exhibit several long thin filopodia and a complete loss of lamellipodia.

Additionally, *arp3* mutant macrophages were generated using the twin-spot technique (Germani et al., 2018). The twin-spot technique relies on an FRT-site combined with a ubiquitously expressed fluorescence marker (Figure 11). Here, the FRT mediated recombination resulted in homozygous mutant cells and the lack of GFP expression. *arp3* mutant macrophages show an overall reduction of branched actin network and exhibit ectopic filopodia leading to a stellate cell shape (Figure 12D, eGFP negative). However, they do not exactly phenocopy the *wave* knock out cells. In isolated cells this technique also allows for a direct internal control.

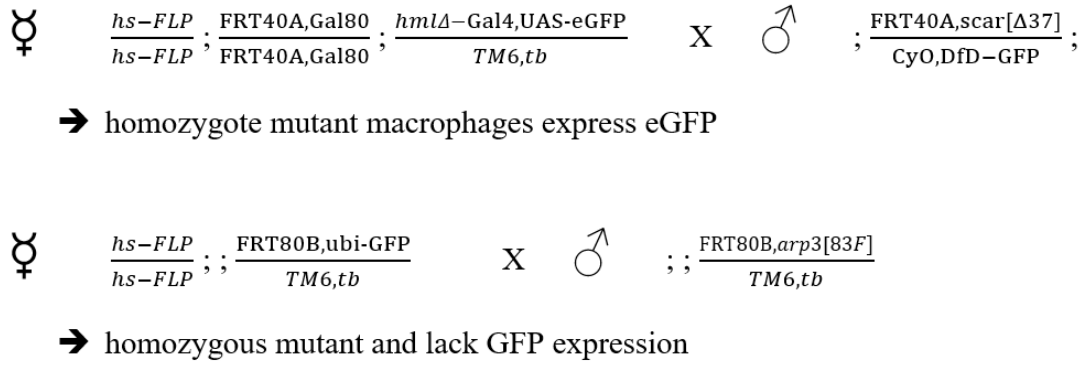

Figure 11: Crossing scheme to generate homozygote mutants in mosaic flies. The heat-shock induction is described in 2.3.3 Mosaic analysis using the FLP/FRT system.

These data confirm previous results generated by RNAi mediated knock down. In *Drosophila* macrophages WAVE is the essential factor regulating Arp2/3 complex dependent lamellipodia formation.

RNAi-mediated gene knock down of the WAVE upstream activator Rac, shows a *wave* mutant-like phenotype (Supplementary Figure 2). However, this phenotype is not as pronounced as observed in *wave* mutant cells. This let assume that other upstream factors are also critical for WAVE activity in macrophages.

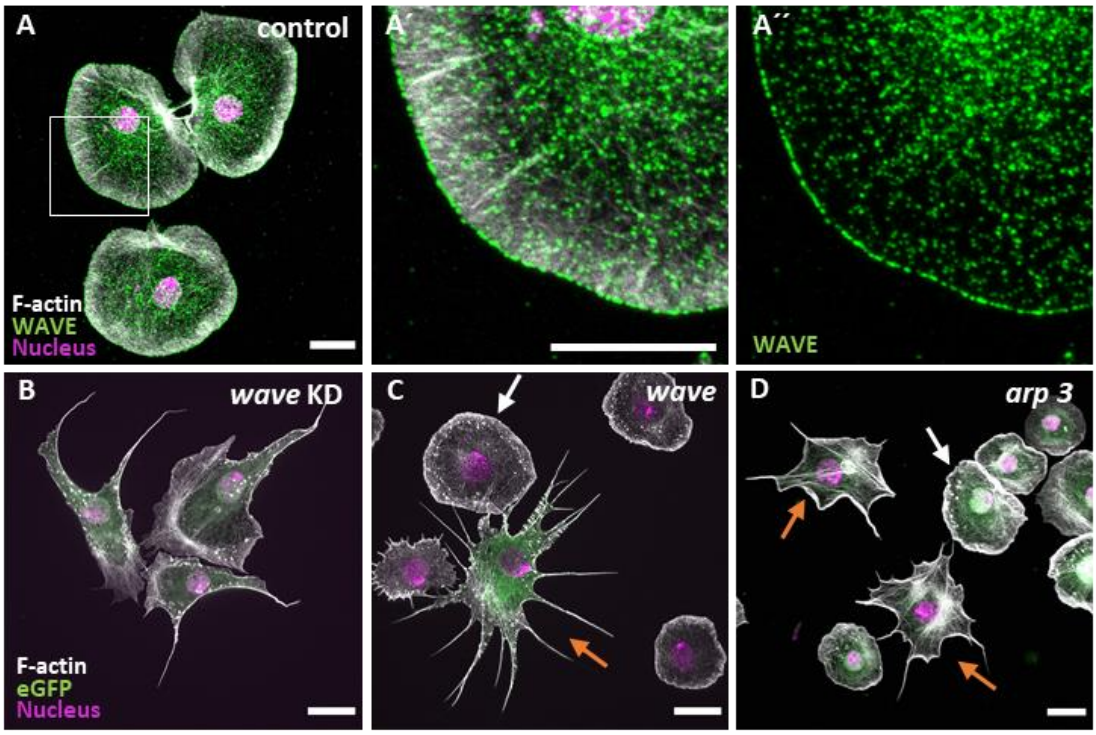

Figure 12: Analysis of WAVE in Drosophila macrophages. (A-A´´) Isolated pupal wild type macrophages plated on ConA stained for F-actin (white), nucleus (magenta) and WAVE (green) spread out show characteristic wild type morphology with broad lamellipodial structures. WAVE is localized in a thin line at the membrane. (B) RNAi-mediated (*hmlΔ*-Gal4) *wave* knockdown in macrophages stained for F-actin (white), nucleus (magenta) and cytoplasmic eGFP expression. Cells almost completely lack lamellipodial structures and exhibit filopodia. (C) Induction of *wave* mutant macrophage clones (eGFP positive, orange arrow) stained for F-actin (white), nucleus (magenta) exhibit extended filopodial structures and completely lack lamellipodia in comparison to wild type cells (white arrow). (D) Induction of *arp 3* mutant macrophage clones (eGFP negative, orange arrow) stained for F-actin (white), nucleus (magenta) in comparison to wild type cells (white arrow). *arp 3* show disturbed lamellipodial and thick actin bundles surrounding the whole cell with filopodial protrusions. Genotypes are indicated. Scale bar = 10 µm.

Previous data emphasize the relevance of lamellipodia protrusions in two dimensional migration on surfaces (Brinkmann et al., 2015; Sander et al., 2013). They provide an extended surface mediating the adhesion to the epidermal surface under physiological conditions (Nagel et al., 2017). In prepupae, sub-epidermal macrophages acquire broad lamellipodia protrusion at the leading edge of the cell initiating random cell migration (Figure 13, Movie 1).

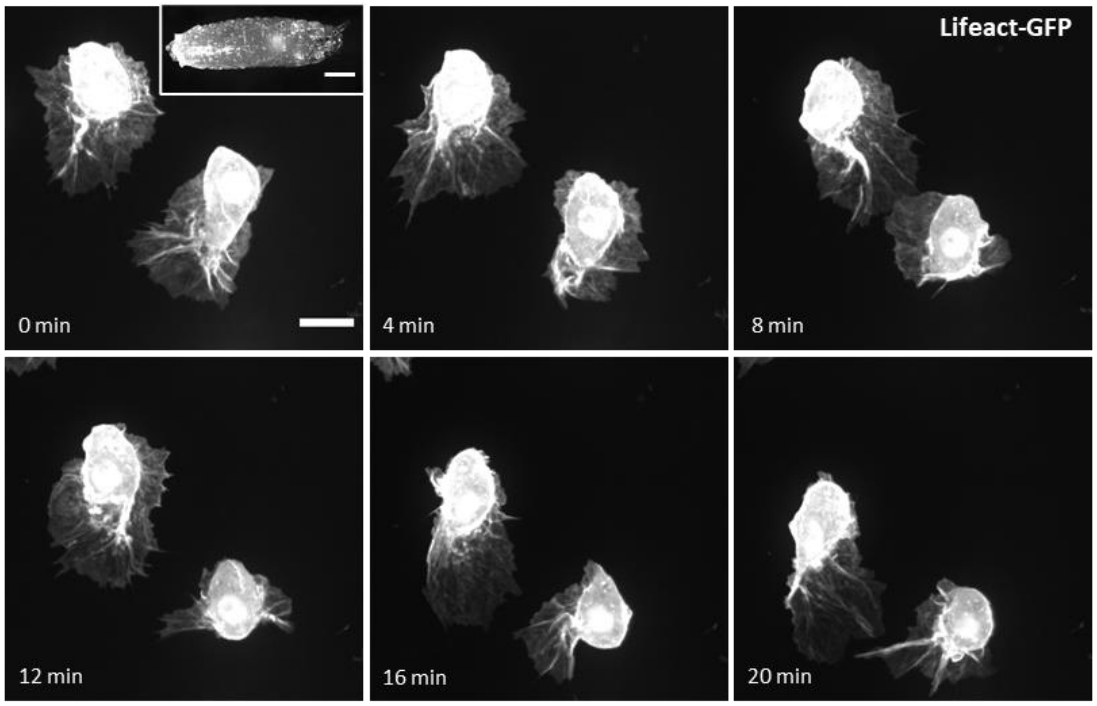

Figure 13: Random migrating macrophages. Frames of time-lapse images of wild type macrophages at the epidermis of a white prepupa (box top-left image). The cells are visualized using macrophage specific expression (*hmlΔ*-Gal4) of lifeact-GFP. At the leading edges, cells exhibit a broad, flat lamellipodium. Scale bar white prepupa = 500 µm, macrophages = 10 µm.

The MARCM system, used for the generation of homozygote *wave* mutant macrophages, allows the expression of the fluorescent marker eGFP only in homozygous mutant cells. It provides a powerful tool to investigate migratory behavior of macrophages lacking lamellipodia formation *in vivo*, to further address their outstanding role and characterize their motion *in vivo*.

Epidermal wild type macrophages expressing cytoplasmic eGFP reveal large protruding lamellipodia (Figure 14A), whereas the *wave* mutant as well as *wave* knock down macrophages completely lack lamellipodia formation. Instead, *wave* depleted macrophages exhibit long and extended filopodial protrusions (Figure 14B+C). In comparison to wild type macrophages, the majority show only rudimentary motion stretching out their filipodia but otherwise staying almost at their origin. Only some macrophages relocated within the 20 min acquisition time. To characterize cell motion of either wild type or *wave* depleted cells, macrophages were tracked during migration using Imaris software. This provides the position of every cell over time and allows the calculation of objective parameters to define cell migratory behavior (2.5.10 Analysis of migration). For better visualization, the color of the trajectories reflects the speed of the cell at each respective timepoint. This show that wild type macrophages move in a continuous motion and homogenous speed. The cell speed mean of

wave depleted cell is significantly reduced in comparison to the wild type macrophages (Figure 14D, Movie 2). The majority of the cell stay sessile at their position. If relocate, they overcome a relatively long distance in a comparatively short time, but then become sessile again. Therefor their motion can be defined an erratic motion (Figure 14B+C, Movie 3).

Straightness of the cell movement (optimal migration distance/migrated distance, (2.5.10 Analysis of migration)) is also reduced, but significantly only in case of *wave* mutant cells (Figure 14E). This result is also reflected in the persistence of the cells (2.5.10 Analysis of migration): wild type cells show a relatively low cell persistence with a mean angle ~30 °, indicating overall straight motion (Figure 14A, F+F´). In *wave* mutant and RNAi mediated *wave* knock down migrating macrophages the persistence angle is significantly increased (Figure 14A, F+F´). Remarkably, the distribution of the median angle shows a high variance within the group. Trajectories show that, if *wave* depleted cells migrate, they do it in a relatively persistent manner. The persistence angle is highly dependent on the more sessile cells, which show a slight local tumbling (Figure 14B+C, Movie 3).

In conclusion, *wave* depletion causes severe migratory defects in random migration of *Drosophila* macrophages. Filopodia can only partially take over the function of lamellipodia. These findings point out the importance of WAVE as actin regulator in lamellipodial cell migration.

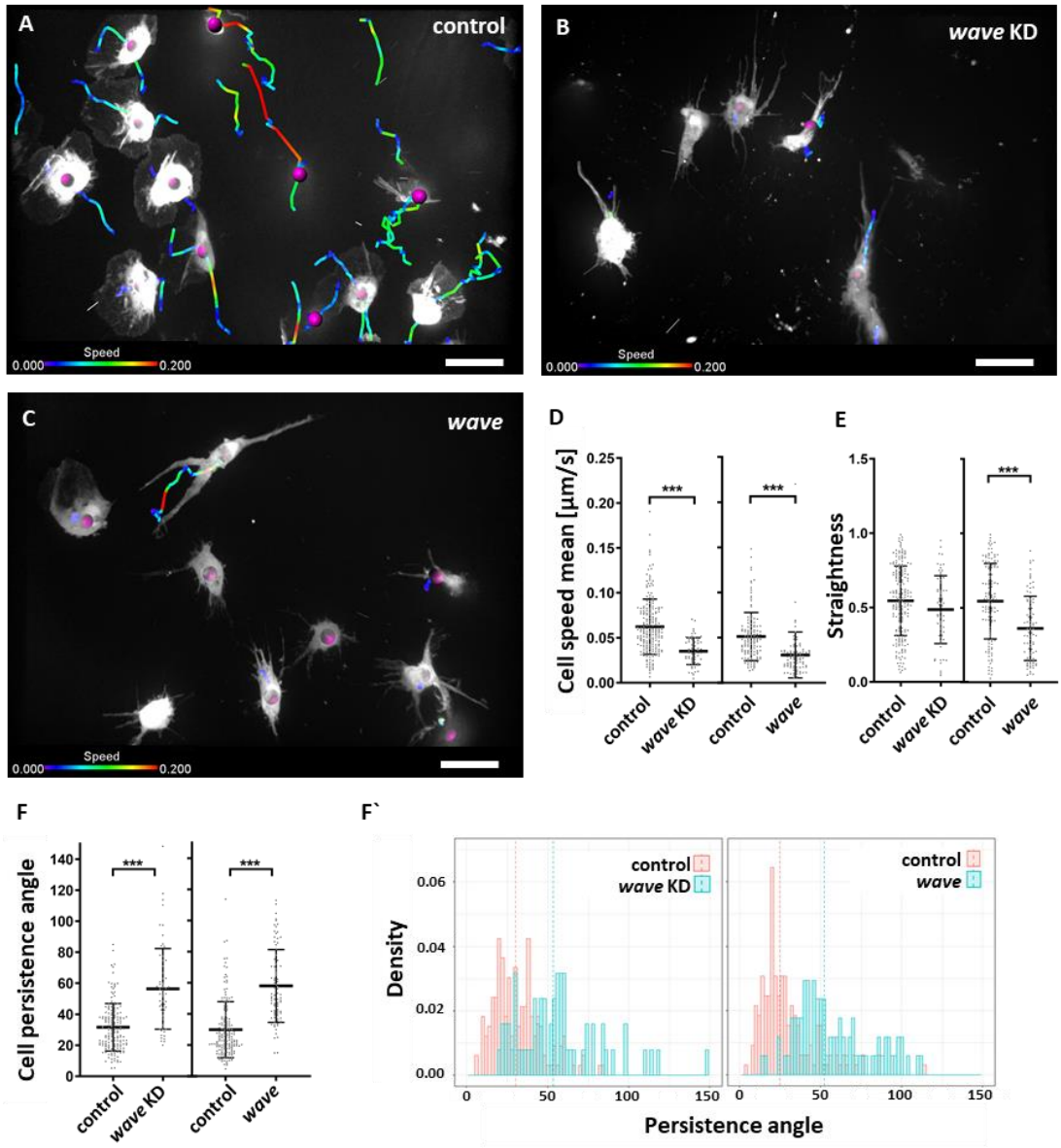

Figure 14: Loss of *wave* causes severe migration defects. (A-C) Still images of randomly migrating pupal macrophages (20 minutes). Cells are tracked with Imaris and trajectories are depicted with speed-color code (in µm/s). (A) Wild type macrophages expressing eGFP show broad lamellipodia attached to the epithelia, migrating constantly. (B) *wave* knock down cells expressing eGFP and (C) induced *wave* mosaic mutant cells (eGFP positive) exhibit long filopodial structures resulting in an altered migratory behavior. (D-F) Graphs are depicted in a scatter dot blot with bars indicating mean and SD. *** = $p \leq 0.001$ (Mann-Whitney-U-Test). In the bias angle histogram one bar depicts the accumulated density of 3 °. Dotted line indicates the median angle of the distribution. (D) Analysis parameter of random migration show a reduced cell speed for *wave* KD and *wave* mutant cells. Cell migration straightness is reduced in *wave* mutant cell but not significantly for *wave* KD. (F) Cell persistence is reduced in *wave* KD and *wave* mutant cells as depicted in persistence angle histogram (F´) which shows a shift in angle distribution to larger angles. Scale bar = 20 µm.

Macrophages respond to immune cues by switching from random explorative motility to directed migration towards the source of chemokine. It is still under debate whether

lamellipodia are indispensable in directed migration upon a chemotactic stimulus (Suraneni et al., 2012; Wu et al., 2012). To address this controversial question, the role of lamellipodia in directed cell migration upon a precise laser induced wounding in pupal wing was analyzed (Figure 15A+B, 2.5.5 Quantification of F-actin staining in imaginal wing).

In comparison to the previous experimental setup, where cells migrate on a two-dimensional epithelial layer, here, cells migrate within the three-dimensional ECM filled cavity of the wing. Protrusions of the cells appear to be more complex, exhibiting lamellipodial as well as filopodial structures (Figure 15C, Sander et al., 2013). Upon wound induction, wild type cells directly switch from random to directed migration (Figure 15C, Movie 4). Protrusions of the cells are re-orientated towards the wounding site. Within 30 minutes, most cells in a distinct radius reach their destination and clot around the induced wound (Figure 15C magenta spot, Movie 4). As in random migration, w*ave* depleted cells extend long filopodia and completely lack lamellipodial structures (Figure 15D+E). Upon laser ablation, cells depleted for *wave* send their long filopodia towards the wound, which indicates that wound response is still intact (Figure 15D+E, Movie 5). However, the cell speed mean is significantly reduced in comparison to wild type (Figure 15F), as also observed in random migration cells. To gain further information about the cell directionality towards the wounding site, the median bias angle for each cell was calculated using a newly established R-script (7.1.3.2 R-script). The analysis is based on the position data of the wound and those of the cells over time. A value close to 0° indicates the highest directionality, whereas cells with a value close to 180° move in opposite direction. In comparison to wild type cells, *wave* depleted cells show no significant differences in directionality (Figure 15G+G´). It should be mentioned, that in wild type cells the cell bias angle also turned out to be unexpectedly high, ranging around 80° in the mean (Figure 15G+G´).

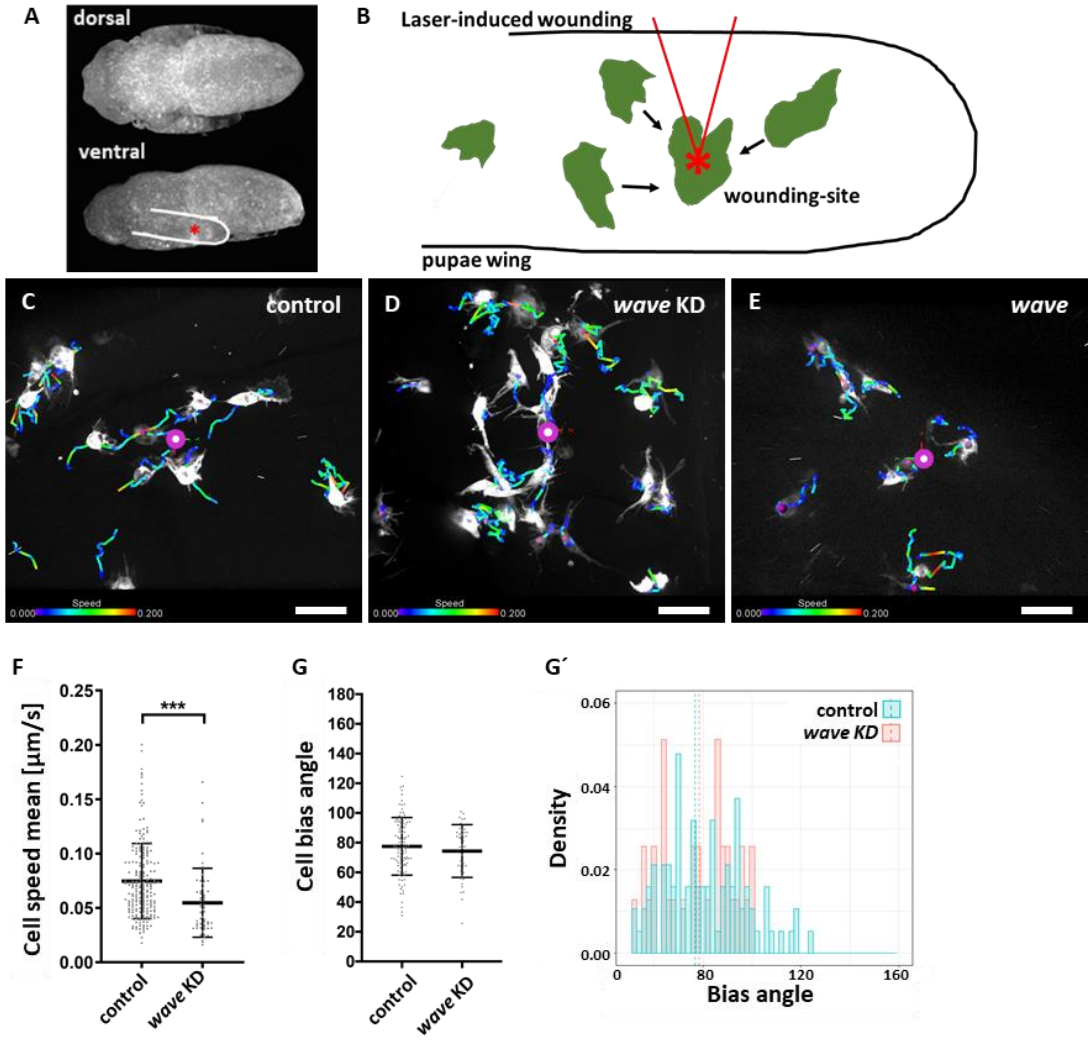

Figure 15: Lamellipodia are dispensable for wound recognition. (A) Dorsal and ventral view of a Drosophila pupa 20 h APF (B) Scheme of laser-induced wounding experiment in the pupal wing (C-E) Stills of time laps images of directed macrophage migration upon wounding of a single cell (magenta dot in the center). Cells are imaged for 30 minutes after ablation in a 30 second interval and tracked afterwards using Imaris. Trajectories with speed color code indicate that wild type and wave depleted macrophages migrate towards the wounding site. (F+G) Graphs are depicted in a scatter dot blot with bars indicating mean and SD. *** = $p \leq 0.001$ (Mann-Whitney-U-Test). In the bias angle histogram one bar depicts the accumulated density of 3 °. Dotted line indicates the median angle of the corresponding distribution (F) Speed is reduced in wave KD macrophages. (G) Cell bias angle ranges around 80 ° in both wild type and wave KD macrophages and bias angle histogram shows no differences in angle distribution (G´). Scale bar = 20 µm.

To summarize, WAVE can be confirmed as a key regulator for branched actin filament formation located at the leading edge of the cell. In the absence of WAVE, cells fail to form lamellipodia. Instead, they exhibit long filopodial structures. This has negative consequences on the migratory behavior of the cells: filopodia barely substitute lamellipodial protrusion,

resulting in reduced cell speed and increased persistence angle. However, despite the absence of WAVE in macrophages, they are still able to detects wounds and respond to them.

3.2 WIRS-ligand binding to the WRC is negligible in macrophage wound response

The loss of lamellipodia causes severe migration defects underlying the importance of proper lamellipodia formation at the leading edge of migrating cells. The local recruitment and activation of Arp2/3 driven branched actin formation via WAVE is an important factor for efficient lamellipodia based directed cell migration. In previous studies a short peptide sequence present in over 100 membrane and membrane-associated proteins was identified (B. Chen et al., 2014). This motive binds to a pocket within the WRC formed by the subunits Sra-1 and Abi and is therefore termed the WAVE interacting regulatory sequence (WIRS). The interaction of WIRS receptor Fat-2 with the WRC is relevant in collective migration of follicle cells driving egg rotation. Disruption of the WIRS binding results in a round egg phenotype (Squarr et al., 2016).

Upon wounding, the actin machinery rearranges to initiate direct motion towards the wounding site. So far, the underling molecular mechanism of chemotactic behavior of pupal macrophages has been poorly addressed. Many potential WIRS ligands are highly expressed in *Drosophila* macrophages suggesting a functional role of WRC-WIRS interaction also in immune response. To identify potential WIRS membrane receptors that might be regulating WRC-driven directed migration, specific RNAi-mediated knockdown of genes of potential candidates were performed. For 28 membrane receptors at least two independent RNAi targets (with exceptions) were screened for defects in directive migration upon wound response. Candidates exclusively expressed in macrophages like Platelet-derived growth factor receptor/ vascular endothelial growth factor receptor (PDGFR/VEGFR) known to be important in chemotaxis of embryonal macrophages during development or Nimrod C1, a phagocytoses receptor, were prioritized (Supplementary Figure 3). However, none of the tested receptors showed a severe defect in wound response.

To analyze the impact of the WRC-WIRS interaction in translating wound signals into changes in cell motility, flies lacking the WIRS binding surface were further investigated. Inducing two point mutations (R106A/G110W, $Abi^{\Delta WIRS}$) into the Abi binding site disrupts the binding-ability of the whole WRC and consequently the interaction with potential WIRS-receptors

required in wound response. To this aim wound response of macrophages ubiquitously re-expressing Abi$^{\Delta WIRS}$ in *abi* mutant (*abi*$^{\Delta 20}$) background was compared with rescue *abi* mutants by re-expressing wild typic Abi (AbiWT). Upon laser-induced wounding of a single cell, macrophages with directed WIRS binding motive are still responding to the wound signal. They show neither any morphological nor obvious migratory defects (Figure 16A+B, Movie 6+7). To test this in more detail, directed migration of macrophages re-expressing Abi$^{\Delta WIRS}$ were compared to wild typic Abi re-expression in *abi* mutant background. The histogram-based macrophage migration score (HMMS, Lammel et al. 2014) was used as an indirect method to analyze macrophage migration upon wounding. It utilizes a radial histogram around the laser induced wound to determine the migration of the macrophages. The score increases over time, when the cells get closer to the wounding site in the center and finally reaches a plateau. The median HMMS for macrophages re-expressing wild type Abi and Abi$^{\Delta WIRS}$ clearly show macrophages responding to the wound signal (Figure 16C). However, the slope of cells with disrupted WIRS binding site is constantly lower than the wild type level. These data suggest that the disruption of the WIRS binding site causes mild wound response defects. Nevertheless, it should be mentioned, that HMMS is sensitive to cell number, size and is only a rough approximation but does not describes cell motion itself. To analyze possible changes in the migratory behavior of single cells in more detail, cells were tracked over time upon wounding. Trajectories of migrating cells show that rescued macrophages by wild typic Abi re-expression as well as an Abi transgene with disrupted WIRS binding surface respond to the wound stimulus and reach the wound within 30 minutes (Figure 16A+B, magenta spot, Movie 6+7). Neither the cell speed mean nor the cell bias angle is affected by the disruption of the WIRS binding motif. This is also visualized in the cell bias histogram showing a high overlap of angle distribution of both groups (Figure 16E´).

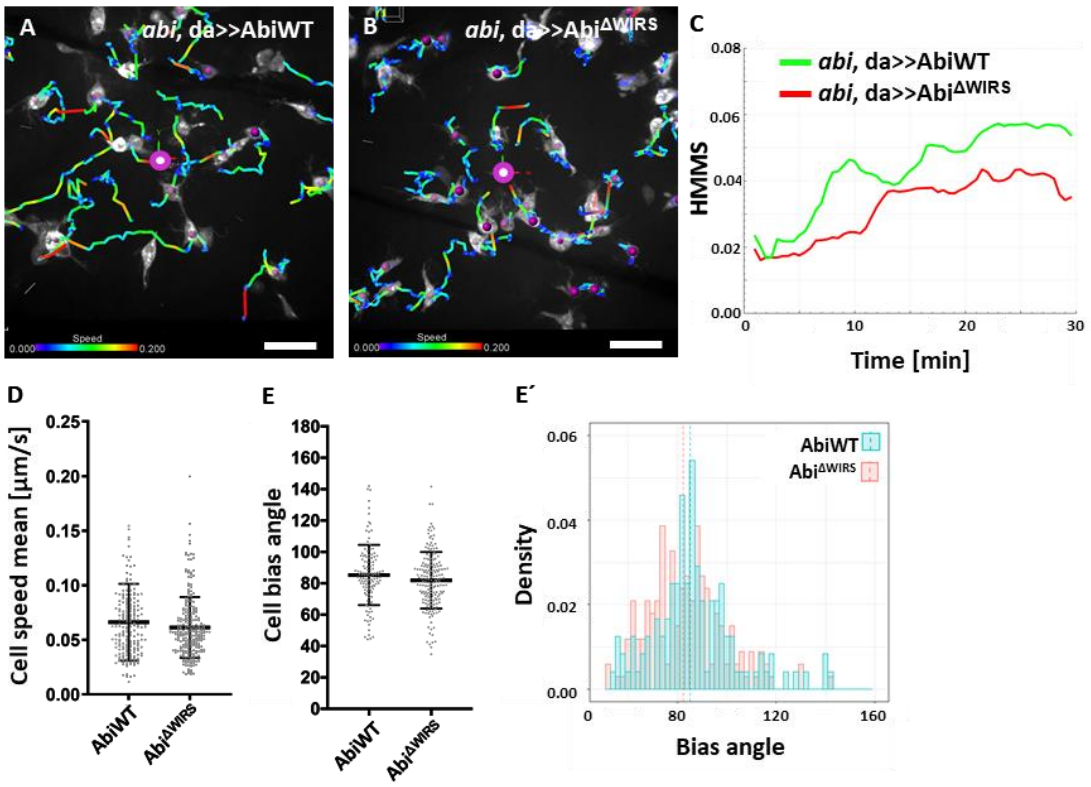

Figure 16: Disruption of the WIRS binding barely affect wound response of *Drosophila* macrophages. Ubiquitously (*da*-Gal4) re-expression of wild typic Abi (AbiWT) or Abi with disrupted WIRS binding site (R106A/G110W, Abi$^{\Delta WIRS}$) in *abi* (*abi*$^{\Delta 20}$) mutant background. (A+B) Stills of time laps images of directed macrophage migration upon wounding of a single cell (magenta dot in the center). Cells are imaged for 30 minutes after ablation in a 30 second interval and tracked afterwards using Imaris. Trajectories with speed color code indicate that AbiWT and Abi$^{\Delta WIRS}$ re-expression in macrophages migrate towards the wounding site. (C) Mean HMMS value of AbiWT (green) and Abi$^{\Delta WIRS}$ (red) determined from movies after laser ablation indicate a slight overall decrease for the Abi$^{\Delta WIRS}$ rescue compared to AbiWT. (D+E) Graphs are depicted in a scatter dot blot with bars indicating mean and SD. *** = $p \leq 0.001$ (Mann-Whitney-U-Test). In the bias angle histogram one bar depicts the accumulated density of 3 °. Dotted line indicates the median angle of the corresponding distribution (D+E) Neither speed nor persistence is altered when disrupting the WIRS binding site in Abi. Scale bar = 20 µm.

In another approach the interaction of WRC with potential WIRS-ligand was tried to be inhibited by the allosteric binding of the WIRS peptide. For this, the WIRS sequence from the human protocadherin 10 (PCDH10) was sequence optimized for *Drosophila* and sequentially linked four times (UASp-WIRS-GGSx4, Kreft, 2017, bachelor thesis). This UASp-construct was established in flies. For a proof of principle, it was expressed in follicle and follicle steam cells (Supplementary Figure 4). It was assumed that the WIRS peptide occupy the WIRS binding site of the WRC and diminish the binding of WIRS ligand Fat2. However, the overexpression of WIRS-GGSx4 does not copied the expected round egg phenotype of *fat2*

mutants and the disruption of the WIRS binding site in the WRC (Supplementary Figure 4). Still, this is a promising approach and need to be pursued.
Taken together, disrupting the WIRS binding site within the WRC does not affect directed cell migration. Detailed analysis of the directionality and the speed of the cells show no evidence for the importance of the WRC-WIRS interaction.

3.3 WAVE is tyrosine-phosphorylated by Abl and Src42A kinase

The non-receptor tyrosine kinase Src and Abl emerged as a promising candidate, as both has previously shown to bind WAVE and influence the activity. They are described as key regulators with an important role in cell proliferation, morphogenesis and cell migration. Both kinases share a N-terminal tandem SH3 and SH2 domain serving as interaction sites for PXXP carrying proteins as well as providing the binding site for phosphorylated tyrosine residues. In the cytoplasm they are present in their folded, autoinhibited kinase inactive form (Brasher and Van Etten, 2000; Nagar et al., 2003; Plattner et al., 1999; Schindler et al., 2000; Xu et al., 1999). Upon growth factor stimulation, they get phosphorylated, regulating the release of the autoinhibited state. Moreover, the interaction with binding partners is associated with the disruption of the intramolecular inhibition. Deregulation of the kinase activity of both kinases is highly associated with cancer. The chromosomal translocation of Abl, leading to a constitutive active form (BCR-Abl), identified Abl as one of the first human oncogenes involved in leukemia (Price et al., 1988). The expression of BCR-Abl is associated with growth factor independent proliferation and reduction of cells undergoing apoptosis (Fogerty et al., 1999).
The ubiquitous expression of the kinase active form BCR-Abl or the constitutively active (CA) Src42A by *da-Gal4* as well as segmental expression by *en*-Gal4 diver causes embryonal lethality (data not shown). Further, the specific ectopic expression in macrophages results in over proliferation and massive cell growth resulting in large macrophages (Figure 17A-C, orange arrow). The expression of BCR-Abl additionally induces lamellocytes differentiation, which under normal conditions only appear upon infection or by other immune cues (Figure 17B, blue arrow). Strikingly, a dense actin network surrounds the e cell (Figure 17B, orange arrow).

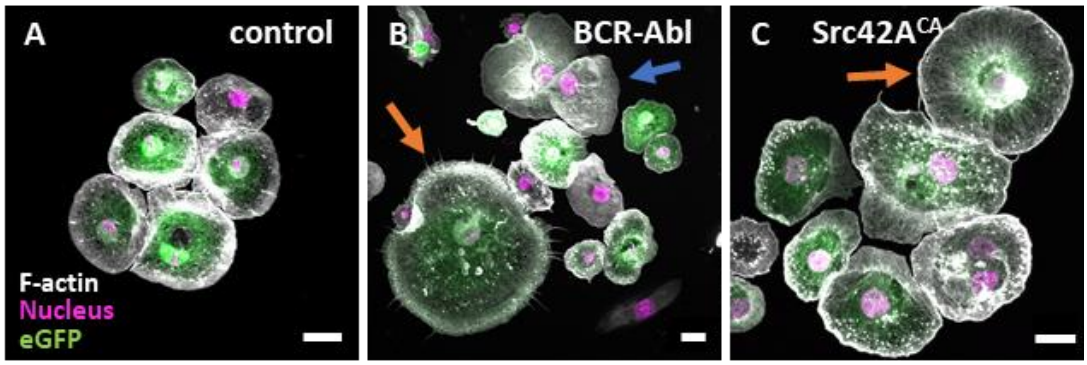

Figure 17: Overexpression of kinase active Abl and Src causes gigantic cell growth. (A-C) Isolated pupal macrophages plated on ConA stained for F-actin (white), nucleus (magenta), cytoplasmic eGFP. Constructs are expressed specifically in macrophages by *hmlΔ*-Gal4 driver. (B+C) Expression of kinase active Abl and Src causes massive cell growth (orange arrow). (B) Expression of kinase active Abl additionally result in differentiation of lamellocytes (blue arrow). Scale bar = 10 µm.

To confirm WAVE being a target of Abl and Scr42A, *Drosophila* S2R+ cells were transfected with either constitutive active Src42A, BCR-Abl or both constructs simultaneously. Protein lysates were treated with Vanadate to preserve phosphorylation state of the cell and then separated on an SDS-PAGE with low bis-acrylamide concentrations of 0.06% to allow for better separation of endogenously WAVE protein (2.4.6 SDS polyacrylamide gel electrophoresis (SDS-PAGE)). It shows that already in the control (eGFP) endogenous WAVE resolves in three separated bands, with the most prominent band at 76 kDa corresponding with the expected molecular weight of WAVE (Figure 18A). Expression of BCR-Abl leads to a shift in molecular weight and WAVE resolves in at least five separate bands, where the uppermost band (~90 kDa) appears to be the prominent one. Surprisingly, the expression of constitutive active Src42A results in the same band pattern as seen in the control expression with EGFP (Figure 18A). The co-expression of BCR-Abl and constitutive active Src42A shows no clear increase in molecular weight of WAVE in comparison to single expression of BCR-Abl alone. It has to be mentioned that the separation of the single band is not as clear as in treatments with BCR-Abl alone.

As the addition of a single phosphoryl group does not necessary lead to a, shift in molecular weight detectable in a SDS page gel. Further experiments were performed to directly detect WAVE tyrosine phosphorylation. To this aim, S2R+ cells were co-transfected with myc-tagged WAVE in combination with the kinase active form of Abl or Src42A. WAVE was precipitated with anti-myc nanobody-coated beads and further analyzed for tyrosine phosphorylation by staining with anti phospho-tyrosine antibody (Figure 18B). The experiment confirmed that BCR-Abl phosphorylates WAVE. Consistent with results

published before, it was shown that constitutive active Scr42A phosphorylates WAVE (Ardern et al., 2006; Leng et al., 2005; Sossey-Alaoui et al., 2007; Stuart et al., 2006).

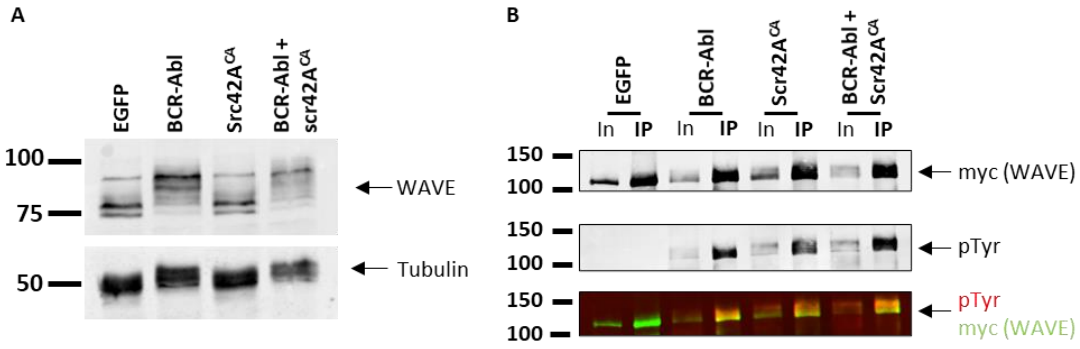

Figure 18: Kinase active form of Abl and Src phosphorylate WAVE. (A) BCR-Abl but not Src42A^{CA} overexpression in transfected S2R+ cells induces a shift in molecular weight of WAVE. (B) Immunoprecipitation with myc-trap beads from lysates of S2R+ cells co-transfected with WAVE-myc and indicated constructs. Anti phospho-tyrosine antibody staining shows phosphorylation of WAVE by BCR-Abl and Src42A^{CA}.

Previous data already demonstrated that Abl directly interacts with WAVE (Mehidi et al., 2019). To identify a possible physiological interaction between Src42A and WAVE in *Drosophila*, co-immunoprecipitation was performed with WAVE and constitutive active Src42A. However, neither for constitutive active Src42A alone nor in the presents of BCR-Abl an interaction of Src42A and WAVE could be detected (Figure 19).

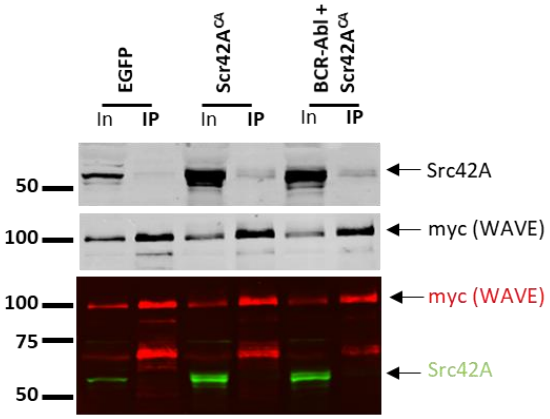

Figure 19: Src42A does not directly interact with WAVE. Co-Immunoprecipitation with myc-trap beads from lysates of S2R+ cells co-transfected with WAVE-myc and Src42A. Src42A is not enriched after co- immunoprecipitation.

In summary, the ectopic expression of the kinase active form of Abl as well as Src42A result in massive cell growth and over-proliferation in isolated macrophages. *In vitro* data reveal that

both kinases are able to phosphorylate WAVE (Chen et al., 2010). For Src42A no directed physiological interaction could be detected under chosen experimental condition. Nevertheless, Src as well as Abl are prime candidates to influence WRC activity via phosphorylation of WAVE.

3.4. Kinase activity of Src42A negatively influences random cell migration but does not impair wound response

For further dissection of Src42A kinase function in regulating WRC activity, random migration of macrophages was investigated in prepupal stage. As the mutation of *src42A* leads to embryonal lethality, macrophage specific RNAi-mediated knockdown of *src42A* was performed. The efficiency of the RNAi-mediated knockdown was determined by measuring protein level via Western Blot (Supplementary Figure 6) showing a remaining protein amount of 25 % in comparison to wild type cells. Random migrating macrophages show no morphological or migratory defect upon RNAi-mediated knockdown (Figure 20 C-E). Further, a dominant negative transgene of Src42A ($Src42A^{DN}$) with lacking kinase activity was overexpressed in macrophages. These cells show no morphological changes in comparison to wild type cells (Figure 20A, Movie 8). Analyzing the migratory behavior in more detail, they show a reduction in speed as well as in straightness (Figure 20C+E). The Cell persistence is not affected (Figure 20D+D´). The overexpression of constitutive active Src42A also lead to a reduction of cell speed (Figure 20C). Further, cell straightness as well as persistence of the migrating macrophages are decreased (Figure 20D-E). Additionally, overexpression of constitutive active Src42A results in gigantic macrophages, which might also influence motion of the cells (Figure 20B, Movie 9).

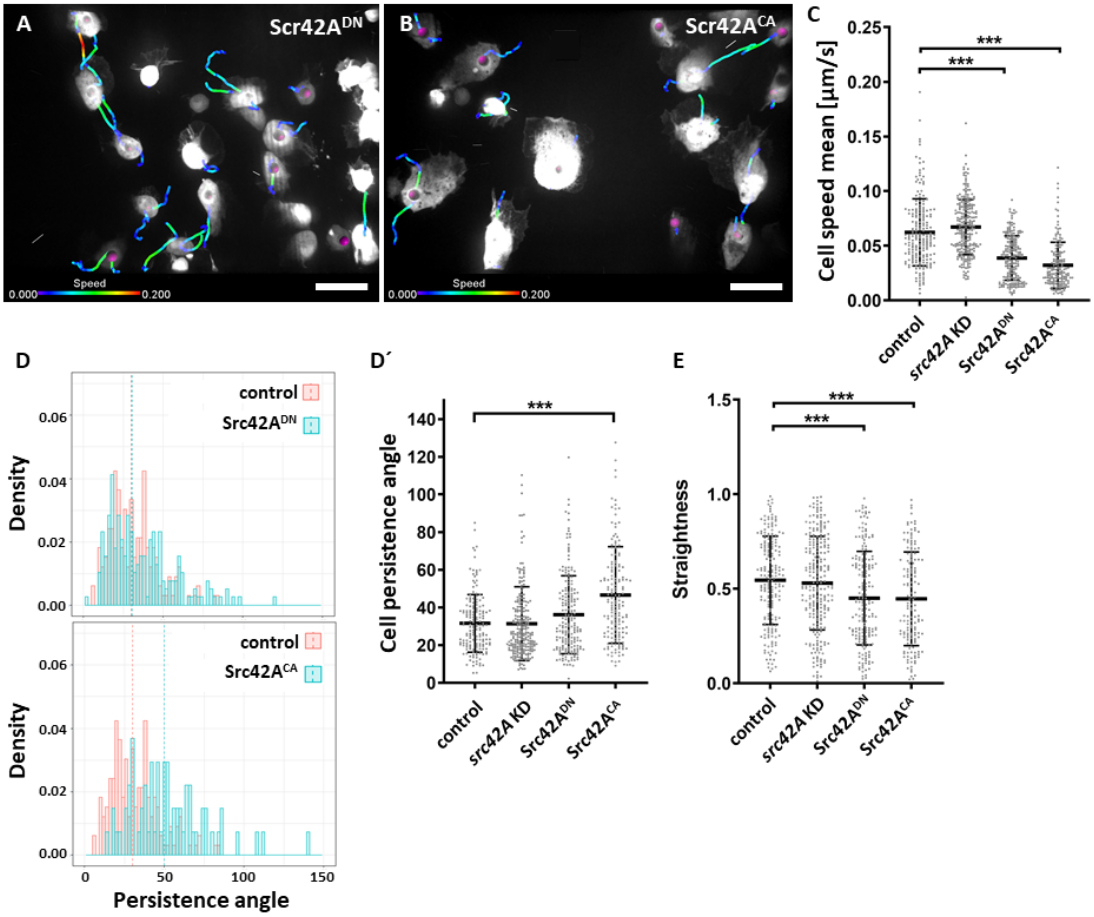

Figure 20: Overexpression of kinase dead and kinase active form of Src impair random cell migration. (A+B) Still images of randomly migrating pupal macrophages. Cells were tracked with Imaris and trajectories are depicted with speed-color code (in µm/s). (A) Macrophages overexpressing kinase dead Src (DN) show no morphological defects but (B) overexpressing kinase active Src (CA) result in giant cells. (C-E) Graphs are depicted in a scatter dot blot with bars indicating mean and SD. *** = $p \leq 0.001$ (non-parametric multiple comparison test). In the bias angle histogram one bar depicts the accumulated density of 3 °. Dotted line indicates the median angle of the corresponding distribution. (C) Cell speed is not altered in src42A KD but reduced in macrophages expressing Src42ADN and Src42ACA (D) Cell persistence is only reduced in macrophages expressing Src42ACA but (E) straightness is impaired in macrophages expressing Src42ADN and Src42ACA. Scale bar = 20 µm.

Previous data in *Drosophila* embryo demonstrated an important role of Src42A in macrophage wound response (Evans et al., 2015). To further analyze Src42A as a potential mediator to transduce the wound signals to the WRC, wounding experiments were performed in pupal wing. Upon ablation of a single cell (magenta spot) in the center of the wing, the surrounding cells start to migrate towards the wound (Figure 21A+B, Movie 4+10). The overexpression of kinase dead Src42A has no effect on cell morphology. Cell speed mean of the cells is slightly but not significantly reduced (Figure 21C). Further, the cell bias angle as an indicator for

directionality shows no significant differences in comparison to wild type wound response (Figure 21, D+D´).

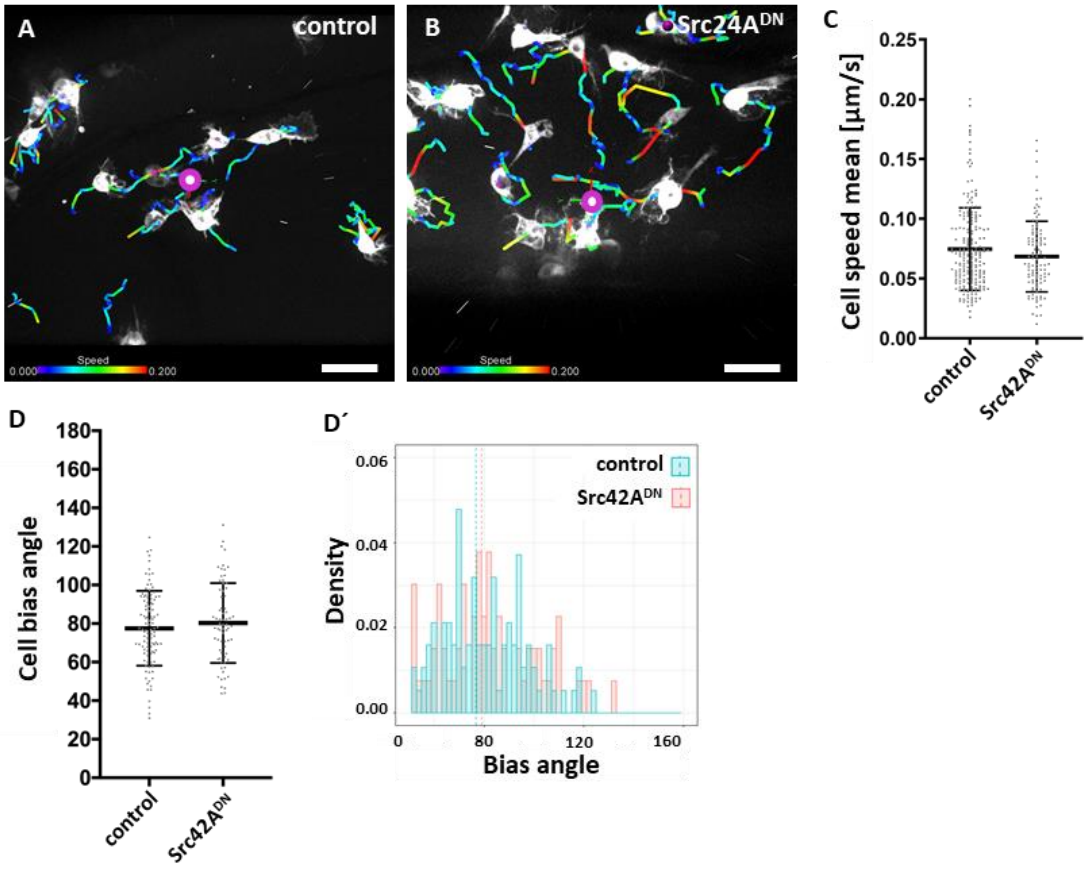

Figure 21: Overexpression of kinase dead Src42A does not alter wound response of *Drosophila* macrophages. (A+B) Stills of time laps images of directed macrophage migration upon wounding of a single cell (magenta dot in the center). Cells were imaged for 30 minutes after ablation in a 30 second interval and tracked afterwards using Imaris. Trajectories with speed color code indicate that wild type and Src42A^{DN} overexpressing macrophages migrate towards the wounding site. (C+D) Graphs are depicted in a scatter dot blot with bars indicating mean and SD. *** = $p \leq 0.001$ (Mann-Whitney-U-Test). In the bias angle histogram one bar depicts the accumulated density of 3 °. Dotted line indicates the median angle of the corresponding distribution. Speed (C) as well as cell bias is not altered in macrophages overexpressing Src42A^{DN}. Scale bar = 20 µm.

Conclusively, Src42A overexpression of either the dominant negative construct or the constitutive active version causes severe defects in 2D randomly migrating macrophages in *Drosophila* white prepupae. These defects have to be considered when further investigating directed migration upon wound signals. However, diverging from previous data, macrophages expressing a kinase dead Src42A transgene still response to wound signals almost as effective as wild type. Hence, these results challenge previously reported outstanding role of Src42A kinase in wound response (Evans et al., 2015).

3.5 Functional characterization of non-receptor tyrosine kinases Abelson function in macrophages

Abl is known for its oncogenic function and appears to be a potential target for corresponding leukemia treatment. Under physiological conditions, Abl is described as being involved in many actin-dependent processes like axon guidance, cell morphogenesis and migration in both vertebrates and invertebrates (Bradley and Koleske, 2009; Fogerty et al., 1999; Gertler et al., 1989). Nevertheless, because the diversity of functions and effector targets the normal cellular function is still not completely understood in its complexity. Abelson's SH2 and SH3 domains as well as the Proline rich motive offer important interaction sites for several other proteins. Many of these interacting proteins, like Ena, Abi and Trio are well known to regulate actin dynamics. During embryogenesis and in later pupal stages, Abl is highly expressed in developing musculature and in the nervous system. Recent publication on axonal growth cone dynamics postulated Abl to act as a mediator between formation of branched actin network and linear filamentous actin polymerization (Kannan et al., 2017).

Beside its function acting as a scaffold interaction platform for other actin regulators, Abl kinase function provides the ability to directly modulate target protein activity via phosphorylation. Abl is known to interact with WAVE and additionally changes its activity by phosphorylation (Leng et al., 2005; Plattner et al., 1999; Sossey-Alaoui et al., 2007; Stuart et al., 2006). Still, the physiological relevance remains poorly understood. Most of these results were obtained from cell culture experiments and have been rarely addressed *in vivo*, so far. As WAVE is known to regulate lamellipodia in *Drosophila* macrophages, the impact of Abl kinase on WAVE activity was further investigated using the macrophage system.

3.5.1 Loss of *abl* promotes lamellipodial cell spreading

Abl is hypothesized to play a critical role in local WAVE activation initiating site-specific branched actin formation. To fulfil this function, Abl is assumed to localize to the leading edge of lamellipodia. To analyze cellular localization of Abl in macrophages, isolated cells were stained with a *Drosophila* Abl specific antibody. In wild type macrophages Abl is mainly localized in the cytoplasm and at the nucleus. Only a weak staining is visible at the cell periphery. (Figure 22A). In macrophages isolated from *abl* mutant pupae (trans-heterozygous abl^{2}/abl^{4}) only a weak signal is detectable, which might be a background signal (Figure 22B). Re-expression of wild typic Abl (AblWT) construct in *abl* mutant background shows a similar staining comparable to wild type control with the same cellular localization (Figure 22C). Ectopically expressed wild type Abl is localized in the cytoplasm, at the nucleus and is also

detectable at the cell membrane (Figure 22D+D´). Macrophages expressing a dominant negative Abl transgene show a loss of nuclear staining while cytoplasmic signal is preserved and increased at the lamellipodium (Figure 22E+E´). In contrast, the ectopic expression of active form of Abl (BCR-Abl) leads to a less prominent staining compared to the overexpression of wild typic Abl or the dominant negative Abl transgene (Figure 22F+F´).

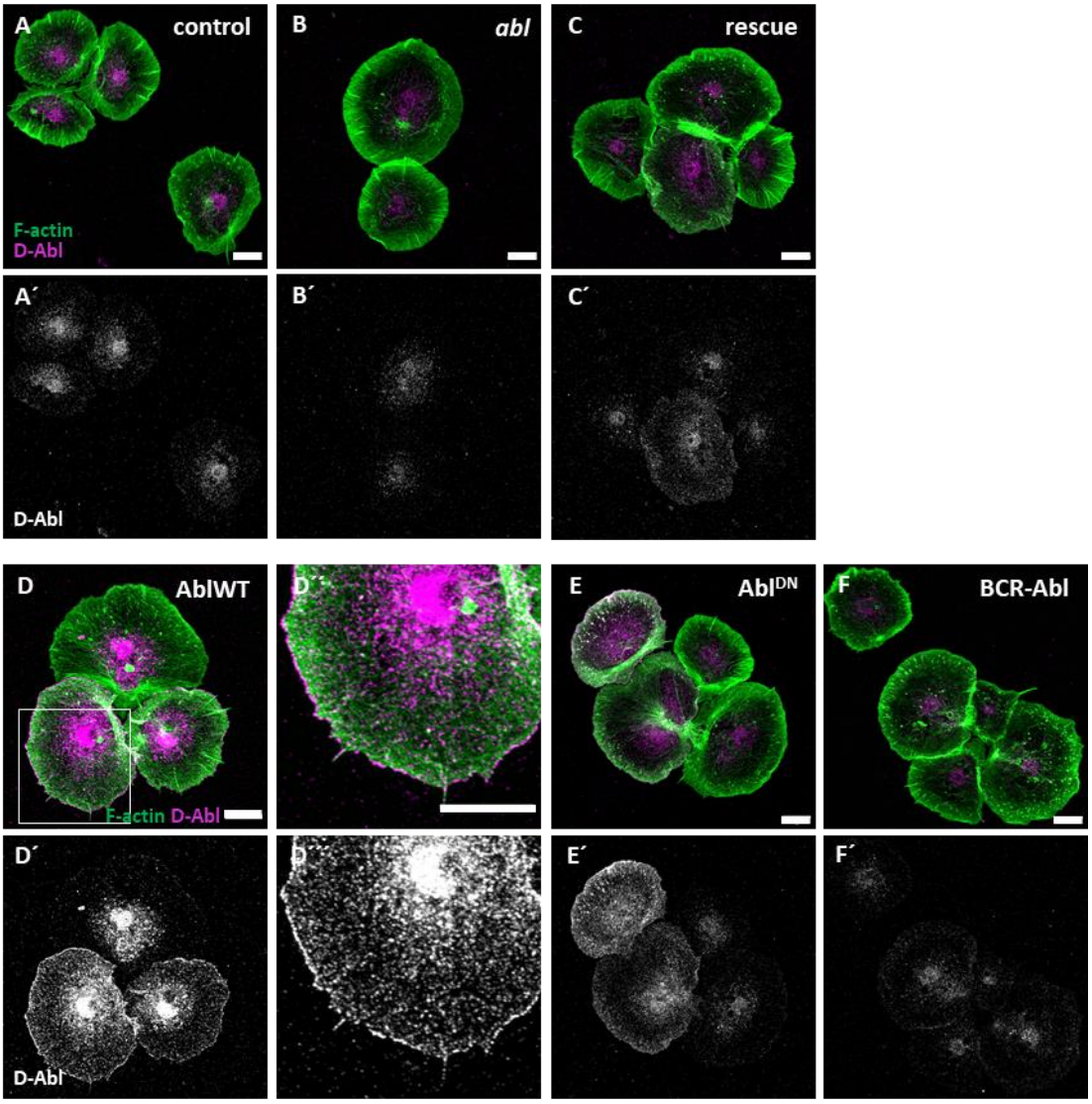

Figure 22: Abl is localized at the membrane as well as in the nucleus. (A-F) Isolated pupal macrophages plated on ConA and stained for F-actin and Abl (staining color code is indicated). (A) Abl expression is weak in wild type macrophages but can be detected in the cytoplasm and the cell periphery and, (B) only a weak cytoplasmic signal is detectable in *abl* mutant macrophages. (C) Expression of AblWT in *abl* mutant macrophages shows the same localization as wild type macrophages. (D-F) Macrophage specific (*hmlΔ*-Gal4) overexpression of indicated Abl constructs. AblWT is localized at the membrane and the nucleus (D-D´´´). Scale bar = 10 µm.

To characterize Abl function in *Drosophila* macrophages, the morphology of isolated macrophages from *abl* mutant pupae were compared with wild typic cells. *abl* mutant macrophages exhibit a broad lamellipodium and no drastic changes in morphology (Figure 23A+B). However, *abl* mutant cells in more detail show them to be increased in size as well as in roundness in compression to wild type macrophages (Figure 23C+D). The same can be observed in macrophages when kinase dead Abl transgene (Abl^{DN}) was specific overexpressed in macrophages. These results can be reproduced in larval as well as prepupal macrophages (Supplementary Figure 5).

Further, in *abl* mutant macrophages 30 % show a round cell morphology, whereas in wild type cells less than 10 % show this specific cell shape (Figure 23E). It can be concluded that the loss of Abl kinase function promotes cell spreading of macrophages.

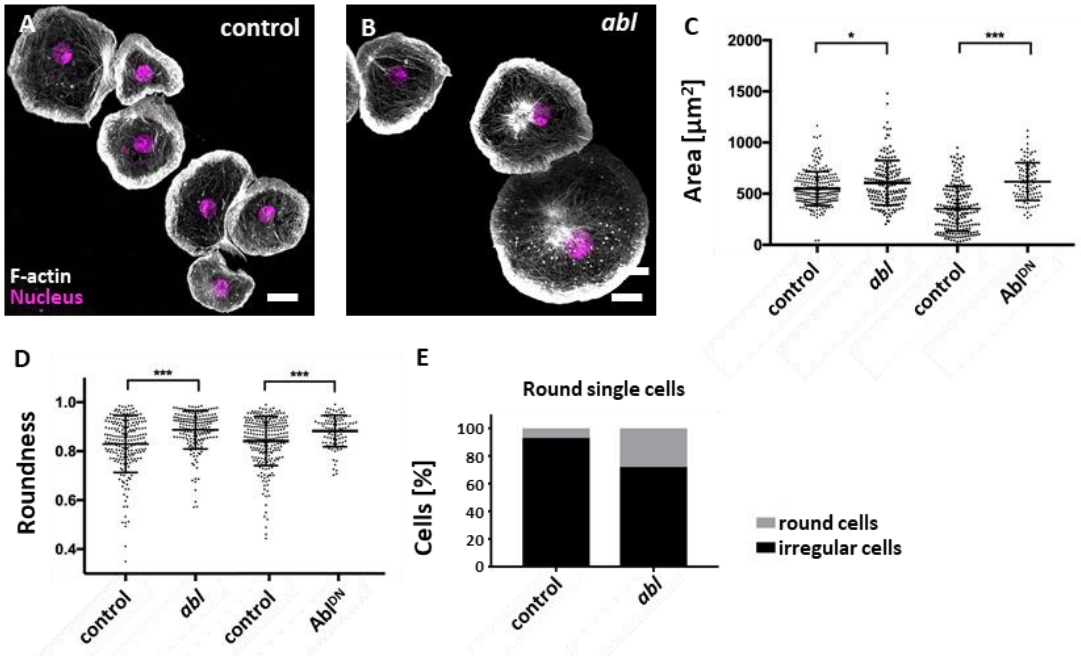

Figure 23: *abl* mutant macrophages were increases in size and roundness. (A+B) Isolated pupal macrophages plated on ConA stained for F-actin (white), nucleus (magenta). Wild typic and *abl* mutant cells both exhibit a broad lamellipodium. (C) Cell shape parameter area and (D) roundness are depicted in a scatter dot blot with bars indicating mean and SD. *** = $p \leq 0.001$ (Mann-Whitney-U-Test). Abl mutant macrophages and macrophages expressing Abl^{DN} construct are increased in size (C) and round rounded up (D) in comparison to their corresponding control. (E) The ratio of round cells to irregular shaped cells is shown, counted in overview images. In *abl* mutant macrophages the number of round cells is increased. Genotypes are indicated. Scale bar = 10 µm.

3.5.2 Random migrating macrophages show reduced explorative behavior in the absence of Abl

The aforementioned results showed the loss of *abl* on influences cell morphology in roundness and size of the cells. To further dissect the impact of Abl on actin dynamics, random migration of pupal macrophages was characterized *in vivo*.

Wild type cells were polarized, with a broad lamellipodium pointing in the direction of migration. In contrast *abl* mutant cells exhibit large protruding lamellipodia with no clear asymmetry (Figure 29A+A´, B+B´). Cell trajectories show wild type macrophages travel long distances within 20 minutes acquisition time (Figure 29A, Movie 11). In contrast, *abl* mutant cells only migrate in region around their origin (Figure 29B, Movie 12). However, migration speed is not impaired in *abl* mutant macrophages (Figure 29D). Unfortunately, the re-expression of wild typic Abl in *abl* mutant background show a slight increase in speed, what has to be considered for further interpretation (Figure 29D, Movie 13). In comparison to wild type macrophages, *abl* mutant cells' persistence is significantly decreased, indicated by an increase in cell persistence angle (Figure 24C and C´). However, the re-expression of wild typic Abl did not rescue cell persistence, challenging the expected effect of the loss of Abl. Further, the cell motion straightness shows a slight but not significant decrease (Figure 24E). Displacement from the origin was calculated to determine the "explorative activity" of a cell. As the parameter "displacement" is highly influenced by the acquisition duration, the track length and speed of the cells and the likelihood of randomly migrating cells returning to their origin by chance is increased over time, the displacement is normalized by time. It turned out that loss of *abl* results in drastically reduced displacement from the origin over time (Figure 24F). The loss of explorative activity could be rescued by re-expressing of wild typic Abl in *abl* mutant background (Figure 24F).

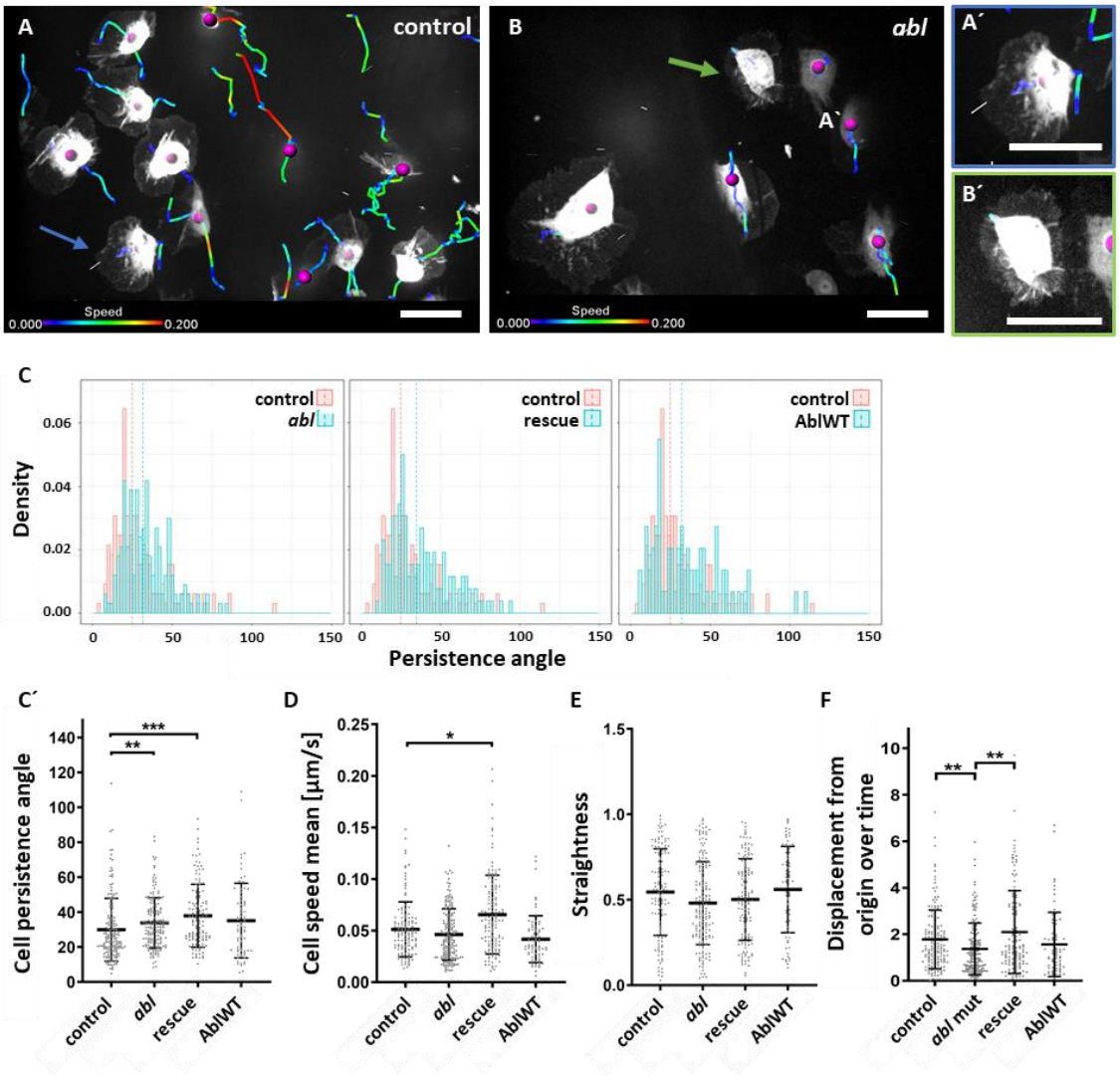

Figure 24: Loss of *abl* impairs explorative behavior of macrophages. (A-B) Still images of random migrating pupal macrophages. Cells are tracked with Imaris and trajectories are depicted with speed-color code (in µm/s). (A) Wild type control macrophages expressing cytosolic eGFP migrating constantly. (A, green arrow, A´ closeup) Cells are polarized with a leading edge with characteristic broad lamellipodium. (B, green arrow, B´ closeup) In *abl* mutant macrophages lamellipodium is surrounding the whole cell. (C-F) Graphs are depicted in a scatter dot blot with bars indicating mean and SD. *** = $p \leq 0.001$ (non-parametric multiple comparison test). In the bias angle histogram one bar depicts the accumulated density of 3 °. Dotted line indicates the median angle of the corresponding distribution. (C) In *abl* mutant cells persistence is decreased but cannot be rescued by re-expression of Abl. (D+E) Cell speed and straightness is not altered (F) Displacement from the origin over time is a value for the explorative behavior of the cells. *abl* mutants show a decreased "explorative ability" and can be rescued by re-expression of Abl. Scale bar = 20 µm.

Previous results demonstrated that the absence of Abl kinase results in lager and round cells, which can be phenocopied by overexpressing dominant negative Abl transgene. Further, the overexpression of BCR-Abl, the kinase active ortholog, causes massive cell growth in isolated

macrophages. To evaluate the influence of kinase activity on cell motion, either dominant negative or BCR-Abl was overexpressed in macrophages. Additionally, RNAi mediated knock-down of *abl* was performed.

Similar to the observations in *abl* mutant macrophages, the expression of the kinase dead transgene of Abl (dominant negative Abl, Abl^{DN}) and the RNAi meditated suppression has negligible effects on cell speed, persistence, and straightness (Figure 25B-D). Nevertheless, the explorative behavior indicated by the displacement from the origin over time in RNAi mediated knock down of *abl* in macrophages and of macrophages, expressing ectopically dominant negative Abl, is significantly reduced (Figure 25E). This finding is consistent with the migratory behavior of *abl* mutant macrophages. Together these results suggest that kinase activity of Abl is a critical factor for the explorative behavior of randomly migrating macrophages.

Under physiological conditions *in vivo* in the living pupa, the overexpression of the kinase active form BCR-Abl results in large cells with huge lamellipodia (Figure 25A, Movie 14). The analysis of the random migration of these cells show that they are almost unable to migrate, which is reflected in a drastic reduction of cell speed mean (Figure 25B). Additionally, cell persistence is significantly decreased, which is also depicted in a shift in the distribution of the overall persistence angle towards lager angles (Figure 25C+C´). These data are consistent with the motion straightness of the cells, which is accordingly significantly decreased (Figure 25D). Because of the huge differences in cell speed in comparison to control cells, displacement from the origin by time is not a suitable value.

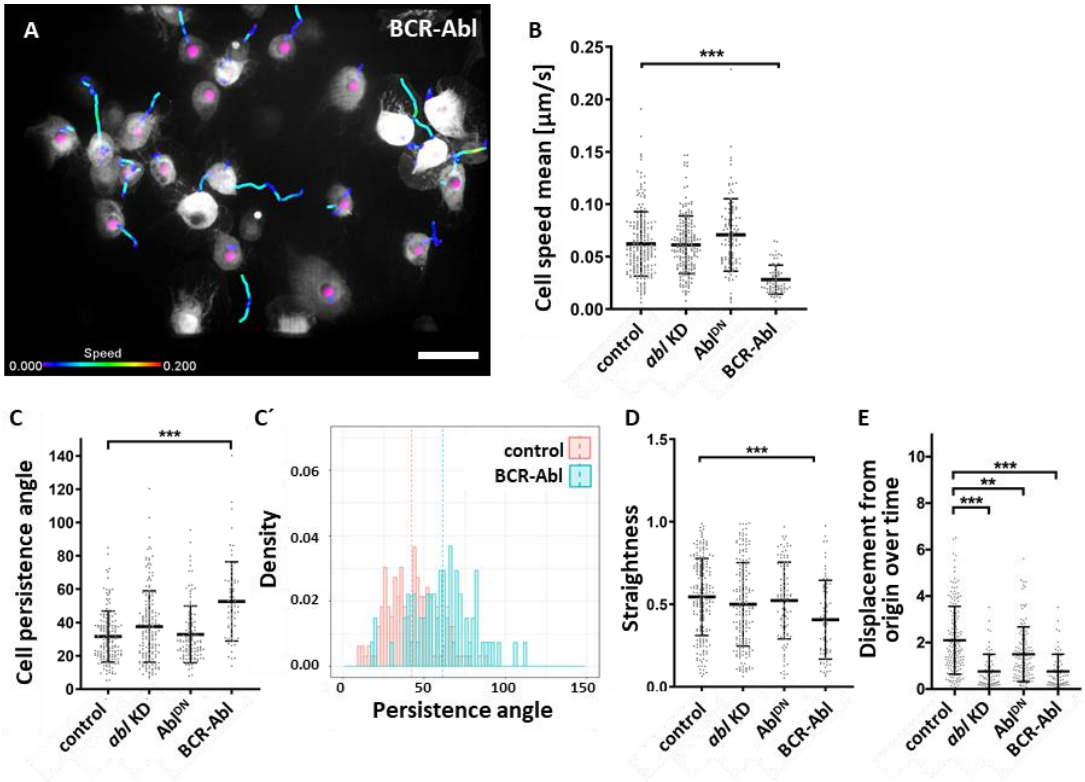

Figure 25: Overexpression of kinase active Abl impairs migration and kinase dead Abl reduced exploratory behavior. (A) Still images of random migrating pupal macrophages. Cells were tracked with Imaris and trajectories are depicted with speed-color code (in µm/s). Morphologically, overexpression of kinase active BCR-Abl results in gigantic cells. (B-E) Graphs are depicted in a scatter dot blot with bars indicating mean and SD. *** = $p \leq 0.001$ (non-parametric multiple comparison test). In the bias angle histogram one bar depicts the accumulated density of 3 °. Dotted line indicates the median angle of the corresponding distribution. (B) Cell speed is not altered when overexpressing kinase dead Abl (DN) or in *abl* KD macrophages but drastically reduced overexpressing BCR-Abl. (C+D) Cell persistence and straightness is reduced in macrophages overexpressing BCR-Abl and not effected in abl KD or kinase dead overexpression. (E) Displacement from the origin over time is a value for the explorative behavior of the cells. *abl* KD and overexpression of kinase dead Abl show a decreased explorative ability. As cell speed is reduced in BCR-Abl overexpressing macrophages, this value is not meaningful. Scale bar = 20 µm.

In conclusion it has been shown that loss of *abl* has mild effects on cell morphology of random macrophage migration *in vivo.* Even more outstanding is the tremendous negative impact of the loss of *abl* as well as the interference with kinase activity on the explorative activity of the cells. Consistent with these findings, in *abl* mutant cells cell speed is not affected but the cells tend to stay close to their origin. Further, the overexpression of the kinase active ortholog BCR-Abl causes reduced speed and less persistence of macrophages randomly migrating in prepupae. Although these large macrophages exhibit broad lamellipodia, their migration is almost blocked.

3.5.3 Wound response is not affected by the loss of *abl*

For an effective wound response, the correct organization of the actin cytoskeleton is as fundamental as for random migration. Previous experiments have shown that in the absence of *wave* macrophages were still able to respond to wound signals but are highly impaired in their migratory behavior. Noteworthy is the reduction of the explorative behavior in comparison to wild type macrophages. This might in particular influence the responsiveness of *abl* mutant macrophages upon wounding.

To determine the role of Abl in directed wound response of macrophage, ablation experiments of a single cell in the pupal wing were performed. Upon wounding wild type macrophages as well as *abl* mutant macrophages switch from random to directed migration towards the wounding site indicated by cell trajectories (Figure 26A+B, Movie 4+16). *abl* mutant cells does not interfere with cell speed nor with the bias angle indication the directionality of migration towards the wound (Figure 26D, E+E´). When removing one *wave* gene copy in *abl* mutant background, analysis showed a reduction in cell speed mean (Figure 26, D) in comparison to wild type cells but the directionality indicated by the cell bias angle is not significantly affected.

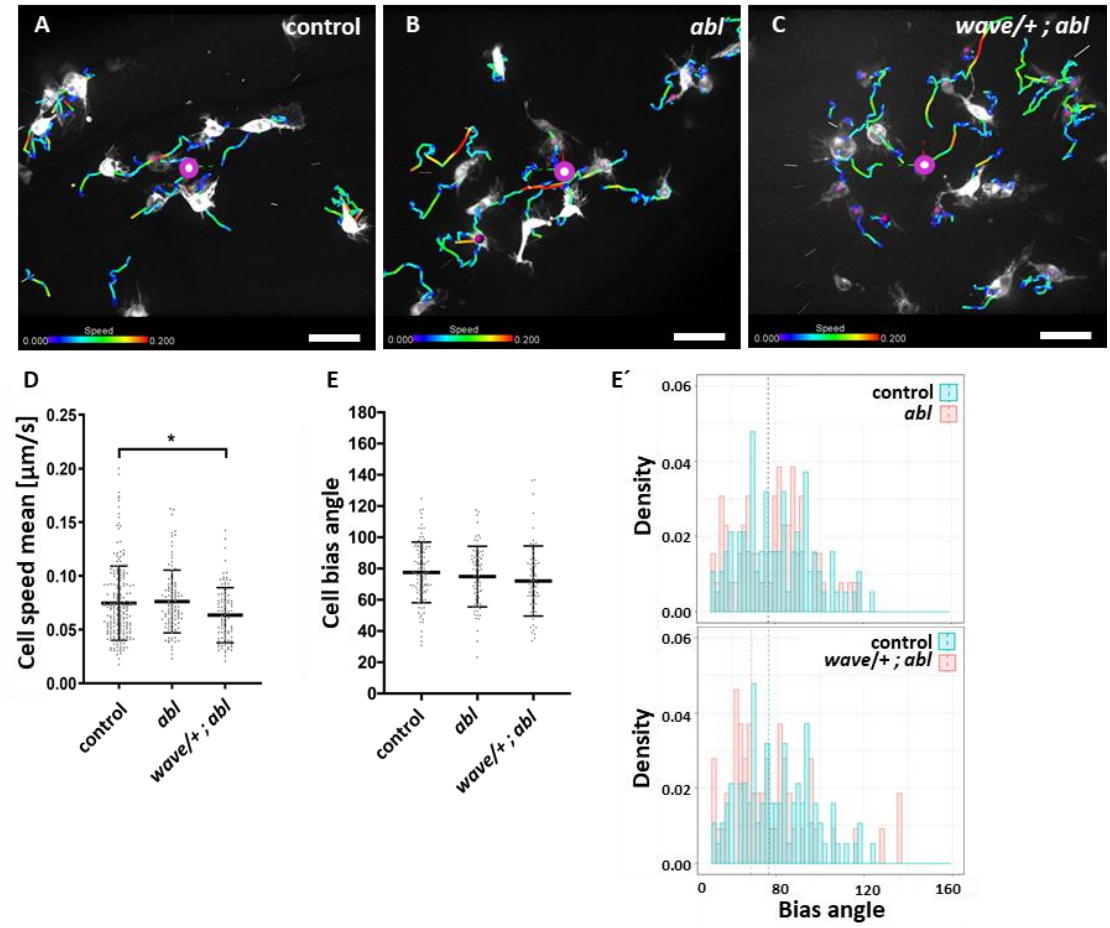

Figure 26: *abl* mutant macrophages still respond to wound signals. (A-C) Stills of time laps images of directed macrophage migration upon wounding of a single cell (magenta dot in the center). Cells were imaged for 30 minutes after ablation in a 30 second interval and tracked afterwards using Imaris. Trajectories with speed color code indicate that wild type, *abl* depleted macrophages and *abl* depleted macrophages lacking one copy of *wave* migrate towards the wounding site. (D+E) Graphs are depicted in a scatter dot blot with bars indicating mean and SD. *** = $p \leq 0.001$ (non-parametric multiple comparison test). In the bias angle histogram one bar depicts the accumulated density of 3 °. Dotted line indicates the median angle of the corresponding distribution. (D) Cell speed mean is not altered in *abl* mutant cells but reduced when eliminating one copy of *wave.* (E) Cell bias angle is not affected in *abl* mutant cells as well as in *abl* mutant macrophages lacking one copy of *wave.* Scale bar = 20 µm.

In conclusion, the absence of the tyrosine kinase abl has no effect on the responsiveness of cells on cell damage. Removing one gene copy of *wave* leads to a slowdown of cells, whereas the directionality is not impaired. Nevertheless, to further understand the underlying principle it has to be investigated whether the loss of one gene copy of *wave* alone shows similar effects.

3.5.4 Src42A protein level is increased in *abl* mutant macrophages and might act compensatory

Abl kinase itself can be activated by tyrosine phosphorylation. One known upstream regulator is Src kinase (Brasher and Van Etten, 2000; Nagar et al., 2003; Plattner et al., 1999; Schindler et al., 2000). Abl and Src kinase show a high structural homology (Figure 7). Furthermore, Src has been described to influence WAVE activity and influence the migration of cells (Ardern et al., 2006; Evans et al., 2015). The hypothesis can be made that Src is able to substitute for the loss of Abl. In *abl* mutant macrophages protein level of Src42A, was increased about 1.2-fold (Figure 27A and A').

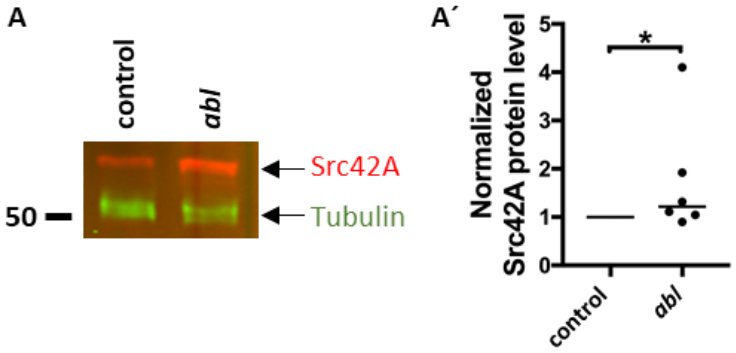

Figure 27: Src42A protein level is slightly increased in *abl* mutant macrophages. (A) Western Blot analyses of isolated larval macrophages. Genotype and antibody staining are indicated. (B) Quantification of Src42A protein level normalized to tubulin expression. Control expression is set to 1.0. Bars depict the median (*abl* mut = 1.214). *** = $p \leq 0.001$ (Mann-Whitney-U-Test).

Increased Src42A level in *abl* mutant background could indicate a compensatory effect. To further address this question, gene dosage experiments for *src42A* in *abl* mutant background were performed and analyzed regarding random macrophage migration. s*rc42A* mutants are lethal and therefore cannot be analyzed in post-embryonal stages.

Cells lacking one gene copy of *src42A* in *abl* mutant background show a wild typic cell morphology (Figure 28B, Movie 16). Cell speed shows no significant difference compared to wild type macrophages or *abl* mutant cells (Figure 28C). The reduction by one gene copy of *src42A* in *abl* mutant background lowers the value of displacement from the origin in a similar scale as the *abl* mutation alone and have no additional effect (Figure 28F). Noteworthy, cell persistence as well as cell motion straightness is decreased in *abl* mutant macrophages lacking one copy of *src42A* (Figure 28D+D´). The loss of one gene copy *src42A* in wild typic background already shows a significant increase in cell speed which has to be taken into account in further conclusions (Figure 28, C). Additionally, cell persistence is decreased in control cells lacking one gene copy of *src42A* (Figure 28, D+D´).

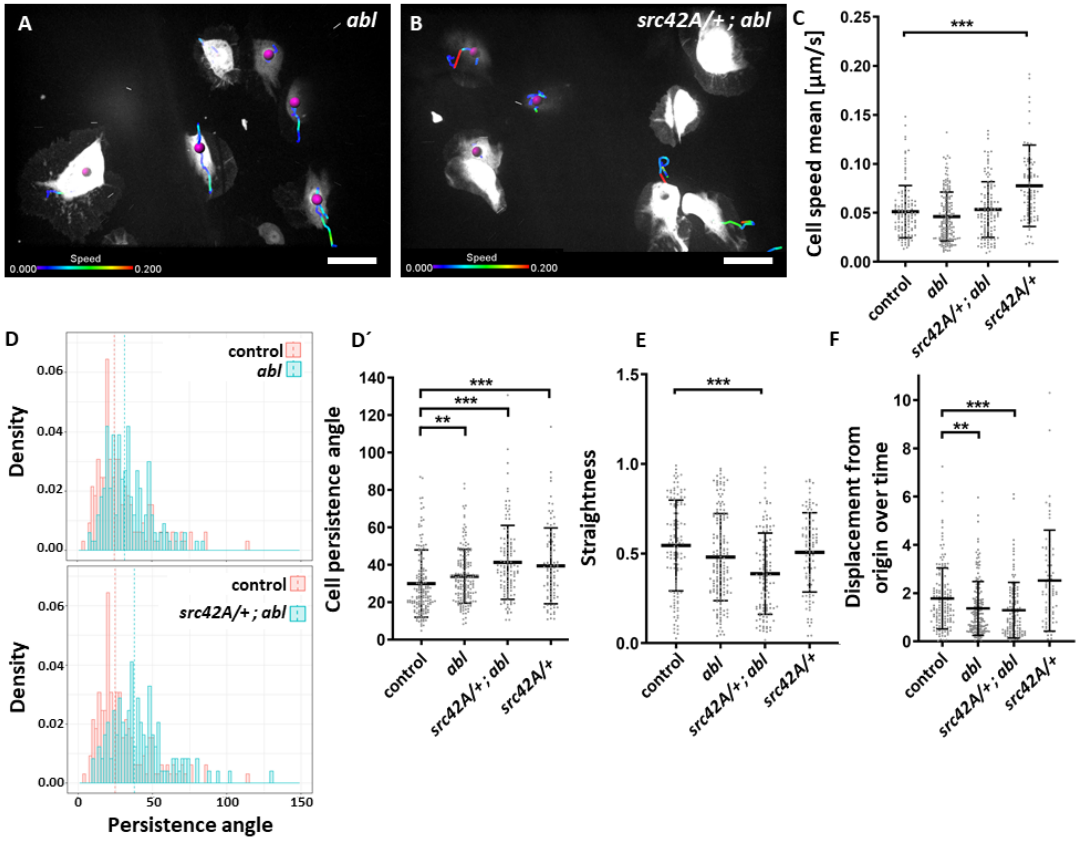

Figure 28: Random macrophage migration in *src42A* gene dosage experiments. (A+B) Still images of random migrating pupal macrophages. Cells were tracked with Imaris and trajectories are depicted with speed-color code (in µm/s). (B) *abl* mutant cells lacking one copy of *src42A* show no morphological defects (C-F) Graphs are depicted in a scatter dot blot with bars indicating mean and SD. *** = $p \leq 0.001$ (non-parametric multiple comparison test). In the bias angle histogram one bar depicts the accumulated density of 3 °. Dotted line indicates the median angle of the corresponding distribution. (C) cell speed is not reduced in *abl* mutant cells lacking one copy of *src42A*. The reduction of one copy of *src42A* in wild typic background leads to increased cell speed. (D) In *abl* mutants lacking one copy of *src42A* cell persistence further decreased but not significantly to *abl* mutation alone. (E) Cell straightness is reduced in *abl* mutants lacking one copy of *src42A*. (F) Displacement from the origin over time is a value for the explorative behavior of the cells. *abl* mutants lacking one copy of *src42A* show a decreased explorative ability comparable to *abl* mutants alone. Scale bar = 20 µm.

In summary, it was demonstrated that Src42A protein level is slightly increased in *abl* mutants. Gene dosage experiment in *abl* mutant background shows that the reduction of one gene copy of *src42A* results in a further decrease in the cell persistence and straightness. However, at least for cell persistence already the reduction of Src42A alone shows a severe effect. This might indicate an Abl independent effect on cell speed and persistence, when reducing *src42A* level. Whether Src42A has a compensatory effect on the loss of Abl cannot be demonstrated conclusively.

3.5.5 *abl* depleted macrophages show an increased WAVE membrane localization

The loss of *abl* is predicted to interfere WAVE activity and with WAVE membrane recruitment. To address this question, the localization of WAVE in wild type macrophages is compared to the localization in *abl* mutant cells. The analysis of WAVE at the membrane show WAVE membrane-localization is increased in *abl* mutants (Figure 29A+A´, B+B´). To compare different cell sizes, the cell perimeter is normalized to 100 % and the median intensity of each tenth of the cell's perimeter was plotted with the corresponding confidence interval (CI) (2.5.3 Fluorescence intensity measurement). The quantification shows an overall and significant increase of WAVE membrane localization (Figure 29C). By subtracting WAVE wild type membrane fluorescence intensity from intensity in *abl* mutant cells, a 1.4-fold increase in WAVE along the whole membrane can be (Figure 29C´). In contrast, correlated total cell fluorescence (CTCF) is only slightly increased in *abl* mutant macrophages (Figure 29D, 2.5.3 Fluorescence intensity measurement). This indicates that the overall WAVE level is stable and only membrane localization of WAVE in influenced in *abl* mutant macrophages.

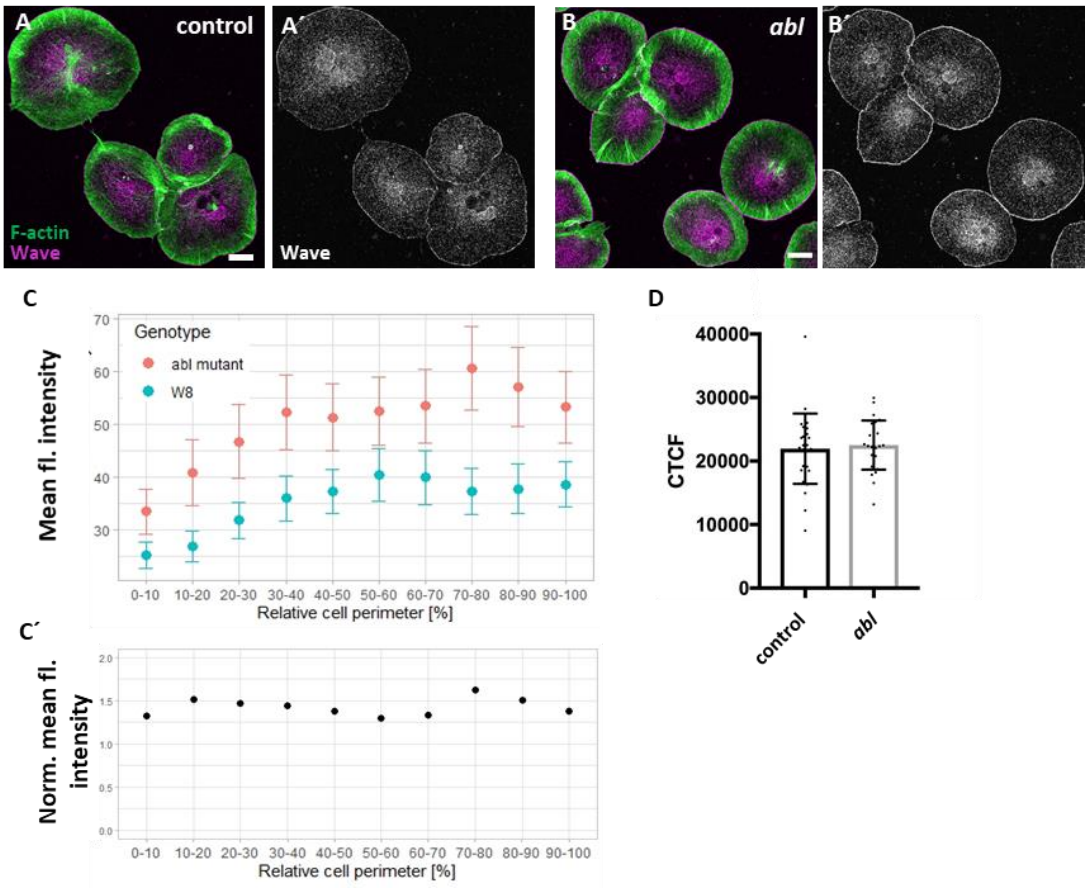

Figure 29: WAVE membrane localization is increased in abl mutant cells. (A+B) Isolated pupal macrophages plated on ConA and stained for F-actin and WAVE (color code for staining is indicated). WAVE membrane localization is increased in abl mutant macrophages. (C) Measurement of WAVE mean fluorescence intensity at the membrane. Cell perimeter is normalized to 100 %. Bars indicate the median of mean fluorescence intensity of a tenth of the cell perimeter and 95 % CI. WAVE mean

fluorescence intensity is increased around 1.4-fold at whole membrane (C´). (D) Measurements of the correlated total cell fluorescence (CTCF). Bars depicts the mean and SD. *** = $p \leq 0.001$ (Mann-Whitney-U-Test). Abl macrophages show only a slight but not significant increase in total WAVE amount by analysing the CTCF. Scale bar = 10 µm.

To confirm these findings, WAVE protein level in *abl* mutant macrophages was analyzed in quantitative Western Blot analysis. WAVE expression is normalized against internal tubulin expression control. In all three independent experiments, WAVE levels are increased in comparison to wild type expression. In median, the expression is increased 1.2-fold. However, the three independent data points show a huge variance, therefore drawing a final conclusion on the effect of the loss of *abl* on WAVE protein level is not possible (Figure 30, Supplementary Figure 7).

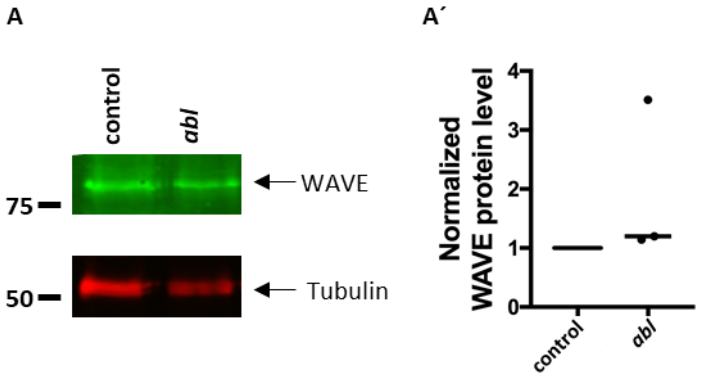

Figure 30: WAVE protein level is slightly increased in *abl* mutant macrophages. (A) Western Blot analyses of isolated larval macrophages. Genotype and antibody staining are indicated. (B) Quantification of WAVE protein level normalized to tubulin expression. Control expression is set to 1.0. Bars depict the median (*abl* mutant = 1.197). *** = $p \leq 0.001$ (Mann-Whitney-U-Test). WAVE is slightly but not significantly increased (also compare Supplementary Figure 7).

Conclusively, loss of Abl leads to increased membrane localization of WAVE continuously by 1.4-fold along the entire membrane. Further, calculating the CTCF show slightly but not significantly increase of WAVE on a cellular level. Further, quantitative Western Blot analyses of the protein level display an increased about 1.2-fold. However, because of a broad distribution of the data point this result needs to be confirmed by additional repetitions.

3.5.6 *wave* reduction in *abl* mutant background further impairs random cell migration

Previous results demonstrated that WAVE localization at the membrane increases in *abl* mutant macrophages. To analyze whether the resulting migratory phenotype is caused by only

an increased presence of WAVE, gene dosage experiments were performed. Each, one gene copy of *wave* is eliminated in *abl* mutant background and in wild typic background.

Control cells lacking one copy of *wave* show no morphological changes and the measured parameters (speed, persistence, straightness, and displacement from the origin) are not affected in these cells in comparison to wild type (Figure 31C-F). The reduction of one *wave* copy alone has no effect on random migrating macrophages.

abl mutant cells missing one copy of *wave* show already morphological differences in comparison to wild type but also to *abl* mutant cells (Figure 31A and B). *abl* mutant cells exhibit a broad lamellipodium (Figure 31A). The reduction of one gene copy of *wave* results in the frequent appearance of filopodial structures (Figure 31B´, Movie 17). In these cells, the persistence and straightness significantly decrease in comparison to wild type cells and slightly in comparison to *abl* mutant cells (Figure 31C and E, Movie 17). Those cells show also a reduced exploratory behavior, indicated by the decreased displacement of the cells for the origin similar to *abl* mutant macrophages (Figure 31F).

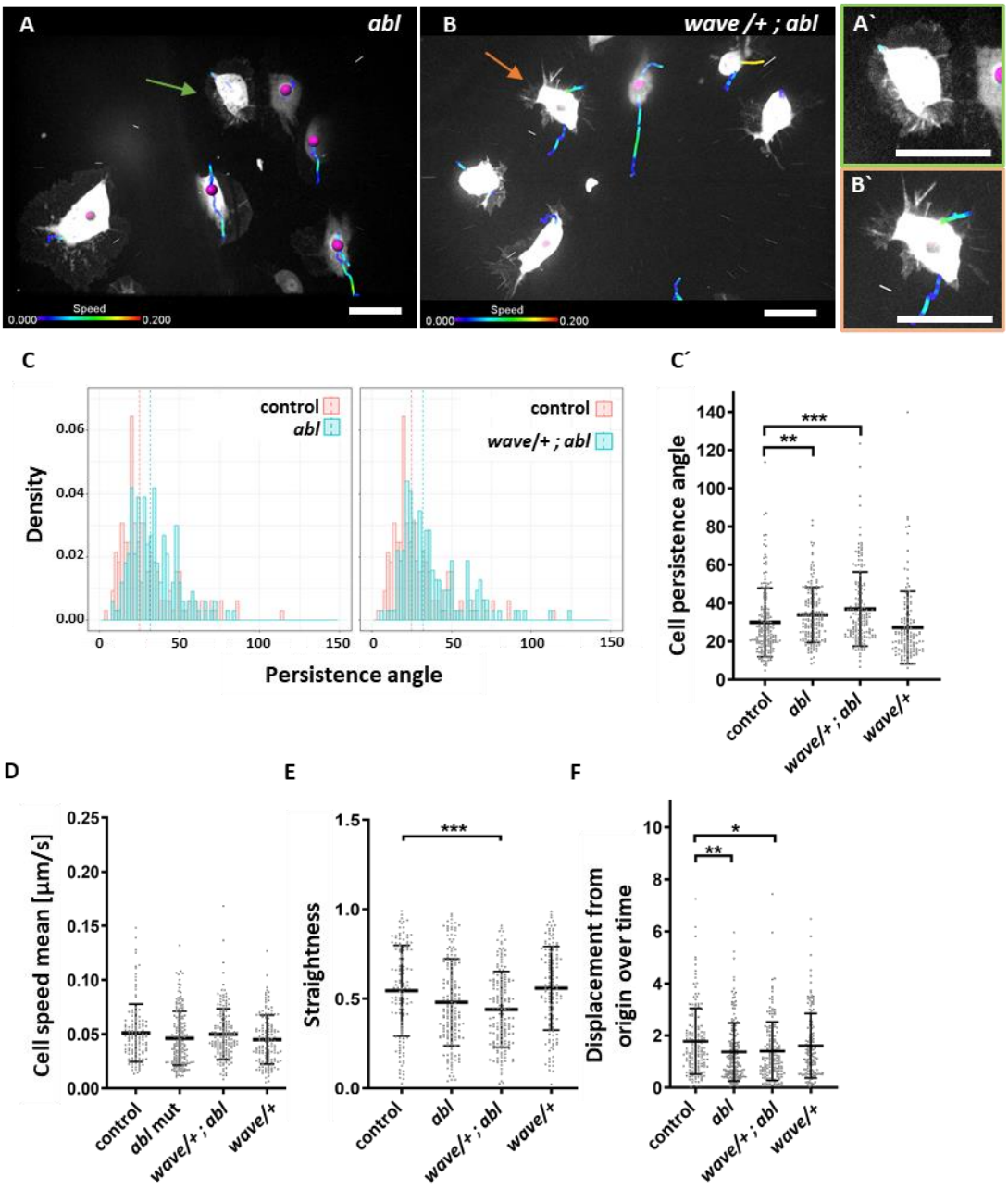

Figure 31: Random macrophage migration in wave gene dosage experiments. (A-B) Still images of random migrating pupal macrophages. Cells were tracked with Imaris and trajectories are depicted with speed-color code (in µm/s). (A, green arrow, A´ closeup) In abl mutant macrophages the lamellipodium is surrounding the whole cell. (B, orange arrow, B´ closeup). Macrophages with only one copy of wave in abl mutant background show more filopodial structures. (C-F) Graphs are depicted in a scatter dot blot with bars indicating mean and SD. *** = $p \leq 0.001$ (non-parametric multiple comparison test). In the bias angle histogram one bar depicts the accumulated density of 3 °. Dotted line indicates the median angle of the corresponding distribution. (C) In abl mutants lacking one copy of wave cell persistence decreased further but not significant to abl mutation alone. (D) Cell speed is not altered. (E) Cell straightness is reduced in abl mutants lacking one copy of wave. (F) Displacement from the origin over time is a value for the explorative behavior of the cells. abl mutants lacking one copy of wave show a decreased explorative ability comparable to abl mutants alone. Scale bar = 20 µm.

Taken together it was shown that the reduction of one gene copy of *wave* in *abl* mutant background only slightly interferes with random cell migration. Persistence of the cells and straightness is further reduced. Additionally, filopodial structures were frequently visible.

3.6 Dissecting the impact of WAVE tyrosine residues in influencing actin polymerization

Phosphorylation is a post-transcriptional modification known to modulate protein folding, influencing their activity and binding ability. WAVE possesses several phospho-residues as potential targets for diverse kinases. The WHD and therein especially tyrosine residues Y153 and Y127 are highly conserved across species (Chen et al., 2010; Krause and Gautreau, 2014; Mendoza, 2013, 1.2.3 The influence of phosphorylation). The phosphorylation of these residues modulates WRC activity in cells by altering the binding affinity of Sra1 to the meandering region. Also, Y153 is targeted by Abl kinase, whereas Y127 residue is phosphorylated by Src42A kinase (Ardern et al., 2006; Leng et al., 2005; Mendoza, 2013). Until now, most studies are performed in cell culture and the impact on migration *in vivo* is barley addressed.

To investigate the impact of distinct tyrosine residues, WAVE transgenes were generated with either a transition of tyrosine to phenylalanine leading to a phospho-abolishing mutation (phospho-mutant) or tyrosine residues, where mutated to glutamic acid achieves a phospho-mimicking mutation. The tissue specific expression allows to further examine the distinct function of the single residues.

3.6.1 WAVE phosphorylation of Y153 induces F-actin formation

In order to determine the impact of phosphorylation of Y127 and Y153 on WAVE dependent F-actin assembly, phospho-mutant and phospho-mimicking constructs were overexpressed tissue-specifically in *Drosophila* macrophages. Isolated macrophages show a wild typic morphology with a broad lamellipodium (Figure 32A). To gain further insights, lamellipodia width was measured. Overexpression of the phospho-mimicking Y153E results in a significant increase of branched actin filaments in comparison to wild type cells (Figure 32B). However, the increase does not significantly differ when comparing WAVE Y153E to wild typic WAVE overexpression. Thus, this could be also an overexpression effect and needs to be investigated in a higher sample size (Figure 32B). The overexpression of the phospho-mimicking WAVE

Y127E does not alter lamellipodia width in comparison to wild type cells. Also, the WAVE transgenes with a mutation in WAVE tyrosine 127 and 153 show no significant increase in lamellipodia width (Figure 32B). On the other hand, the transition of tyrosine to non-phosphorylatable phenylalanine of either one or both tyrosine sides have no significant effects on lamellipodia width.

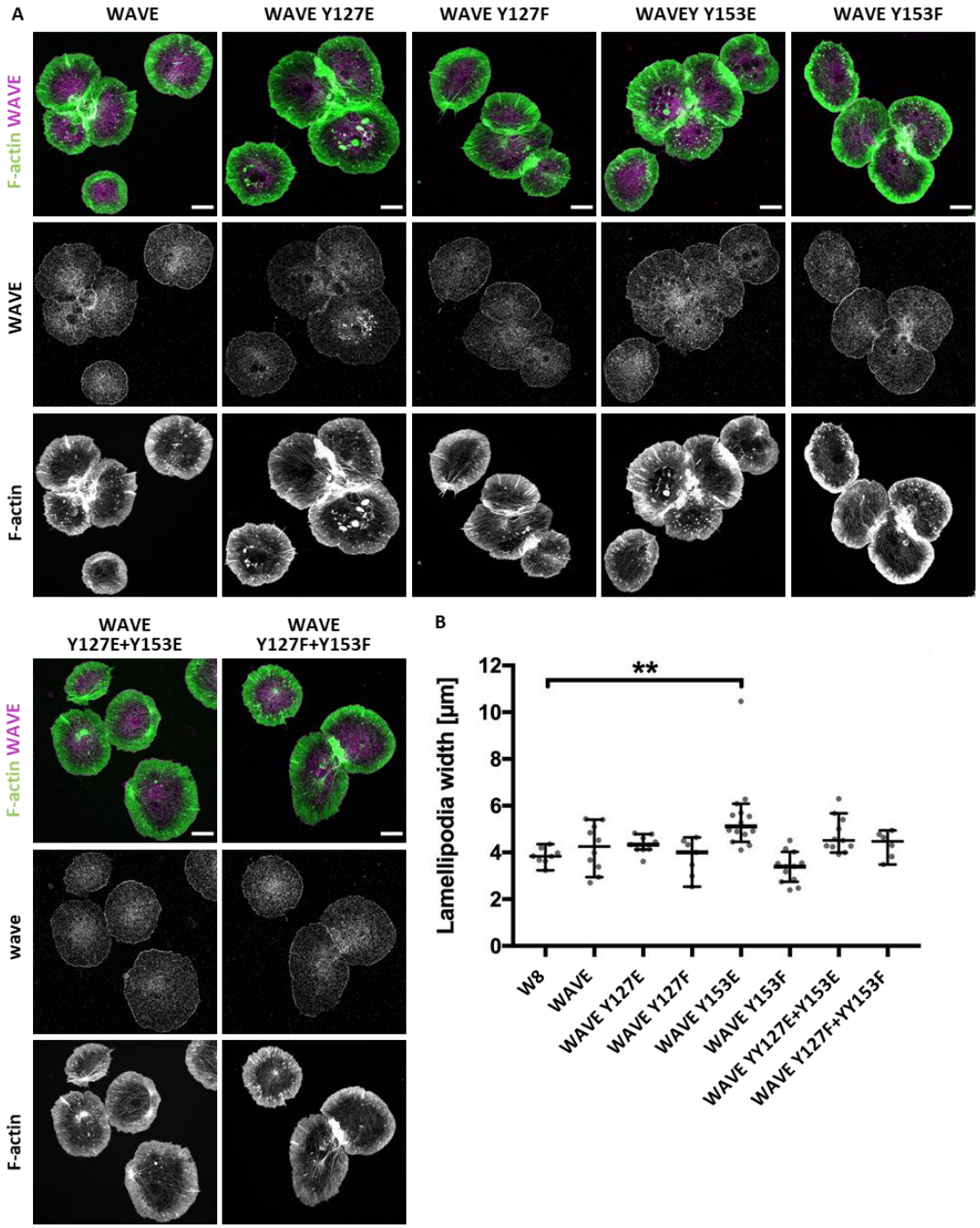

Figure 32: Overexpression of phospho-mimic WAVE Y153E leads to increase of branched actin structures. (A) Isolated pupal macrophages plated on ConA and stained for F-actin and WAVE (color code of staining is indicated). (B) Graphs are depicted in a scatter dot blot with bars indicating mean and SD. *** = $p \leq 0.001$ (non-parametric multiple comparison test). Lamellipodia width is measured as

indicator for branched actin formation. Overexpression of WAVE Y153E leads to increased lamellipodia width in comparison to wild type (W8) cells. Scale bar = 10 µm.

To further fortify this finding, phospho-mutant and phospho-mimicking WAVE were overexpressed in *Drosophila* imaginal wing disc by *en*-Gal4. The anterior-posterior altering expression pattern allows a direct internal comparison of endogenous actin formation versus overexpression dependent effects on F-actin level (2.5.5 Quantification of F-actin staining in imaginal wing discs). Therefore, wing discs were stained for WAVE expression and F-actin. The WAVE staining shows a homogenous expression of all constructs in the posterior site of the wing disc (Figure 33A). The analysis show that the overexpression of phospho-mimicking WAVE Y153E leads to an elevation of F-actin level (Figure 33A, red arrow). The quantification of a ratio between F-actin level of the anterior and posterior site confirms that overexpression of Y153E leads to an increase in F-actin formation (Figure 33B). In contrast, the overexpression of phospho-mimicking WAVE Y127E has no significant effect on F-actin assembly. Compared to wild type WAVE overexpression, the overexpression of phospho-mimicking WAVE with two mutated amino acids (Y127E+Y153E) shows only a slight but not significant increase in F-actin formation. The single or double tyrosine transition of Tyrosine to Phenylalanine (F) has no significant effect on F-actin level (Figure 33B).

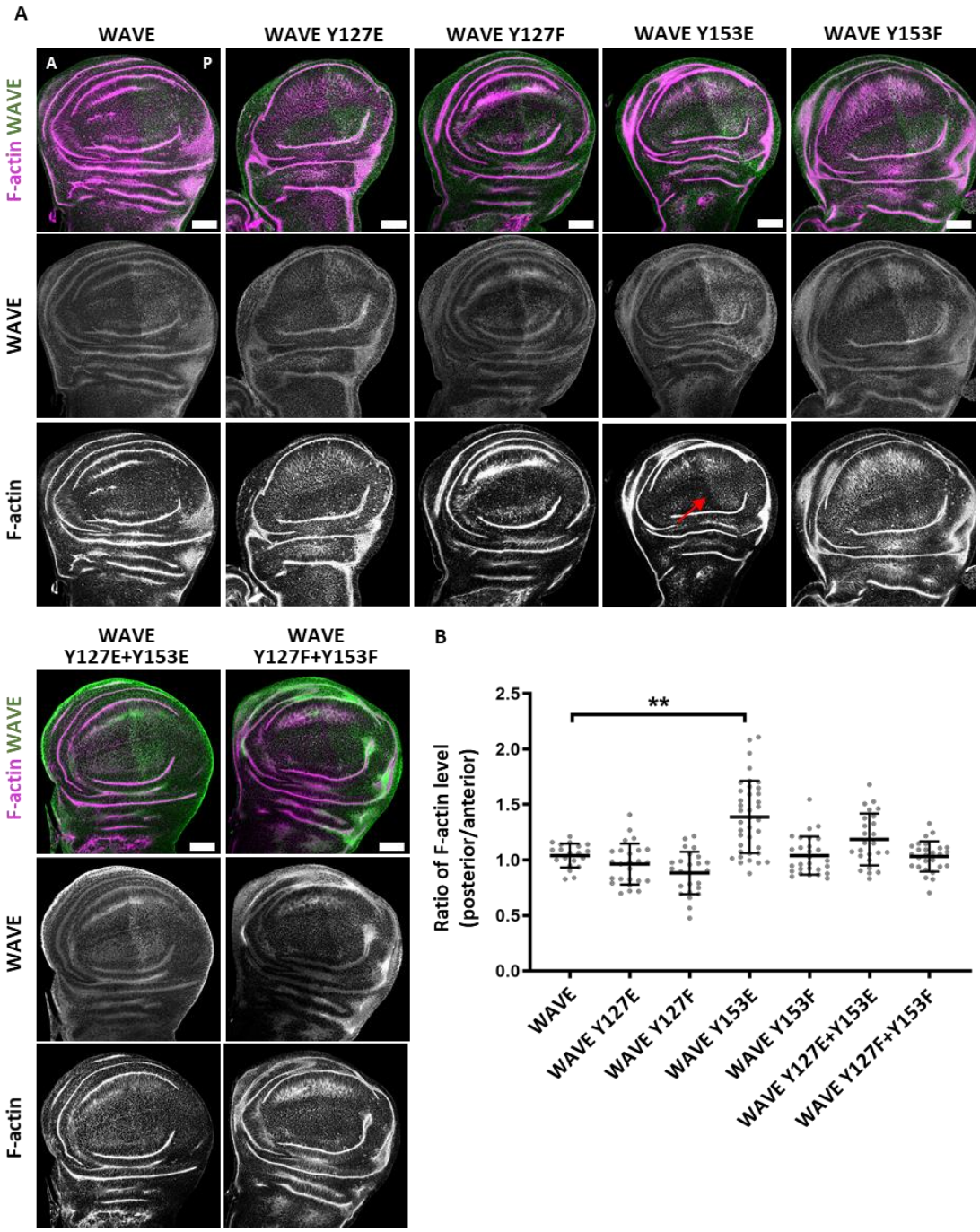

Figure 33: Segmental overexpression of phospho-mimic WAVE Y153E leads to an increase of F-actin level. (A) Isolated wing discs stained for F-actin and WAVE (color code of staining is indicated). Using en-Gal4 driver line constructs were expressed only in the posterior half (P, right) of the imaginal wing disc (anterior =A). WAVE staining is weakly increased in the posterior part due to overexpression. (B) Graphs are depicted in a scatter dot blot with bars indicating mean and SD. *** = $p \leq 0.001$ (non-parametric multiple comparison test). Ratio of F-actin level is depicted for indicated genotypes. F-actin polymerization ratio is increased in wing discs expressing phospho-mimic WAVE Y153E (A, red arrow). Scale bar = 40 μm.

To summarize these results, overexpression of phospho-mimicking WAVE Y153E leads to an increase of WAVE dependent formation of filamentous actin. This is confirmed by measuring the lamellipodia width in macrophages and by calculating the actin formation ratio in wing discs. Both results confirm WAVE phosphorylation of tyrosine 153 modulating WRC activity and directly inducing F-actin formation. However, the phospho-mimicking mutation of WAVE Y127E has neither an effect on lamellipodia width nor F-actin formation in wing disks. Additionally, also the double phospho-mimic version WAVE Y127E+E153E show in both experimental designs only a mild but not significant increase in actin polymerization activity and reduction, when comparing to overexpressing of WAVE Y153E alone.

3.6.2 Mutation of alone Y153 does not impede Abl-dependent WAVE phosphorylation

WAVE tyrosine residue Y153 is phosphorylated by Abl kinase. To test whether the absence of this single residue is sufficient to block Abl mediated phosphorylation of WAVE immune-precipitation experiments were performed. C-terminal myc-tagged wild typic WAVE or phospho-mutant Y153F were co-expressed with eGFP or BCR-Abl to induce phosphorylation. Co-expression control with eGFP shows no WAVE tyrosine phosphorylation while expression of BCR-Abl induced WAVE phosphorylation. Mutated WAVE Y153F still gets phosphorylated (Figure 34).

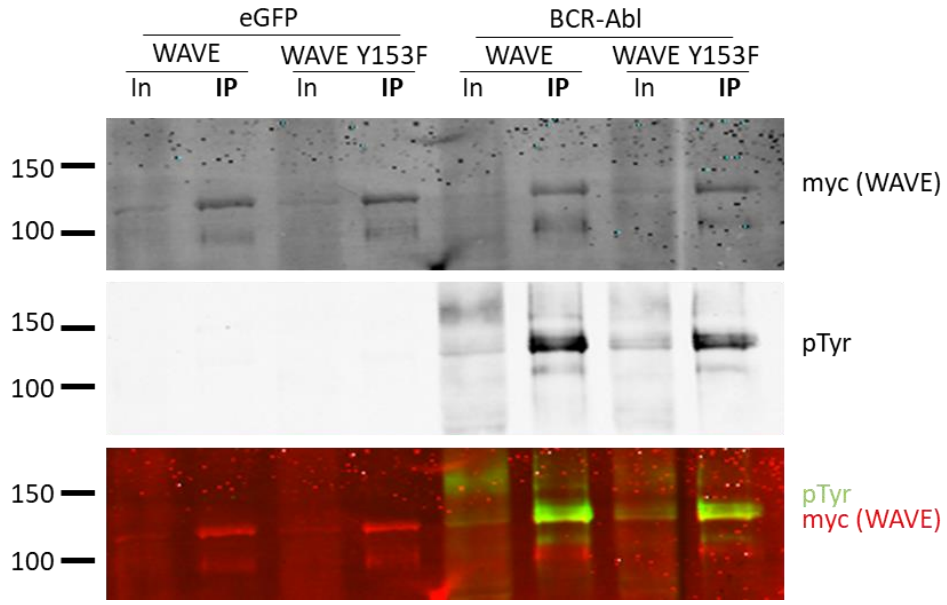

Figure 34: Phospho-mutant WAVE Y153F is not sufficient diminish Abl phosphorylation activity on Wave tyrosine residues. Immunoprecipitation with myc-trap beads from lysates of S2R+ cells. Co-transfection of cells with WAVE-myc or WAVE Y153E-myc and eGFP or BCR-Abl. Co-expression control with EGFP shows negative pTyr staining, whereas pTyr staining is detectable for co-expression of WAVE-myc and WAVE Y153F-myc with BCR-Abl.

This leads to the conclusion that mutated tyrosine residue Y153 alone does not completely diminish Abl dependent WAVE phosphorylation. This suggested that further residues are targeted by Abl and might influences WAVE activity.

3.6.3 WAVE phosphorylation is critical in *Drosophila* development

Since phosphorylation of WAVE is suggested to have an influence on WRC activity, the effect on *Drosophila* development remains to be determined. Phospho-mimicking and phospho-defective WAVE transgenes were ubiquitously re-expressed in *wave* mutant background using *da*-Gal4 driver line. Transgenes with amino acid exchanges of all 15 tyrosine residues (WAVE 15F and 15E) were established in a previous work in a UASt-gateway vector (Kottmeier, 2010, bachelor thesis). The somatic expression is stronger in comparison to transgenes cloned in a UASp vector and so cannot be compared.

Neither phospho-mutant transgenes by transition of tyrosine to phenylalanine of either all nor single tyrosine sites affect viability of the animals (Table 12). The flies also show no morphological defects as it can be observed in *kette* hypomorphic flies in bristle formation (Bogdan et al., 2004, data not shown). In contrast, phospho-mimicking WAVE mutation of all 15 tyrosine residues leads to embryonal lethality. The re-expression of WAVE phospho-mimicking transgenes with mutation of tyrosine Y127E+Y153E is not able to rescue *wave* mutant lethality. In contrast, re-expression of single phospho-mimicking WAVE Y127E and WAVE Y153E completely rescues viability until fly adulthood (Table 12).

Table 12: Survival of flies in *wave* mutant rescue experiments

EXPRESSION IN WAVE MUTANT BACKGROUND	**VIABILITY**
UASt-WAVE	viable
UASt-WAVE 15F	viable
UASt-WAVE 15E	**embryonal lethal**
UASp-WAVE	viable
UASp-WAVE Y127F	viable
UASp-WAVE Y127E	viable

UASp-WAVE Y153F	viable
UASp-WAVE Y153E	viable
UASp-WAVE Y127F+Y153F	viable
UASp-WAVE Y127E+Y153E	**late pupal lethal/ defects in adult eclosion**

The F1 generation of flies re-expressing the phospho-mimicking WAVE transgenes were further analyzed for morphological defects. Flies re-expressing single phospho-mimicking WAVE transgenes for either Y127 or Y153 develop normally until adulthood as those re-expressing wild typic WAVE do (Figure 35). In contrast, re-expression of phospho-mimicking WAVE Y127E+Y153E transgene causes severe developmental defects. In most animals, morphogenesis already terminates in pupal stage (Figure 35A-1). It is also notable, that the pupal case of is often deformed (Figure 35A-2,3). A minority of the animals develop to adult flies whereas the others die. However, these flies showed defects in adult eclosion and finally die in the pupal case (Figure 35B-1,2). Opening the pupal case show some flies to be fully developed. A mild rough eye phenotype caused by eye bristle defects can be observed in WAVE Y127E+Y153E expressing flies (Figure 35D).

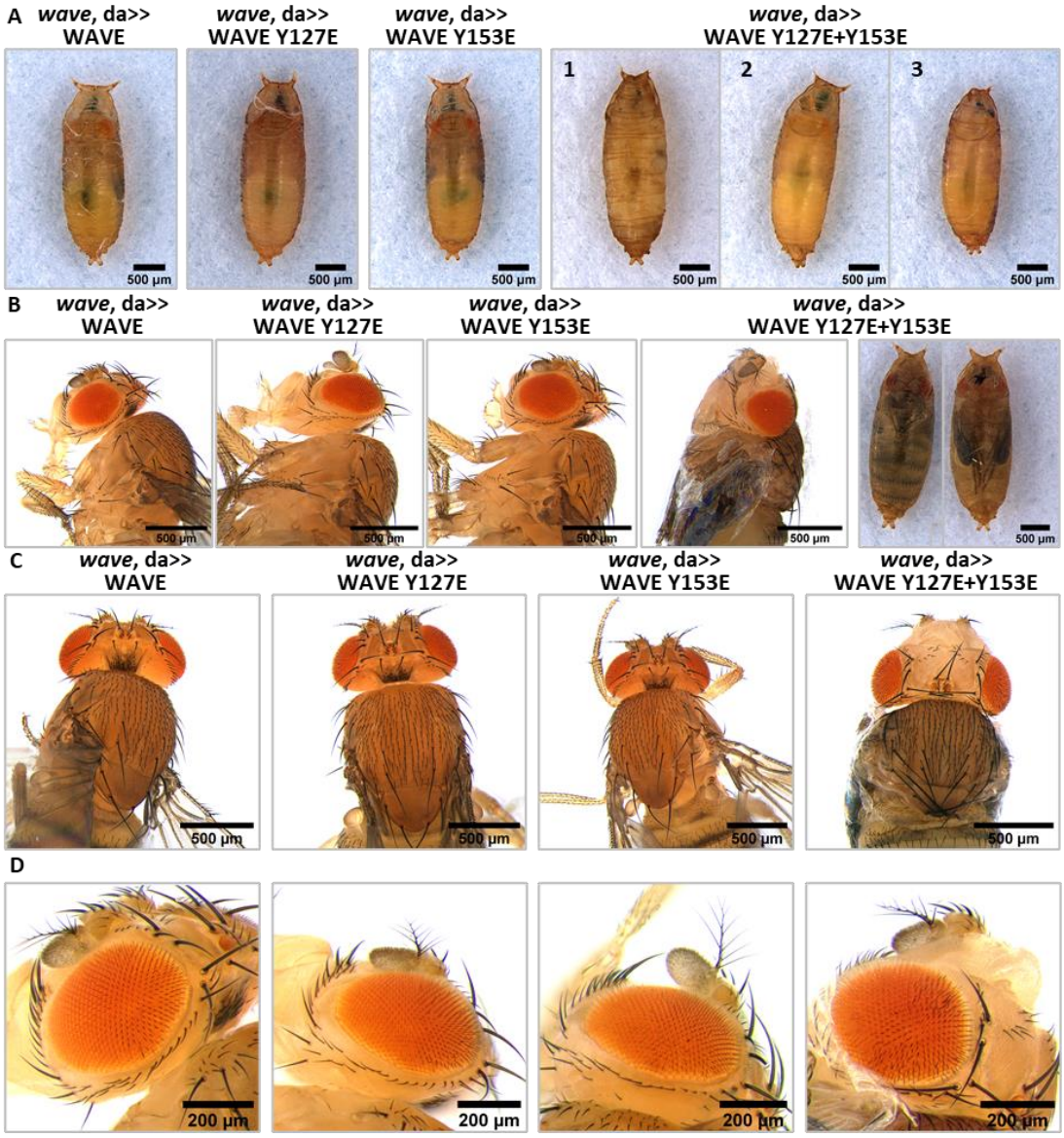

Figure 35: Morphological analysis of *wave* mutant flies rescued by phospho-mimic WAVE constructs. WAVE transgenes were ubiquitously expressed by *da*-Gal4 in *wave* mutant background. (A) 3 days APF the adult fly is almost fully developed. Rescue with WAVE Y127E+Y153E often die in pupal stage (A1). Some develop further but show defects in eclosion (B1+2). (B) Thorax lateral (C) and dorsal view shows intact fly and bristle formation. Flies, rescued with WAVE Y127E+Y153E, are cut out of the pupal case. Adult were fully developed but dead. (D) The eye developments normal, except of flies rescued with WAVE Y127E+Y153E that exhibit a rough eye phenotype.

In conclusion, the re-expression of the WAVE transgenes with executionary non-phosphorylateable tyrosine residues were able to rescue *wave* mutant lethality. In contrast, transgenes mimicking WAVE tyrosine phosphorylation of all 15 tyrosine residues as well as the combined mutation of Y127 and Y153 are not able to restore viability.

3.6.4 WAVE-WHD phosphorylation of Y127 and Y153 affect lamellipodia formation of macrophages

To further analyze the influence of WAVE WHD phosphorylation on actin formation rescue experiments were performed by ubiquitously expressing different WAVE transgenes in *wave* mutant background.

The majority of isolated rescued cells show the wild typic cell shape with a broad lamellipodium at the leading edge and cytoplasmic WAVE staining and at the membrane (Figure 36). As described before, *da*-Gal4 induces a mosaic expression pattern. Even when expressing the wild typic WAVE, few cells of the macrophage do not express the transgene and remain *wave* mutant. These cells are identified by the absence of WAVE staining as well as showing the typical *wave* mutant stellar cell morphology with extended filopodia (Figure 36, orange arrow).

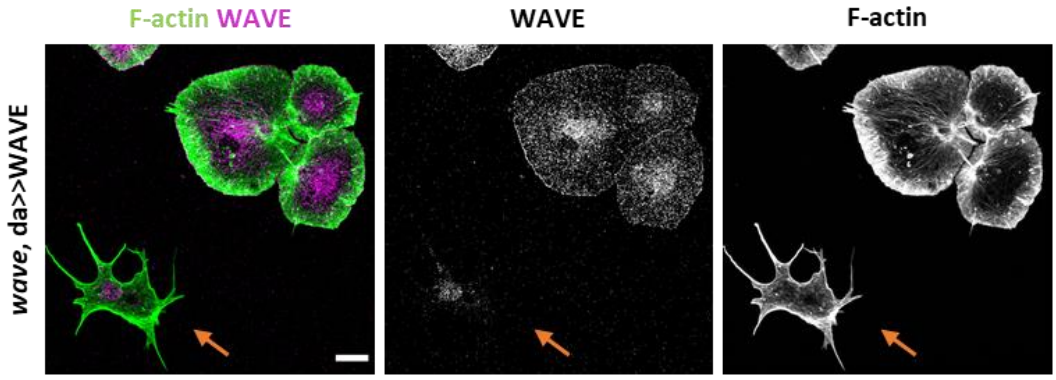

Figure 36: Analysis of WAVE rescue in *Drosophila* macrophages. Isolated pupal macrophages plated on ConA stained for F-actin and WAVE (color code of staining is indicated). WAVE wild type is ubiquitously expressed by *da*-Gal4 in *wave* mutant background. Rescued cells show characteristic wild type morphology with broad lamellipodial structures. Cells failed to be rescued lack WAVE staining and exhibit filopodia instead of lamellipodial structures (orange arrow). Scale bar = 10 µm.

To further study the effect of WAVE tyrosine phosphorylation in macrophages, either single or double phospho-mimicking and phospho-mutant transgenes were re-expressed in *wave* mutant background. Similar to WAVE wild type expression, in all experimental setups, a few cells are not rescued indicated by the absence of WAVE staining.

Re-expression of all transgenes besides phospho-mimicking WAVE Y127E+Y153E were able to restore the wild typic morphology exhibiting a broad, flat lamellipodium, consisting of branched actin structures. (Figure 37A). Cells expressing phospho-mimicking WAVE Y127E+Y153E with two mutation sites show a *wave* mutant like phenotype with extended filopodial structures (Figure 37A). In contrast to *wave* mutant cells, most cells re-expressing

WAVE Y127E+Y153E still show rudimentary lamellipodial structures. They can be clearly distinguished from *wave* mutant cells by WAVE antibody staining.

Further, morphological analysis using shape descriptor parameters showed cells re-expressing phospho-mimicking WAVE Y127E+Y153E were significantly smaller compared to wild type rescue (Figure 37C). Although, roundness in *wave* mutant cells is significantly decreased, it is not a suitable indicator to characterize a stellar cell morphology (Figure 37C´). In contrast, circularity is extremely sensitive to extended protrusions like filopodia (2.5.2 Morphology analyzes of isolated macrophages). The stellar morphology of *wave* mutant macrophages causes a dramatic decrease in circularity. Similar, the re-expression of phospho-mimicking WAVE Y127E+Y153E leads to a strong decrease of circularity in comparison to WAVE wild type expression (Figure 37C´´).

The morphological analysis also shows that re-expression of phospho-mutant WAVE Y127F in macrophages displayed a decreased cell area, but circularity of these cells is comparable to wild typic cells (Figure 37C-C´´).

In *wave* mutant macrophages lamellipodia are completely disrupted and therefore their shape cannot be quantified, whereas the re-expression of phospho-mimicking WAVE Y127E+Y153E causes some rudimentary lamellipodial structures. Consequently, lamellipodial width is drastically reduced. In contrast, macrophages re-expressing the phospho-mimicking WAVE Y153E transgene in *wave* mutant background show an increase in lamellipodia width in comparison to wild type WAVE re-expression (Figure 37B).

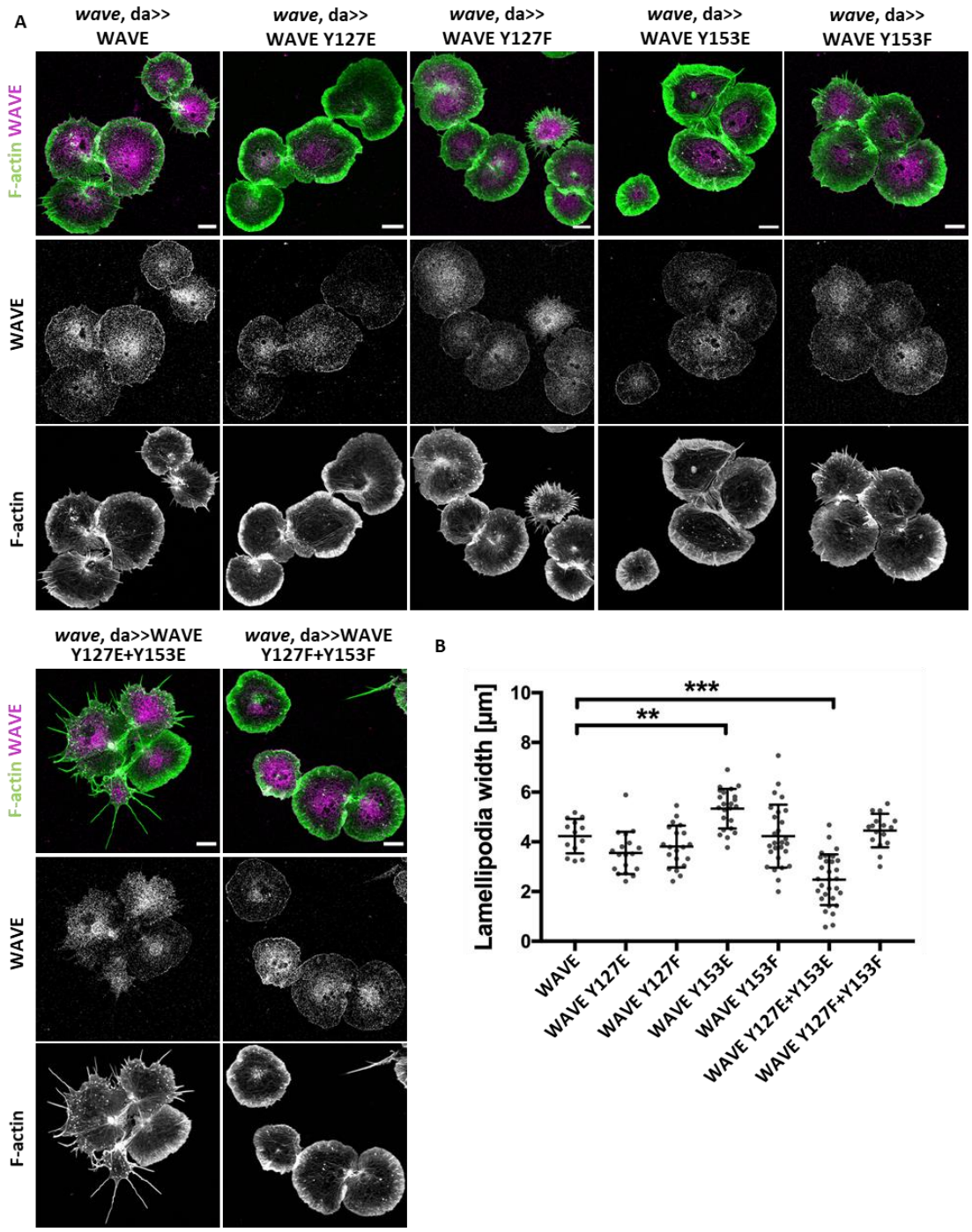
A
wave, da>> WAVE
wave, da>> WAVE Y127E
wave, da>> WAVE Y127F
wave, da>> WAVE Y153E
wave, da>> WAVE Y153F
F-actin WAVE
WAVE
F-actin
wave, da>>WAVE Y127E+Y153E
wave, da>>WAVE Y127F+Y153F
B
Lamellipodia width [µm]
0
2
4
6
8
10
**
***
WAVE
WAVE Y127E
WAVE Y127F
WAVE Y153E
WAVE Y153F
WAVE Y127E+Y153E
WAVE Y127F+Y153F

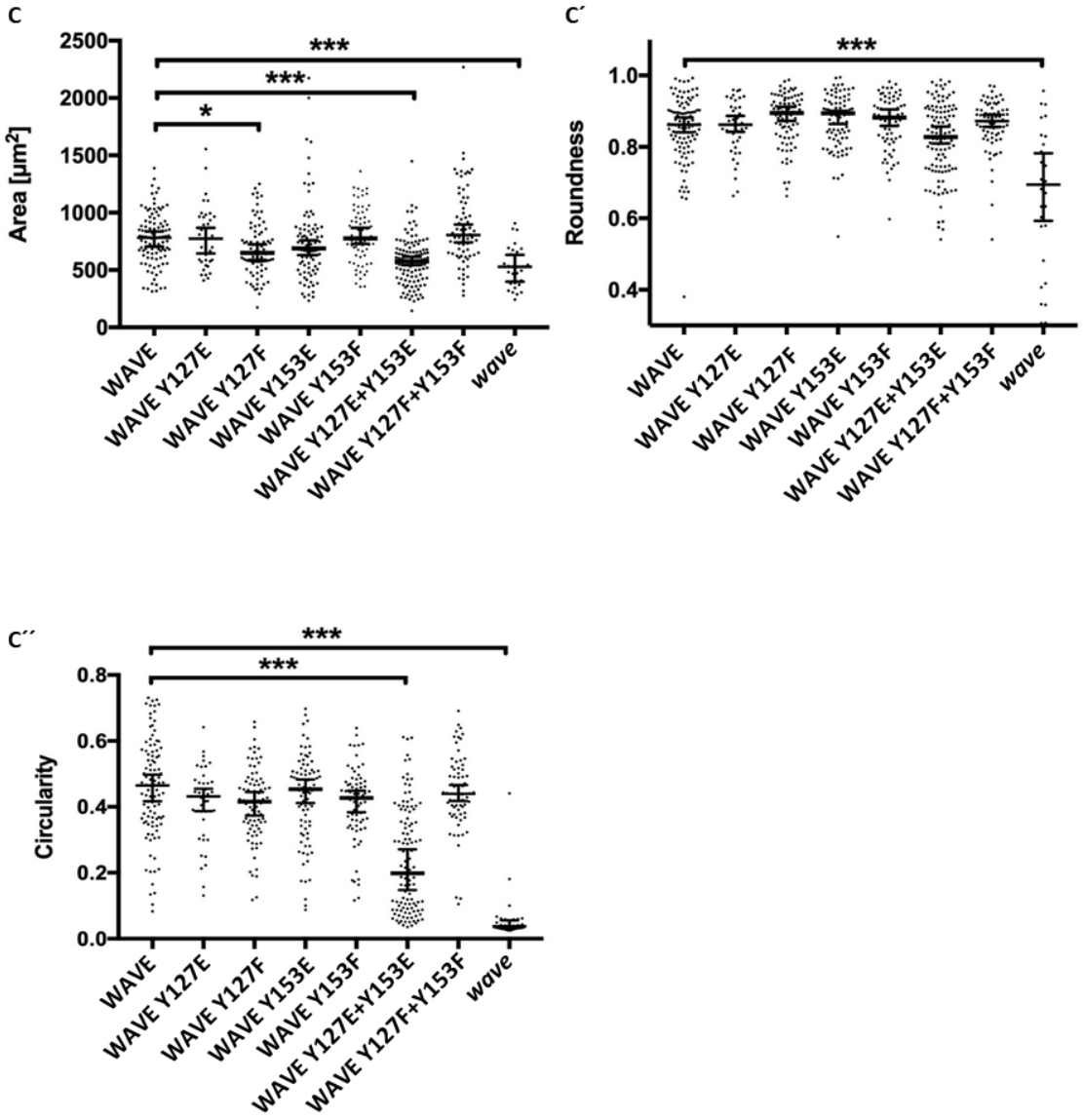

Figure 37: Analyses of WAVE tyrosine phosphorylation in *wave* mutant background in *Drosophila* macrophages. Isolated pupal macrophages plated on ConA stained for F-actin and WAVE (color-code of staining is indicated). WAVE transgenes were ubiquitously expressed by *da*-Gal4 in *wave* mutant background. Cells lack WAVE staining and exhibit filopodia instead of lamellipodial structures were quantified as *wave* mutants (example Figure 36). All constructs except of WAVE Y127E+Y153E can rescue *wave* mutant cells showing characteristic wild type morphology with broad lamellipodial structures. (B+C) Graphs are depicted in a scatter dot blot with bars indicating mean and SD. *** = $p \leq 0.001$ ((B)ANOVA, (C) non-parametric multiple comparison test). (B) Lamellipodia width is increased in macrophages expressing WAVE Y153E and reduced in WAVE Y127E+Y153E expressing cells. In *wave* mutant cells lamellipodial structures are not measurable. (C) Cell shape analyses show a wave mutant like phenotype for macrophages expressing WAVE Y127E+Y153E. Cell size (C) and circularity is decreased. Scale bar = 10 µm.

Analyzing cell morphology demonstrated that the expression of phospho-mutant WAVE constructs completely rescues *wave* mutant phenotype. In contrast, expressing double phospho-mimic WAVE Y127E+Y153E causes severe morphological defects comparable to

wave mutant macrophages. They exhibit only rudimental lamellipodial structures, whereas expression of single phospho-mimic WAVE Y153E lead to extended branched actin lamellipodial structures.

3.6.5 Phosphorylation of WAVE WHD interfere with migration of macrophages

The importance of WAVE regulation in macrophage migration and the consequences of its loss is described in detail in part 3.1. Thus, to get further insights in the regulatory mechanisms of WHD tyrosine residues Y127 and Y153 they are expressed in *wave* mutant background by *da*-Gal4 driver. To visualize migrating macrophages, they are marked with dsRed fused to the macrophage specific truncated *hmlΔ* promotor (Movie 18).

When further analyzing random migratory behavior neither expression of phospho-deficient transgenes with single (Y127F, Y153F, Movie 19+20) nor double tyrosine transition (Y127F+Y153F, Movie 21) of tyrosine to phenylalanine has any severe effect on either speed, straightness or persistence of randomly migrating macrophages (Figure 38E-G). Also, single phospho-mimicking tyrosine side WAVE Y127E does not alter motion of macrophages in comparison to WAVE wild type expression (Figure 38E-G, Movie 22).

Although previous experiments demonstrated that phospho-mimicking of WAVE Y153E leads to an increase in branched F-actin formation, cell speed is significant decreased in random migrating cells (Figure 38E). This is indicated by color-code of the trajectories in comparison to cells expressing WAVE wild type (Figure 38A+C, Movie 18+23). Straightness shows a mild but not significant reduction compared to re-expression of wild type WAVE in mutant cells (Figure 38F).

As described before, double phospho-mimic construct WAVE Y127E+Y153E fails to rescue *wave* mutant lethality and leads to severe morphological defects in isolated macrophages. As expected it also shows migration defects *in vivo* (Figure 38D-G, Movie 24): Cell speed is drastically reduced, (Figure 38D+E, color code of the trajectories, Movie 24), track straightness is highly impaired and cells almost rest at their origin (Figure 38D+F). This is supported by the reduction of the cell persistence (Figure 38G). The distribution of the persistence angle is also massively shifted to higher values (Figure 38G´).

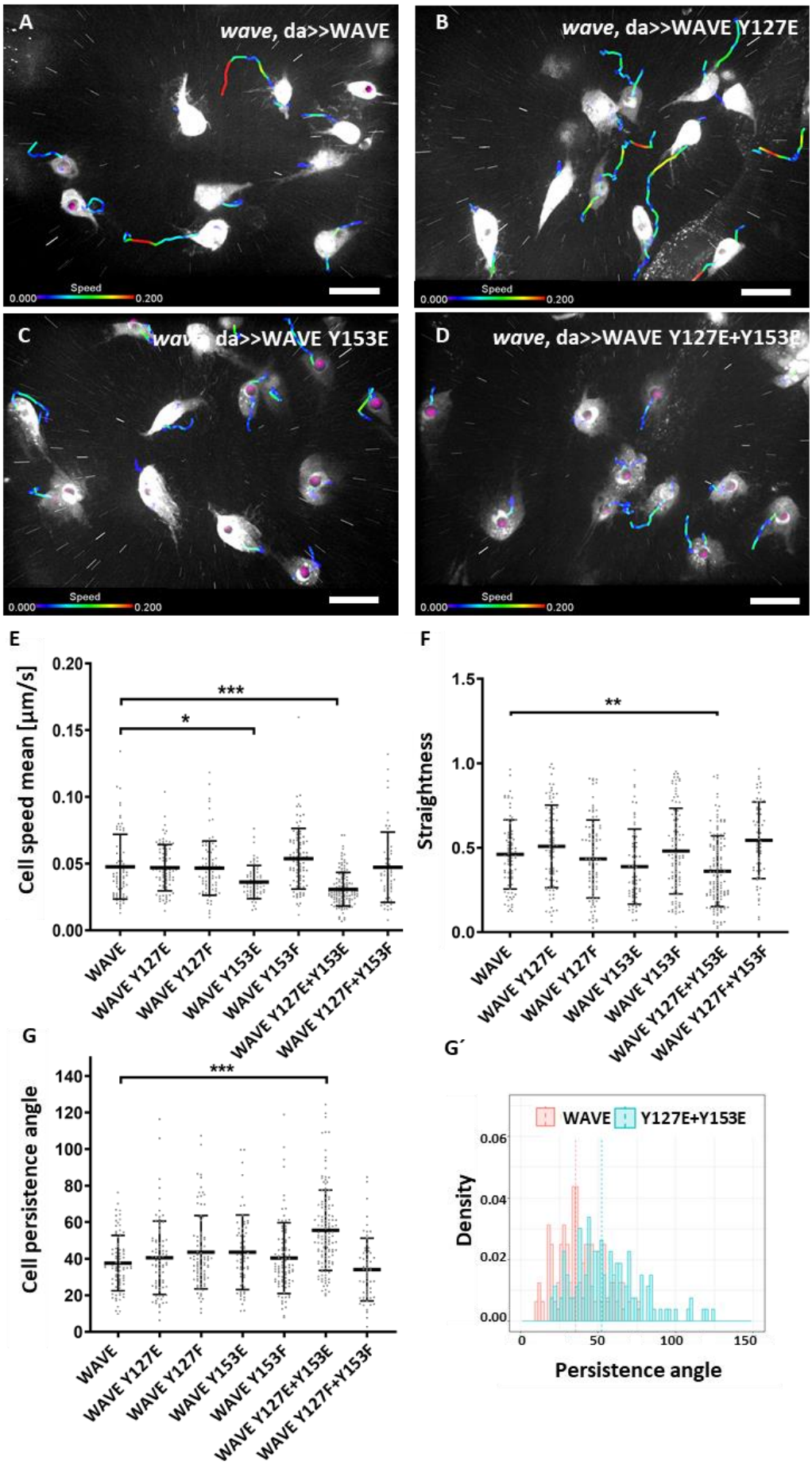
A
wave, da>>WAVE
B
wave, da>>WAVE Y127E
C
wave, da>>WAVE Y153E
D
wave, da>>WAVE Y127E+Y153E
Speed
0.000
0.200
E
Cell speed mean [µm/s]
F
Straightness
G
Cell persistence angle
G´
WAVE
Y127E+Y153E
Density
Persistence angle
WAVE
WAVE Y127E
WAVE Y127F
WAVE Y153E
WAVE Y153F
WAVE Y127E+Y153E
WAVE Y127F+Y153F

Figure 38: Expression phospho-mimic WAVE impairs random cell migration. (A-D) WAVE transgenes were ubiquitously expressed by *da*-Gal4 in *wave* mutant background. Macrophages are marked by *hmlΔ*-dsRed expression. Still images of random migrating pupal macrophages. Cells are tracked with Imaris and trajectories are depicted with speed-color code (in µm/s). (E-G) Graphs are depicted in a scatter dot blot with bars indicating mean and SD. *** = $p \leq 0.001$ (non-parametric multiple comparison test). In the bias angle histogram one bar depicts the accumulated density of 3 °. Dotted line indicates the median angle of the corresponding distribution. (E) Cell speed is reduced in cells expressing WAVE Y153E and WAVE Y127E+Y153E. (F) Cells expressing WAVE Y127E+Y153E show also a reduction in straightness and (G) increase in cell persistence angle as indicated by the right shifted distribution in the persistence angle histogram (G´). Scale bar = 20 µm.

To get further insights of cell morphology, closeup images of migrating cells were recorded with a higher laser intensity. Nevertheless, expression of wild type WAVE in *wave* mutant background completely rescued lamellipodia disruption (Figure 39A, Movie 25). Further, expression of single phospho-mimicking WAVE Y127E and WAVE Y153E exhibit lamellipodial structures (Figure 39B+C). Prepupal macrophages, expressing double phospho-mimic WAVE Y127E+Y153E construct, show a more heterogenous cell population. Some cells exhibit almost wild typic lamellipodia (Figure 39D, blue arrow) whereas other cells show reduced lamellipodial structures but more filopodial protrusions (Figure 39D, orange arrow, Movie 26).

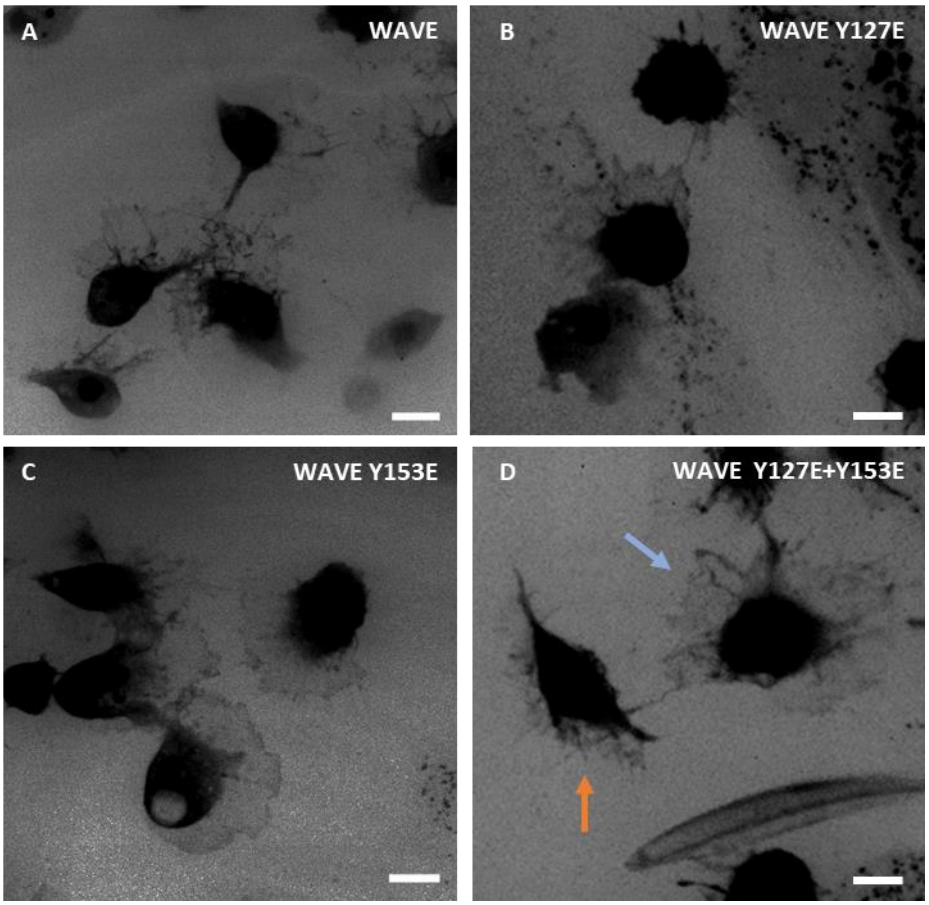

Figure 39: Expression phospho-mimic WAVE Y127E+Y153E show a morphological defect. (A-D) WAVE transgenes were ubiquitously expressed by *da*-Gal4 in *wave* mutant background. Macrophages are marked by *hmlΔ*-dsRed expression. Close-up images of random migrating pupal macrophages. (A) Rescue with WAVE wild type cells show characteristic wild type morphology with broad lamellipodial structures. (B+C) Expression of single phospho-mimic WAVE Y127E and WAVE Y153E show no morphological defects. (D) Rescue with WAVE Y127E+Y153E show a heterogenous macrophage population. Some show wild typic morphology with broad lamellipodial structures (blue arrow) other exhibit predominant filopodial protrusions (orange arrow). Scale bar = 10 µm.

In conclusion, these data show the importance of precise actin regulation in random cell migration. It could be demonstrated that increased lamellipodial branched F-actin formation by the expression of WAVE Y153E interfere with cell migration in *in vivo*. Further, the re-expression of a WAVE transgene with to phospho-mimicking mutations does not rescue the *wave* mutant phenotype.

4 Discussion

4.1 Functions of cell protrusions in random an directed migration

The precise regulation of the Arp2/3 complex via its main activator WAVE is indispensable for efficient lamellipodia-based migration. The investigation of the complex interaction and integration of biochemical signals at the leading edge of lamellipodia has been the focus of research for many decades. Cells provide a powerful setup of regulatory mechanisms to ensure time and space-specific nucleation and elongation of branched actin at the leading edge as driving force for cell motility. The controlled recruitment, activation, and turnover of WAVE within the WRC is crucial for efficient lamellipodia-based migration.

At the leading edge of cells migrating on a flat substrate lamellipodia are the predominant protrusive structure (Abercrombie et al., 1970a; Small, 1988; Small et al., 2002). Depletion of components of the Arp2/3 complex as key nucleator for branched actin filaments leads to complete loss of lamellipodia. This loss is compensated by an extensive outgrowth of filopodial protrusions (Figure 12, Rogers et al., 2003; Sander et al., 2013; Zobel and Bogdan, 2013). The same defects in cell morphology can be observed for most cell types in the absence of WAVE. Previous studies address the consequences of the loss of lamellipodia on migration under cell culture conditions and have provided essential insight for today's knowledge on regulation of the actin machinery.

Building on this data, in this study the relevance of lamellipodia *in vivo* migrating *Drosophila* macrophages as well as in response to wound signals was addressed. Beside RNAi mediated gene suppression of *wave*, the generation of mutant macrophages by MARCM technique allowed the analysis of the migration of *wave* mutant macrophages *in vivo* (Figure 14). The loss of WAVE resulted in a complete disruption of lamellipodial structures and confirmed that in *Drosophila wave* depletion cannot be substituted by other NPFs like WASP. In *Dictyostelium*, depletion of *scar* (*wave*) yields only mild morphological defects as it is partially compensated by WASP function (Veltman et al., 2012). In contrast, *Drosophila wave* mutant macrophage exhibited extended filopodial structures consist of bundled actin filaments. The analysis of their migratory behavior revealed that *wave* mutant cells still showed a rudimental filopodial based migration (Figure 14, Movie 3). They linger at one position starching out their long filopodia until they relocate and overcome a relatively long distance. In contrast to

continuously migrating wildtype macrophages, the migration mode of *wave* mutants can be characterized as an erratic motion.

Consistently, previous studies have drawn a complex picture displaying lamellipodia as a meshwork with bundled actin structures which contribute to a great extent to the formation and dynamics of lamellipodia. F-actin elongators such as Formins and ENA/VASP contribute to the formation. They cooperate with the WRC and elongate preexisting Arp2/3 nucleated filaments (Beli et al., 2008; X. J. Chen et al., 2014; Isogai et al., 2015). Indeed, this study confirmed previous data, showing that filopodia also nucleate independently of branched actin structures (Bischoff et al., 2020; Evans et al., 2013). The *de novo* formation of filopodia reveals a more outstanding role of filopodial structures in cell migration. Cells like nascent myotubes of *Drosophila* testes are highly motile collective migrating cells completely lacking lamellipodia but instead exhibit numerous filopodia driving their migration (Bischoff et al., 2020). In migrating B16-F1 melanoma cells and fibroblasts, loss of Formin FMNL2 and FMNL3 function impairs lamellipodia formation and reduces migration (Kage et al., 2017).

Further, in this work the role of lamellipodia in directed wound response of *Drosophila* pupal macrophages was addressed. Initial publication by Suraneni et al. 2012 and Wu et al. 2012 controversially discusses whether lamellipodial structures are indispensable in directed cell migration. Suraneni and colleagues (2012) showed that *arp3* depleted mouse embryonic fibroblasts (MEFs) lose their ability to follow an EGF-gradient. In contrast, Wu and colleagues (2012) demonstrated in *arp3* KO MEFs that these cells are only affected in speed but still slowly follow a chemotactic PDGF gradient. Consistent with their findings, the results of this study clearly showed that *wave* depleted cells lacking lamellipodia are still able to respond to wound signals (Figure 15, Movie 5). Indeed, they show characteristic stellate morphology and reveal reduction in motility. The loss of WAVE leads to a reduction in cell speed but has influence of directionality of the migrating cells. This is consistent with previous data from macrophages in the *Drosophila* embryo (Evans et al., 2013). The authors show a reduced responsiveness of *wave* mutant macrophages to laser induced wounds. However, consistent with the findings of this work, the main effects occur in the reduction of cell speed, whereas the directionality of the cells is similar to wild type macrophages. Similar data are obtained in *wave* lacking dendritic cells. Furthermore, the depleting WAVE upstream activator Rac does not interfere with the ability of cells to respond to chemotactic cues (Leithner et al., 2016; Monypenny et al., 2009). In conclusion, currently available data highly supports the existence of a chemotactic mechanism independent of the classical GTPase-WAVE-Arp2/3 pathway, in the absence of lamellipodia. A cooperative role of filopodial and branched structures can be also assumed orchestrating efficient directed migration response. Initial chemotactic sensing

could be fulfilled by signaling molecules inducing filapodial filaments, which could serve as template for the further binding of the Arp2/3 complex to induce branched network structures. Recent data show ENA/VASP being critical in Fascin dependent actin bunding in *Drosophila* macrophages. Lamellipodia of *ena* mutant macrophages almost completely lose F-actin bundled structures and exhibit impaired migration speed. However, directionality during inflammatory chemotaxis is not effected (Davidson et al., 2019). As chemotaxis still works in the absence of actin bundles as well as in cells with disrupted branched actin network it can be suggested that both structures also contribute independently to directed migration towards external chemotactic cues.

4.2 WRC-WIRS ligand binding is not crucial in macrophage wound response

Cells need to discriminate between different external signals and adapt their response accordingly. In migratory processes these external stimuli need to be integrated and transferred to the intracellular actin machinery and be further decoded into cell motion.

A previous study has identified a small WCR binding motif, the so-called WRC interacting receptor sequence (WIRS), which is highly conserved across multicellular species (B. Chen et al., 2014). It is present in around 120 proteins, most cell adhesion proteins, membrane receptors but also cytoplasmic proteins. The binding to the WRC is mediated by a pocket formed by the two subunits Sra-1 and Abi. This interaction relays on a complete assembly of the complex indicating its physiological relevance in WRC dependent processes.

The variety of proteins carrying a WIRS motif allow us to draw conclusions about the diversity of biological processes where WIRS mediated interaction with the WRC may be important. WIRS membrane bound proteins can directly recruit the WRC to the membrane and facilitate binding and accumulation of the WRC at distinct locations. The minimum WIRS motive alone does not act on WRC activity, whereas its embedding in complex protein structure comes with further regulatory abilities (B. Chen et al., 2014). The cytoplasmic tail of Protocadherin PCDH10 facilitates Rac dependent WRC activation but PCDH17 inhibits activity *in vitro*.

For the cell adhesions receptor Fat2, the WIRS-WRC interaction was shown to be of high physiological relevance. Mutation of Fat2 causes a round egg phenotype in developing *Drosophila* egg-chambers (Squarr et al., 2016). The receptor binds the WRC *via* the C-terminal cytoplasmic WIRS motive, controlling the collective movement of the follicle cells.

The disruption of the WIRS binding site within the WRC phenocopies *fat2* defects underlines the importance of these interactions in this dynamic migratory process.

Further, the platelet-derived growth factor/vascular endothelial growth factor (PDGF/VDGF) related receptor Pvr has also been listed as a potential WIRS ligand (Supplementary Figure 3). Collective border cell migration is guided by PDGF signaling (Bianco et al., 2007; Duchek et al., 2001). However, it has been shown that the disruption of the WIRS binding site does not interfere with border cell migration (Kreft, 2017). Additionally, the dispersal of *Drosophila* macrophages during embryogenesis is controlled by Pvr and its ligands Pvf2 and Pvf3. However, downstream activation of PI(3)K is essential in wound chemotaxis of embryonic macrophages but not for directed migration during development (Wood et al., 2006). This indicates at least two separate mechanisms that coordinate directed macrophage migration in *Drosophila* embryo. In fibroblasts, PI(3)K is not essential for chemotaxis toward a PDGF gradient, which is consistent with findings in genetic studies in *Dictyostelium* (Hoeller and Kay, 2007; Welf et al., 2012).

In this study WIRS ligands were screened for potential candidates mediating wound response transduction and decoding the signals for the actin machinery in pupal macrophages. These candidates, including Pvr but also 28 other membrane receptors like immune Toll-like receptors, EGF-like phagocytosis receptor Nimrod C1 and receptor tyrosine kinase Ephrin were analyzed regarding their ability to impact the migrating response on laser induced wounding (Supplementary Figure 3). However, none of the candidates showed an apparent impact on the migratory behavior of cells as cells successfully migrate to the wounding site. It must be stated that the initial design of the screen is created to identify strong migration defects. This avoids false positive candidates but on the other hand false negative results cannot been excluded.

To dissect the impact of WIRS-WRC interaction further the wound response of macrophages with disrupted WIRS binding sites was investigated in more detail. First, an analysis using the previously established HMMS score, showed weak defects in wound response (Figure 16, Lammel et al., 2014). However, the HMMS score is an indirect method to analyze the fluorescent signal of macrophages in correlation to their distance to the wounding source. Therefore, it is sensitive to differences in cell size and number of responding cells. To circumvent this, a method to determine directionality of migrating cells towards a wound signal by calculating the bias angle of every cell in a certain radius was established in this work. This, more precise analysis, shows that defected WIRS binding of the WRC does not affect responsiveness nor directionality of macrophages to wounds (Figure 16). These results

suggest that binding of the WRC to certain membrane receptors *via* the WIRS motive plays a minor role in macrophage migration.

The endocytosis of IL-2 highlights another perspective on WAVE interaction with WIRS membrane receptors (Basquin et al., 2015). Generally, endocytosis is a common mechanism to internalize membrane receptors to control their abundance at the membrane. IL-2 uptake is a clathrin-independent mechanism (Grassart et al., 2008). In a first step, WAVE induces outward forces by forming membrane protrusion that simultaneously initializes the invagination of the membrane. The following recruitment and accumulation of IL-2 at the basis of the pit is dependent on WRC binding the WIRS motive of IL2. The authors claim this protrusion, based on endocytosis, to be a potential mechanism for other WIRS carrying membrane receptors, based on the recruitment WIRS motive carrying receptors to the invagination site *via* WRC-WIRS binding (Basquin et al., 2015). A large number of WIRS ligands are adhesion proteins. Therefore, internalization of WIRS-ligands might provide a further regulative mechanism to modulate cell-cell contacts. Evolutionarily, this might be a further explanation for the high conservation of the WIRS motive in membrane receptors. This perspective highlights the diversity of biological processes in which WRC-WIRS interaction might be involved in.

4.3 Phosphorylation as a mechanism to modulate WAVE activity

Phosphorylation of the individual subunits of the WRC, especially WAVE and Abi and its impact on WRC activity has been discussed for a long time. The transfer of the γ-phosphoryl group to either a serine, threonine or tyrosine residue is catalyzed by specific kinases. Kinases and their counterparts – phosphatases – act as molecular switches to change phosphorylation state of proteins and therefore regulate their activity. WAVE and Abi are targets of several kinases, of which none is exclusively specific to a certain regulatory target protein (Krause and Gautreau, 2014; Mendoza, 2013). Additionally, kinases target more than one phospho-residue in one protein with potentially opposing regulatory effects. This makes it challenging to address the question of phosphorylation from the site of kinase or to try to extract the impact of single residues in the phosphorylated and unphosphorylated state (Figure 40).

WAVE proteins possess several phospho-residues, which are found in conserved domains of the protein but not be restricted to them (Figure 6, (Krause and Gautreau, 2014; Mendoza, 2013)). Some of these residues are known to play critical role in regulating WAVE function.

However, the phospho-residues are neither uniformly conserved across different WAVE isoforms nor across species (Supplementary Figure 1). In humans, different WAVE isoforms show only partially overlapping expression patterns (Sossey-Alaoui et al., 2003). Specifically, in tissues, where all isoforms are expressed, it can be assumed that altered phosphorylation patterns might define the individual function of the isoform.

Still, in highly conserved domains like the WHD, PRD and the VCA domain phospho-residues are not uniformly conserved. The PRD is mainly serine phosphorylated by ERK or CDK, respectively (Krause and Gautreau, 2014; Mendoza, 2013). It is speculated that PRD phosphorylation might regulate WAVE by affecting the binding affinity of SH3 domain containing regulators like Abl or Src. In *Drosophila* WAVE, only one Serine is conserved in the PRD.

Focusing on WAVE activation, phosphorylation events within the VCA domain are of great interest. WAVE-VCA carries three highly conserved serine residues (WAVE2 – Ser482, Ser484, Ser488, Supplementary Figure 1) phosphorylated by CK2 (Nakanishi et al., 2007; Pocha and Cory, 2009). Pocha and colleagues (2009) postulate that phosphorylation of the VCA domain is essential for WAVE activity. They show that the phospho-mutation of five serines of WAVE2 leads to a disruption of lamellipodia in fibroblasts. Additionally, phosphorylation of three serines (S488, S489, S497) increases the affinity to the Arp2/3 complex. Remarkably, the same study also demonstrated that increased binding affinity comes with a reduction in Arp2/3 activity (Nakanishi et al., 2007; Pocha and Cory, 2009). This last observation is consistent with data from *Dictyostelium.* Ura et al. (2012) demonstrated that phosphorylation increases intramolecular binding of the VCA domain and thereby keeps the WRC in an inactive state. On the other site, non-phosphorylatable WAVE-VCA increases WAVE activity resulting in extensive WAVE driven protrusions (Ura et al., 2012). Further investigation is crucial to extend the knowledge of VCA phosphorylation and the impact of different Casein kinases.

Like serine phosphorylation, tyrosine phosphorylation is described to modulate WAVE activity. In human and murine isoforms of WAVE, tyrosine residues are distributed over the whole protein. Nevertheless, a functional relevance is only described for those within the WHD. The four tyrosine sites found in *Drosophila* are conserved across species, in particular Y127 as Src kinase and Y153 (dWAVE) as target of Abl kinase are prime candidates to regulate WAVE dependent actin dynamics (Ardern et al., 2006; Leng et al., 2005).

This work addresses the impact of phosphorylation of distinct conserved phospho-residues in the WHD in a multicellular organism for the first time. The overexpression in *Drosophila* wing imaginal discs and macrophages of WAVE transgene, containing a phospho-mimicking

mutation of Y153 leads to an elevation in the level of F-actin (Figure 33). Structural analysis has shown that corresponding Y151 in WAVE1 is located in the α5– α6 loop of the meander region and facilitates the interaction of Sra-1 and WAVE1. Phosphorylation is predicted to destabilize the interaction of the meander region with Sra-1, causing a release of the VCA domain. These results suggest that an additional activation mechanism for WAVE exists, parallel to the Rac activation mode. In conclusion, it can be assumed that in *Drosophila* phosphorylation of WAVE Y153 leads to higher WAVE activity facilitating actin assembly consistent with previous *in vitro* data (Chen et al., 2010). The authors further postulate a similar mechanism for Y125. This residue is part of loop α3 and hydrogen bound to Sra-1 Asp689. Phospho-mimicking mutations of eighter Y125 or Y151 show an increase in lamellipodia formation in HeLa cells (Chen et al., 2010). However, the results from this study could not confirm an increase in F-actin level related to phosphorylation of Y127. Neither the overexpression in imaginal wing discs nor in macrophages show any changes in F-actin staining.

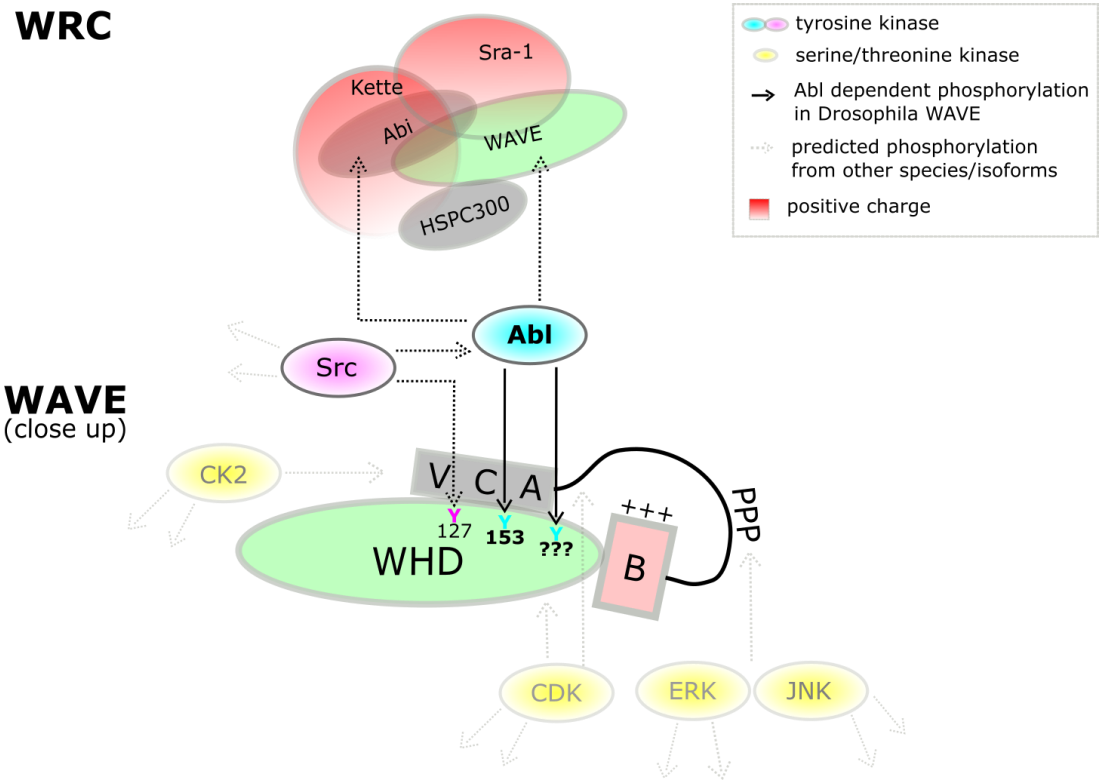

Figure 40: Scheme of complex regulation of WAVE and the WRC by phosphorylation. Abl kinase phosphorylates and directly interacts with the WRC subunit Abi and WAVE. Key phosphorylation events of WAVE and the corresponding effector kinase are depicted. Tyrosine phosphorylation is resticted to the WHD. Abl phosphorylates conserved Y153 (WAVE1/3 Y151, WAVE2 Y150), Src targets Y127 (WAVE1/3 Y125, WAVE2 Y124). Further, so far unknown residues in the WHD (meander region) of WAVE might be targeted by Abl. In mammals, WHD serine/threonine phosphorylation by CDK is reported, but the residues are not conserved in invertebrates. Phosporylation

within the WDH interferes with the inhibitory binding of the VCA, inducing the release. ERK and JNK are targeting WAVE PRD, that has so far only been reported for mamalian WAVE isoforms. CK2 phosporylation of the VCA is partially conserved across species and ifluences WAVE activty as well as binding affinity with the Arp2/3 complex.

In vivo analysis of migrating macrophages shows that cells re-expressing the phospho-mimicking Y153E mutation in a *wave* mutant background exhibit broader lamellipodia (Figure 37). In random migration mode, this leads to a significant reduction in cell speed of these cells (Figure 38). Consistent with this result, the overexpression of the kinase active form of Abl (BCR-Abl) phenocopy this migratory behavior (Figure 25). The proper organization of the lamellipodium is highly dependent on an equilibrium between actin branching on one site and elongation of filaments on the other site (Figure 41). It is postulated an increase of actin branching leads to a stiffer network resulting in a slowing down of protrusion dynamics. The model predicts conversely that shifting the balance in favor of actin elongation, lamellipodia become faster due to an increased persistence (Bear et al., 2002; Krause and Gautreau, 2014). Recent studies have showed that the overexpression of actin assembly factor ENA/VASP in *Drosophila* macrophages increases the speed of the cells (Davidson et al., 2019).The loss of FMNL2 and FMNL3 consistently reduces the speed of lamellipodial protrusions (Kage et al., 2017). However, the overexpression of actin elongators at a certain point limits the accessibility of monomeric actin at the lamellipodial tip by favoring a so-called “non-productive” capturing, which already takes place in the cytosol (Dimchev et al., 2017). A similar effect might be an additional explanation for the decrease in cell speed observed in this study. The results allow the assumption that the expression of a more active form of WAVE might cause an unprecise nucleation of branched structures (Figure 41). This would interfere with the efficiency of cell migration. To test this hypothesis in the future, the recovery rate after bleaching could be determined to analyze the actin turnover rate. Further, high resolution microscopy might give additional insights about the density of the actin-network.

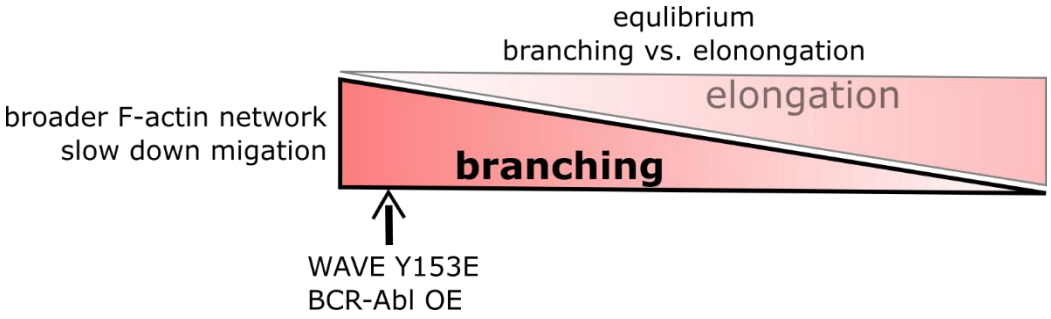

Figure 41: An equilibrium between F-actin branching and elogation is essential for efficient lamellipodia formation. Abl-dependent WAVE phosphorylation of Y153 leads to increased F-actin branching. This results in broader lamellipodia and causes a slow down of random migratin macrophages (modiefied after Krause and Gautreau, 2014).

4.4 Abl kinase is an important but not essential regulator of WRC dependent F-actin formation

The biological function of the non-receptor tyrosine kinase Abl has been in the focus of investigations for many decades. As a consequence, a complex network of biological processes involving Abl was found. A large number of substrates for Abl, including other kinases, adaptor proteins and cytoskeleton regulators have been identified so far (Antoku et al., 2008; Boyle et al., 2007; Fox and Peifer, 2007; Kain and Klemke, 2001; Kannan et al., 2017; Plattner et al., 2003; Sossey-Alaoui et al., 2007). Abl acts as interaction platform carrying a PDR, SH2, SH3 domain and offering a binding site for a diverse set of proteins. Additionally, it is able to modify their activity by phosphorylation. The subcellular localization of Abl cannot be restricted to a certain compartment (Wang, 2014). It is highly expressed in the nucleus but also localizes in the cytoplasm and is further associated with actin structures.

Several studies link Abl activation to cytoskeleton remodeling. Also, cell migration is at least partially mediated through Abl dependent phosphorylation of the WRC. Abi was first identified as interacting with Abl through binding the SH3 and PRD domain, respectively. Further, the direct interaction with WAVE provides an additional interaction site with the WRC (Huang et al., 2007; Leng et al., 2005; Sossey-Alaoui et al., 2007; Stuart et al., 2006). Transfection of S2 cells with an active form of Abl kinase clearly confirms WAVE as a substrate of Abl kinase (Figure 18). In WAVE2, Y150 is the only tyrosine residue targeted by c-Abl (Leng et al., 2005). The authors show that the transition of tyrosine to phenylalanine in Y150 of WAVE2 abrogates phosphorylation of WAVE. For *Drosophila* WAVE, this study could demonstrate that mutation of corresponding Y153 is not sufficient to block Abl

dependent phosphorylation (Figure 34). Similar results have been demonstrated previously for WAVE3, in which three additional tyrosine residues (Y248, Y337, Y486) are phosphorylated by Abl (Sossey-Alaoui et al., 2007). However, only Y486 is conserved in other WAVE isoforms, although it does not carry a canonical Abl motif. None of the residues are conserved in invertebrates (Table 2; Supplementary Figure 1). In *Drosophila* WAVE tyrosine residues Y234 shows an Abl corresponding consensus sequence. Furthermore, Y234, Y247 and Y253 have been identified as a substrate for PTP61F in a tyrosine phospho-proteomics screen in S2 cells (Chang et al., 2008). PTP61F dephosphorylates four conserved tyrosine sites of Abi previously targeted by Abl kinase (Huang et al., 2007), but so far has not been investigated for WAVE phosphorylation status. Until further investigations reveal any functional impact for the other tyrosine residues, WAVE Y153 is the only Abl target that revealed a physiological relevance.

abl mutant flies are partially lethal and show severe actin dependent defects during development. Kinase-dead Abl restores the *abl* mutant viability almost as effectively as wild type Abl (Rogers et al., 2016). To dissect the impact of WAVE phosphorylation, WAVE transgenes with specifically mutated Abl target Y153 as well as abrogated phosphorylation of all 15 tyrosine residues were investigated. The re-expression of WAVE phospho-mutant transgenes were in all combinations able to rescue *wave* lethality. Further, the adult rescued flies reveal no morphological defects (data not shown). From this data it can be concluded that the loss of WAVE tyrosine phosphorylation has a negligible regulatory function in developmental processes. This is consistent with findings for serine phosphorylation in *Dictyostelium.* There, the abrogation of phosphorylation of eight serine residues fully restores *wave* mutant migration defects and partially facilitates migration (Singh et al., 2020). However, it must be considered that the five serine residues within the acidic domain, which previously have been claimed as the important regulators for WAVE activation, were not included. As already mentioned, in *Dictyostelium* WASP can partially substitute the WAVE function. Therefore, *Drosophila* might be the more reliable model organism to investigate this question.

Further investigations in this study addressed the impact of Abl function in macrophage migration as this system is sensitive to changes in WAVE dependent lamellipodia formation. Fibroblast mutant for *abl* and *arg* (*abl2*) fail to induce membrane ruffles in response to PDGF stimulation and show reduced actin fibers in the cell periphery (Kain and Klemke, 2001; Stuart et al., 2006). In contrast, macrophages lacking *abl* are still able to form proper lamellipodia (Figure 23). The shape analyses showed that the cells are increased in size and show a round morphology. This phenotype is phenocopied by overexpressing a dominant negative Abl

construct, revealing the kinase function as essential for macrophage cell morphology (Figure 23). So far, the impact of *abl* depletion on single cell migration has not been addressed *in vivo.* The results of this work showed that *abl* mutant macrophages were still able to migrate with a comparable speed as wildtype cells but lose their explorative behavior (Figure 24).

Interestingly, *abl* mutant macrophages show an increased Src42A protein level. Therefore, it can be suggested, that Src compensates for the loss *abl.* The reduction of one gene copy of *src42A* in *abl* mutant background slightly decreases cell persistence, straightness, and explorative behavior. Nevertheless, the reduction of *src42A* alone already impairs migration. Therefore, no final conclusion can be drawn regarding Src42A potentially substituting Abl in its absence.

A previous study has shown that Abl dependent WAVE phosphorylation correlates with the translocation of WAVE to the membrane (Leng et al., 2005). Surprisingly, the results in this work showed WAVE, in the absence of Abl, to be significantly increased at membrane of macrophages (Figure 29). This could be an explanation for the increase in cell size of *abl* mutant macrophages. However, this does not allow a definitive conclusion on whether WAVE is recruited more efficiently or if the dissociation of WAVE from the membrane is deregulated. Further research into this question will be necessary. It can be assumed that the regulatory defects of WAVE at the membrane might cause the observed migratory defects and the loss of explorative behavior of *abl* mutant macrophages.

4.4.1 Wound-signal transduction in *Drosophila* is not mediated by Abl or Src kinases

The reduced explorative ability in random migration due to loss of *abl* (Figure 24) might indicate that Abl kinase is important in the transmission of extracellular chemotactic guidance cues. As direct binding partner of WRC, direct phosphorylation of WAVE or Abi might transmit the external signal to the actin machinery. Similar to Abl, Src is reported as interacting with WAVE via its SH3 domain. However, in this study we were unable to confirm a direct interaction between the Src42A active form and WAVE in Co-IP experiments (Figure 19). Src42A also carries a SH2 domain binding phospho-tyrosine, which offers the possibility that WAVE might also depend on WAVE phosphorylation and/or activity state. The co-expression of the active form of Abl does not facilitate the Src42A-WAVE binding (Figure 19). Still, other regulatory mechanisms might influence the binding and the exact activation state of WAVE as well as Src.

Abl and Src42A contain a cysteine residue that is conserved in Src family kinases (SFK). In zebra fish leucocyte wound attraction is mediated by SFK Lyn (Yoo et al., 2012, 2011). In this

process, the cysteine residue acts as sensor to transmit H_2O_2 as a damage signal via oxidation to induce the activation of the kinase domain. This makes Abl and Src42A kinase interesting candidates to transmit wound signals to the actin machinery. However, this study could not identify any defects in the wound-response for either Abl or Src42A kinase (Figure 21, Figure 26). These results contradict previous findings in *Drosophila* embryo. They demonstrating that in *src42A* mutants as well as macrophages expressing a dominant negative Src42A transgene the wound response is impaired (Evans et al., 2015). These conflicting results could be explained by the difference of the quantification method. In this work, the cell bias angle was determined to detect directionality of the migrating cells towards the wound on cellular level. For this parameter no significant defects could be detected. In contrast, Evans and colleagues (2016) mainly count the cell number at the wounding site to address the general responsiveness. Their method might be affected by general migratory defects. In their study they already found a reduction of speed in *src42A* mutant macrophages. These findings are consistent with the results of this work. Macrophages expressing kinase dead Src42A show migration defects in random migration independently from external wounding signals (Figure 20). In conclusion, it could be shown that Src42a interferes with macrophage migration but neither Abl nor Src42A are key regulators that transmit an external wounding signal to the actin machinery. These findings are supported by another study by Weavers et al. (2016). They determine the diffusion ability of a potential chemoattractant due to the response time of macrophage upon wounding. Their data excludes quickly diffusing molecules like H_2O_2 and ATP (Weavers et al., 2016).

In collective border cell migration, the anterior-posterior migration is guided by PVR and EGFR signaling (Bianco et al., 2007; McDonald et al., 2006; Montell, 2003). Src, as well as Abl kinase, are activated upon growth factor signaling and therefore seem to be potential candidates to transduce this chemotactic guidance clue to the actin cytoskeleton. Here, the RNAi mediated depletion of *Src42A* or the expression of the kinase dead transgene specifically in border cells reveal strong defects in collective border cell migration (Supplementary Figure 9). However, depletion of Abl or interference with Abl kinase function has no impact on border cell migration (Supplementary Figure 9). Judging by these results, it can be assumed that Src42A might be activated upon the growth factor signaling in border cell migration. Further results, gained by suppressing *wave* by *c306*-Gal4 strong, a specific border cell driver showed an interference of migration in a comparable range as the one determined for Src42A kinase (Supplementary Figure 9). Therefore, further investigations are needed to identify a correlated mechanism of WAVE and Src42A in collected border cell migration.

4.5 Negative regulation of WAVE at the leading edge

In previous studies, phosphorylation of WAVE has mainly been characterized as an additional mechanism to regulate WRC activation to induce actin polymerization (Ardern et al., 2006; Chen et al., 2010). As discussed in the previous chapter, phosphorylation of conserved residue Y153, but not Y127, leads to an elevation of the F-actin level (Figure 33). Interestingly, phosphorylation of both tyrosine residues simultaneously has not been addressed, so far. With this, it is likely that under physiological conditions Y127 as target for Src kinase and Y153, being a substrate for Abl kinase, are phosphorylated at the same time. Abl itself can be activated by Src kinase (Panjarian et al., 2013). Furthermore, Src and Abl both carry a SH2 domain binding to phosphorylated tyrosine residues. It might be that phosphorylation of one residue facilitates the recruitment of the respective kinase and consequently phosphorylation of further residues. Therefore, this study investigates the effects of the exchange of tyrosine Y127 and Y153 to glutamic acid for macrophage migration.

Interestingly, mimicking phosphorylation of both residues does not lead to an increase of F-actin level compared to the exchange of Y153 alone (Figure 33, Figure 37). On the contrary, macrophages exhibit long filipodia and show only a rudimentary lamellipodium when re-expressing the phospho-mimicking transgene with two exchanges in a *wave* mutant background (Figure 37). In random migration, these cells show a drastically reduced cell speed, a lower persistence and straightness in a range that was detected in migration of *wave* mutant cells (Figure 38, Movie 24). This might be a first hint that phosphorylation might also be a negative control mechanism for WAVE.

Until today, negative regulation of WAVE dependent actin polymerization is only poorly investigated in comparison to mechanisms that facilitate WAVE activation. The results of this study show that WAVE with phospho-mimicking mutations of all WAVE 15 tyrosine residues is embryonically lethal (Table 12). Furthermore, the simultaneous phosphorylation of only two important residues, Y127 and Y153, within the WHD domain leads to a late pupal lethality. Consistent with these results, ubiquitous (*da*-Gal4) as well as posterior (*en*-Gal4) overexpression of the active kinase form Src42A and Abl cause embryonal lethality. This might be due to over-proliferation but could be facilitated by actin dysregulation. Furthermore, the overexpressing BCR-Abl expression in the eye leads to a strong rough eye phenotype (Fogerty et al., 1999). The results of this study show that the re-expression of the phospho-mimicking transgene Y127E+Y153E in a *wave* mutant background leads to a milder version of this eye phenotype (Figure 35). Eye development is highly dependent on WRC dependent actin regulation. Depletion of one subunit of the WRC interferes with axon targeting during

eye development (Bogdan et al., 2004; Zallen et al., 2002). Nevertheless, further quantifications are needed to validate the defects observed in this study. Detailed analysis of the interommatidial bristles of the eye via electron microscopy could be performed to get further insights. In summary, it can be predicted that the phosphorylation status of WAVE finetunes the activity of the WRC. Single phosphorylation of Y153 facilitates WAVE activity whereas simultaneous phosphorylation of Y127 and Y153 interferes with its function. Different hypotheses can be stated to mechanistically explain how phosphorylation of WAVE also negatively regulates the WRC.

First, complex integrity of the WRC is crucial for proper WAVE function. The substitution of all 15 tyrosine sites to negatively charges glutamic acid might interfere with the quaternary structure formation of WRC. This is proposed with negative consequences for complex stability and might explain embryonal lethality. The phosphorylation of the different WRC subunits are not independent from each other. WAVE2 needs to be phosphorylated at Y150 until Abi can be phosphorylated respectively (Leng et al., 2005). Mutation of Y150F consequently blocks Abi phosphorylation. Additionally, WAVE2 binding of Abi facilitates Abl dependent phosphorylation of WAVE. In conclusion, this data indicates a strong dependency between those subunits and has to be considered for further experiments. Furthermore, it needs to be investigated whether multiple phosphorylation and consequently the addition of negative charges to WHD interfere with the binding of Abi to WAVE. As mentioned previously, for Sra-1 it has been demonstrated that phosphorylation of a single residue in the meander region of WAVE (WAVE2 Y150, Y124, S137/ WAVE1 T138) destabilizes the binding of these two subunits and induct the release of the VCA (Chen et al., 2010; Miyamoto et al., 2008). These studies did not show whether multiple simultaneous phosphorylation events in the region might further destabilize the binding of Sra1 and WAVE which might cause serious consequences for complex integrity (Figure 42-1). The results in this study show that phosphorylation of two tyrosine residues in the WHD interfere with WAVE function that might be caused by the destabilization of the WRC. Complex integrity is essential for protein stability of the single subunits (Steffen et al., 2004; Stradal and Scita, 2005).

Secondly, the recruitment and localization of WRC at the leading edge is facilitated by a trapping mechanism, immobilizing the free diffusing WRC at the lamellipodium tip (Mehidi et al., 2019, 2018). Therefore the correct binding and orientation of the complex might depend on the charge composition of the complex (Chen et al., 2010). The correct orientation is crucial for the accessibility of the WAVE for upstream activators like RAC, different effector kinases or the binding to the Arp2/3 complex. Interference with these interactions would negatively

influence F-actin formation. Additionally, the addition of multiple negative charges most likely alter the binding ability and orientation of the whole complex to the membrane phospholipids. Tyrosine residues close to the positively charged basic region are particularly likely to interfere with the binding of WAVE with to PIP3 (Figure 42-2). After activating the Arp2/3 complex, the WRC needs to dissociate for efficient elongation of the newly formed daughter filament. This is facilitated by a stronger binding of the WRC to the lamellipodial tip than to the Arp2/3 complex (Mehidi et al., 2018). Additionally, regulatory proteins like Cortactin can bind to the Arp2/3 complex, weakening VCA-Arp2/3 interaction and increasing the turnover efficiency rate of actin nucleators before dissociating from the membrane (Dimchev et al., 2017). Serine phosphorylation of the VCA might be an additional mechanism to facilitate WAVE activation and at the same site weaken Arp2/3 binding. In *abl* mutants it can be assumed that WAVE, but also Abi, are present in a less phosphorylated state than in the presence of Abl. Interestingly, WAVE is found to be increased at the membrane, supporting the notion that a decrease of negative charges might facilitate binding or recruitment of WAVE to the membrane.

Third, the increased membrane localization of WAVE could also be caused by dysregulation of WAVE dissociation from the membrane. Recent studies in T-cells directly link WAVE activation, by the VCA release, from autoinhibiting conformation to proteasomal degradation (Joseph et al., 2017). Since the autoinhibitory conformation of the WRC preserves complex stability, the release of the VCA domain unmasks the particularly highly conserved WAVE2 lysine K45 (dWAVE K48, Supplementary Figure 1). Conclusively, Joseph and colleges claim that activation of WAVE makes the protein simultaneously accessible for the ubiquitination machinery initiating protein degradation (Figure 42-3). Thus, degradation would be a self-controlled mechanism to remove activated WAVE and prevent overshooting activity of the activated WRC. This hypothesis is further supported by data for serine phosphorylation in *Dictyostelium.* In this case, dephosphorylation of serine residues in the VCA domain activate on WAVE. Furthermore, this leads to an accelerated degradation of WAVE, showing that activation rather than phosphorylation is the critical step to regulate WAVE protein level (Ura et al., 2012). Equally, Src-dependent phosphorylation activates N-WASP, but simultaneously initiates degradation *via* ubiquitination (Suetsugu et al., 2002). Furthermore, Abi2 - targeted by Src and Abl kinase is first activated but finally degraded (Dai et al., 2001). Degradation of one complex subunit leads to the degradation of the others WRC members (Kunda et al., 2003; Rogers et al., 2003; Schenck et al., 2004). A recent publication by Cloud et al. (2019) connects WAVE protein level regulation with Ataxin-7, a subunit of the SAGA chromatin remodeling complex. Ataxin-7 binds the deubiquitinase Non-stop. Interestingly, the released and freely

dissociating Non-Stop interacts with the WRC mediated by WIRS motive binding. Depletion of Ataxin-7 or overexpression of Non-Stop results in a drastic increase of WAVE protein levels, blocking ubiquitin regulated degradation (Cloud et al., 2019). This offers a new perspective on phosphorylation dependent WAVE activation. The molecular weight shift that was observed in BCR-Abl expressing S2R+ cells in Western blot analyzes was initially interpreted as having been caused by WAVE phosphorylation. However, a single phosphate group only adds 80 Da, whereas ubiquitin is 8.5 kDa polypeptide and therefore more likely to cause the detected weight differences (Figure 18, A). To prove this hypothesis, WAVE needs to be precipitated and stained with the respective antibody to detect ubiquitination. Just as phosphorylation, ubiquitination is a reversable posttranscriptional protein modification. Following this theory, it could be suggested that WAVE levels are increased in *abl* mutants, as it is expected to be less degraded. Initial data has confirmed this assumption. The overall protein level in *abl* mutants was increased 1.2-fold (Figure 30; Supplementary Figure 7), which is comparable with previous published data. Zhu and Bhat (2011) demonstrate that Abl negatively regulates WAVE protein level while WAVE mRNA stays constant (Zhu and Bhat, 2011). Analyzing the distribution of WAVE in macrophages in the absence of Abl showed that WAVE in particular accumulated at the membrane, while overall cellular WAVE remains almost equal (Figure 29). In comparison to wild type macrophages membrane localization is increased about 1.4-fold. Taken together, these findings suggest that phosphorylation dependent WAVE activation balances protein activation. At the same time, it might regulate a constant turn-over of at the membrane by degradation of activated WAVE. In migrating *abl* mutant cells this leads to a reduction in the explorative behavior.

Finally, the results of this study lead to a new working model (Figure 42). This implies further perspectives for a self-control mechanism to prevent over-activation of the WRC at the membrane. Thereby, all three suggested processes - complex integrity, charge distribution on the WCR surface and finally degradation via ubiquitination - may also work in parallel and facilitate each other. In consequence, this makes tyrosine phosphorylation of WAVE, especially in the WHD domain, a mechanism to fine-tune WRC activity.

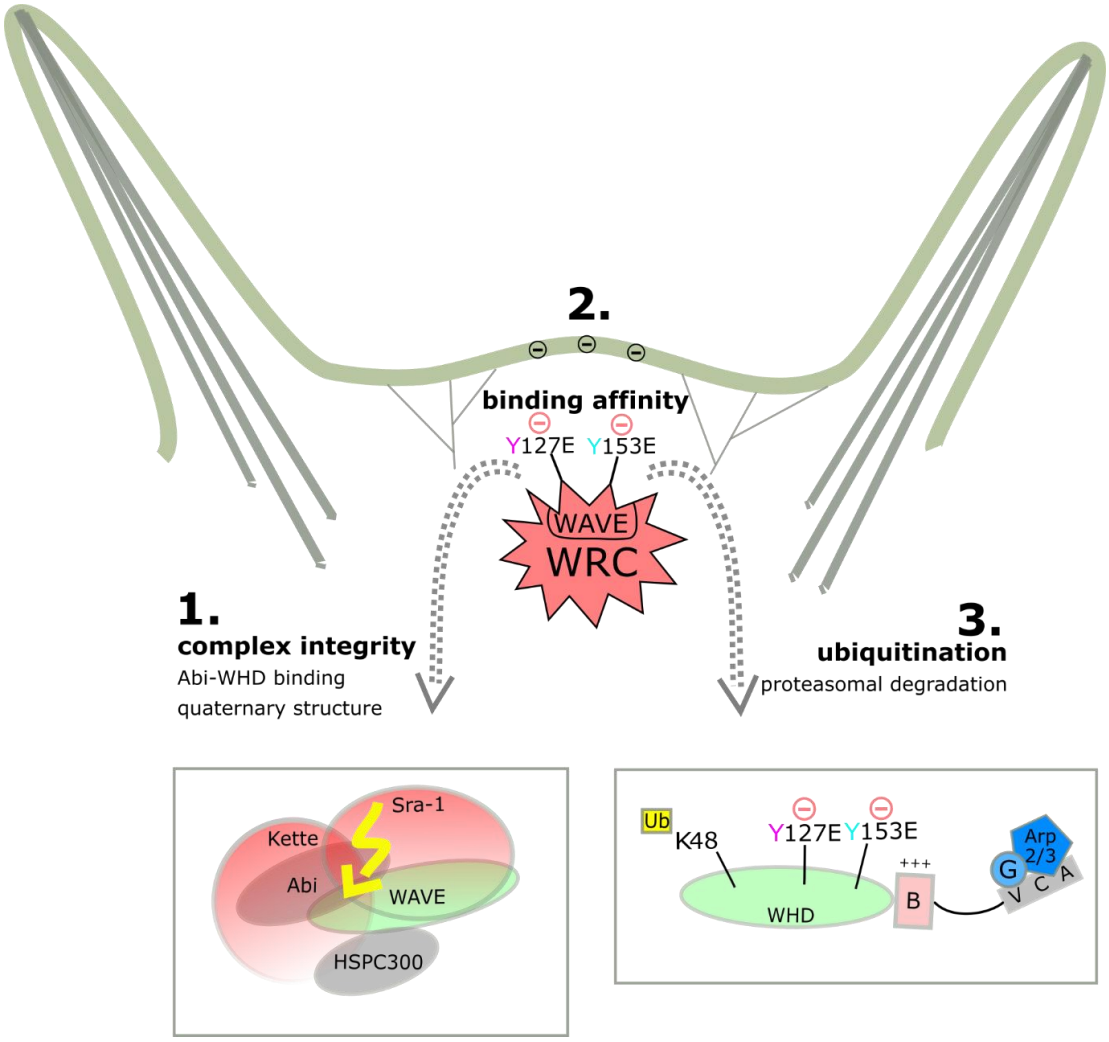

Figure 42: Negative regulation of active WAVE at the leading edge – a working model. Phosphorylation of the two conserved tyrosine residues Y127 and Y153 with WAVE WHD interfere with lamellipodia formation. Three different hypotheses are suggested how phosphorylation might interfere with WAVE dependent F-actin formation at the leading edge. **1)** An increace of negative charges might interfere with the quaternary structure formation of WAVE and the binding affinity to the other subunits of the VRC. **2**) The orientation and binding affinity of the WCR to negatively charged phosphoinositide incorporated in the membrane is suggested to be weakened in highly phosphorylated WAVE. **3**) The activation of WAVE by the release of the VCA domain unmasked K48, which ubiquitination is associated with WAVE degradation.

5 Summary – Zusammenfassung

Cell migration is highly dependent on the precise orchestration of the assembly and disassembly of filamentous actin at their leading edge. Therefore, the temporal and spatial regulation of WAVE activity as the main regulator of Apr2/3 for branched actin polymerization is crucial for efficient lamellipodia-driven cell motility.

This work shows that *wave* mutant *Drosophila* macrophages completely lack lamellipodia that causes severe migration defects. However, they still respond to wound signals by relying on rudimentary filopodia based migration. Furthermore, it could be shown that the disruption of the WIRS receptor binding site within the WRC does not interfere with wound response of macrophages.

The non-receptor tyrosine kinase Abl is assumed to be a key regulator of WAVE, altering its activity via phosphorylation. The results in this study confirm that the active form of Abl is an effector of WAVE. The loss of *abl* and the overexpression of Abl kinase dead transgene leads to an increase of cell spreading. Further, WAVE localization at the membrane is elevated in the absence of Abl. This alteration seems to influence random migration by reducing the explorative behavior of macrophages. However, loss of *abl* did not affect the responsiveness of macrophages to external damage signals. WAVE possesses four tyrosine residues within the WHD: Y127 is a Src kinase target and Y153 of the Abl kinase. The WAVE phospho-mutant Y153F is still phosphorylated via Abl. This indicates that additional tyrosine sites are targeted by Abl. Nevertheless, the phosphorylation of Y153 results in an elevated F-actin level that indicates the physiological relevance of this tyrosine residue. This suggests that phosphorylation of Y153 activates WAVE and the WRC, which is consistent with the results of previous studies. The analysis of random migrating macrophages revealed that this leads to a reduction of cell speed. In contrast, the phosphorylation of Y127 in the WHD showed neither an impact on the F-actin level nor on the migratory behavior of macrophages. Interestingly, the simultaneous phosphorylation of both residues leads to a drastic reduction of lamellipodial structures in macrophages. These cells exhibited extended filopodia and showed a stellar cell shape comparable to *wave* mutant macrophages. Consequently, *in vivo* migrating macrophages show a reduction of cell speed and a negative impact on the persistence of these cells. Individual phospho-mimicking mutation of Y127 or Y153 also do not interfere with the viability of the flies, whereas the simultaneous phosphorylation of both sites lead to late pupal lethality. These results indicate that phosphorylation of multiple tyrosine residues has a negative regulatory effect on WRC function. In conclusion, it can be shown that phosphorylation state of WAVE finetunes WRC activity.

❖

Die Migration von Zellen ist im hohen Maße von dem Auf- und Abbau der Aktinfilamente am Leitsaumen der Zellen abhängig. Dabei ist die lokale und zeitgenaue Regulation von WAVE als Schlüsselregulator des Arp2/3 Komplexes für vernetzte Aktin Polymerisierung entscheidend für eine effiziente, durch das Lamellipodium getriebene, Zellbewegung.
Diese Arbeit zeigt, dass mutierte *wave* Makrophagen in *Drosophila* keine Lamellipodia mehr ausbilden, was starke Migrationsdefekte zur Folge hat. Dennoch reagieren weiter sie auf Wundsignale, die sie mittels einer rudimentären, filopodialen Migration erreichen. Jedoch konnte gezeigt werden, dass die Zerstörung der WIRS Rezeptor-Bindestelle im WRC die Wundantwort der Makrophagen nicht beeinträchtigt.
Die Nicht-Rezeptor-Tyrosinkinase Abl wird als Schlüsselregulatoren für WAVE vermutet, indem sie mittels Phosphorylierung die Aktivität verändert. Die Ergebnisse dieser Studie bestätigen, dass die aktive Form von Abl ein Effektor von WAVE ist. Der Verlust von *abl* sowie die Überexpression des dominant negativen Transgens führen zu einer gesteigerten Zellspreizung. Weiter ist in der Abwesenheit von Abl die Membranlokalisation von WAVE erhöht. Diese Veränderung hat Einfluss auf die freie Migration, indem sie das explorative Verhalten der Zellen senkt. Jedoch hat der Verlust von *abl* keine Auswirkung auf das Reaktionsvermögen von Makrophagen auf externe Beschädigungssignale. WAVE besitzt vier Tyrosine in der WHD: Y127 ist ein vorhergesagtes Ziel der Src Kinase und Y153 der Abl Kinase. Die WAVE Phospho-Mutante Y153F wird jedoch immer noch von Abl phosphoryliert. Das weist darauf hin, dass noch weitere Tyrosine relevante Ziel von Abl sind. Nichtsdestotrotz führt die Phosphorylierung von Y153 zu einer Erhöhung des F-Aktin Level, was die physiologische Relevanz dieses Tyrosins unterstreicht. Es kann angenommen werden, dass die Phosphorylierung von Y153 aktivierend auf WAVE und den WRC wirkt. Dieses Ergebnis ist konsistent mit denen anderer Studien. Die Analyse der Migration von Makrophagen zeigt, dass die Phosphorylierung von Y153 zu einer Reduktion der Geschwindigkeit führt. Im Gegensatz dazu hat die Phosphorylierung von Y127 weder einen Einfluss auf das F-Aktin Level noch auf das Migrationsverhalten der Makrophagen. Interessanterweise führt die gleichzeitige Phosphorylierung von beiden Tyrosinen zu einer drastischen Reduktion von lamellipodialen Strukturen. Diese Zellen stellen verlängerte Filopodien aus und besitzen eine sternförmige Zellform, die mit mutierten *wave* Makrophagen vergleichbar ist. In migrierenden Makrophagen führt dies zu einer Reduktion in der Geschwindigkeit und hat einen negativen Einfluss auf die Persistenz der Zellen. Die individuelle Phosphorylierung von Y127 oder Y153 hat keinen negativen Einfluss auf die Viabilität der Fliegen, wohingegen die gleichzeitige Phosphorylierung zu Letalität im späten

Puppenstadium führt. Diese Ergebnisse deuten darauf hin, dass Phosphorylierung von multiplen Tyrosinen einen negativ regulatorischen Effekt auf die Funktion des WRC hat. Zusammenfassend kann gesagt werden, dass der Phosphorylierungs-Status von WAVE wichtig ist für die Regulation der Aktivität des WRC.

6 References

Abercrombie, M., Heaysman, J.E.M., Pegrum, S.M., 1970a. The locomotion of fibroblasts in culture. Exp. Cell Res. 62, 389–398. https://doi.org/10.1016/0014-4827(70)90570-7

Abercrombie, M., Heaysman, J.E.M., Pegrum, S.M., 1970b. The locomotion of fibroblasts in culture. III. Movements of particles on the dorsal surface of the leading lamella. Exp. Cell Res. 62, 389–398. https://doi.org/10.1016/0014-4827(70)90570-7

Abercrombie, M., Joan, E., Heaysman, M., Pegrum, S.M., 1970c. The locomotion of fibroblasts in culture. II. "Ruffling." Exp. Cell Res. 60, 437–444. https://doi.org/10.1016/0014-4827(70)90537-9

Abou-kheir, W., Isaac, B., Yamaguchi, H., Cox, D., 2008. Membrane targeting of WAVE2 is not sufficient for WAVE2-dependent actin polymerization : a role for IRSp53 in mediating the interaction between Rac and. J. Cell Sci. 121, 379–390. https://doi.org/10.1242/jcs.010272

Aman, A., Piotrowski, T., 2010. Cell migration during morphogenesis. Dev. Biol. 341, 20–33. https://doi.org/10.1016/j.ydbio.2009.11.014

Ammer, A.G., Weed, S.A., 2008. Cortactin branches out: Roles in regulating protrusive actin dynamics, Cell Motility and the Cytoskeleton. https://doi.org/10.1002/cm.20296

Ananthakrishnan, R., Ehrlicher, A., 2007. The Forces Behind Cell Movement. Int. J. Biol. Sci. 3, 303–317. https://doi.org/10.7150/ijbs.3.303

Antoku, S., Saksela, K., Rivera, G.M., Mayer, B.J., 2008. A crucial role in cell spreading for the interaction of Abl PxxP motifs with Crk and Nck adaptors. J. Cell Sci. 121, 3071–3082. https://doi.org/10.1242/jcs.031575

Ardern, H., Sandilands, E., Machesky, L.M., Timpson, P., Frame, M.C., Brunton, V.G., 2006. Src-dependent phosphorylation of Scar1 promotes its association with the Arp2/3 complex. Cell Motil. Cytoskeleton 63, 6–13. https://doi.org/10.1002/cm.20101

Balleza, E., Kim, J.M., Cluzel, P., 2018. Systematic characterization of maturation time of fluorescent proteins in living cells. Nat. Methods 15, 47–51. https://doi.org/10.1038/nmeth.4509

Barrett, K., Leptin, M., Settleman, J., 1997. The Rho GTPase and a Putative RhoGEF Mediate a Signaling Pathway for the Cell Shape Changes in Drosophila Gastrulation 91, 905–915.

Basquin, C., Trichet, M., Vihinen, H., Malardé, V., Lagache, T., Ripoll, L., Jokitalo, E., Olivo-Marin, J., Gautreau, A., Sauvonnet, N., 2015. Membrane protrusion powers clathrin-independent endocytosis of interleukin-2 receptor. EMBO J. 34, 2147–2161. https://doi.org/10.15252/embj.201490788

Bear, J.E., Svitkina, T.M., Krause, M., Schafer, D.A., Loureiro, J.J., Strasser, G.A., Maly, I.V., Chaga, O.Y., Cooper, J.A., Borisy, G.G., Gertler, F.B., 2002. Antagonism between Ena/VASP proteins and actin filament capping regulates fibroblast motility. Cell 109, 509–521. https://doi.org/10.1016/S0092-8674(02)00731-6

Beli, P., Mascheroni, D., Xu, D., Innocenti, M., 2008. WAVE and Arp2/3 jointly inhibit filopodium formation by entering into a complex with mDia2. Nat. Cell Biol. 10, 849–857. https://doi.org/10.1038/ncb1745

Bianco, A., Poukkula, M., Cliffe, A., Mathieu, J., Luque, C.M., Fulga, T. a, Rørth, P., 2007. Two distinct modes of guidance signalling during collective migration of border cells. Nature 448, 362–365. https://doi.org/10.1038/nature05965

Bindels, D.S., Haarbosch, L., Weeren, L.V., Postma, M., Wiese, K.E., Mastop, M., Aumonier, S., Gotthard, G., Royant, A., Hink, M.A., Jr, T.W.J.G., 2017. mScarlet : a bright monomeric red fluorescent protein for cellular imaging 14. https://doi.org/10.1038/nmeth.4074

Bischoff, M.C., Lieb, S., Renkawitz-Pohl, R., Bogdan, S., 2020. Filopodia-based contact stimulated collective migration drives tissue morphogenesis (preprint). Cell Biology. https://doi.org/10.1101/2020.10.19.345082

Blanchoin, L., Pollard, T.D., 2002. Hydrolysis of ATP by Polymerized Actin Depends on the Bound Divalent Cation but Not Profilin † 597–602. https://doi.org/10.1021/bi011214b

Bogdan, S., Grewe, O., Strunk, M., Mertens, A., Klämbt, C., 2004. Sra-1 interacts with Kette and Wasp and is required for neuronal and bristle development in Drosophila. Development 131, 3981–3989. https://doi.org/10.1242/dev.01274

Bogdan, S., Stephan, R., Löbke, C., Mertens, A., Klämbt, C., 2005. Abi activates WASP to promote sensory organ development 7. https://doi.org/10.1038/ncb1305

Bor, B., Bois, J.S., Quinlan, M.E., 2015. Regulation of the formin cappuccino is critical for polarity of Drosophila oocytes. Cytoskeleton 72, 1–15. https://doi.org/10.1002/cm.21205

Boyle, S.N., Michaud, G.A., Schweitzer, B., Predki, P.F., Koleske, A.J., 2007. A Critical Role for Cortactin Phosphorylation by Abl-Family Kinases in PDGF-Induced Dorsal-Wave Formation. Curr. Biol. 17, 445–451. https://doi.org/10.1016/j.cub.2007.01.057

Bradley, W.D., Koleske, A.J., 2009. Regulation of cell migration and morphogenesis by Abl-family kinases: emerging mechanisms and physiological contexts. J. Cell Sci. 122, 3441–3454. https://doi.org/10.1242/jcs.039859

Brasher, B.B., Van Etten, R.A., 2000. c-Abl has high intrinsic tyrosine kinase activity that is stimulated by mutation of the Src homology 3 domain and by autophosphorylation at two distinct regulatory tyrosines. J. Biol. Chem. 275, 35631–35637. https://doi.org/10.1074/jbc.M005401200

Breitsprecher, D., Goode, B.L., 2013. Formins at a glance. J. Cell Sci. 126, 1–7. https://doi.org/10.1242/jcs.107250

Brinkmann, K., Winterhoff, M., O nel, S.-F., Schultz, J., Faix, J., Bogdan, S., 2015. WHAMY is a novel actin polymerase promoting myoblast fusion, macrophage cell motility and sensory organ development. J. Cell Sci. 44, 604–620. https://doi.org/10.1242/jcs.179325

Brühmann, S., Ushakov, D.S., Winterhoff, M., Dickinson, R.B., Curth, U., Faix, J., 2017. Distinct VASP tetramers synergize in the processive elongation of individual actin filaments from clustered arrays. Proc. Natl. Acad. Sci. U. S. A. 114, E5815–E5824. https://doi.org/10.1073/pnas.1703145114

Buracco, S., Claydon, S., Insall, R., 2019. Control of actin dynamics during cell motility [version 1; peer review: 3 approved]. F1000Research 8, 1–10. https://doi.org/10.12688/f1000research.18669.1

Cai, L., Marshall, T.W., Uetrecht, A.C., Schafer, D.A., Bear, J.E., 2007. Coronin 1B Coordinates Arp2/3 Complex and Cofilin Activities at the Leading Edge. Cell 128, 915–929. https://doi.org/10.1016/j.cell.2007.01.031

Campellone, K.G., Welch, M.D., 2010. A nucleator arms race: Cellular control of actin assembly. Nat. Rev. Mol. Cell Biol. 11, 237–251. https://doi.org/10.1038/nrm2867

Carver, R.J., Chen, B., Chou, H.-T., Brautigam, C.A., Xing, W., Yang, S., Henry, L., Doolittle, L.K., Walz, T., Rosen, M.K., 2017. Rac1 GTPase activates the WAVE regulatory complex through two distinct binding sites. eLife 6, e29795–e29795. https://doi.org/10.7554/eLife.29795.001

Cattenoz, P.B., Sakr, R., Pavlidaki, A., Delaporte, C., Riba, A., Molina, N., Hariharan, N., Mukherjee, T., Giangrande, A., 2020. Temporal specificity and heterogeneity of Drosophila immune cells. EMBO J. 39, 1–25. https://doi.org/10.15252/embj.2020104486

Chang, Y.C., Lin, S.Y., Liang, S.Y., Pan, K.T., Chou, C.C., Chen, C.H., Liao, C.L., Khoo, K.H., Meng, T.C., 2008. Tyrosine phosphoproteomics and identification of substrates of protein tyrosine phosphatase dPTP61F in Drosophila S2 Cells by mass

spectrometry-based substrate trapping strategy. J. Proteome Res. 7, 1055–1066. https://doi.org/10.1021/pr700801p

Chen, B., Brinkmann, K., Chen, Z., Pak, C.W., Liao, Y., Shi, S., Henry, L., Grishin, N.V., Bogdan, S., Rosen, M.K., 2014. The WAVE regulatory complex links diverse receptors to the actin cytoskeleton. Cell 156, 195–207. https://doi.org/10.1016/j.cell.2013.11.048

Chen, X.J., Squarr, A.J., Stephan, R., Chen, B., Higgins, T.E., Barry, D.J., Martin, M.C., Rosen, M.K., Bogdan, S., Way, M., 2014. Ena/VASP proteins cooperate with the WAVE complex to regulate the actin cytoskeleton. Dev. Cell 30, 569–584. https://doi.org/10.1016/j.devcel.2014.08.001

Chen, Z., Borek, D., Padrick, S.B., Gomez, T.S., Metlagel, Z., Ismail, A.M., Umetani, J., Billadeau, D.D., Otwinowski, Z., Rosen, M.K., 2010. Structure and control of the actin regulatory WAVE complex. Nature 468, 533–538. https://doi.org/10.1038/nature09623

Cho, N.K., Keyes, L., Johnson, E., Heller, J., Ryner, L., Karim, F., Krasnow, M.A., 2002. Developmental Control of Blood Cell Migration by the Drosophila VEGF Pathway. Cell 108, 865–876. https://doi.org/10.1016/S0092-8674(02)00676-1

Cloud, V., Thapa, A., Morales-Sosa, P., Miller, T.M., Miller, S.A., Holsapple, D., Gerhart, P.M., Momtahan, E., Jack, J.L., Leiva, E., Rapp, S.R., Shelton, L.G., Pierce, R.A., Martin-Brown, S., Florens, L., Washburn, M.P., Mohan, R.D., 2019. Ataxin-7 and Non-stop coordinate SCAR protein levels, subcellular localization, and actin cytoskeleton organization. https://doi.org/10.7554/eLife.49677.001

Cohen, P., 2002. The origins of protein phosphorylation. Nat. Cell Biol. 4. https://doi.org/10.1038/ncb0502-e127

Cooper, J.A., Buhle, E.L., Walker, S.B., Tsong, T.Y., Pollard, T.D., 1983. Kinetic Evidence for a Monomer Activation Step in Actin Polymerization. Biochemistry 22, 2193–2202. https://doi.org/10.1021/bi00278a021

Dai, Z., Kerzic, P., Schroeder, W.G., McNiece, I.K., 2001. Deletion of the Src Homology 3 Domain and C-terminal Proline-rich Sequences in Bcr-Abl Prevents Abl Interactor 2 Degradation and Spontaneous Cell Migration and Impairs Leukemogenesis. J. Biol. Chem. 276, 28954–28960. https://doi.org/10.1074/jbc.M101170200

Davidson, A.J., Millard, T.H., Evans, I.R., Wood, W., 2019. Ena orchestrates remodelling within the actin cytoskeleton to drive robust Drosophila macrophage chemotaxis. J. Cell Sci. 132. https://doi.org/10.1242/jcs.224618

Dimchev, G., Steffen, A., Kage, F., Dimchev, V., Pernier, J., Carlier, M.F., Rottner, K., 2017. Efficiency of lamellipodia protrusion is determined by the extent of cytosolic actin assembly. Mol. Biol. Cell 28, 1311–1325. https://doi.org/10.1091/mbc.E16-05-0334

Duchek, P., Somogyi, K., J??kely, G., Beccari, S., Rorth, P., 2001. Guidance of cell migration by the Drosophila PDGF/VEGF receptor. Cell 107, 17–26. https://doi.org/10.1016/S0092-8674(01)00502-5

Eleftherianos, I., Revenis, C., 2011. Role and Importance of Phenoloxidase in Insect Hemostasis 20052, 28–33. https://doi.org/10.1159/000321931

Evans, I.R., Ghai, P.A., Urbančič, V., Tan, K.-L., Wood, W., 2013. SCAR/WAVE-mediated processing of engulfed apoptotic corpses is essential for effective macrophage migration in Drosophila. Cell Death Differ. 20, 709–720. https://doi.org/10.1038/cdd.2012.166

Evans, I.R., Rodrigues, F.S.L.M., Armitage, E.L., Wood, W., 2015. Draper/CED-1 Mediates an Ancient Damage Response to Control Inflammatory Blood Cell Migration In Vivo. Curr. Biol. CB 25, 1606–12. https://doi.org/10.1016/j.cub.2015.04.037

Fischer, E.H., GRAVES, D.J., CRITTENDEN, E.R., KREBS, E.G., 1959. Structure of the site phosphorylated in the phosphorylase b to a reaction. J. Biol. Chem. 234, 1698–1704.

Fogerty, F.J., Juang, J.L., Petersen, J., Clark, M.J., Hoffmann, F.M., Mosher, D.F., 1999. Dominant effects of the bcr-abl oncogene on Drosophila morphogenesis. Oncogene 18, 219–232. https://doi.org/10.1038/sj.onc.1202239

Fox, D.T., Peifer, M., 2007. Abelson kinase (Abl) and RhoGEF2 regulate actin organization during cell constriction in Drosophila 578, 567–578. https://doi.org/10.1242/dev.02748

Frame, M.C., 2002. Src in cancer: Deregulation and consequences for cell behavior. Biochim. Biophys. Acta - Rev. Cancer 1602, 114–130. https://doi.org/10.1016/S0304-419X(02)00040-9

Galkin, V.E., Orlova, A., Koleske, A.J., Egelman, E.H., 2005. The Arg non-receptor tyrosine kinase modifies F-actin structure. J. Mol. Biol. 346, 565–575. https://doi.org/10.1016/j.jmb.2004.11.078

Gates, J., Mahaffey, J.P., Rogers, S.L., Emerson, M., Rogers, E.M., Sottile, S.L., Van Vactor, D., Gertler, F.B., Peifer, M., 2007. Enabled plays key roles in embryonic epithelial morphogenesis in Drosophila. Development 134, 2027–2039. https://doi.org/10.1242/dev.02849

Genova, J.L., Jong, S., Camp, J.T., Fehon, R.G., 2000. Functional Analysis of Cdc42 in Actin Filament Assembly , Epithelial Morphogenesis , and Cell Signaling during Drosophila Development 194, 181–194. https://doi.org/10.1006/dbio.2000.9671

Germani, F., Bergantinos, C., Johnston, L.A., 2018. Mosaic Analysis in Drosophila 208, 473–490.

Gertler, F.B., Bennett, R.L., Clark, M.J., Hoffmann, F.M., 1989. Drosophila abl tyrosine kinase in embryonic CNS axons: A role in axonogenesis is revealed through dosage-sensitive interactions with disabled. Cell 58, 103–113. https://doi.org/10.1016/0092-8674(89)90407-8

Gertler, F.B., Doctor, J.S., Hoffmann, F.M., 1990. Genetic suppression of mutations in the Drosophila abl proto-oncogene homolog. Science 248, 857–860. https://doi.org/10.1126/science.2188361

Gold, K.S., Brückner, K., 2014. Drosophila as a model for the two myeloid blood cell systems in vertebrates. Exp. Hematol. 42, 717–727. https://doi.org/10.1016/j.exphem.2014.06.002

Goley, E.D., Welch, M.D., 2006. The ARP2/3 complex: an actin nucleator comes of age. Nat. Rev. Mol. Cell Biol. 7, 713–26. https://doi.org/10.1038/nrm2026

Grassart, A., Dujeancourt, A., Lazarow, P.B., Dautry-Varsat, A., Sauvonnet, N., 2008. Clathrin-independent endocytosis used by the IL-2 receptor is regulated by Rac1, Pak1 and Pak2. EMBO Rep. 9, 356–362. https://doi.org/10.1038/embor.2008.28

Han, C., Jan, L.Y., Jan, Y.N., 2011. Enhancer-driven membrane markers for analysis of nonautonomous mechanisms reveal neuron-glia interactions in Drosophila. Proc. Natl. Acad. Sci. U. S. A. 108, 9673–9678. https://doi.org/10.1073/pnas.1106386108

Heit, B., Tavener, S., Raharjo, E., Kubes, P., 2002. An intracellular signaling hierarchy determines direction of migration in opposing chemotactic gradients. J. Cell Biol. 159, 91–102. https://doi.org/10.1083/jcb.200202114

Hoeller, O., Kay, R.R., 2007. Chemotaxis in the Absence of PIP3 Gradients. Curr. Biol. 17, 813–817. https://doi.org/10.1016/j.cub.2007.04.004

Holz, A., 2003. The two origins of hemocytes in Drosophila. Development 130, 4955–4962. https://doi.org/10.1242/dev.00702

Huang, C.H., Lin, T.Y., Pan, R.L., Juang, J.L., 2007. The involvement of Abl and PTP61F in the regulation of Abi protein localization and stability and lamella formation in Drosophila S2 cells. J. Biol. Chem. 282, 32442–32452. https://doi.org/10.1074/jbc.M702583200

Isogai, T., van der Kammen, R., Leyton-Puig, D., Kedziora, K.M., Jalink, K., Innocenti, M., 2015. Initiation of lamellipodia and ruffles involves cooperation between mDia1 and the Arp2/3 complex. J. Cell Sci. 128, 3796–3810. https://doi.org/10.1242/jcs.176768

Johnston, A.B., Collins, A., Goode, B.L., 2015. High-speed depolymerization at actin filament ends jointly catalysed by Twinfilin and Srv2/CAP. Nat. Cell Biol. 17, 1504–1511. https://doi.org/10.1038/ncb3252

Joseph, N., Biber, G., Fried, S., Reicher, B., Levy, O., Sabag, B., Noy, E., Barda-Saad, M., 2017. A conformational change within the WAVE2 complex regulates its degradation following cellular activation. Sci. Rep. 7, 1–16. https://doi.org/10.1038/srep44863

Juang, J.L., Hoffmann, F.M., 1999. Drosophila Abelson interacting protein (dAbi) is a positive regulator of Abelson tyrosine kinase activity. Oncogene 18, 5138–5147. https://doi.org/10.1038/sj.onc.1202911

Kage, F., Winterhoff, M., Dimchev, V., Mueller, J., Thalheim, T., Freise, A., Brühmann, S., Kollasser, J., Block, J., Dimchev, G., Geyer, M., Schnittler, H.J., Brakebusch, C., Stradal, T.E.B., Carlier, M.F., Sixt, M., Käs, J., Faix, J., Rottner, K., 2017. FMNL formins boost lamellipodial force generation. Nat. Commun. 8. https://doi.org/10.1038/ncomms14832

Kain, K.H., Klemke, R.L., 2001. Inhibition of Cell Migration by Abl Family Tyrosine Kinases through Uncoupling of Crk-CAS Complexes. J. Biol. Chem. 276, 16185–16192. https://doi.org/10.1074/jbc.M100095200

Kannan, R., Song, J.K., Karpova, T., Clarke, A., Shivalkar, M., Wang, B., Kotlyanskaya, L., Kuzina, I., Gu, Q., Giniger, E., 2017. The Abl pathway bifurcates to balance Enabled and Rac signaling in axon patterning in Drosophila. Dev. Camb. 144, 487–498. https://doi.org/10.1242/dev.143776

Kim, A.S., Kakalis, L.T., Abdul-Manan, N., Liu, G.A., Rosen, M.K., 2000. Autoinhibition and activation mechanisms of the Wiskott-Aldrich syndrome protein. Nature 404, 151–158. https://doi.org/10.1038/35004513

Kockel, L., Duchek, P., Luque, C.M., Rørth, P., Perrimon, N., 2004. The PDGF / VEGF Receptor Controls Blood Cell Survival in Drosophila 77 Avenue Louis Pasteur 7, 73–84.

Kottmeier, R., 2010. Die Bedeutung der Phosphorylierung von Drosophila SCAR/WAVE.

Kovar, D.R., Harris, E.S., Mahaffy, R., Higgs, H.N., Pollard, T.D., 2006. Control of the assembly of ATP- and ADP-actin by formins and profilin. Cell 124, 423–435. https://doi.org/10.1016/j.cell.2005.11.038

Krause, M., Dent, E.W., Bear, J.E., Loureiro, J.J., Gertler, F.B., 2003. Ena/VASP Proteins: Regulators of the Actin Cytoskeleton and Cell Migration. Annu. Rev. Cell Dev. Biol. 19, 541–564. https://doi.org/10.1146/annurev.cellbio.19.050103.103356

Krause, M., Gautreau, A., 2014. Steering cell migration: Lamellipodium dynamics and the regulation of directional persistence. Nat. Rev. Mol. Cell Biol. 15, 577–590. https://doi.org/10.1038/nrm3861

Kreft, M., 2017. The role of WAVE-dependent actin dynamics in BCC.

Kunda, P., Craig, G., Dominguez, V., Baum, B., 2003. Abi, Sra1, and Kette Control the Stability and Localization of SCAR/WAVE to Regulate the Formation of Actin-Based Protrusions. Curr. Biol. 13, 1867–1875. https://doi.org/10.1016/j.cub.2003.10.005

Laemmli, U.K., 1970. Cleavage of Structura l Proteins during the Assembly of the Head of Bacteriop hage T4 227, 680–685.

Lammel, U., Bechtold, M., Risse, B., Berh, D., Fleige, A., Bunse, I., Jiang, X., Klämbt, C., Bogdan, S., 2014. The Drosophila FHOD1-like formin Knittrig acts through Rok to promote stress fiber formation and directed macrophage migration during the cellular immune response 1366–1380. https://doi.org/10.1242/dev.101352

Lebensohn, A.M., Kirschner, M.W., 2009. Activation of the WAVE Complex by Coincident Signals Controls Actin Assembly. Mol. Cell 36, 512–524. https://doi.org/10.1016/j.molcel.2009.10.024

Lee, T., Luo, L., 2001. Mosaic analysis with a repressible cell marker (MARCM) for Drosophila neural development. Trends Neurosci. 24, 251–254. https://doi.org/10.1016/S0166-2236(00)01791-4

Leithner, A., Eichner, A., Müller, J., Reversat, A., Brown, M., Schwarz, J., Merrin, J., de Gorter, D.J.J., Schur, F., Bayerl, J., de Vries, I., Wieser, S., Hauschild, R., Lai, F.P.L., Moser, M., Kerjaschki, D., Rottner, K., Small, J.V., Stradal, T.E.B., Sixt, M., 2016. Diversified actin protrusions promote environmental exploration but are dispensable for locomotion of leukocytes. Nat. Cell Biol. 18, 1253–1259. https://doi.org/10.1038/ncb3426

Lemaitre, B., Hoffmann, J., 2007. The Host Defense of Drosophila melanogaster. Annu. Rev. Immunol. 25, 697–743. https://doi.org/10.1146/annurev.immunol.25.022106.141615

Leng, Y., Zhang, J., Badour, K., Arpaia, E., Freeman, S., Cheung, P., Siu, M., Siminovitch, K., 2005. Abelson-interactor-1 promotes WAVE2 membrane translocation and Abelson-mediated tyrosine phosphorylation required for WAVE2 activation. Proc. Natl. Acad. Sci. 102, 1098–1103. https://doi.org/10.1073/pnas.0409120102

Lin, H., Spradling, A.C., 1993. Germline Stem Cell Division and Egg Chamber Development in Transplanted Drosophila Germaria. Dev. Biol. 159, 140–152. https://doi.org/10.1006/dbio.1993.1228

Lindsley, D., Zimm, G., 1992. The Genome of Drosophila melanogaster. Academic Press, San Diego.

Litschko, C., Linkner, J., Brühmann, S., Stradal, T.E.B., Reinl, T., Jänsch, L., Rottner, K., Faix, J., 2017. Differential functions of WAVE regulatory complex subunits in the regulation of actin-driven processes. Eur. J. Cell Biol. 0–1. https://doi.org/10.1016/j.ejcb.2017.08.003

Llense, F., Martín-Blanco, E., 2008. JNK Signaling Controls Border Cell Cluster Integrity and Collective Cell Migration. Curr. Biol. 18, 538–544. https://doi.org/10.1016/j.cub.2008.03.029

MacGrath, S.M., Koleske, A.J., 2012. Arg/Abl2 modulates the affinity and stoichiometry of binding of cortactin to F-actin. Biochemistry 51, 6644–6653. https://doi.org/10.1021/bi300722t

Makhijani, K., Alexander, B., Tanaka, T., Rulifson, E., Brückner, K., 2011. The peripheral nervous system supports blood cell homing and survival in the Drosophila larva. Dev. Camb. Engl. 138, 5379–91. https://doi.org/10.1242/dev.067322

Mcdonald, B., Pittman, K., Menezes, G.B., Hirota, S.A., Waterhouse, C.C.M., Beck, P.L., Muruve, D.A., Kubes, P., 2010. Intravascular Danger Signals Guide Neutrophils to Sites of Sterile Inflammation 330, 362–366. https://doi.org/10.1126/science.1195491

McDonald, J.A., Pinheiro, E.M., Kadlec, L., Schupbach, T., Montell, D.J., 2006. Multiple EGFR ligands participate in guiding migrating border cells. Dev. Biol. 296, 94–103. https://doi.org/10.1016/j.ydbio.2006.04.438

Mehidi, A., Kage, F., Karatas, Z., Polesskaya, A., Sainlos, M., 2018. Mechanical regulation of the WAVE complex by actin elongation in the lamellipodium. SSRN Electron. J. https://doi.org/10.2139/ssrn.3192025

Mehidi, A., Rossier, O., Schaks, M., Chazeau, A., Binamé, F., Remorino, A., Coppey, M., Karatas, Z., Sibarita, J.B., Rottner, K., Moreau, V., Giannone, G., 2019. Transient Activations of Rac1 at the Lamellipodium Tip Trigger Membrane Protrusion. Curr. Biol. 29, 2852-2866.e5. https://doi.org/10.1016/j.cub.2019.07.035

Mendoza, M.C., 2013. Phosphoregulation of the WAVE regulatory complex and signal integration. Semin. Cell Dev. Biol. 24, 272–279. https://doi.org/10.1016/j.semcdb.2013.01.007

Mendoza, M.C., Er, E.E., Zhang, W., Ballif, B.A., Elliott, H.L., Danuser, G., Blenis, J., 2011. ERK-MAPK Drives Lamellipodia Protrusion by Activating the WAVE2 Regulatory Complex. Mol. Cell 41, 661–671. https://doi.org/10.1016/j.molcel.2011.02.031

Miyamoto, Y., Yamauchi, J., Tanoue, A., 2008. Cdk5 phosphorylation of WAVE2 regulates oligodendrocyte precursor cell migration through nonreceptor tyrosine kinase fyn. J. Neurosci. 28, 8326–8337. https://doi.org/10.1523/JNEUROSCI.1482-08.2008

Montell, D.J., 2003. Border-cell migration: the race is on. Nat. Rev. Mol. Cell Biol. 4, 13–24. https://doi.org/10.1038/nrm1006

Monypenny, J., Zicha, D., Higashida, C., Oceguera-Yanez, F., Narumiya, S., Watanabe, N., 2009. Cdc42 and Rac Family GTPases Regulate Mode and Speed but Not Direction of Primary Fibroblast Migration during Platelet-Derived Growth Factor-Dependent Chemotaxis. Mol. Cell. Biol. 29, 2730–2747. https://doi.org/10.1128/mcb.01285-08

Moreira, C.G. a, Jacinto, A., Prag, S., 2013. Drosophila integrin adhesion complexes are essential for hemocyte migration in vivo. Biol. Open 2, 795–801. https://doi.org/10.1242/bio.20134564

Moreira, S., Stramer, B., Evans, I., Wood, W., Martin, P., 2010. Prioritization of Competing Damage and Developmental Signals by Migrating Macrophages in the Drosophila Embryo. Curr. Biol. 20, 464–470. https://doi.org/10.1016/j.cub.2010.01.047

Nagar, B., Hantschel, O., Young, M.A., Scheffzek, K., Veach, D., Bornmann, W., Clarkson, B., Superti-Furga, G., Kuriyan, J., 2003. Structural basis for the autoinhibition of c-Abl tyrosine kinase. Cell 112, 859–871. https://doi.org/10.1016/S0092-8674(03)00194-6

Nagel, B.M., Bechtold, M., Rodriguez, L.G., Bogdan, S., 2017. Drosophila WASH is required for integrin-mediated cell adhesion, cell motility and lysosomal neutralization. J. Cell Sci. 130, 344–359. https://doi.org/10.1242/jcs.193086

Nakanishi, O., Suetsugu, S., Yamazaki, D., Takenawa, T., 2007. Effect of WAVE2 phosphorylation on activation of the Arp2/3 complex. J. Biochem. (Tokyo) 141, 319–325. https://doi.org/10.1093/jb/mvm034

Oikawa, T., Yamaguchi, H., Itoh, T., Kato, M., Ijuin, T., Yamazaki, D., Suetsugu, S., Takenawa, T., 2004. PtdIns(3,4,5)P3 binding is necessary for WAVE2-induced formation of lamellipodia 6, 4–6. https://doi.org/10.1038/ncb1125

Olofsson, B., Page, D.T., 2005. Condensation of the central nervous system in embryonic Drosophila is inhibited by blocking hemocyte migration or neural activity. Dev. Biol. 279, 233–243. https://doi.org/10.1016/j.ydbio.2004.12.020

Önel, S.-F., Renkawitz-Pohl, R., 2009. FuRMAS : Triggering Myoblast Fusion in Drosophila 1513–1525. https://doi.org/10.1002/dvdy.21961

Owen-Lynch, J., Whettno, A.D., 1993. Activation of the Abelson Tyrosine Kinase Activity Is Associated with Suppression of Apoptosis in Hemopoietic Cells. Cancer Res. 53, 1735–1738.

Ozaki, K., Hatano, S., 1984. Mechanism of regulation of actin polymerization by Physarum profilin. J. Cell Biol. 98, 1919–1925. https://doi.org/10.1083/jcb.98.6.1919

Panjarian, S., Iacob, R.E., Chen, S., Engen, J.R., Smithgall, T.E., 2013. Structure and dynamic regulation of abl kinases. J. Biol. Chem. 288, 5443–5450. https://doi.org/10.1074/jbc.R112.438382

Pantaloni, D., Le Clainche, C., Carlier, M.F., 2001. Mechanism of actin-based motility. Science 292, 1502–1506. https://doi.org/10.1126/science.1059975

Parsons, B., Foley, E., 2015. Cellular immune defenses of Drosophila melanogaster. Dev. Comp. Immunol. 1–7. https://doi.org/10.1016/j.dci.2015.12.019

Paul, A.S., Pollard, T.D., 2009. Review of the mechanism of processive actin filament elongation by formins. Cell Motil. Cytoskeleton 66, 606–617. https://doi.org/10.1002/cm.20379

Perrimon, N., 1992. Use of a Yeast Site-Specific Recombinase to Generate Embryonic Mosaics in Drosophila 367375.

Plattner, R., Irvin, B.J., Guo, S., Blackburn, K., Kazlauskas, A., Abraham, R.T., York, J.D., Pendergast, A.M., 2003. A new link between the c-Abl tyrosine kinase and phosphoinositide signalling through PLC-γ1. Nat. Cell Biol. 5, 309–319. https://doi.org/10.1038/ncb949

Plattner, R., Kadlec, L., Demali, K.A., Kazlauskas, A., Pendergast, A.M., 1999. c-Abl is activated by growth factors and Src family kinases and has a role in the cellular

response to PDGF. Genes Dev. 13, 2400–2411. https://doi.org/10.1101/gad.13.18.2400

Pocha, S.M., Cory, G.O., 2009. WAVE2 is regulated by multiple phosphorylation events within its VCA domain. Cell Motil. Cytoskeleton 66, 36–47. https://doi.org/10.1002/cm.20323

Pollard, T.D., Borisy, G.G., 2003. Cellular Motility Driven by Assemblyand Disassembly of Actin Filaments. Cell Press 112, 453–465.

Prasad, M., Montell, D.J., 2007. Cellular and Molecular Mechanisms of Border Cell Migration Analyzed Using Time-Lapse Live-Cell Imaging. Dev. Cell 12, 997–1005. https://doi.org/10.1016/j.devcel.2007.03.021

Price, C., Rassool, F., Shivji, M., Gow, J., Tew, C., Haworth, C., Goldman, J., Wiedemann, L., 1988. Rearrangement of the breakpoint cluster region and expression of P210 BCR-ABL in a "masked" Philadelphia chromosome-positive acute myeloid leukemia. Blood 72, 1829–1832. https://doi.org/10.1182/blood.V72.5.1829.bloodjournal7251829

Rasson, A.S., Bois, J.S., Pham, D.S.L., Yoo, H., Quinlan, M.E., 2015. Filament assembly by spire: Key residues and concerted actin binding. J. Mol. Biol. 427, 824–839. https://doi.org/10.1016/j.jmb.2014.09.002

Ratheesh, A., Belyaeva, V., Siekhaus, D.E., 2015. Drosophila immune cell migration and adhesion during embryonic development and larval immune responses. Curr. Opin. Cell Biol. 36, 71–79. https://doi.org/10.1016/j.ceb.2015.07.003

Razzell, W., Evans, I.R., Martin, P., Wood, W., 2013. Calcium flashes orchestrate the wound inflammatory response through duox activation and hydrogen peroxide release. Curr. Biol. 23, 424–429. https://doi.org/10.1016/j.cub.2013.01.058

Reichman, C., Singh, K., Liu, Y., Singh, S., Li, H., Fajardo, J.E., Fiser, A., Birge, R.B., 2005. Transactivation of Abl by the Crk II adapter protein requires a PNAY sequence in the Crk C-terminal SH3 domain. Oncogene 24, 8187–8199. https://doi.org/10.1038/sj.onc.1208988

Ridley, A.J., Paterson, H.F., Johnston, C.L., Diekmann, D., Hall, A., 1992. The small GTP-binding protein rac regulates growth factor-induced membrane ruffling. Cell 70, 401–410. https://doi.org/10.1016/0092-8674(92)90164-8

Rodal, A.A., Del Signore, S.J., Martin, A.C., 2015. Drosophila comes of age as a model system for understanding the function of cytoskeletal proteins in cells, tissues, and organisms. Cytoskeleton 72, 207–224. https://doi.org/10.1002/cm.21228

Rogers, E.M., Spracklen, A.J., Bilancia, C.G., Sumigray, K.D., Allred, S.C., Nowotarski, S.H., Schaefer, K.N., Ritchie, B.J., Peifer, M., 2016. Abelson kinase acts as a robust, multifunctional scaffold in regulating embryonic morphogenesis. Mol. Biol. Cell 27, 2613–2631. https://doi.org/10.1091/mbc.e16-05-0292

Rogers, S.L., Wiedemann, U., Stuurman, N., Vale, R.D., 2003. Molecular requirements for actin-based lamella formation in Drosophila S2 cells. J. Cell Biol. 162, 1079–1088. https://doi.org/10.1083/jcb.200303023

Rüder, M., Nagel, B.M., Bogdan, S., 2018. Analysis of Cell Shape and Cell Migration of Drosophila Macrophages In Vivo. Springer Methods Mol. Biol. 1749, 227–238. https://doi.org/10.1007/978-1-4939-7701-7

Safer, D., Nachmias, V.T., 1994. Beta thymosins as actin binding peptides. BioEssays 16, 473–479. https://doi.org/10.1002/bies.950160706

Sampson, C.J., Williams, M.J., 2012. Real-time analysis of Drosophila post-embryonic haemocyte behavior. PLoS ONE 7. https://doi.org/10.1371/journal.pone.0028783

Sander, M., Squarr, A.J., Risse, B., Jiang, X., Bogdan, S., 2013. Drosophila pupal macrophages - A versatile tool for combined ex vivo and in vivo imaging of actin dynamics at high resolution. Eur. J. Cell Biol. 92, 349–354. https://doi.org/10.1016/j.ejcb.2013.09.003

Satoh, S., Tominaga, T., 2001. mDia-interacting Protein Acts Downstream of Rho-mDia and Modifies Src Activation and Stress Fiber Formation *. Biol. Cell 276, 39290–39294. https://doi.org/10.1074/jbc.M107026200

Schafer, D.A., Jennings, P.B., Cooper, J.A., 1996. Dynamics of capping protein and actin assembly in vitro: Uncapping barbed ends by polyphosphoinositides. J. Cell Biol. 135, 169–179. https://doi.org/10.1083/jcb.135.1.169

Schäfer, G., Weber, S., Holz, A., Bogdan, S., Schumacher, S., Müller, A., Renkawitz-Pohl, R., Önel, S.F., 2007. The Wiskott-Aldrich syndrome protein (WASP) is essential for myoblast fusion in Drosophila. Dev. Biol. 304, 664–674. https://doi.org/10.1016/j.ydbio.2007.01.015

Schaks, M., Singh, S.P., Kage, F., Thomason, P., Klünemann, T., Steffen, A., Blankenfeldt, W., Stradal, T.E., Insall, R.H., Rottner, K., 2018. Distinct Interaction Sites of Rac GTPase with WAVE Regulatory Complex Have Non-redundant Functions in Vivo. Curr. Biol. 28, 3674-3684.e6. https://doi.org/10.1016/j.cub.2018.10.002

Schenck, A., Qurashi, A., Carrera, P., Bardoni, B., Diebold, C., Schejter, E., Mandel, J.L., Giangrande, A., 2004. WAVE/SCAR, a multifunctional complex coordinating different aspects of neuronal connectivity. Dev. Biol. 274, 260–270. https://doi.org/10.1016/j.ydbio.2004.07.009

Schindler, T., Schindler, T., Bornmann, W., Bornmann, W., Pellicena, P., Pellicena, P., Miller, W.T., Miller, W.T., Clarkson, B., Clarkson, B., Kuriyan, J., Kuriyan, J., 2000. Structural mechanism for STI-571 inhibition of abelson tyrosine kinase. Science 289, 1938–1942.

Schirenbeck, A., Bretschneider, T., Arasada, R., Schleicher, M., Faix, J., 2005. The Diaphanous-related formin dDia2 is required for the formation and maintenance of filopodia. Nat. Cell Biol. 7, 619–625. https://doi.org/10.1038/ncb1266

Shellard, A., Mayor, R., 2016. Chemotaxis during neural crest migration. Semin. Cell Dev. Biol. 55, 111–118. https://doi.org/10.1016/j.semcdb.2016.01.031

Shemesh, T., Otomo, T., Rosen, M.K., Bershadsky, A.D., Kozlov, M.M., 2005. A novel mechanism of actin filament processive capping by formin: Solution of the rotation paradox. J. Cell Biol. 170, 889–893. https://doi.org/10.1083/jcb.200504156

Shindo, M., Wada, H., Kaido, M., Tateno, M., Aigaki, T., Tsuda, L., Hayashi, S., 2008. Dual function of Src in the maintenance of adherens junctions during tracheal epithelial morphogenesis. Development 135, 1355–1364. https://doi.org/10.1242/dev.015982

Sian, H., Cheong, J., Nona, M., Guerra, S.B., Vanberkum, M.F., 2020. The first quarter of the C-terminal domain of Abelson regulates the WAVE regulatory complex and Enabled in axon guidance 1–19.

Siekhaus, D., Haesemeyer, M., Moffitt, O., Lehmann, R., 2010. RhoL controls invasion and Rap1 localization during immune cell transmigration in Drosophila. Nat. Cell Biol. 12, 605–610. https://doi.org/10.1038/ncb2063

Silver, D.L., Geisbrecht, E.R., Montell, D.J., 2005. Requirement for JAK/STAT signaling throughout border cell migration in Drosophila. Dev. Camb. Engl. 132, 3483–3492. https://doi.org/10.1242/dev.01910

Sinenko, S. a, Mathey-Prevot, B., 2004. Increased expression of Drosophila tetraspanin, Tsp68C, suppresses the abnormal proliferation of ytr-deficient and Ras/Raf-activated hemocytes. Oncogene 23, 9120–9128. https://doi.org/10.1038/sj.onc.1208156

Singh, S.P., Thomason, P.A., Lilla, S., Schaks, M., Tang, Q., Goodei, B.L., MacHesky, L.M., Rottner, K., Insall, R.H., 2020. Cell-substrate adhesion drives scar/wave activation and phosphorylation by a ste20-family kinase, which controls pseudopod lifetime. PLoS Biol. 18. https://doi.org/10.1371/JOURNAL.PBIO.3000774

Sixt, M., 2012. Cell migration: Fibroblasts find a new way to get ahead. J. Cell Biol. 197, 347–349. https://doi.org/10.1083/jcb.201204039

Skruber, K., Read, T.A., Vitriol, E.A., 2018. Reconsidering an active role for G-actin in cytoskeletal regulation. J. Cell Sci. 131. https://doi.org/10.1242/jcs.203760

Small, J.V., 1988. The actin cytoskeleton. Electron Microsc. Rev. Volume 1, Pages 155-174. https://doi.org/10.1016/s0892-0354(98)90010-7

Small, J.V., Stradal, T., Vignal, E., Rottner, K., 2002. The lamellipodium : where motility begins 12, 112–120.

Sorrentino, R.P., Carton, Y., Govind, S., 2002. Cellular immune response to parasite infection in the Drosophila lymph gland is developmentally regulated. Dev. Biol. 243, 65–80. https://doi.org/10.1006/dbio.2001.0542

Sossey-Alaoui, K., Head, K., Nowak, N., Cowell, J.K., 2003. Genomic organization and expression profile of the human and mouse WAVE gene family. Mamm. Genome 14, 314–322. https://doi.org/10.1007/s00335-002-2247-7

Sossey-Alaoui, K., Li, X., Cowell, J.K., 2007. c-Abl-mediated phosphorylation of WAVE3 is required for lamellipodia formation and cell migration. J. Biol. Chem. 282, 26257–26265. https://doi.org/10.1074/jbc.M701484200

Squarr, A.J., Brinkmann, K., Chen, B., Steinbacher, T., Ebnet, K., Rosen, M.K., Bogdan, S., 2016. Fat2 acts through the WAVE regulatory complex to drive collective cell migration during tissue rotation. J. Cell Biol. 212, 591–603. https://doi.org/10.1083/jcb.201508081

Steffen, A., Rottner, K., Ehinger, J., Innocenti, M., Scita, G., Wehland, J., Stradal, T.E.B., 2004. Sra-1 and Nap1 link Rac to actin assembly driving lamellipodia formation. EMBO J. 23, 749–759. https://doi.org/10.1038/sj.emboj.7600084

Stephan, R., Gohl, C., Fleige, A., Klämbt, C., Bogdan, S., 2011. Membrane-targeted WAVE mediates photoreceptor axon targeting in the absence of the WAVE complex in Drosophila. Mol. Biol. Cell 22, 4079–4092. https://doi.org/10.1091/mbc.E11-02-0121

Stradal, T.E.B., Scita, G., 2005. Protein complexes regulating Arp2 / 3-mediated actin assembly 4–10. https://doi.org/10.1016/j.ceb.2005.12.003

Stuart, J.R., Gonzalez, F.H., Kawai, H., Yuan, Z.M., 2006. c-Abl interacts with the WAVE2 signaling complex to induce membrane ruffling and cell spreading. J. Biol. Chem. 281, 31290–31297. https://doi.org/10.1074/jbc.M602389200

Suetsugu, S., Hattori, M., Miki, H., Tezuka, T., Yamamoto, T., Mikoshiba, K., Takenawa, T., 2002. Sustained Activation of N-WASP through Phosphorylation Is Essential for Neurite Extension 3, 645–658.

Suraneni, P., Rubinstein, B., Unruh, J.R., Durnin, M., Hanein, D., Li, R., 2012. The Arp2/3 complex is required for lamellipodia extension and directional fibroblast cell migration. J. Cell Biol. 197, 239–251. https://doi.org/10.1083/jcb.201112113

Takahashi, M., 2005. Requirements of genetic interactions between Src42A, armadillo and shotgun, a gene encoding E-cadherin, for normal development in Drosophila. Development 132, 2547–2559. https://doi.org/10.1242/dev.01850

Takenawa, T., Suetsugu, S., 2007. The WASP–WAVE protein network: connecting the membrane to the cytoskeleton. Nat. Rev. Mol. Cell Biol. 8, 37–48. https://doi.org/10.1038/nrm2069

Tanaka, K., Takeda, S., Mitsuoka, K., Oda, T., Kimura-Sakiyama, C., Maéda, Y., Narita, A., 2018. Structural basis for cofilin binding and actin filament disassembly. Nat. Commun. 9, 1–3. https://doi.org/10.1038/s41467-018-04290-w

Tateno, M., Nishida, Y., Adachi-yamada, T., 2000. Regulation of JNK by Src During Drosophila Development 287, 324–328.

Tepass, U., Fessler, L.I., Aziz, A., Hartenstein, V., 1994. Embryonic origin of hemocytes and their relationship to cell death in Drosophila. Development 120, 1829–1837.

Theopold, U., Krautz, R., Dushay, M.S., 2014. The Drosophila clotting system and its messages for mammals. Dev. Comp. Immunol. 42, 42–46. https://doi.org/10.1016/j.dci.2013.03.014

Thuma, L., Carter, D., Weavers, H., Martin, P., 2018. Drosophila immune cells extravasate from vessels to wounds using Tre1 GPCR and Rho signaling. J. Cell Biol. jcb.201801013-jcb.201801013. https://doi.org/10.1083/jcb.201801013

Tilney, L.G., Tilney, M.S., Guild, G.M., 1995. F actin bundles in Drosophila bristles 130, 629–638. https://doi.org/10.1083/jcb.130.3.629

Ura, S., Pollitt, A.Y., Veltman, D.M., Morrice, N.A., MacHesky, L.M., Insall, R.H., 2012. Pseudopod growth and evolution during cell movement is controlled through SCAR/WAVE dephosphorylation. Curr. Biol. 22, 553–561. https://doi.org/10.1016/j.cub.2012.02.020

Urbano, J.M., Torgler, C.N., Molnar, C., Tepass, U., López-Varea, A., Brown, N.H., de Celis, J.F., Martín-Bermudo, M.D., 2009. Drosophila laminins act as key regulators of basement membrane assembly and morphogenesis. Development 136, 4165–4176. https://doi.org/10.1242/dev.044263

Urbano, M., Comber, K., Dragu, A., Wood, W., Stramer, B., Sa, B.J., 2017. Drosophila Embryonic Hemocytes Produce Laminins to Strengthen Migratory Response Report Drosophila Embryonic Hemocytes Produce Laminins to Strengthen Migratory Response 1461–1470. https://doi.org/10.1016/j.celrep.2017.10.047

Veltman, D.M., King, J.S., Machesky, L.M., Insall, R.H., 2012. SCAR knockouts in Dictyostelium: WASP assumes SCAR's position and upstream regulators in pseudopods. J. Cell Biol. 198, 501–508. https://doi.org/10.1083/jcb.201205058

Vicente-Manzanares, M., Choi, C.K., Horwitz, A.R., 2009. Integrins in cell migration - the actin connection. J. Cell Sci. 122, 1473–1473. https://doi.org/10.1242/jcs.052894

Waksman, G., Kumaran, S., Lubman, O., 2004. SH2 domains: Role, structure and implications for molecular medicine. Expert Rev. Mol. Med. 6, 1–21. https://doi.org/10.1017/S1462399404007331

Wang, J.Y.J., 2014. The Capable ABL : What Is Its Biological Function ? 34, 1188–1197. https://doi.org/10.1128/MCB.01454-13

Weavers, H., Liepe, J., Sim, A., Wood, W., Martin, P., Stumpf, M.P.H., 2016. Systems Analysis of the Dynamic Inflammatory Response to Tissue Damage Reveals Spatiotemporal Properties of the Wound Attractant Gradient. Curr. Biol. 26, 1975–1989. https://doi.org/10.1016/j.cub.2016.06.012

Welch, H.C.E., Coadwell, W.J., Stephens, L.R., Hawkins, P.T., 2003. Phosphoinositide 3-kinase-dependent activation of Rac. FEBS Lett. 546, 93–97. https://doi.org/10.1016/S0014-5793(03)00454-X

Welf, E.S., Ahmed, S., Johnson, H.E., Melvin, A.T., Haugh, J.M., 2012. Migrating fibroblasts reorient directionality: By a metastable, PI3K-dependent mechanism. J. Cell Biol. 197, 105–114. https://doi.org/10.1083/jcb.201108152

Wodarz, A., Hinz, U., Engelbert, M., Knust, E., 1995. Expression of crumbs confers apical character on plasma membrane domains of ectodermal epithelia of drosophila. Cell 82, 67–76. https://doi.org/10.1016/0092-8674(95)90053-5

Wood, W., Faria, C., Jacinto, A., 2006. Distinct mechanisms regulate hemocyte chemotaxis during development and wound healing in Drosophila melanogaster. J. Cell Biol. 173, 405–416. https://doi.org/10.1083/jcb.200508161

Wu, C., Asokan, S.B., Berginski, M.E., Haynes, E.M., Sharpless, N.E., Griffith, J.D., Gomez, S.M., Bear, J.E., 2012. Arp2/3 is critical for lamellipodia and response to extracellular matrix cues but is dispensable for chemotaxis. Cell 148, 973–987. https://doi.org/10.1016/j.cell.2011.12.034

Wynn, T.A., Chawla, A., Pollard, J.W., 2013. Macrophage biology in development, homeostasis and disease. Nature 496, 445–455. https://doi.org/10.1038/nature12034

Xu, W., Doshi, A., Lei, M., Eck, M.J., Harrison, S.C., 1999. Crystal Structures of c-Src Reveal Features of Its Autoinhibitory Mechanism 3, 629–638.

Yoo, S.K., Freisinger, C.M., LeBert, D.C., Huttenlocher, A., 2012. Early redox, Src family kinase, and calcium signaling integrate wound responses and tissue regeneration in zebrafish. J. Cell Biol. 199, 225–234. https://doi.org/10.1083/jcb.201203154

Yoo, S.K., Starnes, T.W., Deng, Q., Huttenlocher, A., 2011. Lyn is a redox sensor that mediates leukocyte wound attraction in vivo. Nature 480, 109–112. https://doi.org/10.1038/nature10632

Zallen, J.A., Cohen, Y., Hudson, A.M., Cooley, L., Wieschaus, E., Schejter, E.D., 2002. SCAR is a primary regulator of Arp2/3-dependent morphological events in Drosophila. J. Cell Biol. 156, 689–701. https://doi.org/10.1083/jcb.200109057

Zhu, Z., Bhat, K.M., 2011. The Hem protein mediates neuronal migration by inhibiting WAVE degradation and functions opposite of Abelson tyrosine kinase. Dev. Biol. 357, 283–294. https://doi.org/10.1016/j.ydbio.2011.06.025

Zigmond, S.H., Evangelists, M., Boone, C., Yang, C., Dar, A.C., Sicheri, F., Forkey, J., Pring, M., 2003. Formin Leaky Cap Allows Elongation in the Presence of Tight Capping Proteins. Curr. Biol. 13, 1820–1823. https://doi.org/10.1016/j.cub.2003.09.057

Zobel, T., Bogdan, S., 2013. A high resolution view of the fly actin cytoskeleton lacking a functional WAVE complex. J. Microsc. 251, 224–231. https://doi.org/10.1111/jmi.12020

7. Appendix

7.1 Supplementary Material

7.1.1 Primer

Supplementary Table 1: List of Primer

NAME	SEQUENCE	FINAL VECTOR
***hmlΔ*-Topo-fwd**	CACCCCAAAAGTTATTTCTGTAGGC	pDEST-HemmarG-eGFP/Stinger-eGFP
***hmlΔ*-rev**	TTTGTTAGGCTAATCGGAAATTG	pDEST-HemmarG-eGFP/Stinger-eGFP
mScarlet_F_XhoI	GAACTCGAGATGAGTAAAGGAGAAGCTGTGA	pBlueScript_mScarlet
mScarlet_R_XhoI	GAACTCGAGTTTTTGTATAGTTCATCCATGCC	pBlueScript_mScarlet
Scarlet_seq_F	CAAGTGGGAACGCGTAATGA	Scarlet(-I) sequencing Primer
mScarlet-H_XhoI_F	GAACTCGAGATGGTGAGCAAGGGCGAGG	pBlueScript_mScarlet-H
mScarlet-H_XhoI_R	GAACTCGAGTTCTTGTACAGCTCGTCCATGC	pBlueScript_mScarlet-H
Scarlet-H_seq _F	GCGTGATGAACTTCGAGGAC	Scarlet(-H) sequencing Primer
mScarlet_RNheI	GAAGCTAGCTTATTTGTATAGTTCATCCATGCC	mScarlet/Scarlet-I

mScarlet_F_NheI	GAAGCTAGCATGAGTAAAGGAGAAGCTGTGAT	mScarlet/Scarlet-I
mScarlet-H_NheI_F	GAAGCTAGCATGGTGAGCAAGGGCGAGG	mScarlet-H
mScarlet-H_NheI_R	GAAGCTAGCTTACTTGTACAGCTCGTCCATGC	mScarlet-H
WAVE-Y153F-sense	GGATGGTCTTAAGTTCTTCACGGATCCGAACTAC	pUASp-attB-WAVE/ pUASp-attB-myc-WAVE Y→F at referred site
WAVE-Y153E-sense	GCAAGGATGGTCTTAAGTTCGAAACGGATCCGAACTACTTC	pUASp-attB-WAVE/ pUASp-attB-myc-WAVE Y→E at referred site
Y127E-sense	CCGGCACCAATGATGGACACAGAAGCCCAGTGCGA	pUASp-attB-WAVE/ pUASp-attB-myc-WAVE Y→E at referred site
Y127F-sense	CGGCACCAATGATGGACACATTTGCCCAGTGCG	pUASp-attB-WAVE/ pUASp-attB-myc-WAVE Y→F at referred site
WAVE-Y153E antisense	GAAGTAGTTCGGATCCGTTTCGAACTTAAGACCATCCTTGC	pUASp-attB-WAVE/ pUASp-attB-myc-WAVE Y→E at referred site
WAVE-Y153F antisense	GTAGTTCGGATCCGTGAAGAACTTAAGACCATCC	pUASp-attB-WAVE/ pUASp-

		attB-myc-WAVE Y→F at referred site
Y127E-antisense	TCGCACTGGGCTTCTGTGTCCATCATTGGTGCCGG	pUASp-attB-WAVE/ pUASp-attB-myc-WAVE Y→E at referred site
Y127F-antisense	CGCACTGGGCAAATGTGTCCATCATTGGTGCCG	pUASp-attB-WAVE/ pUASp-attB-myc-WAVE Y→F at referred site

7.1.2 R-scripts for analyses migratory behavior

Cell are tracked by Imaris software using following parameters.

Supplementary Table 2: Tracking Parameters

Random migration - hole cell	**Directed migration - hole cell**	**Directed migration - nucleus**
[Algorithm] Enable Region Of Interest = true Process Entire Image = false Enable Region Growing = false Enable Tracking = true [Region of Interest] Region1: XYZT from [1 1 1 1] to [608 960 26 61] [Source Channel] Source Channel Index = 1 Estimated Diameter = 10.0 um Background Subtraction = true	[Algorithm] Enable Region Of Interest = false Enable Region Growing = false Enable Tracking = true [Source Channel] Source Channel Index = 1 Estimated Diameter = 10.0 um Background Subtraction = true [Classify Spots] "Quality" above 12.5 [Tracking]	[Algorithm] Enable Region Of Interest = true Process Entire Image = false Enable Region Growing = false Enable Tracking = true [Region of Interest] Region1: XYZT from [1 1 1 2] to [608 864 21 61] [Source Channel] Source Channel Index = 2 Estimated Diameter = 6.00 um Background Subtraction = true

[Classify Spots] "Quality" above 20.9 [Tracking] Algorithm Name = Autoregressive Motion MaxDistance = 15.0 um MaxGapSize = 2 Fill Gap Enable = false [Classify Tracks] "Track Duration" above 110 s	Algorithm Name = Autoregressive Motion MaxDistance = 20.0 um MaxGapSize = 2 Fill Gap Enable = false [Classify Tracks] "Track Duration" above 300 s	[Classify Spots] "Quality" above 15.0 "Distance from Origin Reference Frame" between 15.0 um and 70.0 um [Tracking] Algorithm Name = Brownian Motion MaxDistance = 15.0 um MaxGapSize = 2 Fill Gap Enable = false [Classify Tracks] "Track Duration" above 250 s

The following R-scripts are used to analyze cell migration. The following order structure is recommended to run the scripts. Otherwise, working directories would have to be changed within the single scripts. Further descriptions are included in more detail in the method chapter or as comments within the script (2.5.10 Analysis of migration).

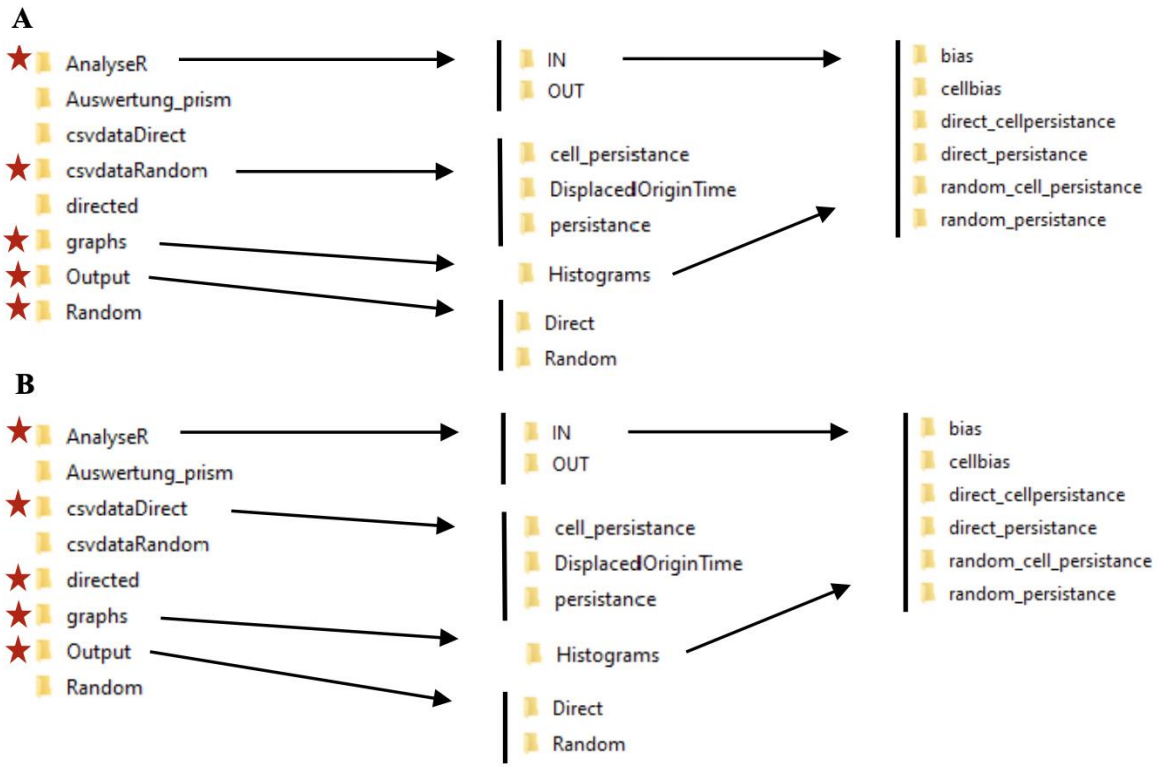

Figure 43: Recommended folder structure to analyse A) random migration B) directed migration

7.1.2.1 Analysis of random cell migration (RCM)

```
#library(data.table)
#install.packages("ggplot2")
#library(ggplot2)
#install.packages("xlsx")
#library("xlsx")

#list data and set working directory
rm(list = ls())
wd <- "E:/Imaris/Done/Random"
folder <- list.files(wd, full.names=FALSE)
setwd(wd)

#loop folder in random
for (x in 1:length(folder)){
  Mig<-data.frame()
  cell_c <- data.frame()
  cell_angle_P <- data.frame()
  wd1 <- paste0(wd,"/",folder[x])
  setwd(wd1)
  paste0(wd,"/",folder[x])

#migration analyses
  for (f in list.files(pattern = "Position_Reference_Frame.csv", recursive =
TRUE)){

    obj <- read.csv(f, header=TRUE, skip=3)

    sortTrackID <-obj[order(obj$TrackID),]             #sort data by Track ID

    richtungsvektor<-    data.frame(matrix(nrow=nrow(sortTrackID),    ncol=3))
       #motionvector of all cells
    for (i in 2:(nrow(sortTrackID))) {
      if (sortTrackID$TrackID[i]==sortTrackID$TrackID[i-1]){
              #as long track ID identical calculate motion vector
        richtungsvektor[i,1]<-          c((sortTrackID$Position.X[i])-
        (sortTrackID$Position.X[i-1]))
        richtungsvektor[i,2]<-          c((sortTrackID$Position.Y[i])-
        (sortTrackID$Position.Y[i-1]))
        richtungsvektor[i,3]<-          c((sortTrackID$Position.Z[i])-
        (sortTrackID$Position.Z[i-1]))
      }
    }

       richtungsvektor$Steplenght<-
       c(sqrt(((richtungsvektor$X1)**2)+((richtungsvektor$X2)**2)+((richtungsv
       ektor$X3)**2)))

    sortTrackID$richtungsvektor <- richtungsvektor

scalar<-          data.frame(matrix(nrow=nrow(sortTrackID),          ncol=1))
#matrix(nrow=nrow(sortTrackID_Radius), ncol=1)

    for (i in 2:(nrow(richtungsvektor))) {
       scalar[i,1]    <-    c((richtungsvektor$X1[i]*richtungsvektor$X1[i-1])+
       (richtungsvektor$X2[i]*richtungsvektor$X2[i-1]+
       (richtungsvektor$X3[i]*richtungsvektor$X3[i-1]))) #scalar persitance
    }
```

```
names(scalar)<- c("scalar")

    sortTrackID$scalar <- scalar

    results<- data.frame(matrix(nrow=nrow(sortTrackID), ncol=2))

    for (i in 2:(nrow(sortTrackID))) {
       results[i,1]                                                    <-
       c(acos((scalar$scalar[i])/((richtungsvektor$Steplenght[i])*
       (richtungsvektor$Steplenght[i-1]))))
        #radians / Bogenmaß
      results[i,2]                                                     <-
c((acos((scalar$scalar[i])/((richtungsvektor$Steplenght[i])*
       (richtungsvektor$Steplenght[i-1]))))*(360/(2*pi)))
        #angle / Winkel
      results[i,3] <- c(sortTrackID$TrackID[i])
      results[i,4] <- c(sortTrackID$Time[i])
      results[i,5] <- c(folder[x])
    }

    names(results)                                                     <-
c("bogenmas","persitanceangel","TrackID","Time","Genotype")

    sortTrackID$results <- results

    #filter out tracks with exact 0 od 180 degree, just show up when track gaps
     are connected connection
    results<-subset(results, results$persitanceangel<180)
    results<-subset(results, results$persitanceangel>0)

    Mig<-rbind.data.frame(Mig,results)

    #calcultes cell mean angle
       cell_mean             <-             aggregate(results$persitanceangel,
       by=list(results$TrackID), FUN=mean, na.rm=T)
    #calcultes cell median angle
       cell_median            <-             aggregate(results$persitanceangel,
       by=list(results$TrackID), FUN=median, na.rm=T)

    cell_c <- cbind(cell_mean,cell_median)

    cell_angle_P <-rbind.data.frame(cell_angle_P,cell_c)
  }

  #Genotype
  for(i in 1:(nrow(cell_angle_P))){
    cell_angle_P[i,5]<- (folder[x])
  }
    names(cell_angle_P)          <-          c("TrackID","Cell_mean_p_angle",
       "TrackID2","Cell_median_p_angle","Genotype") #"Cellpersistanceangle"

  #save data as csv in new folder (see folderstructure)
    setwd("E:/Imaris/Done/csvdataRandom/cell_persistance")
    write.csv(cell_angle_P,file=(paste0(folder[x],".","csv")))
    #write.xlsx(cell_angle_P,file=(paste0(folder[x],".","xlsx")))

    setwd("E:/Imaris/Done/csvdataRandom/persistance")
    write.csv(Mig,file=(paste0(folder[x],".","csv")))
    #write.xlsx(Mig,file=(paste0(folder[x],".","xlsx")))
}
```

7.1.2.2 Analysis of directed cell migration (DCM)

```
#library(data.table)
#install.packages("ggplot2")
#library(ggplot2)

rm(list = ls())
#wd <- "E:/Imaris/Done/directed/RNAi"
wd <- "E:/Imaris/Done/directed/Mutant"
folder <- list.files(wd, full.names=FALSE)
setwd(wd)

for (x in 1:length(folder)){
  Mig_persit <-data.frame()
  Mig_bias <-data.frame()
  cell_c <-data.frame()
  cell_angle_P <-data.frame()
  cell_angle_B <-data.frame()
  wd1 <- paste0(wd,"/",folder[x])
  setwd(wd1)
  paste0(wd,"/",folder[x])

  for (f in list.files(pattern = "Position_Reference_Frame.csv", recursive =
TRUE)){
  #for (f in list.files(pattern = "Detailed.csv", recursive = TRUE)){
    obj <- read.csv(f, header=TRUE, skip=3)

    #Sort tracks via ID
    sortTrackID <-obj[order(obj$TrackID),]

       obj$disRefPoint<-
       c(sqrt(((obj$Position.X.Reference.Frame)**2)+((obj$Position.Y.Reference
       .Frame)**2)+((obj$Position.Z.Reference.Frame)**2)))
    #calculates distance from all point towards the wound (0/0/0) to every
timepoint

  #Set radius within cells should be analysed
       radius<-subset(obj, obj$disRefPoint<=70 & obj$disRefPoint>=15)    #zellen
       die sich wärend der Aufnahme im radius X aufhalten
       sortTrackID_Radius <-radius[order(radius$TrackID),]  #again, sorting

    #calculations for general cell persistance in wounding experiments
        richtungsvektor<-      data.frame(matrix(nrow=nrow(sortTrackID_Radius),
ncol=3))
        for (i in 2:(nrow(sortTrackID_Radius))) {
          if (sortTrackID_Radius$TrackID[i]==sortTrackID_Radius$TrackID[i-1]){

              richtungsvektor[i,1]<-
              c((sortTrackID_Radius$Position.X.Reference.Frame[i])-
              (sortTrackID_Radius$Position.X.Reference.Frame[i-1]))
              richtungsvektor[i,2]<-
              c((sortTrackID_Radius$Position.Y.Reference.Frame[i])-
              (sortTrackID_Radius$Position.Y.Reference.Frame[i-1]))
              richtungsvektor[i,3]<-
              c((sortTrackID_Radius$Position.Z.Reference.Frame[i])-
              (sortTrackID_Radius$Position.Z.Reference.Frame[i-1]))
          }
        }
```

```
            richtungsvektor$Steplenght<-
      c(sqrt(((richtungsvektor$X1)**2)+((richtungsvektor$X2)**2)+((richtungsv
      ektor$X3)**2)))

       sortTrackID_Radius$richtungsvektor <- richtungsvektor

       scalar<- data.frame(matrix(nrow=nrow(sortTrackID_Radius), ncol=1))
       for (i in 2:(nrow(richtungsvektor))) {
            scalar[i,1]   <-   c((richtungsvektor$X1[i]*richtungsvektor$X1[i-
            1])+(richtungsvektor$X2[i]*richtungsvektor$X2[i-
            1]+(richtungsvektor$X3[i]*richtungsvektor$X3[i-1])))      #scalar
            persistance
       }
       names(scalar)<- c("scalar")

       sortTrackID_Radius$scalar <- scalar

       results_persit<-      data.frame(matrix(nrow=nrow(sortTrackID_Radius),
ncol=2))
       for (i in 2:(nrow(sortTrackID_Radius))) {
      results_persit[i,1]                                                  <-
      c(acos((scalar$scalar[i])/((richtungsvektor$Steplenght[i])*(richtungsve
      ktor$Steplenght[i-1]))))
      results_persit[i,2]                                                  <-
      c((acos((scalar$scalar[i])/((richtungsvektor$Steplenght[i])*(richtungsv
      ektor$Steplenght[i-1]))))*(360/(2*pi)))
      results_persit[i,3] <- c(sortTrackID$TrackID[i])
      results_persit[i,4] <- c(sortTrackID$Time[i])
      results_persit[i,5] <- c(folder[x])
       }

      names(results_persit)                                                <-
      c("bogenmass","persistanceangel","TrackID","Time","Genotype")

     #calculates mean and median angle for cell persistance
      cell_mean         <-         aggregate(results_persit$persistanceangel,
      by=list(results_persit$TrackID), FUN=mean, na.rm=T)
      cell_median        <-        aggregate(results_persit$persistanceangel,
      by=list(results_persit$TrackID), FUN=median, na.rm=T)
      cell_c <- cbind(cell_mean,cell_median) #bind median table and mean table
      columwise

       cell_angle_P <-rbind.data.frame(cell_angle_P,cell_c) #rowbind different
experiments per loop run for one genotype

       sortTrackID_Radius$results_persit <- results_persit

       Mig_persit<-rbind.data.frame(Mig_persit,results_persit)

#calcluates scalar of bias angle, angle towards wound
     scalar_bias<-  data.frame(matrix(nrow=nrow(sortTrackID_Radius),  ncol=1))
#matrix(nrow=nrow(sortTrackID_Radius), ncol=1)
     for (i in 2:(nrow(sortTrackID_Radius))) {
      scalar_bias[i,1]    <-    c((sortTrackID_Radius$richtungsvektor$X1[i]*(-
      (sortTrackID_Radius$Position.X.Reference.Frame[i-
      1])))+(richtungsvektor$X2[i]*                                        (-
      (sortTrackID_Radius$Position.Y.Reference.Frame[i-
      1])))+(richtungsvektor$X3[i]*                                        (-
      (sortTrackID_Radius$Position.Z.Reference.Frame[i-1]))))          #scalar
      persitance
```

```
      }

      names(scalar_bias)<- c("scalarbias")

      sortTrackID_Radius$scalar_bias <- scalar_bias

      results_bias<- data.frame(matrix(nrow=nrow(sortTrackID_Radius), ncol=2))

    for (i in 2:(nrow(sortTrackID_Radius))) {
       results_bias[i,1]                                                    <-
       c(acos((scalar_bias$scalarbias[i])/((sortTrackID_Radius$disRefPoint[i-
       1])*(sortTrackID_Radius$richtungsvektor$Steplenght[i]))))
      results_bias[i,2]                                                     <-
      c(acos((scalar_bias$scalarbias[i])/((sortTrackID_Radius$disRefPoint[i-
      1])*(sortTrackID_Radius$richtungsvektor$Steplenght[i])))*(360/(2*pi)))
      results_bias[i,3] <- c(sortTrackID$TrackID[i])
      results_bias[i,4] <- c(sortTrackID$Time[i])
      results_bias[i,5] <- c(folder[x])

    }

    names(results_bias)                                                     <-
c("bogenmass_bias","biasangel","TrackID","Time","Genotype")

    sortTrackID_Radius$results_bias <- results_bias

    Mig_bias<-rbind.data.frame(Mig_bias,results_bias)

    #calculate cellbias angle
      cell_mean              <-              aggregate(results_bias$biasangel,
      by=list(results_bias$TrackID), FUN=mean, na.rm=T)
      cell_median             <-             aggregate(results_bias$biasangel,
      by=list(results_bias$TrackID), FUN=median, na.rm=T)
      cell_c <- cbind(cell_mean,cell_median) #bind median table and mean table
      columwise

      cell_angle_B  <-rbind.data.frame(cell_angle_B,cell_c)  #rowbind  different
      experiments per loop run for one genotype
  }


  #create header for cell angle table
    for(i in 1:(nrow(cell_angle_B))){
      cell_angle_B[i,5]<- (folder[x])
    }

    names(cell_angle_B)           <-           c("TrackID","Cell_mean_b_angle",
"TrackID2","Cell_median_b_angle","Genotype")


    for(i in 1:(nrow(cell_angle_P))){
      cell_angle_P[i,5]<- (folder[x])
    }
    names(cell_angle_P)           <-           c("TrackID","Cell_mean_p_angle",
"TrackID2","Cell_median_p_angle","Genotype")


  #save calculation in corresponding folders
    setwd("E:/Imaris/Done/csvdataDirect/cell_persistance")
    write.csv(cell_angle_P,file=(paste0(folder[x],".","csv")))
```

```
    setwd("E:/Imaris/Done/csvdataDirect/cell_bias")
    write.csv(cell_angle_B,file=(paste0(folder[x],".","csv")))

    setwd("E:/Imaris/Done/csvdataDirect/persistance")
    write.csv(Mig_persit,file=(paste0(folder[x],".","csv")))

    setwd("E:/Imaris/Done/csvdataDirect/bias")
    write.csv(Mig_bias,file=(paste0(folder[x],".","csv")))

}
```

7.1.2.3 Creation of angle histogram for random and directed migration

```
#library(data.table)
#install.packages("ggplot2")
#library(ggplot2)

#Put Data from "Migrations analyse csv" in Analyse IN folder, Name it correctly
for blot names

#low part: Run for all blot in advance until "specific part"

  rm(list = ls())
  wd <- "E:/Imaris/Done/AnalyseR/IN"
  folder <- list.files(wd, full.names=FALSE)
  setwd(wd)

  for (x in 1:length(folder)){
    wd1 <- paste0(wd,"/",folder[x])
    AllDataBind <- data.frame()
    setwd(wd1)
    paste0(wd,"/",folder[x])

    #bind data to analyse
    for (f in list.files(pattern = ".csv", recursive = TRUE)){
      obj <- read.csv(f, header=TRUE)    #data<-read.csv(f, header = FALSE, sep
= ",")

      AllDataBind <- rbind.data.frame(AllDataBind,obj)

      setwd("E:/Imaris/Done/AnalyseR/OUT")
      write.csv(AllDataBind,file=(paste0(folder[x],".","csv")))
      setwd(wd1)
    }
  }

  library(ggplot2)
  library(plyr)

  rm(list = ls())
  wd <- "E:/Imaris/Done/AnalyseR/OUT"
  folder <- list.files(wd, full.names=FALSE)
  setwd(wd)

#spezific part
```

```
  #Random-Cell-Persistance Angle

for (f in list.files(pattern = "random_cell_persistance.csv", recursive = TRUE))
{
        df <- read.csv(f, header=TRUE)
        }

      mu          <-          ddply(df,          "Genotype",          summarise,
grp.median=median(Cell_mean_p_angle))

       hist_RCP_mean     <-ggplot(df,     aes(x=Cell_mean_p_angle,fill=Genotype,
       color=Genotype))+
       geom_histogram(alpha=0.2,      position="identity",      binwidth      =
       2,aes(y=..density..)) +
       theme_bw()+   theme(legend.position="bottom")+   xlim(0,150)   +   ylim
(0,0.07)+
       geom_vline(data=mu,      aes(xintercept=grp.median,      color=Genotype),
       linetype="dashed")

      mu          <-          ddply(df,          "Genotype",          summarise,
grp.median=median(Cell_median_p_angle))

       hist_RCP_median  <-  ggplot(df,  aes(x=Cell_median_p_angle,fill=Genotype,
       color=Genotype))+
       geom_histogram(alpha=0.2,      position="identity",      binwidth      =
       2,aes(y=..density..))  +
       theme_bw()+   theme(legend.position="bottom")+   xlim(0,150)   +   ylim
(0,0.07)+
       geom_vline(data=mu,      aes(xintercept=grp.median,      color=Genotype),
       linetype="dashed")

      #save histograms and name it like file
      wd <- ("E:/Imaris/Done/AnalyseR/IN/random_cell_persistance")
      setwd(wd)
      name <- list.files(wd,full.names=FALSE)

      setwd("E:/Imaris/Done/graphs/Histograms/random_cell_persistance")

      # 1. Open jpeg file and name it like analyse in data
       png(paste0("RCP-MEAN_",
       (sub(".csv","",name[1])),"+",(sub(".csv","",name[2])),".png"))
      # 2. Create the plot
      plot(hist_RCP_mean)
      # 3. Close the file
      dev.off()

       png(paste0("RCP-MEDIAN_",
       (sub(".csv","",name[1])),"+",(sub(".csv","",name[2])),".png"))
       plot(hist_RCP_median)
       dev.off()

#Random Persistence Angle

      for  (f  in  list.files(pattern  =  "random_persistance.csv",  recursive  =
TRUE)){
        df <- read.csv(f, header=TRUE)   #data<-read.csv(f, header = FALSE, sep
= ",")
      }
```

```
      mu          <-          ddply(df,          "Genotype",          summarise,
grp.median=median(persitanceangel))

      ggplot(df, aes(x=persitanceangel,fill=Genotype, color=Genotype))+
       geom_histogram(alpha=0.2,    position="identity",    binwidth    =    2,
       aes(y=..density..))  +
       theme_bw()+ theme(legend.position="bottom")+
       geom_vline(data=mu, aes(xintercept=grp.median, color=Genotype),
                  linetype="dashed")


      #save histograms and name it like file
      wd <- ("E:/Imaris/Done/AnalyseR/IN/random_persistance")
      setwd(wd)
      name <- list.files(wd,full.names=FALSE)

      setwd("E:/Imaris/Done/graphs/Histograms/random_persistance")

      # 1. Open jpeg file and name it like analyse in data
      png(paste0("RP-MEAN_",
     (sub(".csv","",name[1])),"+",(sub(".csv","",name[2])),".png"))
      # 2. Create the plot
      plot(hist_RCP_mean)
      # 3. Close the file
      dev.off()


#Direct-cellbias Angle

      for (f in list.files(pattern = "cellbias.csv", recursive = TRUE)){
        df <- read.csv(f, header=TRUE) #data<-read.csv(f, header = FALSE, sep =
","")
        }

        mu          <-          ddply(df,          "Genotype",          summarise,
grp.median=median(Cell_mean_b_angle))

          hist_CBA_mean  <-  ggplot(df,  aes(x=Cell_mean_b_angle,fill=Genotype,
              color=Genotype))+
          geom_histogram(alpha=0.2,    position="identity",    binwidth    =    2,
          aes(y=..density..))  +
          theme_bw()+    theme(legend.position="bottom")+    xlim(50,160)    +
ylim(0,0.07)+
          geom_vline(data=mu, aes(xintercept=grp.median, color=Genotype),
                     linetype="dashed")

        mu          <-          ddply(df,          "Genotype",          summarise,
grp.median=median(Cell_median_b_angle))

       hist_CBA_median  <-  ggplot(df,  aes(x=Cell_median_b_angle,fill=Genotype,
       color=Genotype))+
       geom_histogram(alpha=0.2,    position="identity",    binwidth    =    2,
       aes(y=..density..))  +
       theme_bw()+     theme(legend.position="bottom")+     xlim(50,160)     +
ylim(0,0.06)+
       geom_vline(data=mu, aes(xintercept=grp.median, color=Genotype),
                  linetype="dashed")

        #save histograms and name it like file
        wd <- ("E:/Imaris/Done/AnalyseR/IN/cellbias")
```

```
        setwd(wd)
        name <- list.files(wd,full.names=FALSE)

        setwd("E:/Imaris/Done/graphs/Histograms/cellbias")

        # 1. Open jpeg file and name it like analyse in data
        png(paste0("CBA-MEAN_",
        (sub(".csv","",name[1])),"+",(sub(".csv","",name[2])),".png"))
        # 2. Create the plot
        plot(hist_CAB_mean)
        # 3. Close the file
        dev.off()

        png(paste0("CBA-MEDIAN_",
        (sub(".csv","",name[1])),"+",(sub(".csv","",name[2])),".png"))
        plot(hist_CBA_median)
        dev.off()


  #Direct-bias Angle

     for (f in list.files(pattern = "bias.csv", recursive = TRUE)){
        df <- read.csv(f, header=TRUE) #data<-read.csv(f, header = FALSE, sep =
","")
        }

     mu <- ddply(df, "Genotype", summarise, grp.median=median(biasangel))

      hist_BA <- ggplot(df, aes(x=biasangel,fill=Genotype, color=Genotype))+
      geom_histogram(alpha=0.2,     position="identity",     binwidth     =     2,
aes(y=..density..))+
      theme_bw()+ theme(legend.position="bottom")+
      geom_vline(data=mu, aes(xintercept=grp.median, color=Genotype),
                    linetype="dashed")

#save histograms and name it like file
      wd <- ("E:/Imaris/Done/AnalyseR/IN/bias")
      setwd(wd)
      name <- list.files(wd,full.names=FALSE)

      setwd("E:/Imaris/Done/graphs/Histograms/bias")

      # 1. Open jpeg file and name it like analyse in data

       png(paste0("BA_",(sub(".csv","",name[1])),"+",(sub(".csv","",name[2])),
       ".png"))
        # 2. Create the plot
        plot(hist_BA)
        # 3. Close the file
        dev.off()

  #Direct-cellpersistance-angle

    for (f in list.files(pattern = "direct_cellpersistance.csv", recursive =
TRUE)){
          df <- read.csv(f, header=TRUE) #data<-read.csv(f, header = FALSE, sep
= ",")
        }
```

```
    mu          <-          ddply(df,          "Genotype",          summarise,
grp.median=median(Cell_mean_p_angle))

      hist_DCP_mean    <-    ggplot(df,    aes(x=Cell_mean_p_angle,fill=Genotype,
      color=Genotype))+
      geom_histogram(alpha=0.2,       position="identity",       binwidth       =
2,aes(y=..density..))+
      theme_bw()+ theme(legend.position="bottom")+
      geom_vline(data=mu, aes(xintercept=grp.median, color=Genotype),
                           linetype="dashed")

    mu          <-          ddply(df,          "Genotype",          summarise,
grp.median=median(Cell_median_p_angle))

      hist_DCP_median  <-  ggplot(df,  aes(x=Cell_median_p_angle,fill=Genotype,
      color=Genotype))+
     geom_histogram(alpha=0.2,     position="identity",     binwidth     =     2,
aes(y=..density..))+
     theme_bw()+ theme(legend.position="bottom")+
     geom_vline(data=mu, aes(xintercept=grp.median, color=Genotype),
                    linetype="dashed")

        #save histograms and name it like file
        wd <- ("E:/Imaris/Done/AnalyseR/IN/direct_cellpersistance")
        setwd(wd)
        name <- list.files(wd,full.names=FALSE)

        setwd("E:/Imaris/Done/graphs/Histograms/direct_cellpersistance")

        # 1. Open jpeg file and name it like analyse in data
        png(paste0("DCP-MEAN_",
        (sub(".csv","",name[1])),"+",(sub(".csv","",name[2])),".png"))
        # 2. Create the plot
        plot(hist_DCP_mean)
        # 3. Close the file
        dev.off()

        png(paste0("DCP-MEDIAN_",
        (sub(".csv","",name[1])),"+",(sub(".csv","",name[2])),".png"))
        plot(hist_DCP_median)
        dev.off()


#Direct-persistanceangel

     for  (f  in  list.files(pattern  =  "direct_persistance.csv",  recursive  =
TRUE)){
       df <- read.csv(f, header=TRUE) #data<-read.csv(f, header = FALSE, sep =
",")
     }

     mu          <-          ddply(df,          "Genotype",          summarise,
grp.median=median(persistanceangel))

     hist_DP      <-      ggplot(df,      aes(x=persistanceangel,fill=Genotype,
color=Genotype))+
          geom_histogram(alpha=0.2,   position="identity",   binwidth   =   2,
             aes(y=..density..))  +
             theme_bw()+ theme(legend.position="bottom")+
             geom_vline(data=mu, aes(xintercept=grp.median, color=Genotype),
```

```
                linetype="dashed")

    #save histograms and name it like file
    wd <- ("E:/Imaris/Done/AnalyseR/IN/direct_persistance")
    setwd(wd)
    name <- list.files(wd,full.names=FALSE)

    setwd("E:/Imaris/Done/graphs/Histograms/direct_persistance")

    # 1. Open jpeg file and name it like analyse in data

    png(paste0("DP_",(sub(".csv","",name[1])),"+",(sub(".csv","",name[2])),".
    png"))
    # 2. Create the plot
    plot(hist_DP)
    # 3. Close the file
    dev.off()
```

7.1.2.4 Displacement over time (DOT)

```
#just for random migration!
#library(data.table)
#install.packages("ggplot2")
#library(ggplot2)
rm(list = ls())
wd <- "E:/Imaris/Done/Random"
folder <- list.files(wd, full.names=FALSE)
setwd(wd)

for (x in 1:length(folder)){

  wd1 <- paste0(wd,"/",folder[x])
  setwd(wd1)
  paste0(wd,"/",folder[x])
  Min1<- data.frame()
  Max1<-data.frame()
  MinMax<- data.frame()
  Hit<-data.frame()


  for (f in list.files(pattern = "Position_Reference_Frame.csv", recursive =
TRUE)){

    obj <- read.csv(f, header=TRUE, skip=3)
    obj <-obj[order(obj$TrackID),]

    Min1 <- obj[1,]
    MinMax <- rbind.data.frame(MinMax,Min1)


    for(i in 2:(nrow(obj)))     #Starting point of vector
      if (obj$TrackID[i]>obj$TrackID[i-1])
      {
        Hit<-obj[i-1,]
        MinMax <- rbind.data.frame(MinMax,Hit)
        Hit<-obj[i,]
        MinMax <- rbind.data.frame(MinMax,Hit)
      }
```

```
    Max1 <- obj[nrow(obj),]     #Endpoint of vector
    MinMax <- rbind.data.frame(MinMax,Max1)

    richtungsvektor<- data.frame(matrix(nrow=nrow(MinMax), ncol=3))

    for(i in 2:(nrow(MinMax))){
      if (MinMax$TrackID[i]==MinMax$TrackID[i-1]){
        richtungsvektor[i,1]<-   c((MinMax$Position.X[i])-(MinMax$Position.X[i-
1]))
        richtungsvektor[i,2]<-   c((MinMax$Position.Y[i])-(MinMax$Position.Y[i-
1]))
        richtungsvektor[i,3]<-   c((MinMax$Position.Z[i])-(MinMax$Position.Z[i-
1]))
        richtungsvektor[i,4]<-           c((MinMax$Time[i])-(MinMax$Time[i-1]))
       #frame length
      }
    }

       richtungsvektor$Steplenght                                          <-
       c(sqrt(((richtungsvektor$X1)**2)+((richtungsvektor$X2)**2)+((richtungsv
       ektor$X3)**2)))

  }

   MinMax$OriVector<-richtungsvektor

   MinMax$PerMin <- c((MinMax$OriVector$V4)/3) #Frame in this case 20 seconds
V4(Frame numbre / 3 equals minutes)

   MinMax$OriDisTime    <-    c((MinMax$OriVector$Steplenght)/(MinMax$PerMin))
#Steplength of displacemnt normalized by time (in this case bay miuntes)

   setwd("E:/Imaris/Done/csvdataRandom/DisplacedOriginTime")
   write.csv(MinMax,file=(paste0(folder[x],".","csv")))

}
```

7.1.2.5 Track speed calculation – random and direct

```
#library(ggplot2)
#list data and set working direktory
rm(list = ls())
data<- data.frame()
wd <- "E:/Imaris/Done/Random"
folder <- list.files(wd, full.names=FALSE)
setwd(wd)

#loop folder in random
for (x in 1:length(folder)){
  wd1 <- paste0(wd,"/",folder[x])
  setwd(wd1)
  paste0(wd,"/",folder[x])

  #binding speed data
  for (f in list.files(pattern = "Track_Speed_Mean.csv", recursive = TRUE)){

    obj <- read.csv(f, header=TRUE, skip=3)
```

```
    for(i in 1:(nrow(obj))){
      obj$Genotype<- (folder[x])
    }

    data <- rbind.data.frame(data,obj)
  }
}

ggplot(data, aes(Genotype,Track.Speed.Mean))+
  geom_jitter(color = "gray50", size=0.5)+
  geom_boxplot(fill=gray(0.9), outlier.size = 0.5, alpha = 0.4)+theme_bw()+
  theme(axis.text.x = element_text(angle = 45, hjust = 1,face="bold", size= 12),
axis.text.y = element_text(face="bold", size=12))

Anova_Results <- aov(Track.Speed.Mean ~ Genotype, data = data)
summary(Anova_Results)
TukeyHSD(Anova_Results)
plot(TukeyHSD(Anova_Results))


#save data as csv in new folder (see folderstructure), subsitute "name"
setwd("E:/Imaris/Done/Trackspeed")
write.csv(data,file=(paste0("name","Random-Trackspeed",".","csv")))


### Track speed mean in direct migration

#library(data.table)
#install.packages("ggplot2")
#library(ggplot2)

rm(list = ls())
Trackspeedmean_G<- data.frame()
Trackspeedmean_S <- data.frame()
Trackspeedmean <- data.frame()
#wd <- "E:/Imaris/Done/directed/RNAi"
wd <- "E:/Imaris/Done/directed/Mutant"
folder <- list.files(wd, full.names=FALSE)
setwd(wd)

for (x in 1:length(folder)){
  Trackspeedmean <- data.frame()
  wd1 <- paste0(wd,"/",folder[x])
  setwd(wd1)
  paste0(wd,"/",folder[x])

  for (f in list.files(pattern = "Position_Reference_Frame.csv", recursive =
TRUE)){
   # for (f in list.files(pattern = "Detailed.csv", recursive = TRUE)){
    obj <- read.csv(f, header=TRUE, skip=3)

    #Sort tracks via ID
    sortTrackID <-obj[order(obj$TrackID),]

       obj$disRefPoint<-
       c(sqrt(((obj$Position.X.Reference.Frame)**2)+((obj$Position.Y.Reference
       .Frame)**2)+((obj$Position.Z.Reference.Frame)**2)))
    #calculates distance from all point towards the wound (0/0/0) to every
timepoint
```

```
    #Set radius within cells should be analysed
       radius<-subset(obj, obj$disRefPoint<=70 & obj$disRefPoint>=15)    #zellen
       die sich wärend der Aufnahme im radius X aufhalten
    sortTrackID_Radius <-radius[order(radius$TrackID),]      #again, sorting

    #calculations for general cell persistance in wounding experiments
    richtungsvektor<- data.frame(matrix(nrow=nrow(sortTrackID_Radius), ncol=3))
    for (i in 2:(nrow(sortTrackID_Radius))) {
      if (sortTrackID_Radius$TrackID[i]==sortTrackID_Radius$TrackID[i-1]){

       richtungsvektor[i,1]<-
       c((sortTrackID_Radius$Position.X.Reference.Frame[i])-
       (sortTrackID_Radius$Position.X.Reference.Frame[i-1]))
       richtungsvektor[i,2]<-
       c((sortTrackID_Radius$Position.Y.Reference.Frame[i])-
       (sortTrackID_Radius$Position.Y.Reference.Frame[i-1]))
       richtungsvektor[i,3]<-
       c((sortTrackID_Radius$Position.Z.Reference.Frame[i])-
       (sortTrackID_Radius$Position.Z.Reference.Frame[i-1]))
      }
    }

       richtungsvektor$Steplenght<-
       c(sqrt(((richtungsvektor$X1)**2)+((richtungsvektor$X2)**2)+((richtungsv
       ektor$X3)**2)))

       richtungsvektor$Speed <- c((richtungsvektor$Steplenght)/30) #20 seconds
       timeframe

    data <- cbind.data.frame(sortTrackID_Radius,richtungsvektor)

    #print(s)
    Trackspeedmean_S <- aggregate(data, by = list(data$TrackID), FUN = mean,
na.rm=T)

    for(i in 1:(nrow(Trackspeedmean_S))){
      Trackspeedmean_S$Genotype<- (folder[x])


    }

       Trackspeedmean_G <- rbind.data.frame(Trackspeedmean_G,Trackspeedmean_S)

  }
       Trackspeedmean<- rbind.data.frame(Trackspeedmean,Trackspeedmean_G)

}

setwd("E:/Imaris/Done/Trackspeed")
write.csv(Trackspeedmean,file=(paste0("name","Trackspeedmean-
direct",".","csv")))
```

7.1.3 Analysis of Border cell migration

7.1.3.1 FIJI Macro

Source: Luis Garcia Rodrigues, University of Münster (unpublished)

```
input = getDirectory("Input directory");
output = getDirectory("Output directory");

Dialog.create("File type");
Dialog.addString("File suffix: ", ".tif", 5);
Dialog.show();
suffix = Dialog.getString();

processFolder(input);


function processFolder(input) {
	run("Clear Results");
	list = getFileList(input);
	for (i = 0; i < list.length; i++) {
		if(File.isDirectory(input + list[i]))
			processFolder("" + input + list[i]);
		if(endsWith(list[i], suffix))
			processFile(input, output, list[i]);
	}
	saveAs("Results",output+"results.csv");
	waitForUser("Results has been saved in"+output+"results.csv "+"\n click
OK to close");
	while (nImages>0) {
	   selectImage(nImages);
	   close();
	}
}

function processFile(input, output, file) {
	setTool("multipoint");
	open(input+file);
	redo = true;
	skip = false;
	while (redo){
		waitForUser("Measure", "Waiting for the reference points.");
		getSelectionBounds(selectionx,selectiony,w,h);

		if (selectionx == 0 && selectiony == 0){
			x=newArray(1);
			y=newArray(1);
			//this is just a quick (and dirty) solution for skip
			skip = getBoolean("Ok Mate, seems that you want to skip this
image. \n Are you sure? \n (cancel will stop the macro)");
			if(skip){
				totaldistance=-1;
				migrationdistance=-1;
			}else{
				totaldistance=-2;
				migrationdistance=-1;
			}
		}else{
```

```
                    getSelectionCoordinates(x,y);
                    if (x.length < 3 && x.length > 1){
                           x0 = newArray(x[0],y[0]);
                           x1 = newArray(x[1],y[1]);
                           totaldistance = distance(x0,x1);
                           migrationdistance = totaldistance;
                    }else if(x.length == 1){
                                  totaldistance = 1;
                                  migrationdistance = 0;

                    }else{
                           result = line_intersection(x,y);
                           x0 = newArray(x[0],y[0]);
                           x1 = newArray(x[1],y[1]);
                           x5 = newArray(result[0], result[1]);
                           totaldistance = distance(x0,x1);
                           migrationdistance = distance(x0,x5);
                    }
             }
             if (totaldistance >= migrationdistance){
                    redo = false;
             }else{
                    selectImage(nImages);
                    close();
                    if (totaldistance == -2){
                           waitForUser("Ok, let's try again.");
                    }else{
                           waitForUser("Total   distance   was   smaller   than
migrated distance, \n please be careful with the points, repeat measure.");
                    }
                    open(input+file);
             }
       }

       row = nResults;
       if (skip == false){
       setResult("image", row, file);
       setResult("migration D", row, migrationdistance);
       setResult("total D", row, totaldistance);
       updateResults();
       }
       selectImage(nImages);
    close();
    if (row == 99){
       waitForUser("Congrats!", "WOW, you have completed a set of 100 images.
\n You should take a rest.");
       }
}

function line_intersection(x, y){

             k = ((y[1]-y[0]) * (x[2]-x[0]) - (x[1]-x[0]) * (y[2]-y[0])) /
((y[1]-y[0])^2 + (x[1]-x[0])^2);
             x3= x[2] - k * (y[1]-y[0]);
             y3 = y[2] + k * (x[1]-x[0]);
             drawLine(x[0], y[0], x[1], y[1]);
             drawLine(x[2], y[2], x3, y3);

             xdiff = newArray(x[0]-x[1],x[2]-x3);
             ydiff = newArray(y[0]-y[1],y[2]-y3);
```

```
              div = det(xdiff,ydiff);
              if (div == 0) {
                     print('lines do not intersect');
                     return -1;
              }
              a0 = newArray(x[0],y[0]);
              a1 = newArray(x[1],y[1]);
              a2 = newArray(x[2], y[2]);
              a3 = newArray(x3,y3);
              d1 = det(a0,a1);
              d2 = det(a2,a3);
              d = newArray(d1,d2);
              x = det(d,xdiff)/div;
              y = det(d,ydiff)/div;

              intersection_point = newArray(x,y);
              makePoint(x,y);

              return intersection_point;
}
function det(a,b){
       return a[0]*b[1]-a[1]*b[0];
}

function distance(a,b){
       d1 = a[0]-b[0];
       d2 = a[1]-b[1];
       dis = sqrt(pow(d1,2)+pow(d2,2));
       return dis;
       }
```

7.1.3.2 R-script

Source: Luis Garcia Rodrigues, University of Münster

```
library("data.table")
library("ggplot2")

migration_analysis <- function(folder){
  obj<-data.table()
  for (f in list.files(folder,pattern = ".csv", recursive = TRUE)){
    print(f)
    obj<-rbind(obj,analysis_individual(paste(folder,f,sep=""), f),fill=TRUE)
  }

  #plot<-ggplot(obj,  aes(quadrant))+geom_bar(aes(fill  =  genotype),position  =
position_stack()) +
  #coord_flip() +
  #theme(legend.position = "top")
  #print(plot)

  plot2<-ggplot(obj,  aes(genotype))+geom_bar(aes(fill  =  quadrant),position  =
position_stack()) +
    coord_flip() +
    theme(legend.position = "top")
  print(plot2)
```

```
    plot3<-ggplot(obj,                                          aes(x=quadrant,
group=genotype))+geom_bar(aes(y=..prop.., fill=factor(..x..)) )+
    coord_flip() + facet_grid(~genotype)
    theme(legend.position = "top")
  print(plot3)

  plot3<-ggplot(data=unique(obj[,.(genotype,quadrant,      quadrant_percent)]),
aes(x=genotype, y=quadrant_percent, fill=quadrant))+geom_bar(stat="identity" )+
    coord_flip() +
    theme(legend.position = "top")+
    labs(x="Ratio")

  print(plot3)

  return(obj)
}

analysis_individual<- function(filePath, fileName){
  dt <- fread(filePath)
  dt[,normalized_migration:= `migration D`/`total D`]
  dt[,genotype:=paste(strsplit(fileName,".csv"))]
  dt[,quadrant:=paste(((normalized_migration-0.00001)%/%0.25)+1)]
  total_entries <- nrow(dt)
  total_by_quadrant <- dt[, length(genotype), by=quadrant]

  dt[,quadrant_percent:=percent(genotype,dt),by=quadrant]

  dt<-dt[order(normalized_migration)]
  return (dt)
}

percent<-function(vector, dt){
  return(length(vector)/nrow(dt))
}
```

7.1.3.3 Manual for statistical analysis of BCM-data

Create an analysis folder and set it as working directory. Then, call function (R-script) migration_analysis("./") or one of the other.

Further save results as .csv file in working directory:

command: results<- migration_analysis("./")
write.csv(results,file=("name.csv")) #saved in working directory

GraphPad:

Create contingency table with outcome --> 100-75, 75-50, 50-25, 25-0

use "quadrant_percent" information to create the bars.

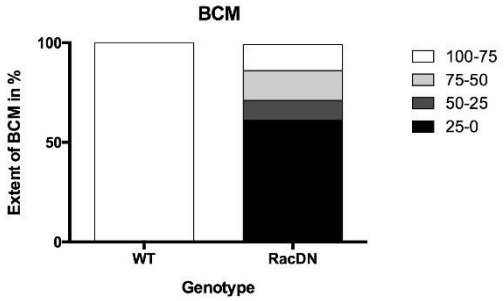

Example for BCM quantification

Statistics:

use column statistics: data --> normalized_migration

make a non-parametric test (Mann–Whitney U test)

7.2 Supplementary Figures

7.2.1 Alignment WAVE isoforms and orthologs

Supplementary Figure 1: Multiple sequence alignment by NCBI clustal W2.

7.2.2 Rac depletion in macrophages

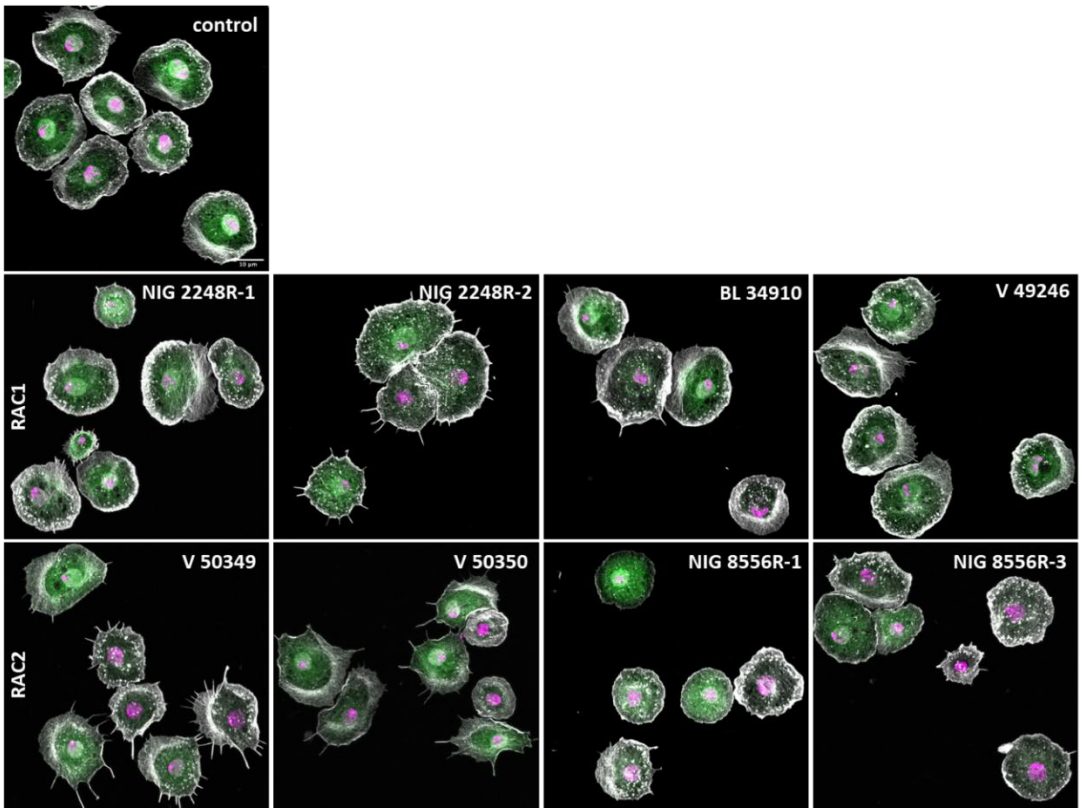

Supplementary Figure 2: Test of Rac RNAi-mediated knockdown. Isolated larval macrophages plated on ConA and stained for F-actin and nucleus, expressing cytoplasmic eGFP (see color code).

Supplementary Table 3: Compression of results gained by RNAi mediated Rac suppression in macrophages (Supplementary Figure 2) with previous performed experiments.

	CHROMO-SOME	OFF TARGETS	HEMOZYTE–MORITZ SANDER	TESTIS – MAIK BISCHHOFF	HEMOZYE – THIS THESIS
RAC1					
NIG-Fly 2248R-1	I	?	NO	NO	NO
NIG-Fly 2248R-2	I	?	NO	NO	stellate (weak)
Bloomington 349110	III	?	NO	NO	NO

VDRC 49246	II	RAC2	spiky (strong)	NO	NO
RAC2					
VDRC 50349	III	RAC1	spiky (strong)	NO	spiky
VDRC 50350	III	RAC1	spiky (strong)	NO	spiky
NIG-Fly 8556R-1	III	?	stellate	YES	small cells with reduced lamellipodia
NIG-Fly 8556R-3	III	?	spiky	YES	small cells with reduced lamellipodia

7.2.3 WIRS-ligand screen

Gene name	Protein ID	Human ortholog	Protein family	Molecular function (predicted)	Expression (reported)
CG8222	Q8T4M0	PDGFR/VEGFR	PDGF- and VEGF-receptor	hemocyte migration	hemocytes
CG17752	Q9VDV7	SLC22A25	solute carrier family	cation transporter	hemocytes
CG10413	Q9VJ75	SLC12A9	solute carrier family	cation transporter	hemocytes
CG5853	Q9VL61	ABCG4	ABC transporter	ABC transporter	hemocytes
CG3829	961K6	CDC36/SCARB3	CD36 antigen (collagen receptor)	scavenger receptor activity	hemocytes
CG8942	Q9VJU5	KRTAP9-9	Nimrod C1/ EGF-like	Phagocytosis, immune defense	hemocytes
CG6890	Q9V477	TLR9	Toll/interleukin-1 receptor	Axis formation, immune response	Ovary, gut, hemocytes
CG18241	Q9VLE6	IL18R1	Toll/interleukin-1 receptor	immune response	Testis, gut, fat body, hemocytes
CG8595	Q7KIN0	TLR7	Toll/interleukin-1 receptor	immune response	Brain, testis, hemocytes
CG7121	Q9NBK8	TLR4	Toll/interleukin-1 receptor	immune response	CNS, ovary, gut, fat body, hemocytes
CG6210	Q95ST2	WLS	Wntless, Wnt-protein binding	Epithelial morphogenesis	CNS, gut, ovary, salivary gland, hemocytes
CG1511	O96435	EPHB1	Eph receptor tyrosine kinase	Photoreceptor axon guidance, oogenesis, anti-parasitoid immune response	CNS, eye, ovary, hemocytes
CG10671	Q9VRJ2	FITM2	FIT (Fat storage transmembrane) protein family	lipid storage, cell shape	Gut, heart, fat body, hemocytes
CG7250	Q9NBK9	TLR3	Toll/interleukin-1 receptor	immune response	Brain, CNS, hemocytes
CG17800	Q9VS29	DSCAML1	Down syndrome cell adhesion molecule (DSCAM)	Axon guidance, immune system (phagocytosis)	CNS, fat body, gut, hemocytes
CG8856	A1Z8V0	MAMDC2	Scavenger receptor classC	Phagocytosis, immune defense	ubiquitous
CG6899	Q24495	PTPRB	transmembrane receptor protein tyrosine	axon guidance	ubiquitous
CG5248	Q9VCX1	RGS12	GPRC binding	Glia differentiation, cell cortex and cortical cytoskeleton	ubiquitous
CG32475	Q9W0V7	Not known	G-protein coupled receptor 2 family	Lifespan, response to starvation	ubiquitous
CG18402	C7C417	IGF1R	Insulin-like receptor	Axon guidance, oogenesis, stress response	ubiquitous
CG31009	Q5D716	PCDH15	Cadherin protein family	calcium-dependent cell adhesion	CNS, eye, ovary, hindgut,
CG1232	P48613	not known	sodium channel regulator	heat response	Brain, gut, testis
CG1817	P35992	PTPRB	receptor protein tyrosine phosphatase	regulation of growth cones from the emryonic midline	Hindgut, ovary, trachea, CNS
CG5227	O97394	SDK2	sidekick cell adhesion molecules, immunoglobulin superfamily	photoreceptor cell differentiation	CNS, Ovary, trachea, salivary glands,
CG31116	Q9VGH7	CLCN2	Chloride channel family	Chloride transport	Brain, eye, fat body, midgut
CG4894	Q24270	CACNA1D	Calcium channel family	Calcium ion transport	Brain, eye, heart
CG12734	Girdin	Girdin			
CG8433	Q9Y169	EXT2	Glycosyltransferase 47 protein family	role in heparan sulfate proteoglycans (HSPGs) biosynthesis	CNS, eye, ovaryfat body

Supplementary Figure 3: Tested potential WIRS-ligands that has been tested for directed wound response in this thesis. At least two independent RNAi were used in hemocyte specific knock down by *hml*Δ-Gal4.

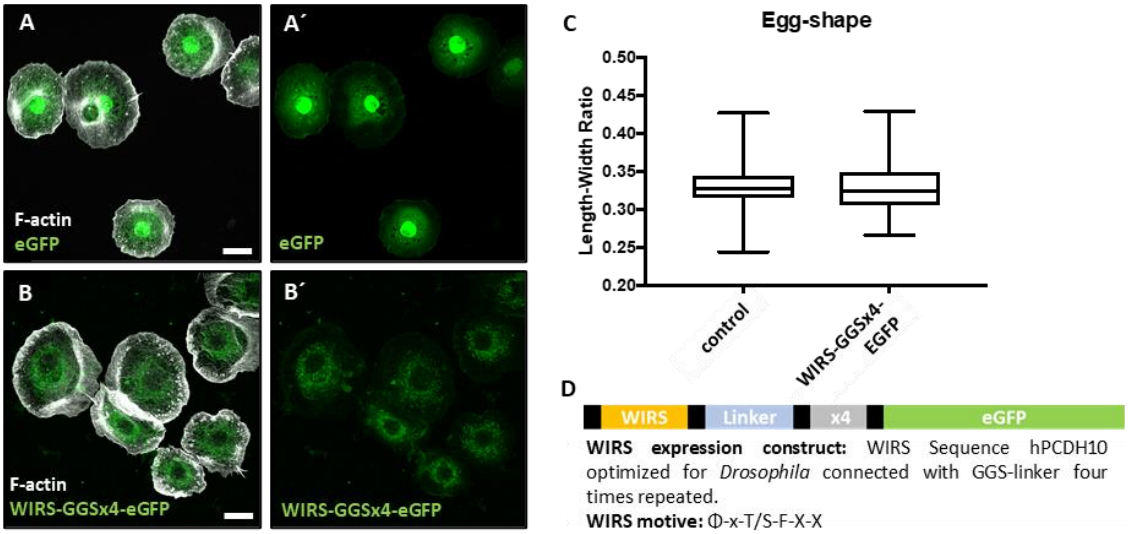

Supplementary Figure 4: Expression test of WIRS-GGSx4-eGFP. (A+B) Isolated larval macrophages plated on ConA and stained for F-actin (white) and cytoplasmic expression of eGFP (A) or WIRS-GGSx4-eGFP (B) by *hmlΔ*-Gal4. (C) Expression of eGFP or WIRS-GGSx4-eGFP in follicle cells (*gr1*-Gal4). Egg-shape analysis show no differences. (D) Scheme of WIRS-GGSx4-eGFP expression construct.

7.2.4 Shape analysis of *abl* mutant larval macrophages

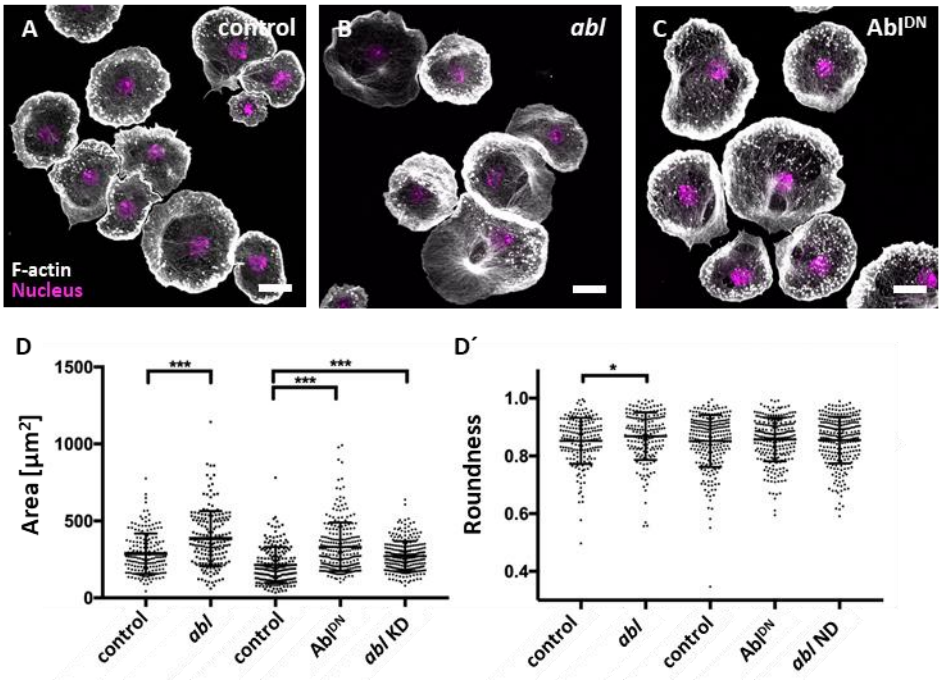

Supplementary Figure 5: *abl* mutant larval macrophages are increases in size and rounded up. (A+C) Isolated larval macrophages plated on ConA stained for F-actin (white), nucleus (magenta). Morphologically both show a broad lamellipodium. (C) Cell shape parameter area and roundness are depicted in a scatter dot blot with bars indicating mean and SD. *** = $p \leq 0.001$ (Mann-Whitney-U-Test). (D) *abl* mutant macrophages, macrophages expressing Abl^{DN} construct and *abl* RNAi-mediated knockdown are increased in size in comparison to their corresponding control. (D´) *abl* mutant macrophages are also rounded up. Scale bar = 10 µm.

7.2.5 *src42A* RNAi efficiency test

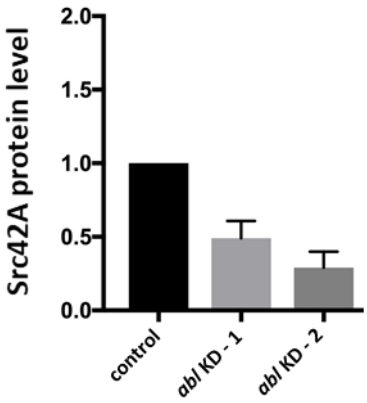

Supplementary Figure 6: Result of quantitative analysis of indicated *src42A* RNAi constructs by Western blot. Src42A protein level normalized to respective actin level and Src42A expression in eGFP control transfected cells. Abl KD -1 = VDRC *Src42A* RNAi line 100708, *Abl* KD -1 = Bloomington *Src42A* RNAi line 55868

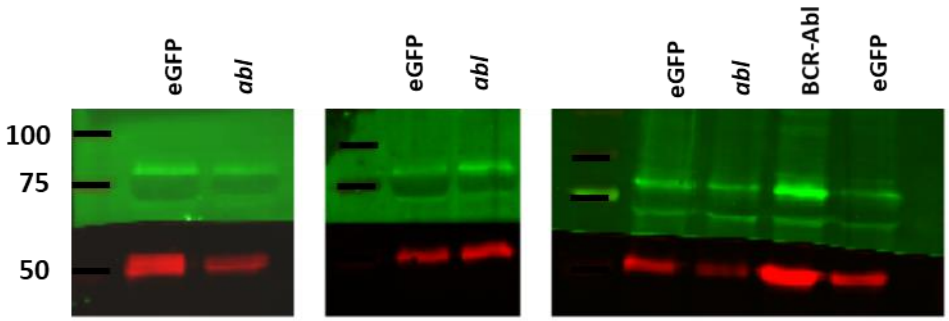

Supplementary Figure 7: Western Blot analyses of isolated larval macrophages. Genotype and antibody staining are indicated. Three independent experiments. Quantification Figure 30.

In a site experiment the function of WAVE, Abl and Src42A was investigated in collective cell migration in border cell migration. Recent work manly used *slbo*-Gal4 for ectopic tissue specific expression in border cells, were not able to detect any effect of *wave* and other WRC complex members on border cell migration. Here, another border cell driver *c306*-Gal4 were tested and compared with the expression level and timepoint in egg chamber development (Supplementary Figure 8). The results show an earlier and almost 2 times stronger expression of eGFP.

7.2.6 Border cell migration: the impact of WAVE, Abl and Src42A

Tissue specific suppression with RNAi expression by *c306*-Gal4 show 40 % overall and 10 % severe border cell migration defects (Supplementary Figure 9). When analyzing the effect of two important kinases Abl and Src42A that are known acting on WAVE activity, only interference with Src function result in impaired border cell migration (Supplementary Figure 9).

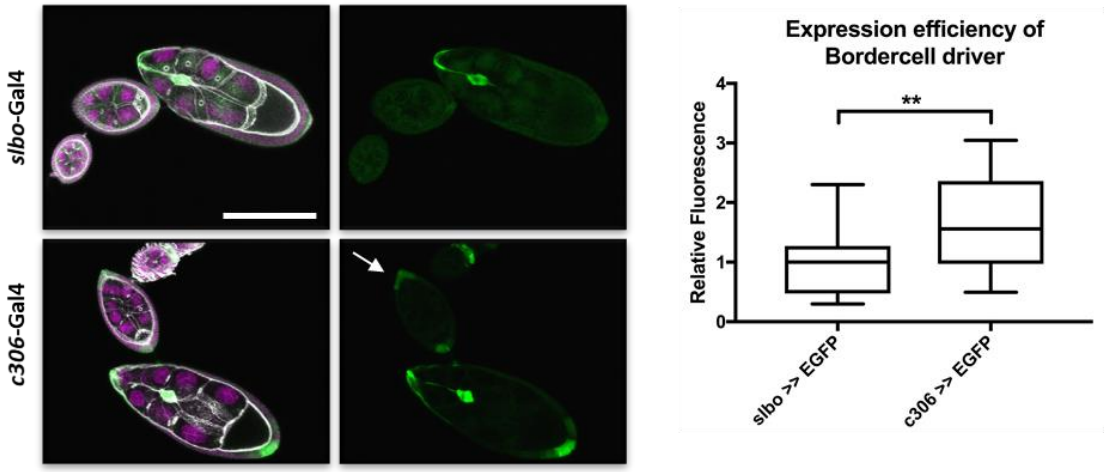

Supplementary Figure 8: Comparison of expression pattern of two different border cell driver. eGFP expression is in median 1.5-fold increased driven by *c306*-Gal4 in comparison to *slbo*-Gal4. Additionally, *c306*-Gal4 expresses already in earlier egg chamber stages (white arrow).

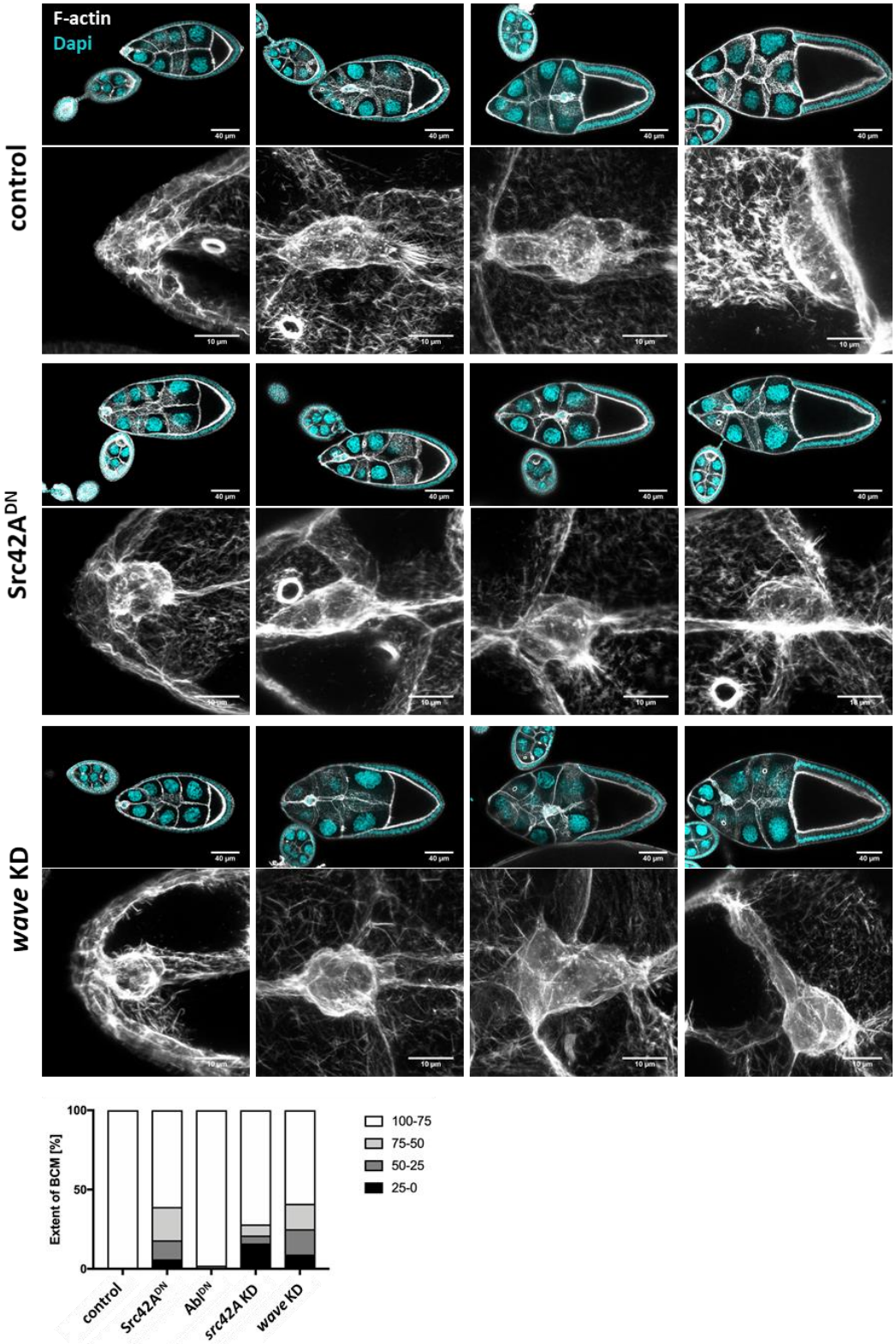

Supplementary Figure 9: Analysis of Border cell migration (BCM). Expression of indicated RNAi by *c306*-Gal4. Control egg chamber show wild typic BCM. Step 1. delamination, step 2. Collective cell migration through the nurse cells, step 3. Reaching the oocyte in stage 10A (100 % migration, see method part 2.5.4). BCM is analyzed, when expressing indicated constructs. Depletion of *wave* as well as *src42A* or the expression of Src42A^{DN} show severe defects in BCM. The expression of Abl^{DN} has no effect on BCM.

7.2.7 Three variances of Scarlet, a new bright monomeric red fluorescent protein

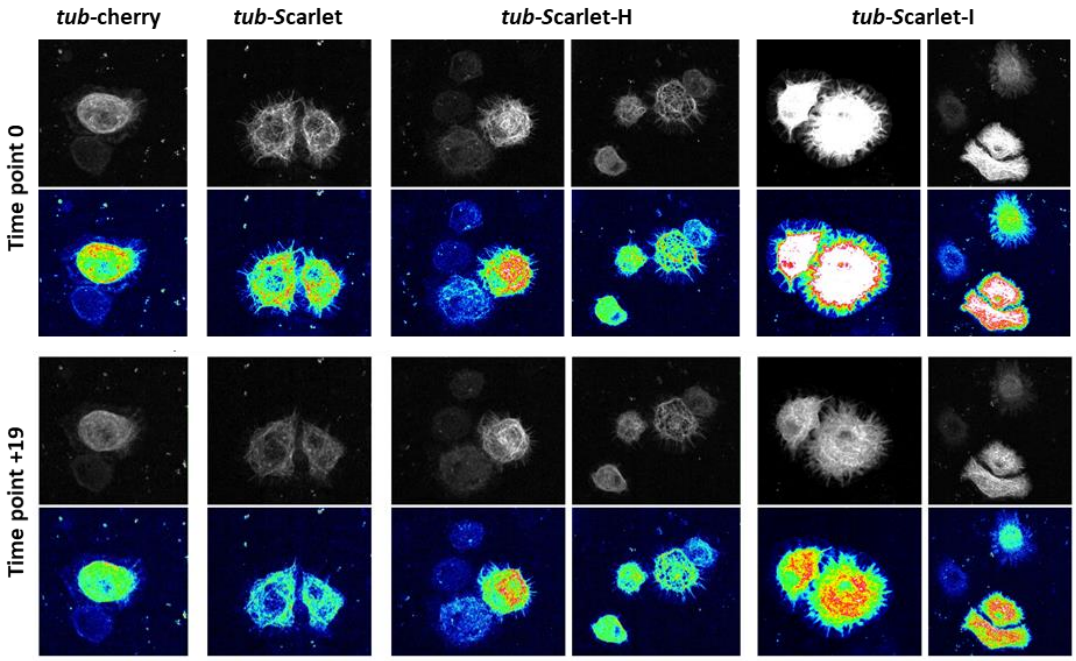

Construct	Start intensity	Bleaching
cherry	0	0
Scarlet	0	+
Scarlet-H	+	- -
Scarlet-I	+ + +	+ +

Supplementary Figure 10: Novel fluorophore mScarlet: Expression test of three different variants. Still images of time laps. Comparison of brightness at imaging start and 19 timepoints later. Tubulin driven cherry expression is used as control for a classic red fluorescent protein. Table illustrated performance in comparison to cherry ((+ more, - less), Bindels et al., 2017).

Verzeichnis der akademischen Lehrer/-innen

Christian-Albrechts-Universität zu Kiel	Prof. Dr. Dr. Ulrich Lüning
Dr. Christiana Anagnostou	Prof. Dr. Dietrich Ober
Prof. Dr. Michael Bauer	Dr. Björn Raabe
Prof. Dr. Wolfgang Bilger	Prof. Dr. Thomas Roeder
Prof. Dr. Dr. Thomas Bosch	Prof. Dr. Stefan Rose-John
Dr. Dirk Brandis	Prof. Dr. Margareta Sauter
Prof. Dr. Heinz Brendelberger	Prof. Dr. Axel Scheidig
Prof. Dr. Manuela Dittmar	Prof. Dr. Peter Schönheit
Prof. Dr. Helmut Fickenscher	Prof. Dr. Hinrich Graf von der Schulenburg
Prof. Dr. Gernot Friedrichs	Prof. Dr. Rüdiger Schulz
Prof. Dr. Christoph Garbers	Prof. Dr. Ruth Anne Schmitz-Streit
Prof. Dr. Stanislav Gorb	Prof. Dr. Felix Tuczek
Prof. Dr. Günther Hartl	Prof. Dr. Richard Weidmann
PD Dr. Holger Heine	
Prof. Dr. Frank Kempken	**University of Edinburgh**
Prof. Dr. Karin Krupinska	Prof. Tom Little, Ph.D.
Prof. Dr. Matthias Leippe	

Danksagung

Ich blicke auf die letzten Jahre mit viel Dankbarkeit aber auch mit Demut zurück.
Dankbarkeit für die vielen bereichernden Erfahrungen, Dankbarkeit für die vielen spannenden Momente, Dankbarkeit frei Forschen zu können. Besonders bin ich aber dankbar und demütig für das Privileg den höchsten Bildungsabschluss anstreben zu dürfen.
Dies alles wäre nicht möglich ohne die Menschen, die mich auf diesem Weg begleitet haben. Ihnen gilt meine tiefe Dankbarkeit.

Erst möchte ich mich bei Sven bedanken, für das spannende Projekt und das Vertrauen, das du nicht nur in meine Arbeit, sondern besonders während des Umzuges nach Marburg, in mich gesetzt hast. Danke für deine vielen Ratschläge und deine Geduld, die du mit mir hattest. Du hast immer gefördert, dass ich auf viele Konferenzen fahren konnte und mich dort mit Wissenschaftler*innen aus der ganzen Welt austauschen konnte.
Ich bin hier in der besonderen Situation in gleich zwei Instituten danken zu dürfen. Begonnen hat alles in der Badestraße in Münster, wo mich Christian mit offenen Armen und viel Herzlichkeit aufgenommen hat. Danke für die schöne Zeit und das immerwährende Gefühl willkommen zu sein. Ein riesen Dank geht an die erste „Bogdan-Crew“: Bene, Meike, Lena, Julia und Klaus. Ihr habt mich unfassbar herzlich und offen bei euch aufgenommen. Ich werde die zwar kurze aber schöne Zeit mit euch nie vergessen. Danke an Klaus für die vielen Stunden Zerstreuung in der Boulderhalle und meinen ersten Einbruch. Liebe Lena, auf dich und deine Freundschaft konnte und kann ich mich immer verlassen – vielen Dank.
Vielen lieben Dank auch an alle anderen tollen Menschen in der Badestraße, die „Kämbts“, die „Schirmeiers“, die „Luschnigs“, die „Rumpfs“ und die „Stanewskys“. Ihr habt mir nicht nur immer mit Rat und Tat zur Seite gestanden, sondern mich auch in Traditionen des Karnevals eingeführt und mir die kleine Hütte im schönsten Skigebiet der Welt gezeigt. Danke, Helen, Anne, Kerem, Jonas, Svende, Sandra, Rafael, Holger, Felix, Rita, Johanna, Ellen, Simone, Astrid, Selen, Nils und allen anderen.
Lieber Bene, ohne dich hätte ich den Umzug nach Marburg nicht gemeistert. Danke für dein Sofa im schönen Allna und die Geduld mir der du mit mir über 2000 Fliegenstämme neue sortiert hast. Danke auch an die mittlerweile echt große Labor-Truppe in Marburg – Caro, Steffi, Maik, Wiebke, Susanne Ö., Alex, Vignesh, Mila und Regina. Danke für die netten Mittagsrunden und die Gespräche in den kleinen Arbeitspausen. Liebe Wiebke, dein offenes Ohr und dein stetiger Optimismus haben mich an vielen Tagen aufgebaut. Danke Alex, dass ich mich immer auf deine Hilfe verlassen kann. Danke Susanne B. für deine unvergleichbare

Geduld, deine Hilfsbereitschaft bei allen Fragen und deine immer offene Tür. Ein großer Dank geht an die drei Frauen, die guten Geister, die helfenden Hände - Kirsten, Doris und Andrea. Sie halten in Marburg den Laden am Laufen. Ihr seid nicht nur eine Stütze für alle von uns im Labor, sondern habt auch so immer ein offenes Ohr, ein liebes Wort oder einen Not-Sekt im Kühlschrank. Ich werde euer schallendes Lachen, dass über die Flure hallt, vermissen. Einen besonderen Dank gilt hier Andrea, die mich in meinem letzten Jahr im Labor so tatkräftig unterstützt hat und meinen doch manchmal wirren Kopf immer wieder ertragen hat. Nicht zuletzt gilt mein Dank Armin – dem Herrn der Fliegen (und allem was dazu gehört). Wie du uns die Arbeit erleichterst, merkt man immer am eindrücklichsten, wenn du nicht da bist.

Ein besonderer Dank geht an alle meine lieben, verrückten, großartigen und besten Menschen in Kiel, Hamburg, Münster, Freiburg, Homburg, Köln und wo ihr nicht sonst noch so steckt. Euer Vertrauen und eure Freundschaft sind ein riesen Geschenk, für das ich jeden Tag aufs Neue dankbar bin. Danke Vero, Francie, Tanja, Lisa, Anica, Daniel und noch so vielen mehr. Danke Vero für den vielen Kaffee und den starken Rückhalt. Danke an all die Genossen, die zusammen mit mir diese Welt zu einem gerechteren, solidarischen Ort machen. Anna-Lena, Sophie, Philipp und Clara und ihr anderen – mit euch ziehe ich in jede Schlacht.

Daniel – Danke, für deinen Vertrauen in mich, deine Unterstützung, deine Geduld und dass du mich auch in schwierigen Zeiten immer wieder zum Lachen bringst. Gemeinsam haben wir fünf Jahre Fernbeziehung in einer echt verrückten Zeit gemeistert. Was soll da jetzt noch kommen?

Der letzte und größte Dank geht an meine Familie: An meine beiden kleinen, großen Brüder, auf die ich unfassbar stolz bin und auf die ich mich immer verlassen kann. Meinen Eltern, die immer mein größter Rückhalt sind und mir ein Grundvertrauen in mich und die Welt geschenkt haben, ohne dass ich sicher nicht so weit gekommen wäre.